Pulsating Burners - Controlling Mechanisms and Performance

Final Report

January 1, 1987 - June 30, 1990

Prepared by

J.I. Jagoda, B.R. Daniel and B.T. Zinn

School of Aerospace Engineering

Georgia Institute of Technology

For

Gas Research Institute

Grant No. 5087-260-1466

GRI Project Managers

James A. Kezerle and Thomas R. Roose, Ph. D.

Combustion

January 1991

GRI DISCLAIMER

LEGAL NOTICE: This report was prepared by the Georgia Institute of Technology as an account of work sponsored by the Gas Research Institute (GRI). Neither GRI, members of GRI, nor any person acting on behalf of either:

a. Makes any warranty or representation, express or implied, with respect to the accuracy, completeness, or usefulness of the information contained in this report, or that the use of any apparatus, method, or process disclosed in this report may not infringe privately owned rights; or

b. Assume any liability with respect to the use of, or for damages resulting from the use of, any information, apparatus, method, or process disclosed in this report.

50272-101

REPORT DOCUMENTATION PAGE | 1. REPORT NO. | 2. | 3. Recipient's Accession No.

4. Title and Subtitle
"Pulsating Burners - Controlling Mechanism and Performance"

5. Report Date
January 1991

6.

7. Author(s)
J.I.Jagoda, B.R.Daniel and B.T.Zinn

8. Performing Organization Rept. No.
-

9. Performing Organization Name and Address
School of Aerospace Engineering
Georgia Institute of Technology
Atlanta, Georgia 30332

10. Project/Task/Work Unit No.
E-16-601

11. Contract(C) or Grant(G) No.
(C) 5087-260-1466
(G)

12. Sponsoring Organization Name and Address
Gas Research Institute
8600 West Bryn Mawr Avenue
Chicago, IL 60631

13. Type of Report & Period Covered
Final
Jan.'87-June '90

14.

15. Supplementary Notes

16. Abstract (Limit: 200 words)

The objective of this study was to increase our understanding of the physical processes which control the mixing and heat release processes in valved, natural gas fired, pulse combustors. The effects of combustor geometry and heat transfer upon the performance of the pulse combustor were investigated. The flow and flame spread in the pulse combustor were visualized using high speed shadowgraphy and radical imaging, respectively. In addition, the flow field has been quantified using laser Doppler velocimetry. The resulting data were used to explain the dependence of the pulse combustor's performance upon the timing of the entry of the reactants and the complex interaction between the fuel and air jets. Furthermore, the reasons for the existence of lean and rich limits of operation were determined. Under a separate task, the acoustic characteristics of the various parts which make up a pulse combustor were determined using an impedance tube technique. Finally, an analytical scheme was developed which allows the calculation of the admittance of entire sections of the pulse combustor from measured admittances of its component parts.

17. Document Analysis a. Descriptors

Pulse Combustion

b. Identifiers/Open-Ended Terms

Performance, Flow Visualization, Reignition, Flame Spread, Limits of Operation, Admittance Measurements.

c. COSATI Field/Group Combustion

18. Availability Statement:
Distribution Unlimited

19. Security Class (This Report)
unclassified

20. Security Class (This Page)
unclassified

21. No. of Pages

22. Price

See ANSI-Z39.18) See Instructions on Reverse OPTIONAL FORM 272 (4-77)
(Formerly NTIS-35)
Department of Commerce

RESEARCH SUMMARY

Title: Pulsating Burners - Controlling Mechanisms and Performance

Contractor: Georgia Tech Research Corporation

Contract Number: 5087-260-1466

Reporting Period: January 1987- June 1990, Final Report

Principle Investigators: B. T. Zinn, B. R. Daniel and J. I. Jagoda

Objective: The objectives of this study were to gain further insights into the detailed physical mechanisms which control the mixing and heat release processes in pulse combustors. In addition, the acoustic damping characteristics of various components and subsystems of the pulse combustor were to be determined over a range of operating conditions.

Technical Perspective: Natural gas fired pulse combustors have been on the market for a number of years. Nevertheless, their controlling mechanisms are still not sufficiently well understood to permit the design

of pulse combustors for different applications without resorting to costly trial and error development efforts. Proper operation of pulse combustors requires that the timing of the mixing, cycle to cycle reignition and flame spread processes produce oscillatory heat release in phase with the pressure oscillations. In addition, the thus generated driving must be sufficient to overcome the damping by the pulse combustor. To develop a rational design procedure for pulse combustors, it is necessary that the various processes responsible for energy addition to and removal from the pulsations be understood. Furthermore, data describing the acoustic properties of various pulse combustor components under different operating conditions are needed. Finally, the interaction between the acoustic characteristics of the various combustor components and the fundamental fluid mechanical, heat transfer and combustion processes must be understood.

Technical Approach: In order to elucidate the mechanisms which control the operation of a natural gas fired, Helmholtz type, pulse combustor and to determine the acoustic characteristics of different components and

subsystems which make up this pulse combustor, the following tasks were performed:

1) The flow field characteristics, mixing and heat release distributions in the pulse combustor were investigated using LDV, Schlieren, mixing visualization and radical radiation imaging.

2) The acoustic characteristics of various components and subsystems which make up the pulse combustor were measured using the impedance tube technique.

Results: A natural gas fired, valved, Helmholtz type, pulse combustor based upon an AGA design was studied. High speed shadowgraphy showed that the injection of the fuel jet leads the entry of the air jet. The latter creates large axial and transverse vortices in the mixing chamber. Comparison of the flow field with spatially and time resolved heat release measurements indicated that the order in which the reactants enter the combustor is critical to the spread of the combustion process through the mixing chamber. While the fuel jet begins to react with air left over from the previous cycle as soon as it enters the mixing chamber, the main ignition of the new fuel occurs near the combustor wall opposite of the fuel port. Combustion is then convected by the leading edge vortex of the air jet through the remainder of the mixing chamber. It is

this complex interaction between the fuel and air jets which stabilizes the combustion process in the mixing chamber. An increase in the combustor temperature was found to lower the lean limit of operation of the pulse combustor. However, the period of pulsations had to be extended or combustion air had to be supplied under pressure to extend its rich limit. This rich limit occurs near stoichometric conditions because no air is left over from the previous cycle. The combustion process is then confined to the time interval between the entry of the new air jet and the quenching of the reaction by the combustion products returning to the mixing chamber. For the standard AGA combustor this time is too short to permit sufficient heat release to drive the pressure oscillations. Further investigation of the importance of the timing between the heat release and the pressure oscillations revealed that at low operating frequencies the combustion process can excite higher pressure harmonics in the combustor unless the timing of the heat release is delayed. Furthermore, reduction of heat transfer to the combustor walls was found to significantly reduce the operating frequency of the device. The results of ensemble averaged mean velocity and turbulence intensity measurements are used to

qualitatively describe the complex, turbulent flow field in the mixing chamber at various instants during the cycle. These measurements are currently being completed by the graduate student as part of his Ph. D. thesis work. Under a separate task, an impedance tube technique was used to measure the acoustic characteristics (i.e., the admittance) of the fuel and air valves and of the mixing chamber fitted with both valves. These measurements indicated that, while the fuel valve behaves acoustically like a hard termination, the damping by the air valve increases with increasing frequency and valve opening and decreases with increasing pressure amplitude. Comparisons of the admittance measurements of the mixing chamber with those of the entire combustor showed that the damping by the Helmholtz volume formed by the combustion chamber overshadows the effect of the damping by the air flapper valve for the pulse combustor configuration under investigation. In addition to these measurements, an analytical scheme was developed which permits the determination of the admittance of the entire mixing chamber - valve assembly from the measured admittances of its component parts.

Project Implications: To be completed by the GRI technical manager.

TABLE OF CONTENTS

LIST OF FIGURES

11. Locations at which the Laser Doppler Velocimeter Results Shown in Figures 12 through 29 were Obtained. Each Location is Labeled (m,n).

12. Variation of the Vertical Mean Velocity During a Cycle for Locations along the Line m = 1. The Top Plot includes the Pressure Trace for Reference.

13. Variation of the Vertical Mean Velocity During a Cycle for Locations along the Line m = 2. The Top Plot includes the Pressure Trace for Reference.

14. Variation of the Vertical Mean Velocity During a Cycle for Locations along the Line m = 3. The Top Plot includes the Pressure Trace for Reference.

15. Variation of the Axial Mean Velocity During a Cycle for Locations along the Line m = 1. The Top Plot includes the Pressure Trace for Reference.

16. Variation of the Axial Mean Velocity During a Cycle for Locations along the Line m = 2. The Top Plot includes the Pressure Trace for Reference.

17. Variation of the Axial Mean Velocity During a Cycle for Locations along the Line m = 3. The Top Plot includes the Pressure Trace for Reference.

18. Variation of the Vertical Turbulence Intensity During a Cycle for Locations along the Line m = 1. The Top Plot includes the Pressure Trace for Reference.

19. Variation of the Vertical Turbulence Intensity During a Cycle for Locations along the Line m = 2. The Top Plot includes the Pressure Trace for Reference.

INTRODUCTION

A recent increase in interest in pulse combustors has been driven by such advantages as high combustion and thermal efficiencies, excellent heat transfer characteristics and low CO, NO_x and soot emissions. Development of new pulse combustor applications has been hampered, however, by a lack of adequate understanding of the fundamental processes which control the operation of these devices. It was the purpose of this program to shed new light upon the mechanisms which control the operation of pulse combustors and to provide the designer with additional insight which would help him in the development of new and the scaling of existing pulse combustion devices.

The natural gas fired, valved, Helmholtz type, pulse combustor whose operating characteristics were investigated in this program is based upon an AGA design. It is shown schematically in Fig. 1. The combustor consists of cylindrical mixing and combustion chambers, a tailpipe, a cylindrical decoupling chamber and a short vent pipe. Natural gas and air enter the combustor at right angle to each other through separate flapper valves attached to the curved side wall of the mixing chamber. During start up, the reactants are allowed to mix and are ignited using a spark plug. As the natural gas burns (a process which has previously been shown to take place primarily in the mixing chamber) the pressure in the combustor rises. This closes the flapper valves which prevents further reactants from entering the mixing chamber. This pressure rise also pushes the combustion products out through the tail pipe. The momentum of the

expelled exhaust gases causes the pressure in the mixing chamber to drop which reopens the flapper valves. New reactants now enter the combustor where they mix and are ignited by burning pockets of gas left over from the previous cycle. The cycle now repeats itself. Thus, pulse combustion operation can be maintained indefinitely without the use of the spark plug.

The gap in the fuel flapper valve is fixed while that in the air valve can be adjusted using a micrometer, see Fig. 2. The overall equivalence ratio in the pulse combustor is, therefore, varied by adjusting the air flapper valve setting which changes the air flow rate.

OBJECTIVES

It was the objective of this study to gain further insight into the fundamental processes responsible for the operation of pulse combustors in general and natural gas fired, valved, Helmholtz type, pulse combustors in particular. Emphasis was placed upon obtaining practical information which will permit designers to develop new and/or larger scale pulse combustors without resorting to costly trial and error based development efforts.

More specifically, the goal was to determine the effect of the combustor geometry and temperature upon its performance. In addition, the velocity, mixing and heat release distributions in the mixing and combustion chambers were measured both qualitatively and quantitatively and used to establish the nature of the interaction between

the combustion process and the acoustics of the combustor. This would lead to a physical explanation of the operating characteristics of the natural gas fired, valved, Helmholtz type, pulse combustor. In addition, the admittance of various components and subsystems which make up the pulse combustor were to be determined under a variety of operating conditions.

PROGRAM PLAN

The program is divided into three major tasks as outlined below:

Task I: Investigation of the Oscillatory Flow and Heat Release Fields and their Interaction in the Pulse Combustor

A. Performance Evaluation A limited number of measurements were carried out in modified, gas fired, valved, Helmholtz and Schmidt type pulse combustors in order to complement the performance studies carried out under a previous contract.

B. Shadow Visualization High speed shadowgraph cinematography was carried out parallel and normal to the axis of the combustor. These shadowgrams were then correlated in order to obtain a complete picture of the three-dimensional flow field in the pulse combustor.

C. Mixing Visualization An attempt was made to visualize mixing patterns photographically by heavily seeding one of the reactant flows and illuminating the combustor using an expanded laser sheet.

D. Spectroscopy Local and global heat release in the pulse combustor were determined by measuring the radical radiation emitted from the combustor. Instantaneous readings were ensemble averaged using the pressure signal as a clock. Planar spectroscopy using an intensified CCD camera resulted in local heat release measurements with excellent spatial and temporal resolution.

E. Laser Doppler Velocimetry Velocities were measured in the periodically varying, turbulent flow field at selected locations in the combustor. These velocities were then ensemble averaged which permitted the determination of mean velocities and turbulence intensities at various locations, at each instant during the cycle.

All Task I measurements were carried out in a pulse combustor whose mixing and combustion chambers were fitted with flat windows. The results from the different investigations outlined above were then correlated with each other and with the phase in the cycle at which they were obtained using the pressure oscillation as a clock. Such a coordination between the pressure, flow field and heat release measurements was

necessary to shed further light upon the fundamental processes which control the operation of the pulse combustor.

Task II: Admittance Measurements of Pulse Combustor Components

The acoustic admittances of various components and subsystems which make up a natural gas fired, valved, Helmholtz type, pulse combustor were measured using an impedance tube technique. These measurements yielded information on the frequency and amplitude dependances of the damping caused by the various pulse combustor subsystems. In addition, a methodology was developed which permits the designer to predict the damping in the pulse combustor from the acoustic properties of its component parts.

Task III: Reporting

As per contract agreement.

TECHNICAL PROGRESS AND RESULTS

Task I

Performance Evaluation:

This part of the study dealt with the investigation of the dependance of the performance of the pulse combustor upon the combustor geometry, the temperature in the combustion chamber and the relative duration and phase between the heat release and pressure oscillations.

Effect of the Combustor Geometry. The AGA based pulse combustor design consists of a small diameter mixing chamber attached to a larger diameter combustion chamber, see Fig. 1 . This introduces a step at the interface between the mixing and combustion chambers which has long been assumed to be critical for stabilizing the combustion process. This hypothesis was tested by constructing a pulse combustor with the same combustion chamber volume but without the step; i.e., a combustor whose mixing and combustion chamber diameters are equal. Tests revealed that the performance characteristics of the stepless pulse combustor are identical to those of the standard combustor. The combustion process in this type of pulse combustor is, therefore, not stabilized by the flow behind the backward facing step but by the complex interaction between the fuel and air jets in the mixing chamber.

Investigations under a previous contract have shown that the Helmholtz type pulse combustor fitted with a standard tailpipe (i.e.,183 cm long) operates well for equivalence ratios between 0.61 and 1.03. When the tailpipe of the Helmholtz combustor was extended to 366 cm the rich limit of operation increased to an equivalence ratio 1.43. On the other hand, when the tailpipe was shortened to 69 cm the lean limit of operation was lowered to an equivalence ratio of 0.56. For tailpipes shorter than 69 cm the air supply had to be significantly pressurized in order to maintain the pulsation. If the pressurization was reduced the combustor switched from a pulsating to a non-pulsating mode of operation. The reasons for the existence of the limits of operation mentioned above will be addressed later.

Effect of Temperature upon Combustor Performance. The temperature in the pulse combustor was increased by insulating its mixing and combustion chambers either externally or internally. When the combustor was externally insulated the temperature increased by approximately 30 ^{o}K. Nevertheless, the kinetics of the combustion process were noticeably affected. For example, the CO level in the exhaust increased by 15%. However, the amplitude of the pressure pulsations remained unchanged. More importantly, the addition of thermal insulation lowered the lean limit of operation from an equivalence ratio of 0.64 to 0.55. The rich limit of operation was not affected by the increase in temperature. This suggests that the lean limit of operation of the pulse combustor is, at least in part, kinetically controlled. A more detailed explanation of the reason for the existence of the rich limit will be given later.

The temperature in the pulse combustor was more significantly increased by insulating the combustor internally using high temperature ceramic padding. However, the acoustic losses caused by this insulating material significantly decreased the amplitude of the pulsations. Since the mass flow rates of the reactants through the flapper valves depend upon the pressure amplitudes, the operating range of the pulse combustor was decreased. In some cases it was necessary to increase the gap in the air flapper valve and/or to pressurize the air supply to maintain the pulsations. In addition, it was noted that the internal insulation decreased the frequency of the pulsations. An analytical model currently being developed under a new program does, indeed, predict a dependence of

the frequency of pulsation upon the rate of heat transfer to the walls of the combustor. More details of the effect of temperature upon the operating characteristics of the pulse combustor are given in Ref. 1.

Effect of Heat Release Duration and Timing. The effect of the relative timing between the heat release and pressure oscillations were investigated by changing the duration of the pressure cycle. Both the Helmholtz and a Schmidt tube pulse combustors were used in this investigation. The Schmidt (or quarter wave) pulse combustor used the same fuel and air injection system as the Helmholtz pulse combustor. However, the mixing chamber, the combustion chamber and the tail pipe were replaced by a single, constant diameter pipe.

Tests showed that lengthening of the tailpipe of the Helmholtz combustor caused a decrease in the pulsating frequency until a tailpipe length of 550 cm was reached. Then the operating frequency of the combustor "jumped" to the tailpipe's first harmonic, see Fig. 3a. If the tailpipe was further lengthened, the frequency continued to decrease. A similar trend was observed when the Schmidt pulse combustor was lengthened, as shown in Fig. 3b. It should be noted that a "jump" to the higher harmonic of the Helmholtz combustor's tailpipe and of the Schmidt pulse combustor causes a doubling and tripling of the frequencies, respectively. However, if the mixing of the reactants and, therefore, the heat release process was delayed with respect to the pressure oscillations this frequency jump could be avoided. Such a delay could be introduced by moving the fuel injection port 7.5 cm downstream of its normal location.

The above phenomena can be explained using Rayleigh's criterion which states that an oscillating heat release will drive pressure fluctuations if both are in phase. The timing and duration of the heat release due to the combustion process are determined by the injection of the reactants and their mixing. At relatively high frequencies (i.e., short cycle durations) the heat release is primarily in phase with the fundamental mode of the combustor, as is shown schematically in Fig. 4a. If the frequency of pulsations is decreased the cycle duration lengthens. The heat release is then confined to the early part of the fundamental pressure fluctuation (see Fig. 4b). However, the same figure also shows that the heat release is now more in phase with the first harmonic of the pressure oscillation. Therefore, it is this harmonic that is excited. Finally, if the combustion process is delayed the heat release is, once again, in phase with the fundamental pressure oscillation, see Fig. 4c. This causes the fundamental mode to be excited. This work is described in more detail in Refs. 1 and 2.

Finally, pressure amplitude measurements along the axis of the Schmidt pulse combustor indicated that as long as the air valve is in place this pulse combustor behaves like a true quarter wave tube, see Fig. 5. However, once the air valve is removed the standing wave pattern is closer to that characteristic of a Rijke tube. In that configuration the combustor is open at both ends, at the valve housing and at the downstream end, both of which are pressure nodes. Combustion takes place at approximately one quarter of the combustor length from the air inlet. Since in the Rijke tube the length of the combustor represents one

half of the acoustic wavelength, compared with one quarter of the wavelength in the Schmidt tube, the frequency of pulsations increases once the air valve is removed. This is discussed in more detail in Ref. 2.

Shadow Visualization

During a previous contract, the flow in the mixing chamber was visualized using high speed shadowgraphy through flat quartz walls at the end of the mixing chamber and the quartz transition between the combustion chamber and the tailpipe, see Fig 6. Briefly, a fast moving, highly turbulent fuel jet was seen to enter the mixing chamber followed by a wider, slower moving air jet, see Fig. 7. The air jet impinges upon the fuel jet at approximately the same instant at which the latter reaches the mixing chamber wall opposite the fuel port. The leading edge vortex of the air jet then rapidly "scoops up" the fuel and sets up two, counter rotating vortices in the mixing chamber. Combustion occurs under conditions of intense, small scale turbulence and is nearly completed when the fuel for the next cycle enters the mixing chamber. Some of these shadow visualizations were repeated under different operating conditions during the present contract period. These tests indicated that the entry of the air jet is delayed as the fuel - air ratio in the combustor is increased.

In addition, the axial flow field in the pulse combustor was visualized using high speed shadow photography through the flat quartz windows in the curved side walls of the mixing and combustion chambers, see Fig. 8. Particular attention was focused on the flow field in the mixing chamber and in the vicinity of the combustion chamber - tail pipe interface.

Since the air and fuel ports are located off axis, the flow field is not cylindrically symmetric. Once again, the high speed shadowgraphy showed that the fuel jet enters the mixing chamber shortly after the pressure there has passed through its maximum. Just before the pressure minimum is reached the air jet enters the mixing chamber. The addition of this air into the combustor increases the axial flow velocities further downstream in the mixing chamber. A little later, during the combustion phase of the cycle, a large, axial recirculation region forms in the mixing chamber. As the pressure maximum is reached the flow becomes axial again. Shortly thereafter, the new fuel jet enters and the cycle repeats itself.

High speed shadowgraphy was also carried out at the downstream end of the combustion chamber where the combustor connects with the tail pipe. As the pressure in the combustor decreases, combustion products from the tail pipe are seen to flow back into the combustion chamber. This backflow penetrates a distance of only two to three inches back into the combustor. As the acoustic pressure begins to rise again the flow reverses and reenters the tail pipe.

Mixing Visualization

Attempts were made to visualize the mixing process between the fuel and air as they enter the mixing chamber. For this purpose, the air jet was heavily seeded with micron sized titanium dioxide particles while the fuel jet was left unseeded. As the reactants entered the mixing chamber, slices through this chamber were illuminated using vertical sheets of light produced by expanding the beam from a five watt argon ion laser using a

cylindrical lens. The resulting light scattered by the particles in the flow was then recorded using a high speed camera capable of framing rates of up to 11,000 frames per second.

These visualization experiments were not very successful. In spite of mirror generated, multiple traverses by the laser sheet through the mixing chamber not enough light was scattered by the particles to mark the film at framing rates above 2,500 frames per second. At these framing rates it was difficult to freeze the fast moving flow. In addition, seed particles remaining in the mixing chamber from previous cycles tended to obscure the details of the mixing flow field of the newly entering reactants. It was, therefore, decided to abandon this part of the investigation, at least until a more powerful pulsed laser, such as a copper vapor becomes available at this laboratory.

Spectroscopy

This investigation makes use of the fact that the intensity of spontaneously emitted CH, CC or OH radiation has been shown to be a measure of the local reaction rate. Under a previous contract the temporal oscillations of the overall reaction rate in the combustor were compared with those of the pressure. It was shown that the global radiation from the combustor fluctuates with the same frequency as the combustor pressure. The heat release fluctuations lead those of the pressure by a phase angle which decreases as the equivalence ratio in the combustor is increased. As predicted by Rayleigh's criterion, this leads to an increase in sound pressure level in the combustor when the equivalence ratio is

increased. At the same time it was shown that the combustion process never stops entirely during the cycle.

Under the present contract these experiments were extended to cover spatially as well as temporally resolved radiation measurements. A newly acquired intensified imaging system was used in these experiments. The radiation from the combustor is allowed to pass through a quartz window in the combustor wall before being focused through an interference filter onto an image intensifier. The intensifier is connected via an optical fiber bundle to the face plate of an 128 x 128 pixel CCD array. The array is read by an Omnicomp frame grabber and the data are transfered to the memory of a MicroVAX II workstation. The workstation is equipped with a 200 Mbite disk and a tape drive. The image intensifier can be gated which results in exposure times down to 50 nanoseconds, faster than necessary to freeze the fast, highly turbulent flow in the combustor. Images can be read and transfered at a rate of 200 frames per second from the array to the computer. In addition, up to four channels of scalars can be recorded simultaneously with the images. In these studies, the acoustic pressure signal was recorded and used to identify the instant during the cycle at which the image was obtained.

Once the images have been obtained they can be manipulated using a wide range of software. Images can be sorted, added, subtracted and averaged, contrasts can be enhanced and contour maps can be plotted using false colors. Furthermore, the intensities recorded by selected, individual pixels during consecutive frames can be plotted versus time. The frequency of any oscillations in these signals can be determined by

Fourier analysis and the phase angle between the fluctuations in the pixel intensities and the pressure signal can be calculated. This allows the determination of the local driving of the pulsations by the combustion process using Rayleigh's criterion.

Local radical radiation and, therefore, heat release rates in the combustor were measured by imaging CC radiation through the flat quartz window at the upstream end of the mixing chamber. Images obtained at the same instants during consecutive cycles indicate that while the overall features of the flame shape are very similar at given instants during the cycle, the precise path over which the flame has spread varies somewhat from cycle to cycle. Figure 9 shows four frames which indicate the locations of the ignition and flame spread during one cycle in the pulse combustor. Each "frame" actually represents the average of 128 separate images obtained at the same phase during different cycles. The mechanism of flame spread is best illustrated by comparing the instantaneous flow fields and heat release distributions in Fig. 9. Early in the cycle (Fig. 9a), as the fuel jet enters the mixing chamber, it begins to react weakly with the air left over from the previous cycle. Main ignition of the new fuel occurs at the time and location where the fuel jet impinges upon the opposite wall, as shown in Fig. 9b. At that instant the new air jet has just reached the center of the mixing chamber. Shortly thereafter, the upper part of the leading mushroom vortex of the air jet entrains the reacting fuel which intensifies the combustion process and spreads it throughout the upper part of the mixing chamber(Fig. 9c). Only after a pair of counter-rotating vortices have established themselves does

the flame spread throughout the entire mixing chamber, as shown in Fig. 9d.

In order to quantify the flame spread in the mixing chamber, software was developed which permits the calculation of the phase angle between the maximum heat release rate at every location and the maximum pressure. The distribution of these phase angles then gives an indication of the instantaneous shape of the flame and of its spread through the combustor. Figure 10 shows a contour plot obtained using this technique. The numbers indicate the phase by which the local heat release leads the pressure. The flame, thus, spreads from the upper left hand side of the mixing chamber, opposite the fuel port, towards the lower left hand side and, finally, towards the right hand side of the mixing chamber into the region between the fuel and air ports.

These results indicate that, for the present valve configuration, it is essential that the fuel enter the mixing chamber prior to the air jet. Otherwise the momentum of the air jet would prevent the fuel jet from penetrating significantly into the mixing chamber. This would result in poor mixing of the fuel and air. At the same time, a different fuel and air port configuration or dual fuel inlets would, probably, result in a quicker, more uniform distribution of the combustion process in the mixing chamber. The results of these heat release measurements are discussed further in Refs. 3 and 4.

Laser Doppler Velocimetry

Velocity measurements in the mixing chamber were carried out using a two component LDV system based on a five watt argon ion laser. The results of the flow visualization experiments had indicated that reverse flow exists in the mixing chamber. Therefore, Bragg cells were incorporated into both components of the system. Because the flow in the combustor is periodic, mean flow velocities and turbulence intensities at different instances during the cycle had to be determined using conditional sampling. This was achieved by detecting the start of each cycle which was taken to be the positive zero crossing of the pressure signal. Each cycle was then divided into 60 equal time intervals based upon the previously obtained operational frequency of the combustor. Finally, the data were sorted into the relevant bins according to their time of arrival during the cycle. Ensemble averaged mean and RMS velocities were, thus, obtained at 60 equi-spaced instances during the cycle.

Early tests of the performance of the LDV indicated that the system and its data reduction software produced reproducible mean velocities which were in good agreement with quantitative observations from the flow visualization, see Ref. 5. However, the apparent level of turbulence, as measured by the RMS value of the conditionally sampled velocities, was considerably higher than that observed in other turbulent flows, (e.g. in the turbulent shear layer behind a backward facing step). It is important to realize that it is possible that only a part of this RMS may be due to true turbulence. Since the values of the velocity fluctuations were obtained by ensemble averaging, they may contain contributions due to 1) the finite width of the slots into which each cycle was divided; 2) the

slight variations in the flow field from cycle to cycle; and 3) slight variations in the combustor frequency during the experiment. In order to eliminate at least the effect of variations in the operating frequency of the combustor the data reduction software was modified. In the updated data reduction routine the pulse duration for each cycle was determined from the actual pressure oscillations measured during the experiment rather than from a previously determined mean frequency.

Typical spatially and temporally resolved mean velocity and turbulence intensity data in the axial (u) and vertical (v) directions are shown in Figs. 11 through 29. Figure 11 shows the locations at which these LDV data were obtained. All measurement points lie in a plane which bisects the right angle between the fuel and air injection ports, equi-spaced along lines which are normal to the axis of the combustor. Each measurement location is labeled (m,n) where m represents the number of the line counting from the flat end of the mixing chamber and n denotes the point number on this line counting from the curved wall of the chamber opposite to the fuel and air ports.

Each of the velocity and turbulence intensity figures represents one cycle starting at the negative zero crossing of the pressure signal; i.e., at an instant after the fuel has started to enter but before the air has entered the mixing chamber. Figures 12 through 23 represent velocity and turbulence intensity traces at each of the ten points along one measurement line; i.e., along a given value of m. In order to avoid having ten data traces superimposed upon each other each of these figures consists of three plots one of which also shows the pressure signal for

reference. Figures 24 through 29 show a different representation of the same data which is more qualitative but conveys a better physical picture of the variation of the complex flow field in the mixing chamber during a cycle. These are three - dimensional "carpet plots" in which one axis represents the location of the measurement station along a given measurement line, the second axis represents the normalized time (i.e., 0 to 1 for one cycle) and the third axis shows either the u or v components of the velocity. This results in two carpet plots (one for u and one for v) for each value of m.

Figures 24, 25 and 26 show the carpet plots of the vertical velocities for the three measurement lines closest to the closed, upstream end of the mixing chamber. These are best analyzed in conjunction with the instantaneous velocity vs. time plots in Figs. 12, 13 and 14. Large positive (upward) velocity peaks are seen early in the cycle along all three lines. At m = 3, which lies in the paths of the fuel and air jets, (Fig. 26) the maximum occurs very early in the cycle, near the center of the mixing chamber (n = 4 to 7). Further upstream, at m = 1 and 2 (Figs 24 and 25), the peaks occur later, and are confined to locations n = 9 and 10, which lie close to the curved mixing chamber wall between the fuel and air ports. Immediately following the peak at m = 3 and coincident with the peaks at m = 1 and 2, deep, wide and wide valleys (downward velocities) are seen near the center of all three measurement lines. The early peak at m = 3 is caused by the entry of the fuel jet which results in an upward component of velocity. The valley observed later in the cycle is due to the downward component of the velocity of the entering air jet. Since the positive peaks along m = 1 and 2 occur at the same instant in the cycle as the valley they

must be due to the leading edge vortex of the air jet observed in the flow visualization. Later in the cycle the flow near the wall opposite to the inlet ports is generally upward while that near the ports is directed downward. This suggests the existence of a large vortex in the plane normal to the axis of the combustor.

The time dependence of the instantaneous axial velocities and their carpet plots at the same locations are shown in Figs. 15 through 17 and 27 through 29, respectively. Early in the cycle, when the fuel jet enters the mixing chamber, a significant downstream velocity directed towards the combustion chamber is observed. These positive velocity peaks are particularly large along lines m = 2 and 3 (Figs. 16 and 17), where the effect of the fuel jet is felt most strongly. It is also confined to the area near the curved mixing chamber wall opposite the injection ports. This wall deflects the incoming jet. In addition, the initial combustion process and the associated expansion of the combustion products are concentrated in this area. Shortly thereafter, the air jet enters the mixing chamber. It has very little effect upon the axial velocities along the line m = 3 which coincides with the centerline of the jet. However, at locations m = 1 and 2 large valleys representing upstream velocities can be seen. These are formed by the leading edge vortex of the incoming air jet which has an upstream component of velocity. After this vortex has passed, a small upstream velocity continues to be observed. This flow causes the acoustic pressure in the mixing chamber to increase. As the acoustic pressure approaches its maximum the flow reverses direction and the combustion products exhaust towards the combustion chamber for the remainder of the cycle.

The instantaneous turbulence intensities for all measurement lines are plotted versus phase in the cycle in Figs. 18 through 23. Early in the cycle the turbulence levels at all locations are relatively low. At the central locations (n = 3,4,5 and 6) along the lines m = 2 and 3, which lie directly in the path of the fuel jet, the turbulence intensity increases as soon as this jet enters the mixing chamber. At all other locations the turbulence intensity does not significantly increase until the entry of the air jet is detected in the mean velocities. The turbulence levels then remain elevated for part of the cycle and then slowly drop to their initial values.

These LDV measurements are presently continuing as part of the Ph.D. thesis work of the graduate student responsible for this work. Velocity measurements in the mixing chamber will be completed and velocity measurements at the combustion chamber - tailpipe interface will be added. The complete set of velocity results will then be submitted for publication to a suitable journal and as a "Topical Report" to GRI.

Rich Limit of Pulse Combustor Operation

As mentioned in the section dealing with performance measurements, the Helmholtz type pulse combustor fitted with the standard, 163 cm long tail pipe has a rich limit of operation at an equivalence ratio of 1.03. This limit exists even though the pulse combustor appears to be operating near its optimal condition immediately before this limit is reached. This operational limit can, however, be extended if the tail pipe is lengthened; i.e., the period of the pulsations is prolonged, or if the combustion air is supplied under pressure. Based

upon the results of the measurements discussed above, the following mechanism appears to control this rich limit.

In order to attain pulse combustion, the driving of the pulsations by the combustion process must overcome the acoustic damping due to, for example, viscous dissipation and acoustic radiation from the combustor. A limit of operation of the pulse combustor occurs if this balance between the driving and damping processes fails to materialize. According to Rayleigh's criterion, the driving by the combustion process can be quantified by the Rayleigh efficiency η which is defined by

$$\eta = \frac{R}{C_p \bar{P} \bar{Q}} \int_0^1 P' Q \, d\tau \approx \frac{|P||Q| \cos \theta}{C_p \bar{P} \bar{Q}}$$

where P and Q are the total pressure and combustion heat release rate, θ is the phase angle between the pressure and the heat release rate oscillations, R and Cp are the ideal gas constant and the specific heat at constant pressure, respectively, and τ is the time normalized by the duration of one cycle. Bars, primes and brackets represent the steady state, oscillating components and amplitudes of the indicated quantities, respectively.

Figure 30 shows the variation of the Rayleigh efficiency of the combustor fitted with a standard tailpipe and an extended tailpipe as a function of equivalence ratio, ϕ. The maximum ϕ at which each curve stops represent the rich limit of operation for each configuration. Clearly, near the lean limit the driving is small, just enough to overcome the damping

in the system. In contrast, near the rich limit for the combustor fitted with a standard tailpipe the driving is close to its maximum. Thus, the mechanism which controls this rich limit appears fundamentally different from that which is responsible for the lean limit.

The Rayleigh efficiencies presented in Fig. 30 were calculated from the measured fluctuations of pressure and heat release and the phase angle between them. The dependences of these three variables upon the equivalence ratio in the combustor are shown in Figs. 31 and 32. The amplitudes of both, the pressure and heat release fluctuations reach their maxima near stoichometric conditions. The phase angle by which the heat release leads the pressure, on the other hand, decreases with increasing equivalence ratio until it asymptotically reaches a constant value which depends upon the length of the tailpipe.

In order to understand the combustor behavior described above, it is helpful to consider the relative phases of the pressure and radiation oscillations and the instants of fuel and air injection. Figure 33 shows one normalized period of oscillation for both rich and lean operating conditions. The arrows indicate the instants at which fuel and air jets enter the mixing chamber. Horizontal lines at the top of the figure indicate those parts of the cycle when the combustion products move away from or towards the mixing chamber where most of the combustion process occurs. Finally, the points marked "X" indicate the instants at which the new fuel charges reignite, as indicated by the increase in the radiation signal. All this information is based upon the high speed shadowgrams, pressure and CC radiation measurements described above.

Figure 33 indicates that for lean operation the new fuel ignites before the new air enters the mixing chamber. This is possible since there is air left over from the previous cycle. As the equivalence ratio is increased, less air is available from the previous cycle and ignition is delayed until, under stoichometric conditions, ignition of the fuel jet must await the entry of the air jet. Since the oscillations of heat release always lead those of pressure, the phase angle between the two decreases as the equivalence ratio is decreased, see Fig. 32. Since with decreasing phase angle the pressure and heat release fluctuations are more in phase, the Rayleigh criterion causes the pressure amplitudes in the combustor increase with increasing equivalence ratio, as observed in Fig. 31.

The rich limit of operation can now be explained with the aid of Fig. 33. The time available for the reactants to mix and burn is limited to the time interval between the instants when the new fuel charge ignites and when the reaction is quenched by the combustion products returning from the combustion chamber to the mixing chamber. If ignition is delayed this time interval is too short and not enough heat is released to drive the pulsations. This occurs at the rich limit.

When the duration of the cycle is prolonged by extending the tailpipe the time available for combustion is increased and the rich limit is significantly extended. A similar result is obtained if ignition of the new fuel is advanced by forcing the air to enter earlier or if mixing is improved by injecting the air jet under pressure. Conversely, delaying the entry of the air jet by, for example, extending the pipe which connects the air valve to the mixing chamber reduced the rich limit to an equivalence

ratio of less than one. A more detailed description of this part of the work is given in Refs. 6 and 7.

Task II

In this task, the impedance tube technique was used to measure the admittances (i.e., the complex ratio between the acoustic velocity and pressure) of different pulse combustor components. The admittance is a complex quantity which describes the acoustic behavior of the system. As discussed later, the magnitude of the real part of the admittance describes whether the system drives or damps the acoustic pressure oscillations. All components which make up the pulse combustor damp the pressure oscillations in the absence of combustion. Therefore, the measured, real part of the admittance of the cold combustor provides an indication of how much driving the combustion process will have to provide to assure pulse operation.

In the impedance tube set-up, the investigated component is attached to one end of a long tube, see Fig. 34. An electro-pneumatic, acoustic driver is attached to the wall just upstream of the opposite, open end of the tube. The acoustic driver is used to excite an incident acoustic wave which moves towards the tested component. The interaction of this wave with the investigated sample produces a reflected wave with modified amplitude and phase. The incident and reflected waves combine to establish a standing wave in the impedance tube. A piezo-electric pressure transducer mounted near the tested sample measures the acoustic pressure amplitude at the upstream end of the tube. A second

pressure transducer, mounted at the end of a long rod, is translated inside the tube to measure the axial variation of the standing wave pressure amplitude along the impedance tube.

When measuring the admittance of a hard termination (i.e., zero admittance), the incident wave is reflected without a change in amplitude or a shift in phase. In this case, the combination of incident and reflected waves produces a standing wave with a zero-amplitude pressure minimum located one quarter of the wavelength ($\lambda/4$) from the hard termination, see Fig. 35a. On the other hand, if the complex admittance of the termination is non-zero, see Fig. 35b, the minimum pressure amplitude is non-zero and it occurs at a location other than $\lambda/4$ from the tested sample. Physically, the termination changes the pressure amplitude of the reflected wave and introduces an apparent change in the length of the pipe by introducing a phase shift in the reflection process. The measured values of P_{max}, P_{min} and the distance of P_{min} from the tested sample can be used to determine the real and imaginary parts of the admittance of the termination and, thus, of the component under investigation. A more detailed analysis shows that the real part of the admittance, which is calculated from the difference between the maximum and minimum pressure amplitudes (i.e., $P_{max} - P_{min}$) determines the damping (or driving) provided by the component under investigation. On the other hand, the imaginary part of the admittance provides information which affects the frequency of the system which utilizes the tested component.

The above described technique was used to measure the real and imaginary parts of the admittances of different pulse combustor components under cold and "hot" operating conditions. Admittance measurements under cold conditions were completed as part of this project. The system was also prepared for measurements with combustion under the present program but most actual measurements were carried out under a new contract.

The admittances were measured under cold flow conditions for the following configurations: (1) a hard termination at the end of the impedance tube; (2) the gas valve and its decoupler at the end of the tube; (3) the air valve at the end of the tube; (4) the mixing chamber fitted with the air valve only; and (5) the mixing chamber fitted with both the fuel and the air valves. The air valve opening was varied between 0 and .018 inches for configurations 3, 4 and 5. In these tests the acoustic driver was set to generate sound pressure levels of approximately 160 dB near the tested component. This corresponds to typical dB levels in pulse combustors. Furthermore, the driving frequencies were varied between 20 and 170 Hz. In addition, the admittance of the air flapper valve and of the entire pulse combustor including valves, mixing and combustion cambers were measured as a function of amplitude. All tests were carried out at mean pressures in the impedance tube equal to the previously determined boost pressure in the pulse combustor.

Before presenting the obtained results, it would be helpful to consider Fig. 36. It shows the dependence of the real part of the admittance upon ΔP (i.e., $P_{max} - P_{min}$). Clearly, when the magnitude of

the real part of the admittance (i.e., Y_r) is small, the value of Y_r is relatively insensitive to the accuracy of the measurement of ΔP. However, as the magnitude of Y_r increases, the sensitivity of the Y_r to the measured ΔP increases rapidly. Thus, the error in the determined Y_r increases with increasing value Y_r. In addition, while the real part of the admittance depends largely upon the value of ΔP, the value of the imaginary part of the admittance is primarily determined by the location of P_{min}. Since the standing pressure wave has a relatively flat minimum, especially at low frequencies, it was easier to determine the value of the minimum than its location. The real parts of the admittances were, therefore, measured with better accuracy than their imaginary parts.

The real parts of the admittances for the above configurations with the air valve (when included) closed and open (to .012 inches) measured over a 20 to 170 Hz frequency range are shown in Fig. 37. An air valve opening of .012 inches was selected since it corresponds to a typical setting for the pulse combustor under normal operating conditions. Both, the hard termination and the fuel flapper valve with its decoupling chamber showed no damping over the entire range of investigated frequencies (i.e., $Y_r = 0$). This indicates that the fuel valve orifice behaves, essentially, like a solid surface.

For all of the tested configurations which contain an air flapper valve Y_r is essentially zero at low frequencies as long as the air valve is closed. As the frequency is increased, Y_r and, thus, the damping by the air valve and its housing increases until it becomes quite significant at high

frequencies. The real part of the admittance is increased even further if the closed air valve is attached via an elbow to the mixing chamber. On the other hand, adding the fuel valve to the mixing chamber - air valve assembly has no significant effect upon the admittance at any investigated frequency. This provides further indication that the fuel valve behaves like a solid surface.

Figure 37 also shows that opening the air valve substantially increases the real part of the admittance over the entire range of investigated frequencies. Once again, the effect of attaching the air valve housing to the side of the mixing chamber is significantly greater than adding the fuel valve to the mixing chamber - air valve assembly. The increase in the real part of the admittance with increasing air valve opening is illustrated in more detail in Fig. 38 for a range of valve openings and driving frequencies for the mixing chamber fitted with both valves.

The variation of the measured imaginary part of the admittance (i.e., Y_i) for these configurations over the 20 to 170 Hz frequency range are shown in Fig. 39. Once again, Y_i is zero for the hard termination as well as for the fuel valve only. However, once the closed air valve was added to any of the three investigated configurations the imaginary part of the admittance increased substantially. The latter effect increased with increasing frequency. This occurred because adding the valve assembly moves the termination, in the form of the valve plates, further away from the end of the impedance tube, see Fig. 40. The minimum of the standing pressure wave in the impedance tube was, therefore, moved upstream

resulting in an increase in Y_j. Because of the size of the mixing chamber and the elbow that connects the air valve to it, this effect is more pronounced for the valve - mixing chamber assembly than for the air valve alone.

Once the air valve is opened the pressure anti-node moves away from the valve plates towards the driver end of the impedance tube, see Fig. 40. (If the valve plates are completely removed the resulting open end corresponds to a pressure node). This causes the decrease in the magnitude of Y_j observed in Fig. 39. Because of the above discussed difficulty in determining the precise location of the minimum of the standing pressure wave, no clear difference between the imaginary part of the impedance of the air valve only and that of the valve - mixing chamber assembly could be established. However, Fig. 41 clearly shows that the magnitude of Y_j decreases as the opening of the air valve increases. This effect is particularly pronounced at higher frequencies. The lack of smoothness of the curves is, once again, due to the difficulty in determining the precise location of the flat minimum of the standing wave.

Additional admittance measurements were carried out in which either the mixing chamber with its valves or the entire combustor consisting of mixing and combustion chambers and the flapper valves were attached to the impedance tube. In these tests, the admittances were measured as a function of applied sound pressure level for a given air valve opening. Figure 42 shows that for the mixing chamber assembly only the damping decreases with increasing sound pressure level. Since it

has been shown that the only significant acoustic losses in the mixing chamber assembly occur in the air flapper valve it can be concluded that it is the damping in the air valve that decreases with increasing acoustic excitation. However, the damping of the entire combustor (including the combustion chamber) increases with increased applied sound pressure level, as shown in Fig. 42. This suggests that the damping in the Helmholtz volume formed by the combustion chamber overshadows the effect of the damping in the air flapper valve for this pulse combustor configuration.

In addition to the above detailed measurements an analytical scheme was developed which permits the determination of the admittance of the entire mixing chamber - valve assembly from the measured admittances of its component parts. As shown in Fig. 43, the assembly was divided into five sections. The admittance at location "1" was calculated from that of the solid wall ($\bar{Y} = 0$) which closes the upstream end of the mixing chamber using a transfer function. The admittance at "2" was determined from the measured admittance values of the valve. The admittance at "3" was taken to be zero since the fuel valve had been shown to behave like a solid surface. The acoustic mass conservation equation was then applied to the control volume bounded by interfaces 1,2,3 and 4 to calculate the admittance at "4" from the admittances at the other interfaces. Finally, the admittance at "5" was calculated from that at "4" using a transfer function. Details of these calculations are given in Ref. 8. The results of these calculations for different valve openings and over a range of frequencies are compared with the experimentally measured values of the real and imaginary parts of the admittance of the mixing chamber - valve assembly in Figs. 44 and 45. Clearly, the agreement is excellent.

At the end of this contract the impedance tube set up was modified to accommodate tests with combustion. Because of heat transfer to the impedance tube wall a temperature gradient existed along the axis of the impedance tube. A measurement technique was developed to determine the temperature gradient using thermocouples and the classical impedance tube theory was modified to account for it. The actual measurement of the driving by the unsteady combustion process was initiated and completed under a new contract.

Task III

Apart from the semiannual and annual reports specified in the contract, the following papers were presented and published during the contract period. They are listed in the order in which they are referenced in the above text:

1. "Dependence of Pulse Combustion Performance upon Interior Temperature, Acoustic Losses and Combustion Time", X.C. Cheng, B.R. Daniel, J.I. Jagoda and B.T. Zinn, International Gas Research Conference, Tokyo, Japan, November, 1989.
2. "Dependence of Pulse Combustor Frequency upon Combustion Process Timing", X.C. Cheng, B.R. Daniel, J.I. Jagoda and B.T. Zinn, Twelfth Annual Energy Sources Technology Conference and Exhibition, Fossil Fuels Combustion Symposium, PD-Vol. 25, pp 39-42, Houston, TX, January, 1989.
3. "Radiation Measurements in a Gas Fired Pulse Combustor", S.H. Ku, X.C. Cheng, B.R, Daniel and B.T. Zinn, Proceedings of the Spring Technical

Meeting, Central States Section of The Combustion Institute, Chicago, IL, May, 1987.

4. "The Interaction between Fluid Mechanics and Combustion in a Helmholtz Type Pulse Combustor", J.M. Tang, B.R. Daniel, J.I. Jagoda and B.T. Zinn, Fall Technical Meeting, Eastern Section of The Combustion Institute, Orlando, FL, December, 1990.
5. "Frequency Modeling and Velocity Measurements in Gas Fired, Valved Pulse Combustors", Fall Technical Meeting, Eastern Section of The Combustion Institute, Clearwater Beach, FL, December, 1988.
6. "Flame Spread and Limits of Operation of Gas Fired, Mechanically Valved Pulse Combustor", S.H. Ku, B.R. Daniel, J.I. Jagoda and B.T. Zinn, Poster at the Twenty-Second Symposium (International) on Combustion, Seattle, WA, August, 1988.
7. "Controlling the Rich Limit of Operation of Pulse Combustors", J.M. Tang, S.H. Ku, B.R. Daniel, J.I. Jagoda and B.T. Zinn, Twenty-Third Symposium (International) on Combustion, Orleans, France, August 1990, (in print).
8. "The Acoustic Characteristics of Pulse Combustor Flapper Valves and Mixing Chambers", D. Xu, B.R. Daniel, J.I. Jagoda and B.T. Zinn, Thirteenth Annual Energy Sources Technology Conference and Exhibition, Fossil Fuel Combustion Symposium, PD-Vol. 30, pp 21-28, New Orleans, LA, January, 1990.

CONCLUSIONS

The physical mechanisms which control the performance of a natural gas fired, valved Helmholtz type pulse combustor were investigated. Comparison of flow and flame spread visualization indicated that the fuel

jet enters the mixing chamber ahead of the air jet. Under lean operating conditions the fuel begins to react as soon as it enters the combustor. Main ignition occurs once the fuel is scooped up by the leading edge vortex of the air jet. Combustion then spreads by the convection of this vortex throughout the mixing chamber. It is this complex interaction between the fuel and air jets entering the mixing chamber which stabilizes the combustion process. The lean limit of operation of the pulse combustor could be extended by reducing the heat losses to the combustor walls while its rich limit was increased by reducing the pulsation frequency or supplying the combustion air under pressure. The rich limit of operation near stoichometric conditions exists because of the limited time available for combustion during the cycle if no air from the previous cycle is available for early ignition. In addition to the visualization experiments the flow field is currently being quantified by laser Doppler velocimetry.

Under a separate task the acoustic characteristics of the air flapper valve were determined by an impedance tube technique. In addition, an analytical scheme was developed which allows the determination of the admittance of entire sections of a pulse combustor from the measured admittances of its component parts.

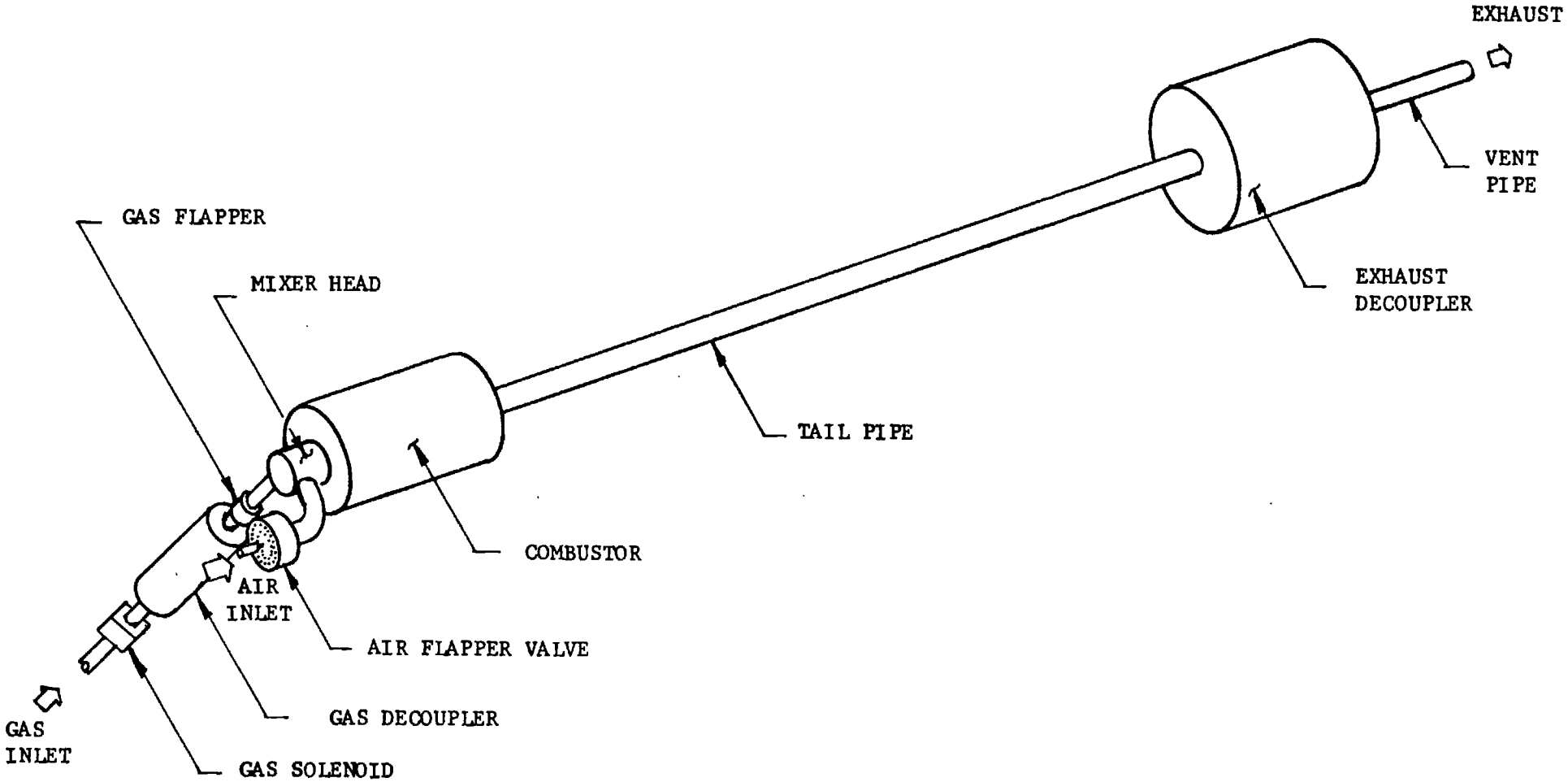

Fig. 1 Schematic of the Helmholtz Type Pulse Combustor

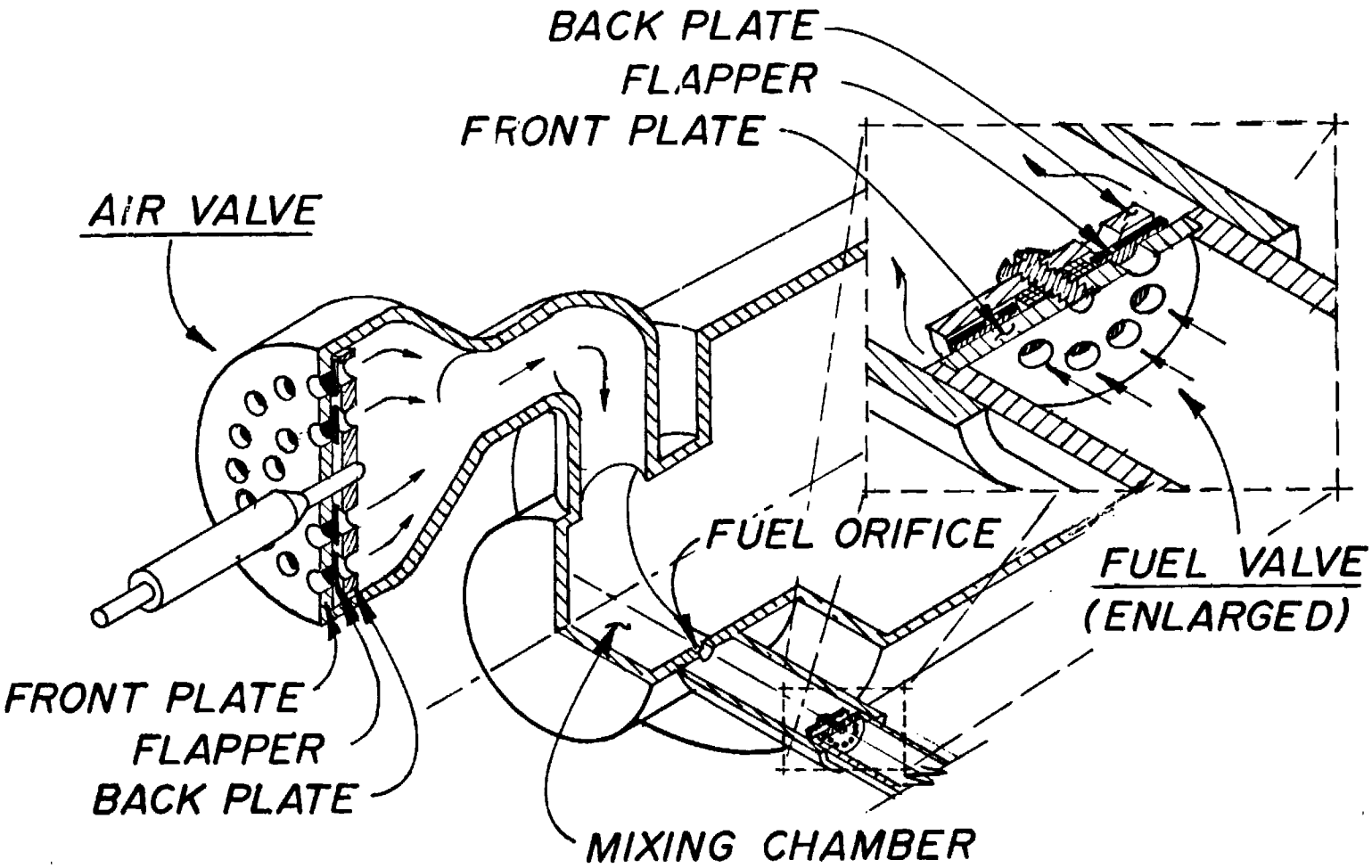

Fig. 2 Schematic of the Mixing Chamber Showing the Fuel and Air Flapper Valves

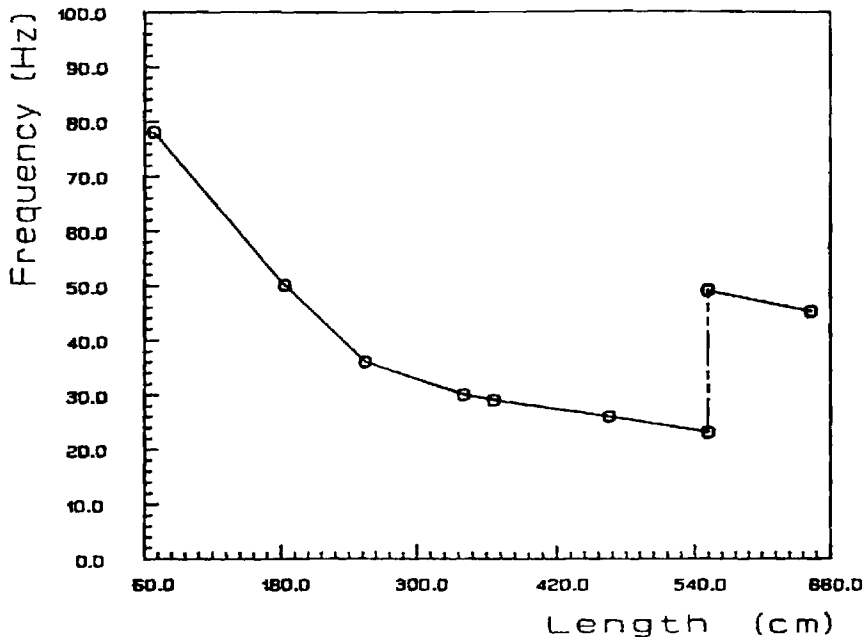

a

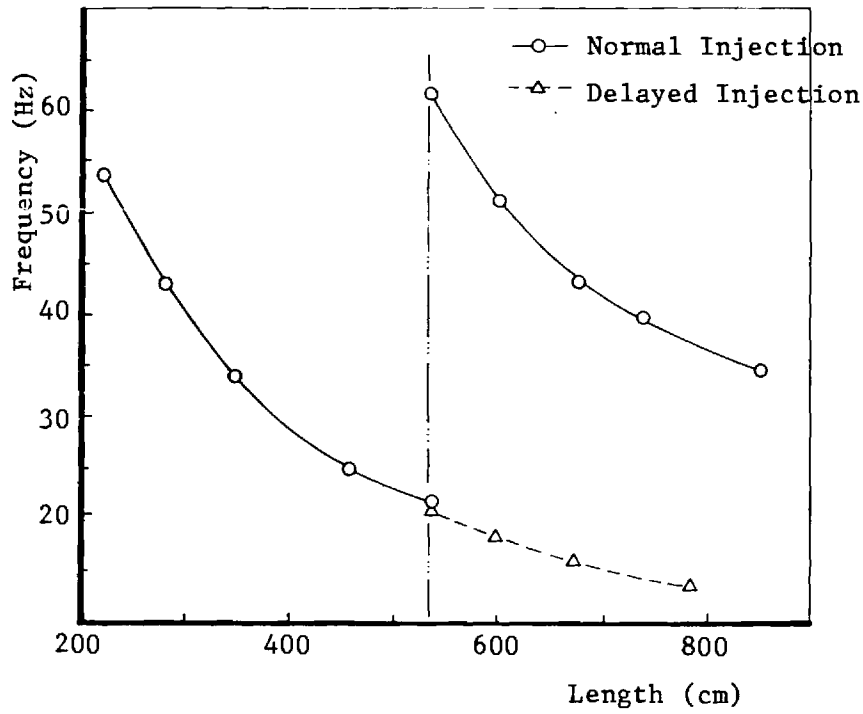

b

Fig. 3 Operational Frequency of the a) Helmhotz and b) Schmidt Combustors as a Function of Tailpipe or Combustor Length Respectively.

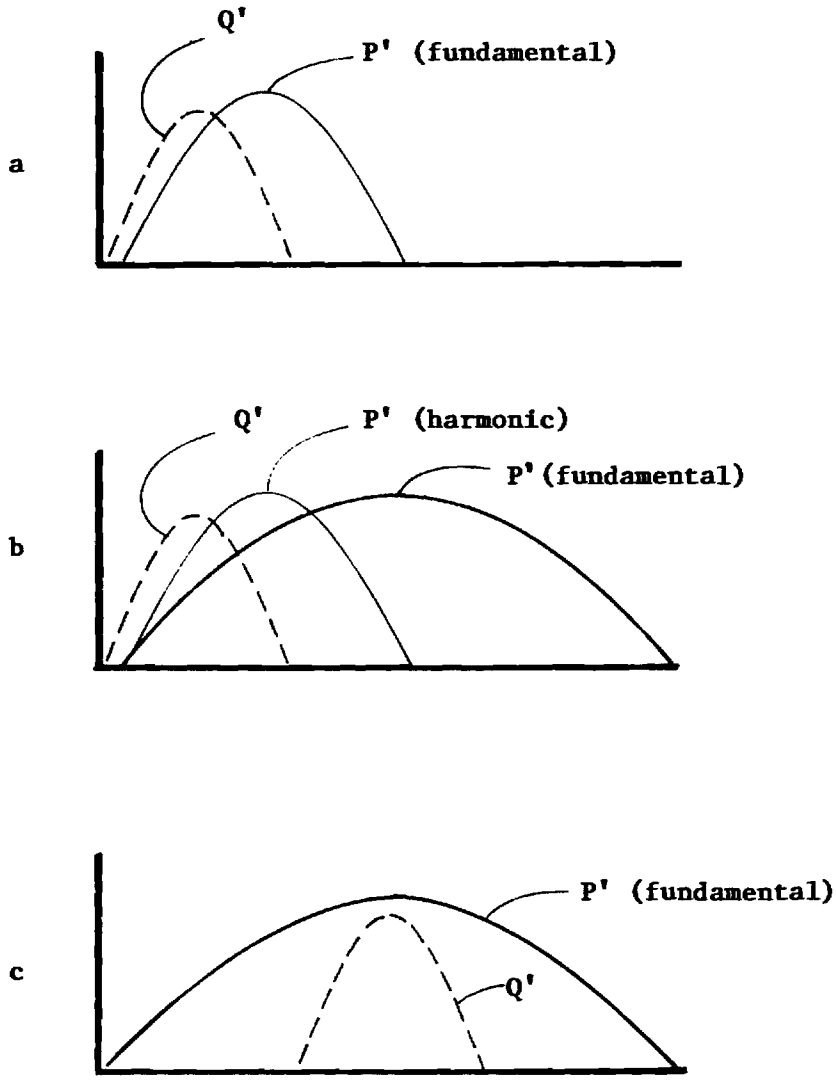

Fig. 4 Schematic of Relative Timing of Heat Release (Q') and Pressure (P') Oscillations for a) High Frequencies, b) Low Frequencies with Standard Fuel Injection and c) Low Frequencies with Displaced Fuel Injection Leading to Delayed Heat Release.

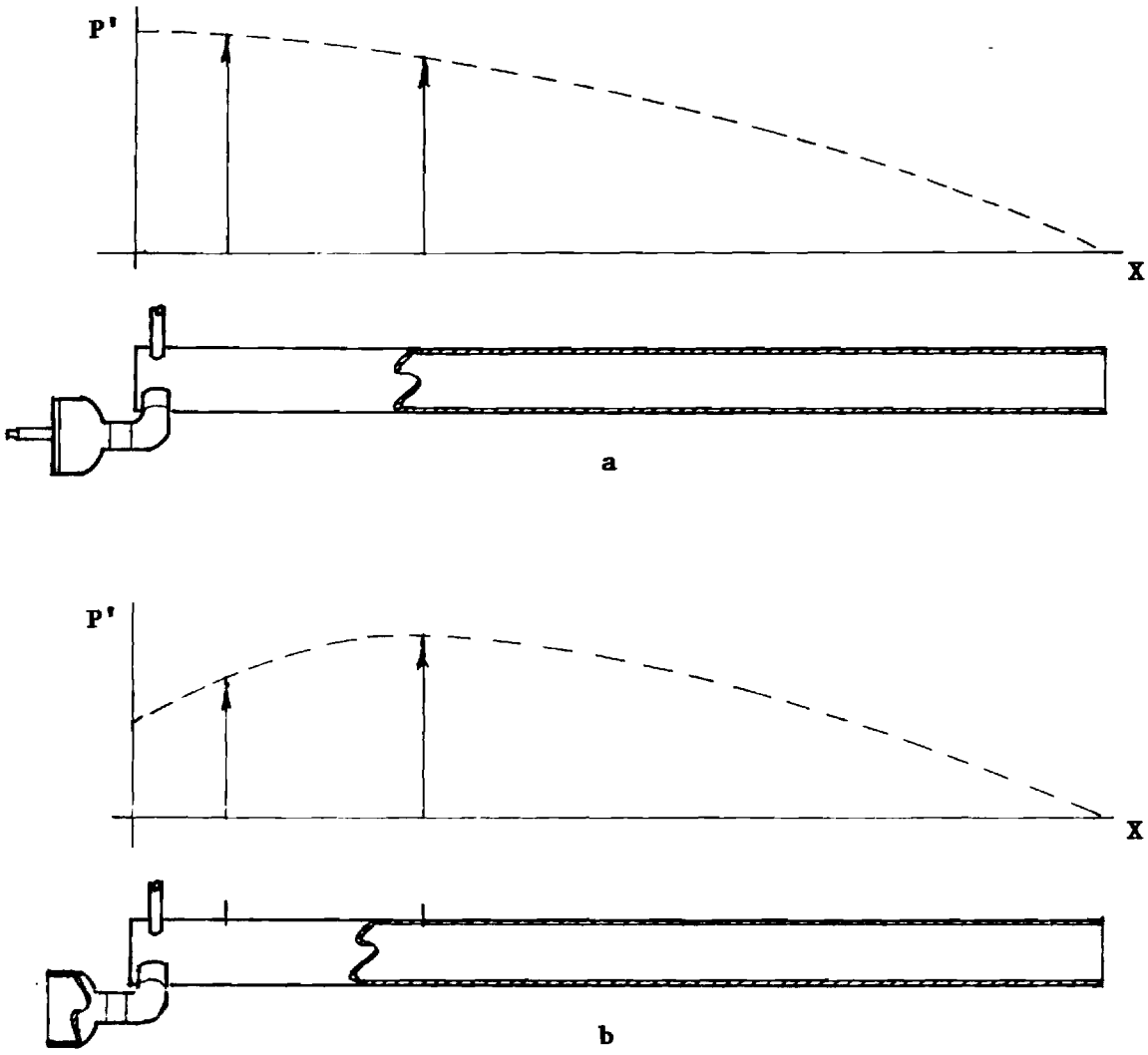

Fig. 5 Standing Wave Pattern along Schmidt Combustor a) with Air Valve and b) without Air Valve.

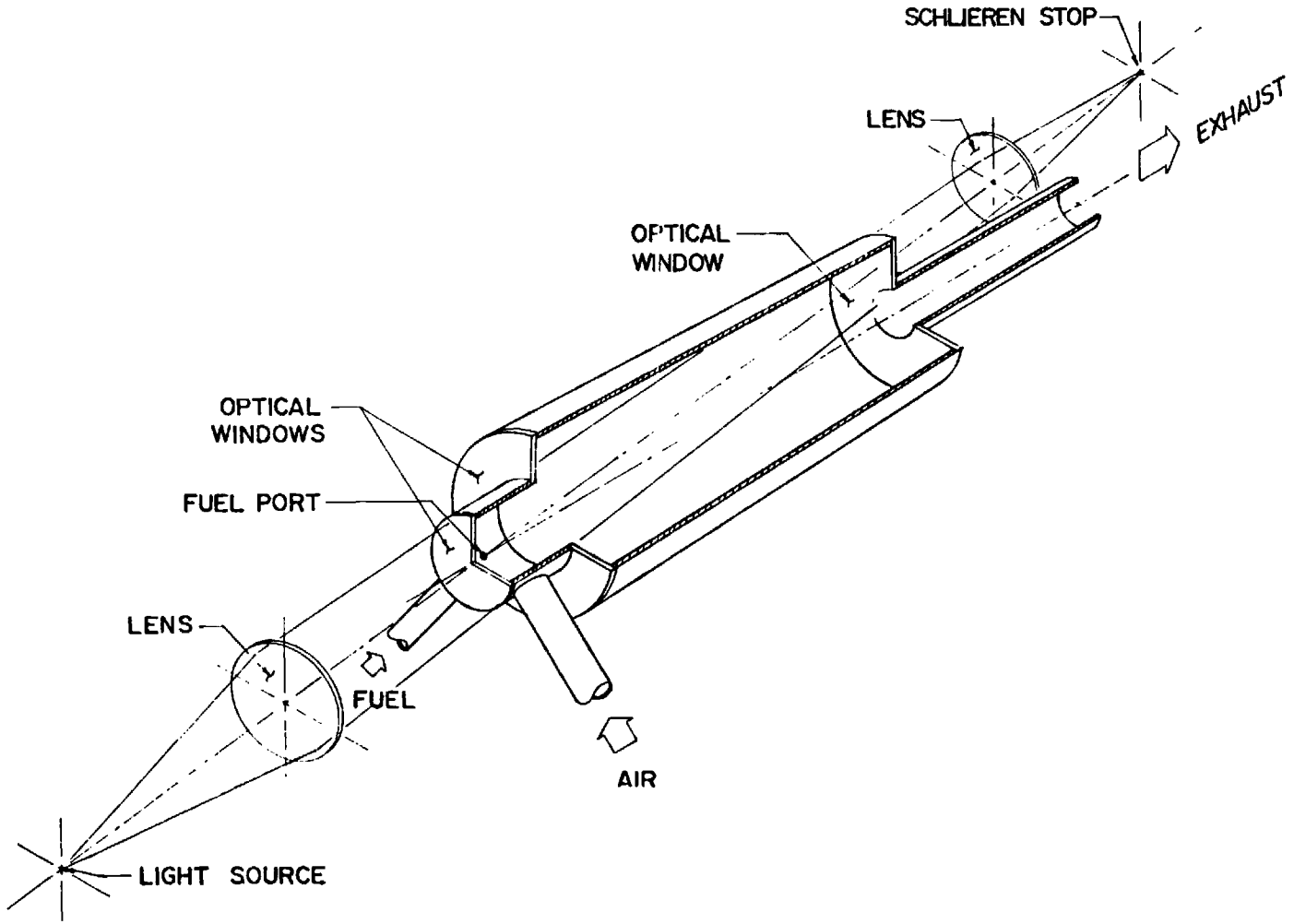

Fig. 6 Schematic of the Schlieren Set-up along the Combustor Axis

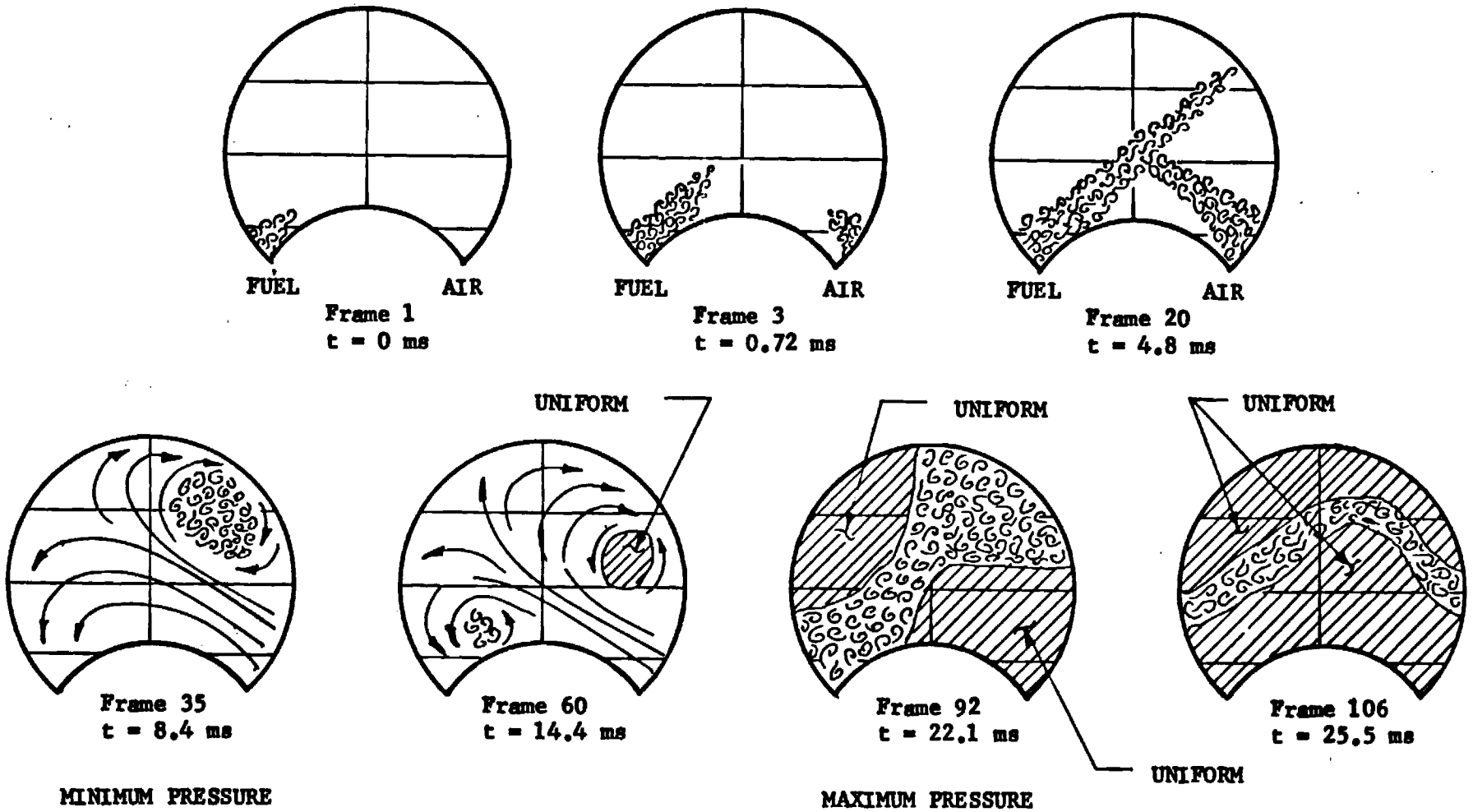

Fig. 7 Schematic of Selected Frames from the High Speed Shadow Movie Showing the Flow Field at Different Instances during the Cycle as Seen along the Combustor Axis

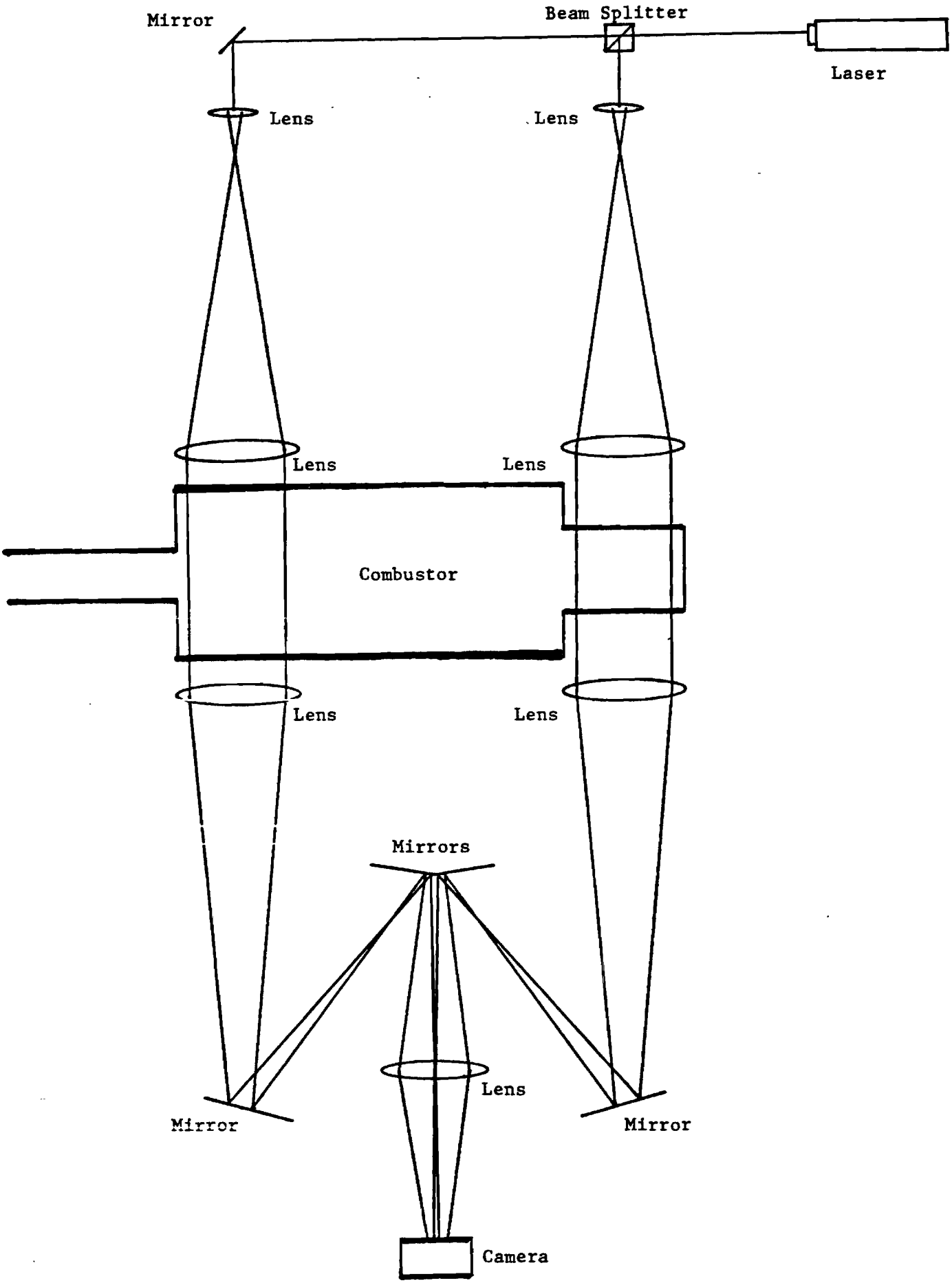

Fig. 8 Schematic of the Schlieren Set-up normal to the Combustor Axis

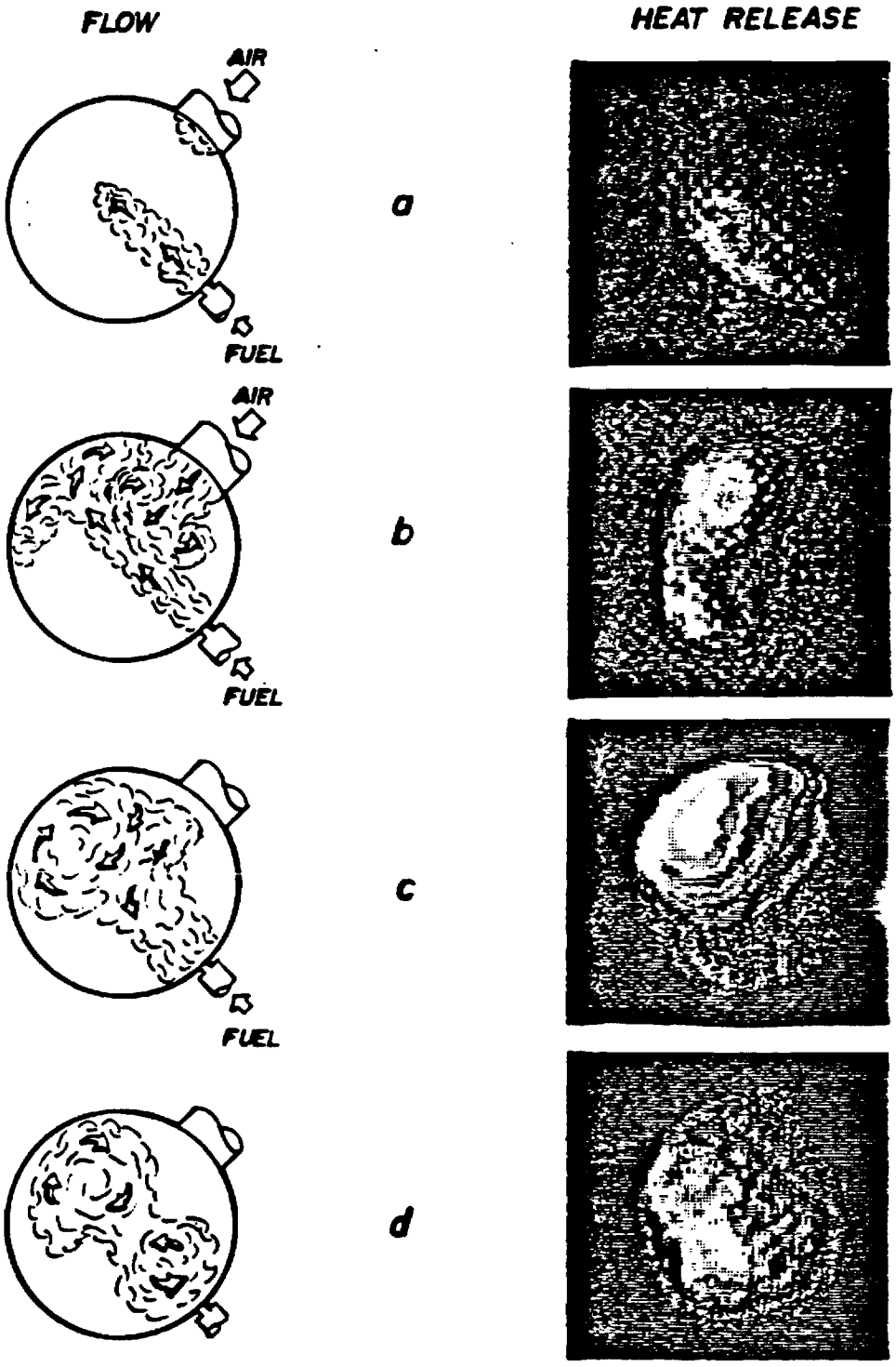

Fig. 9 Comparison of the Flow Field and the Heat Release Distribution as Seen along the Combustor Axis at Four Instants during the Cycle.

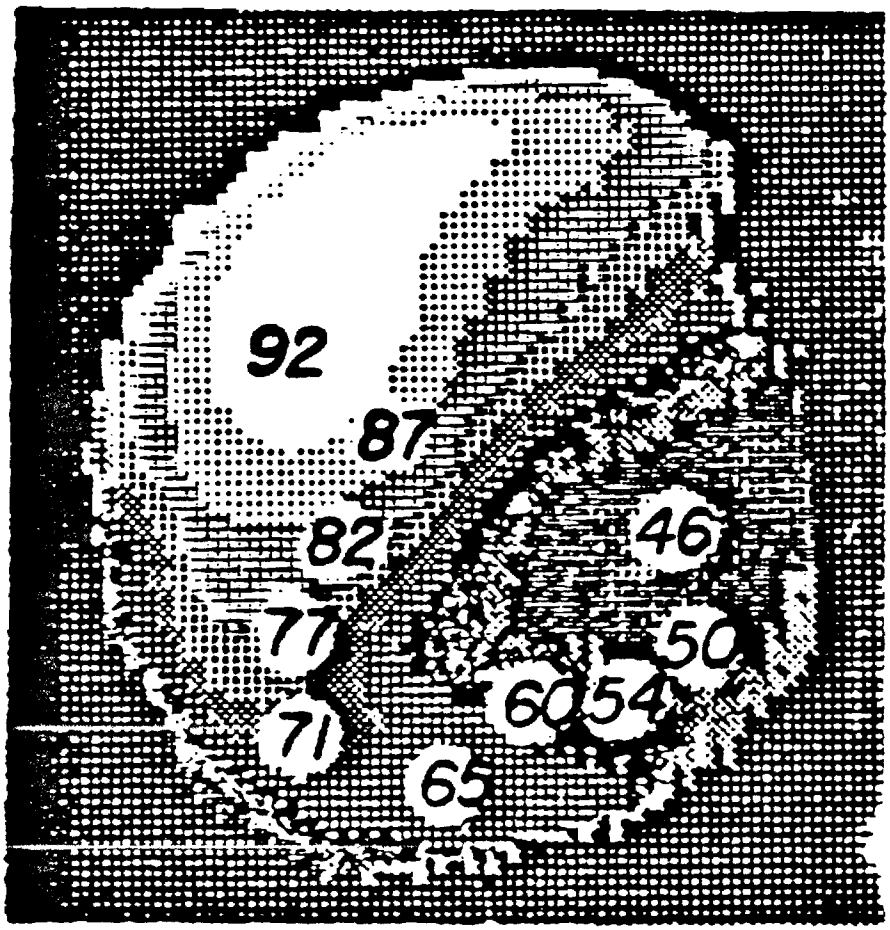

Fig. 10 Contour Plot of Phase Angle by which the Heat Release Oscillations Lead the Pressure Oscillations.

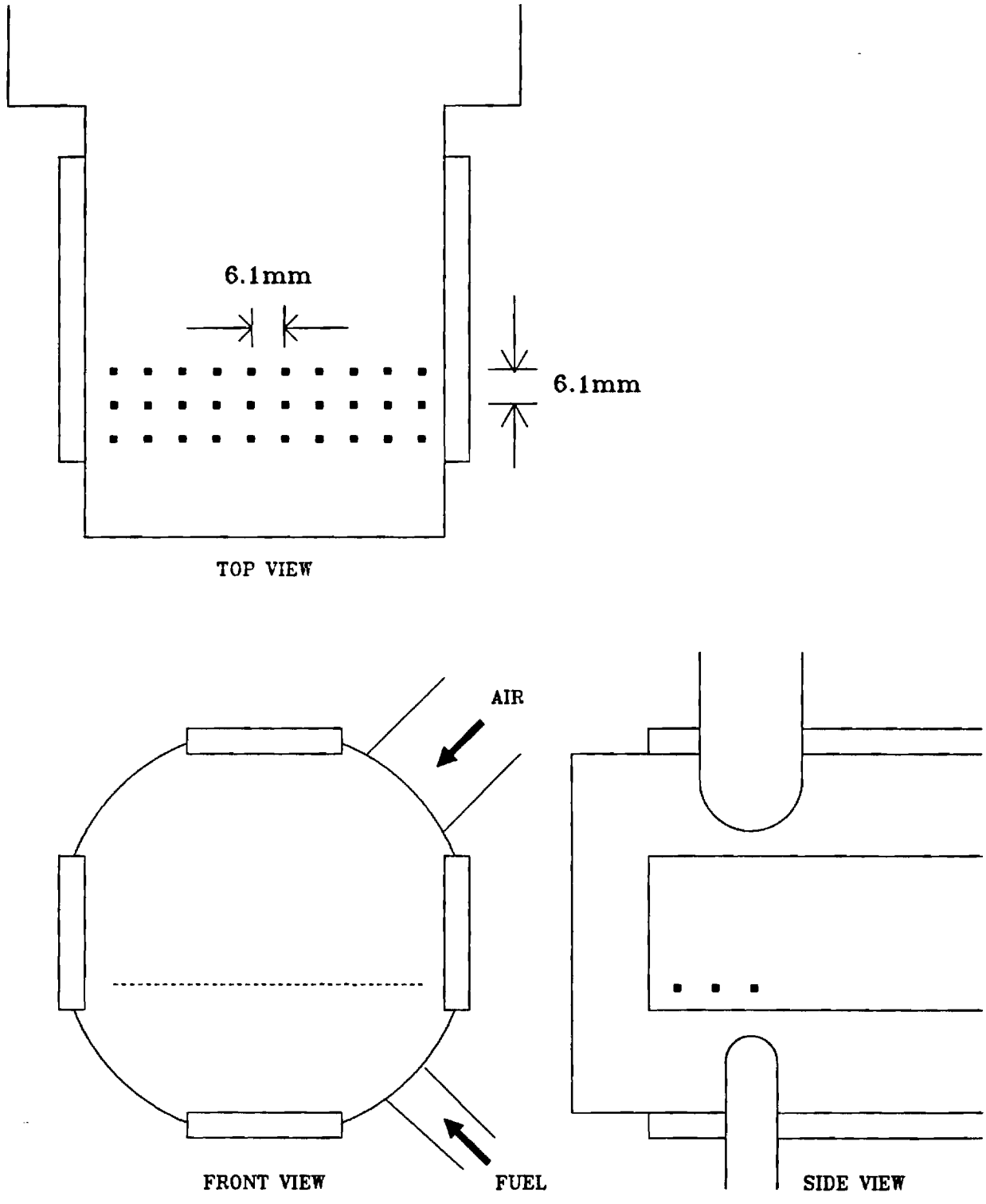

Fig. 11 Locations at which the Laser Doppler Velocimeter Results Shown in Figures 12 through 29 were Obtained. Each Location is Labeled (m,n).

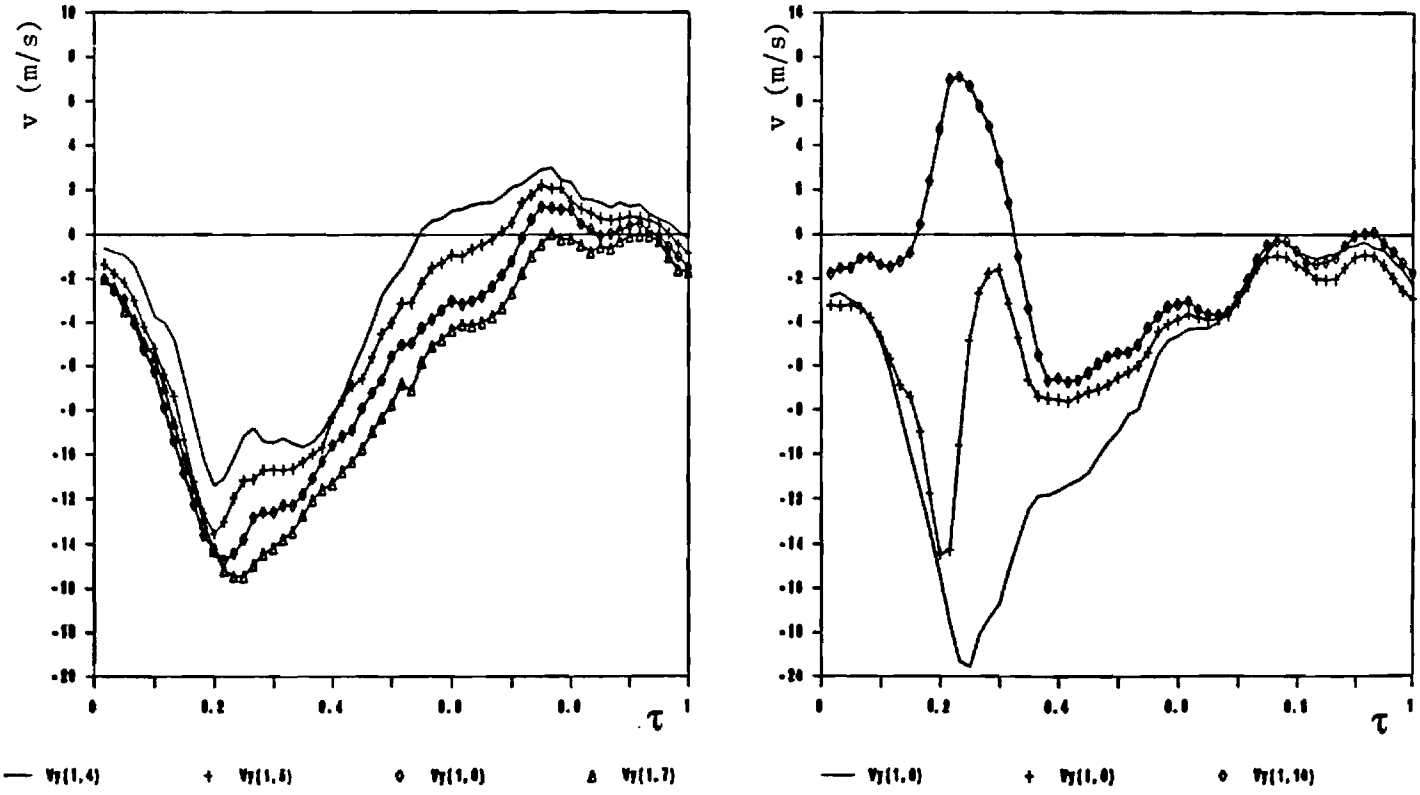

Fig. 12 Variation of the Vertical Mean Velocity During a Cycle for Locations along the Line m = 1. The Top Plot includes the Pressure Trace for Reference.

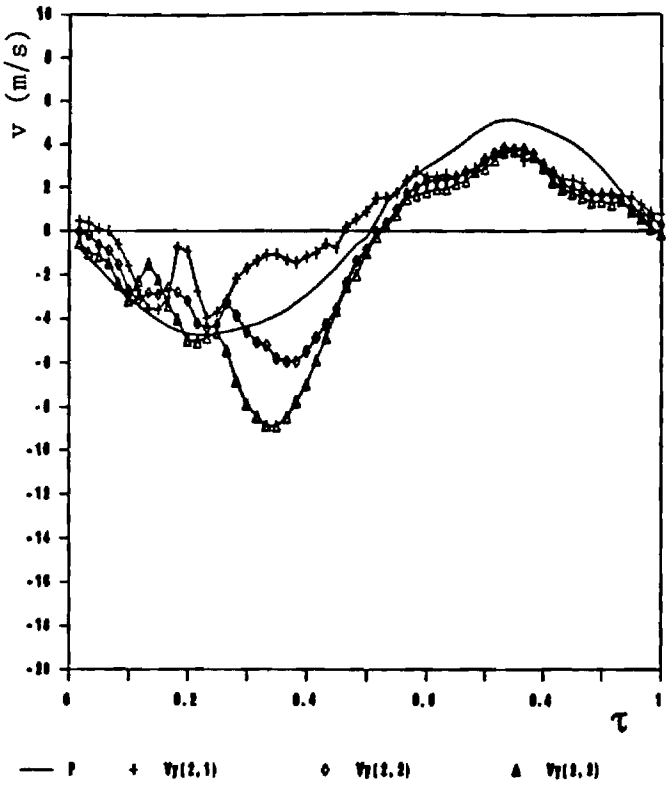

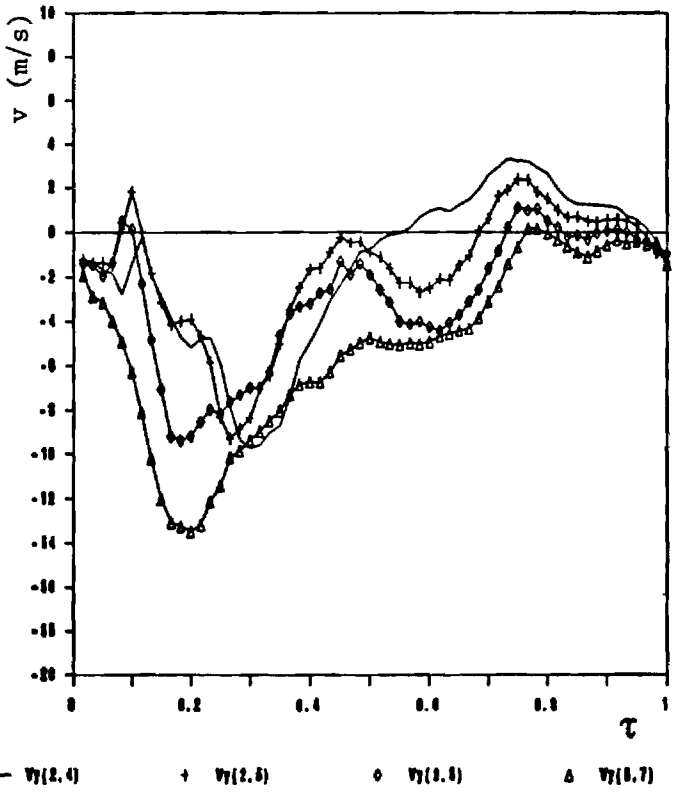

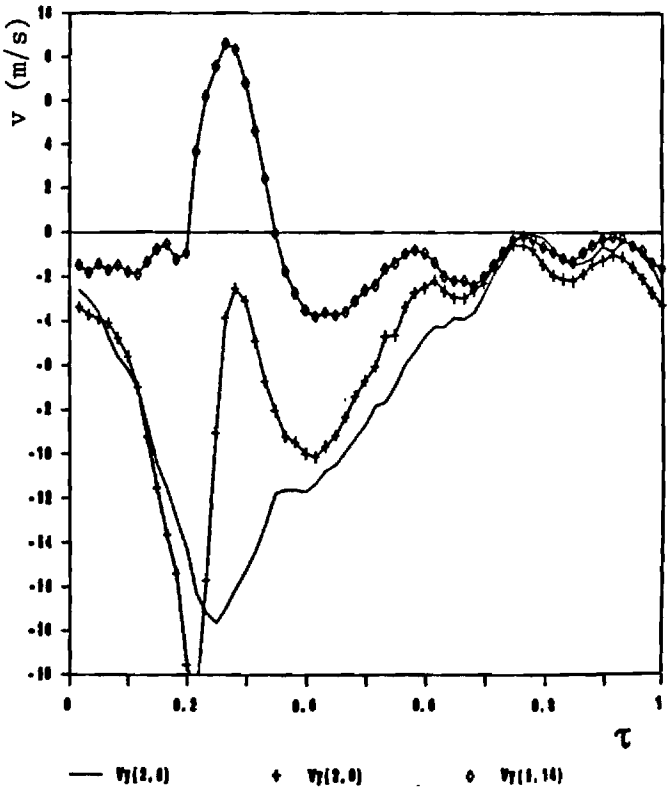

Fig. 13 Variation of the Vertical Mean Velocity During a Cycle for Locations along the Line m = 2. The Top Plot includes the Pressure Trace for Reference.

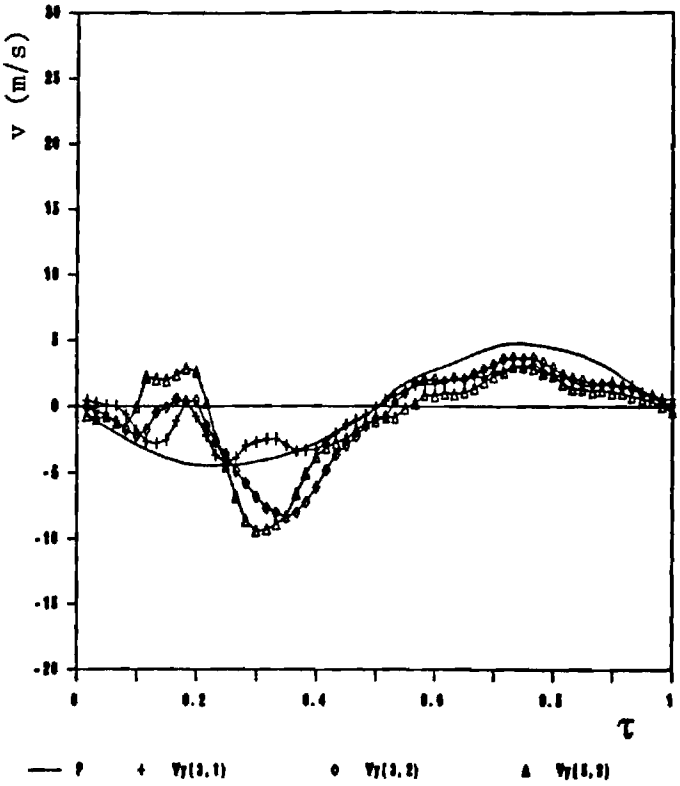

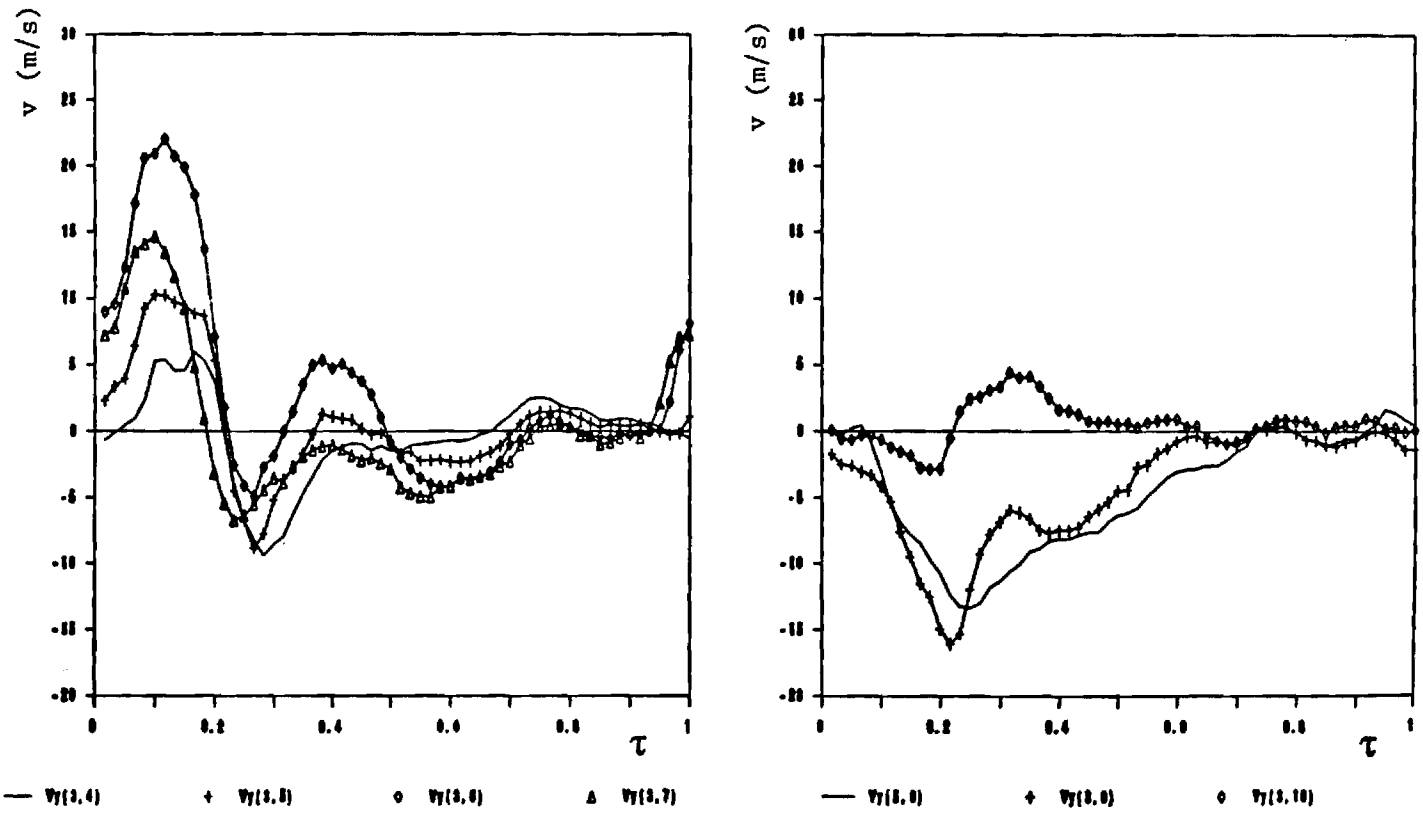

Fig. 14 Variation of the Vertical Mean Velocity During a Cycle for Locations along the Line m = 3. The Top Plot includes the Pressure Trace for Reference.

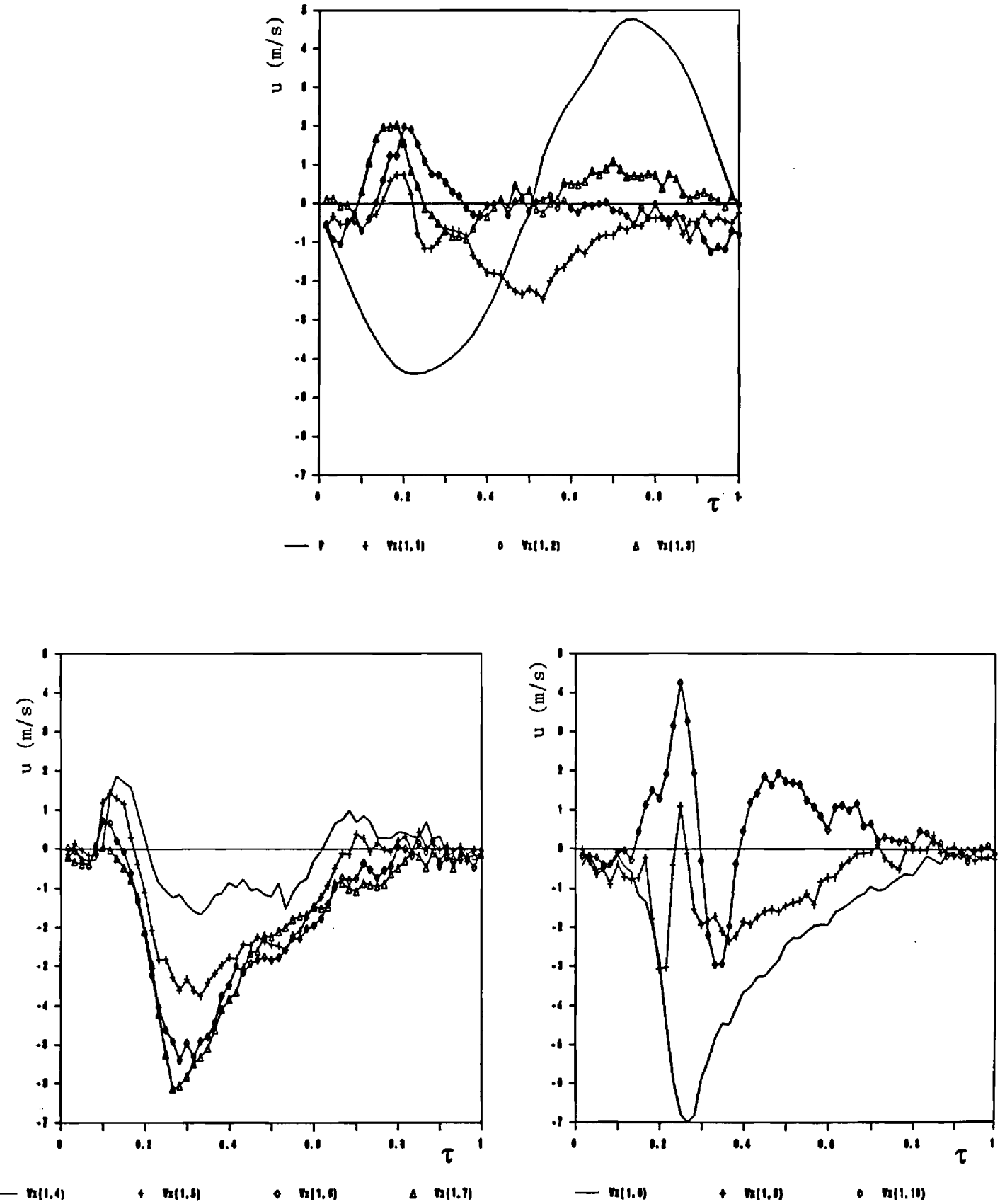

Fig. 15 Variation of the Axial Mean Velocity During a Cycle for Locations along the Line m = 1. The Top Plot includes the Pressure Trace for Reference.

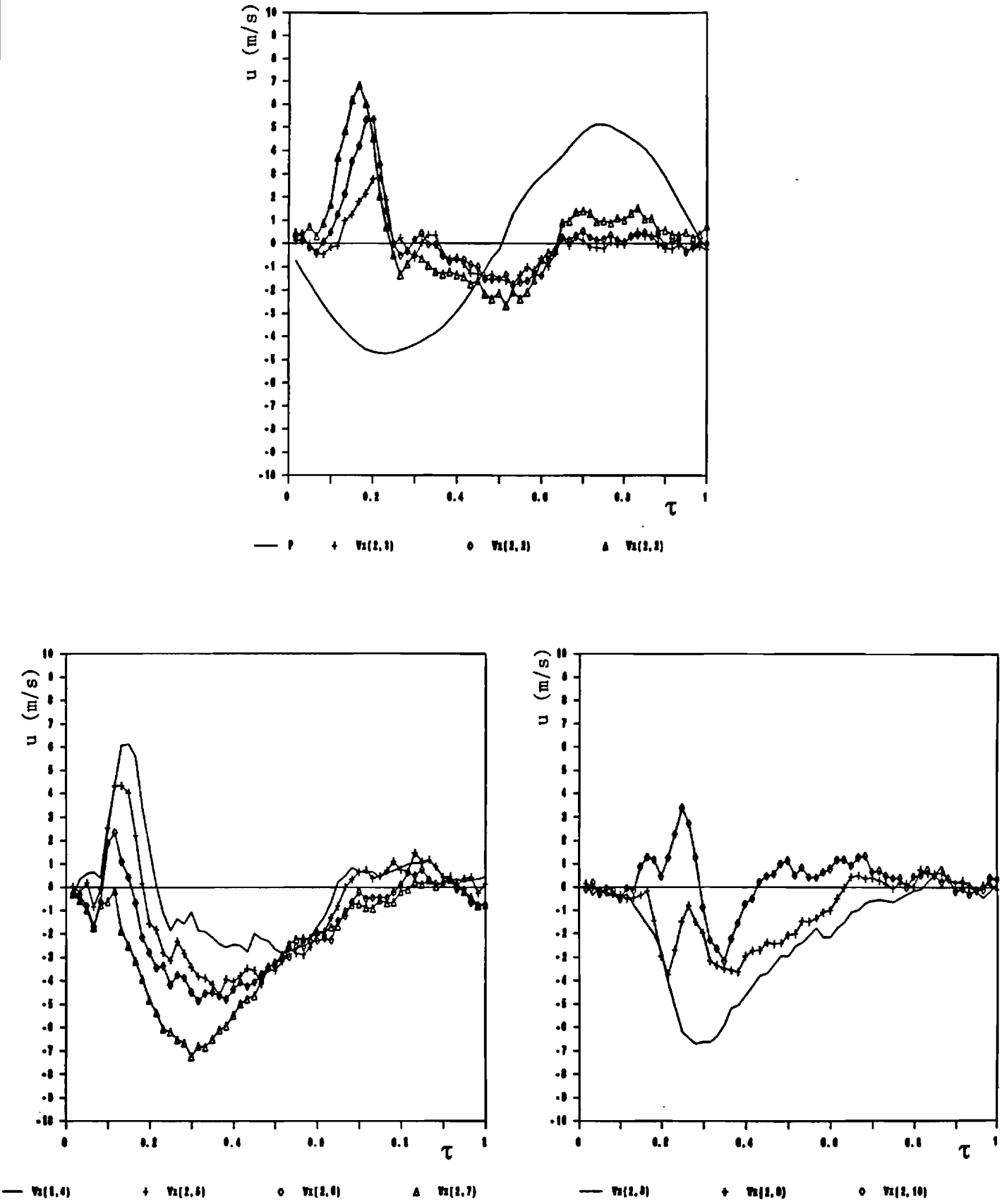

Fig. 16 Variation of the Axial Mean Velocity During a Cycle for Locations along the Line m = 2. The Top Plot includes the Pressure Trace for Reference.

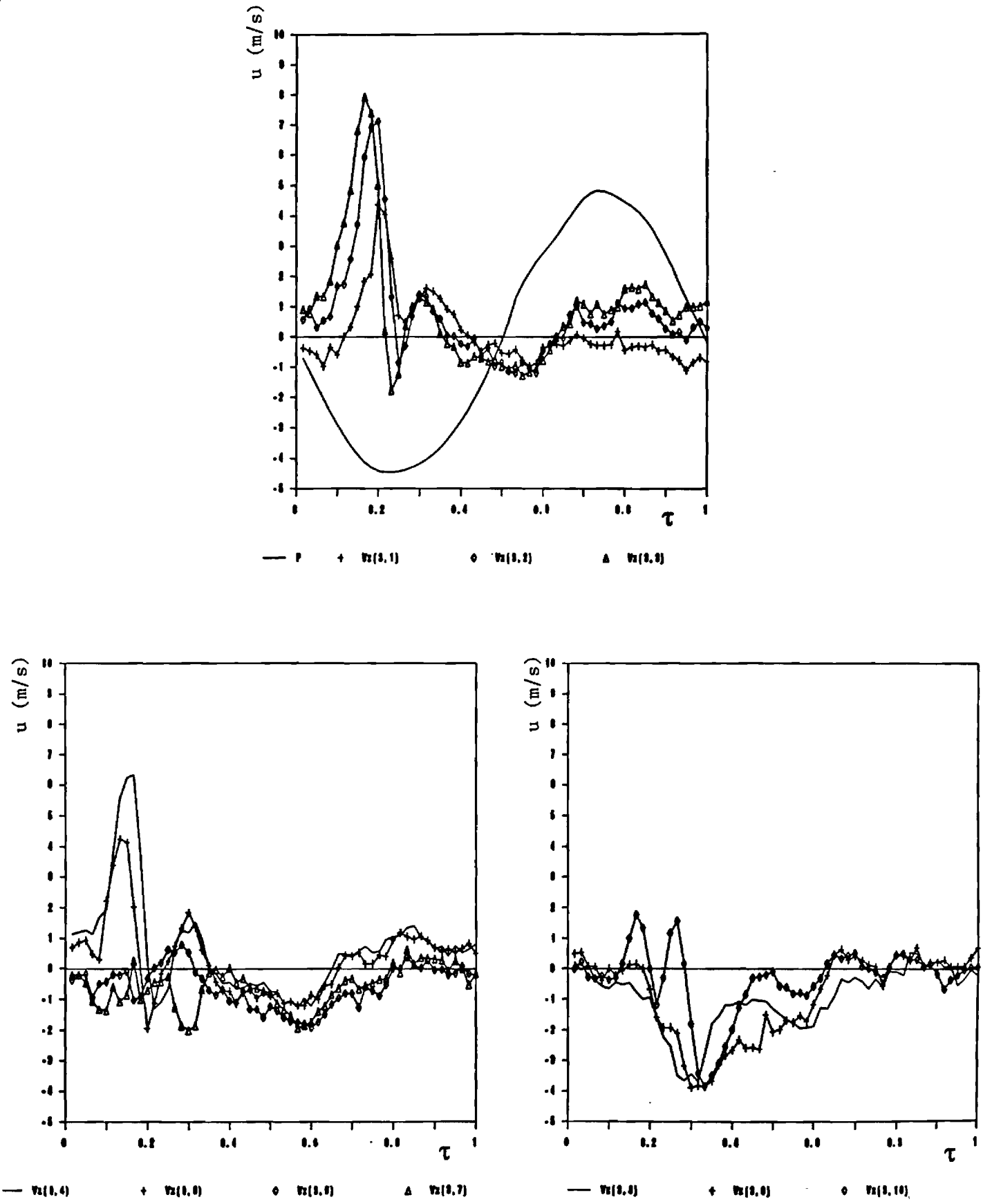

Fig. 17 Variation of the Axial Mean Velocity During a Cycle for Locations along the Line m = 3. The Top Plot includes the Pressure Trace for Reference.

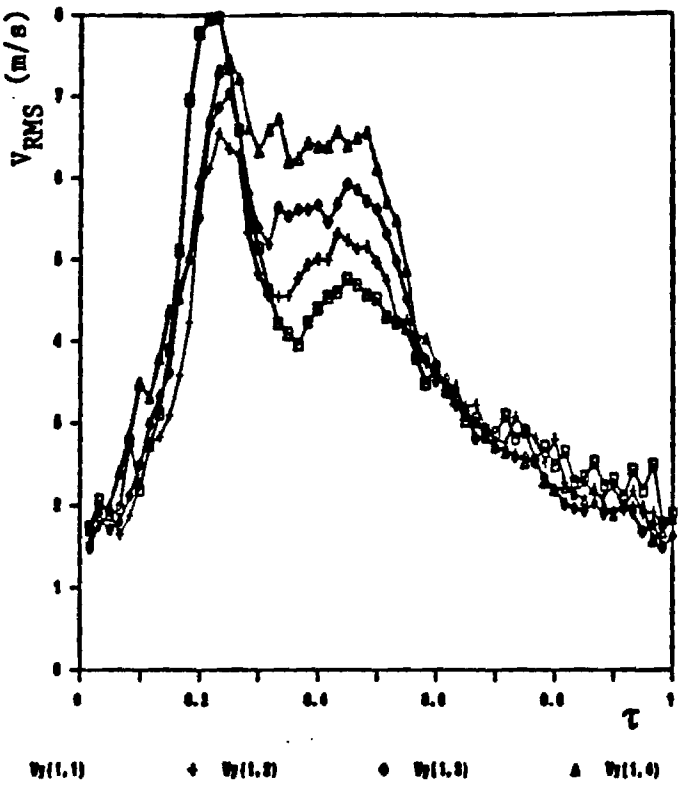

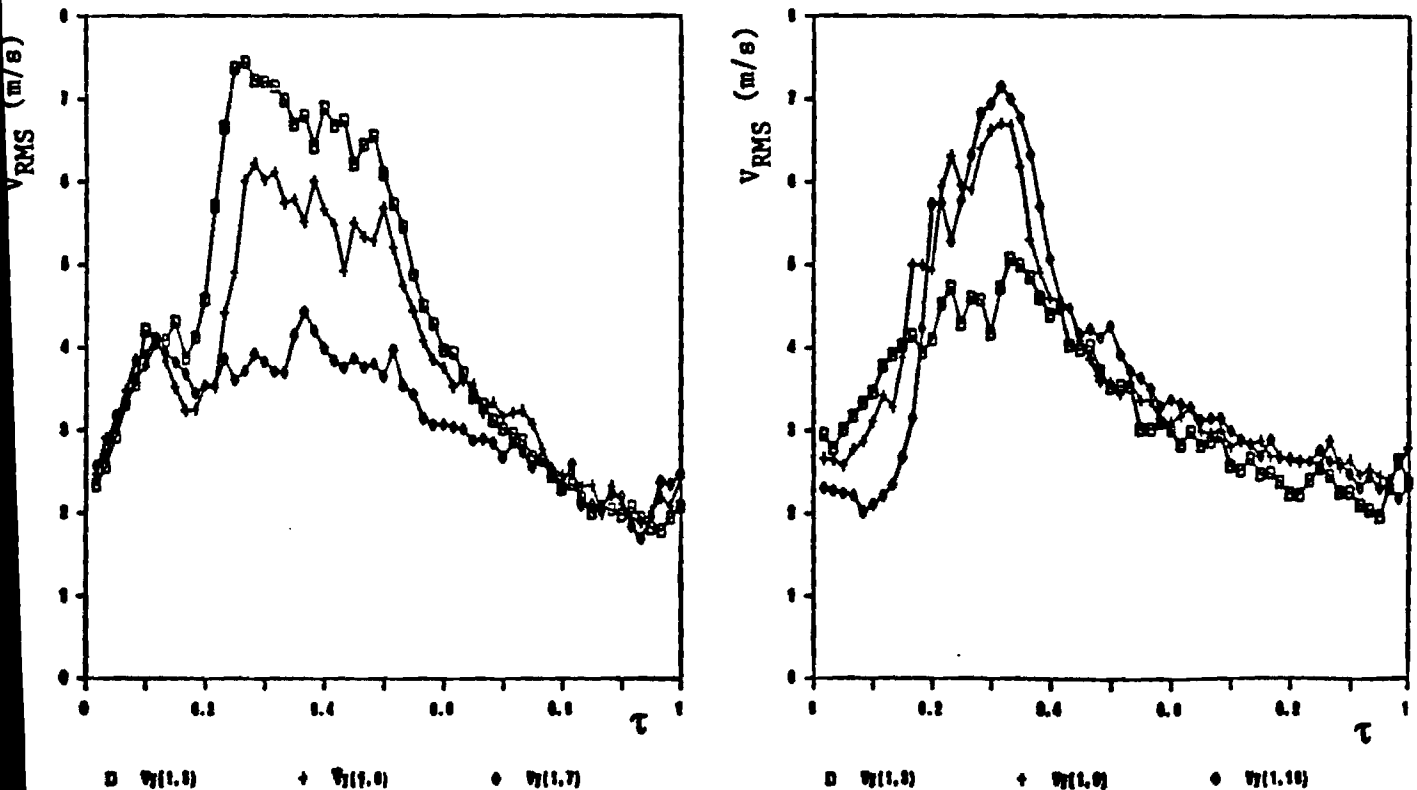

Fig. 18 Variation of the Vertical Turbulence Intensity During a Cycle for Locations along the Line m = 1.

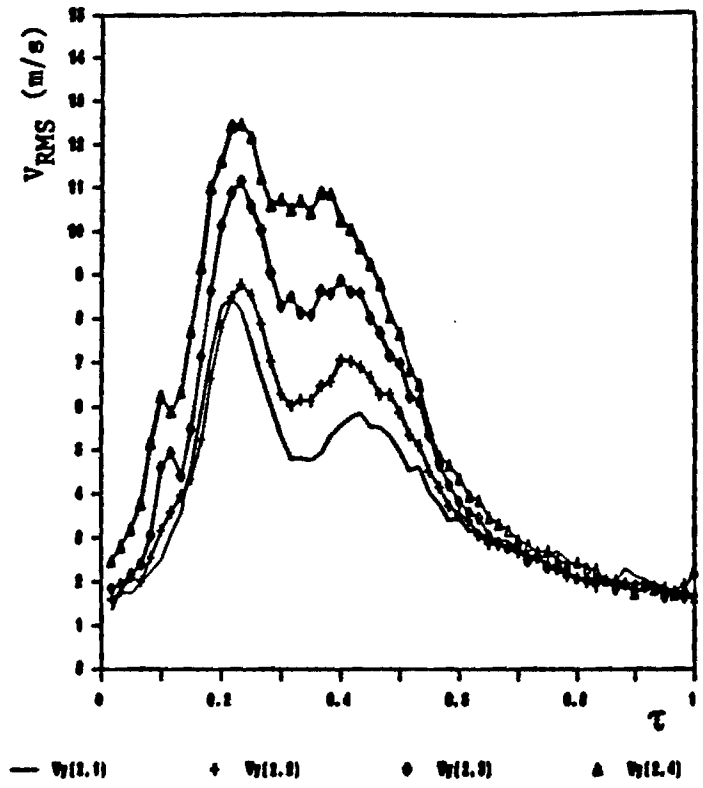

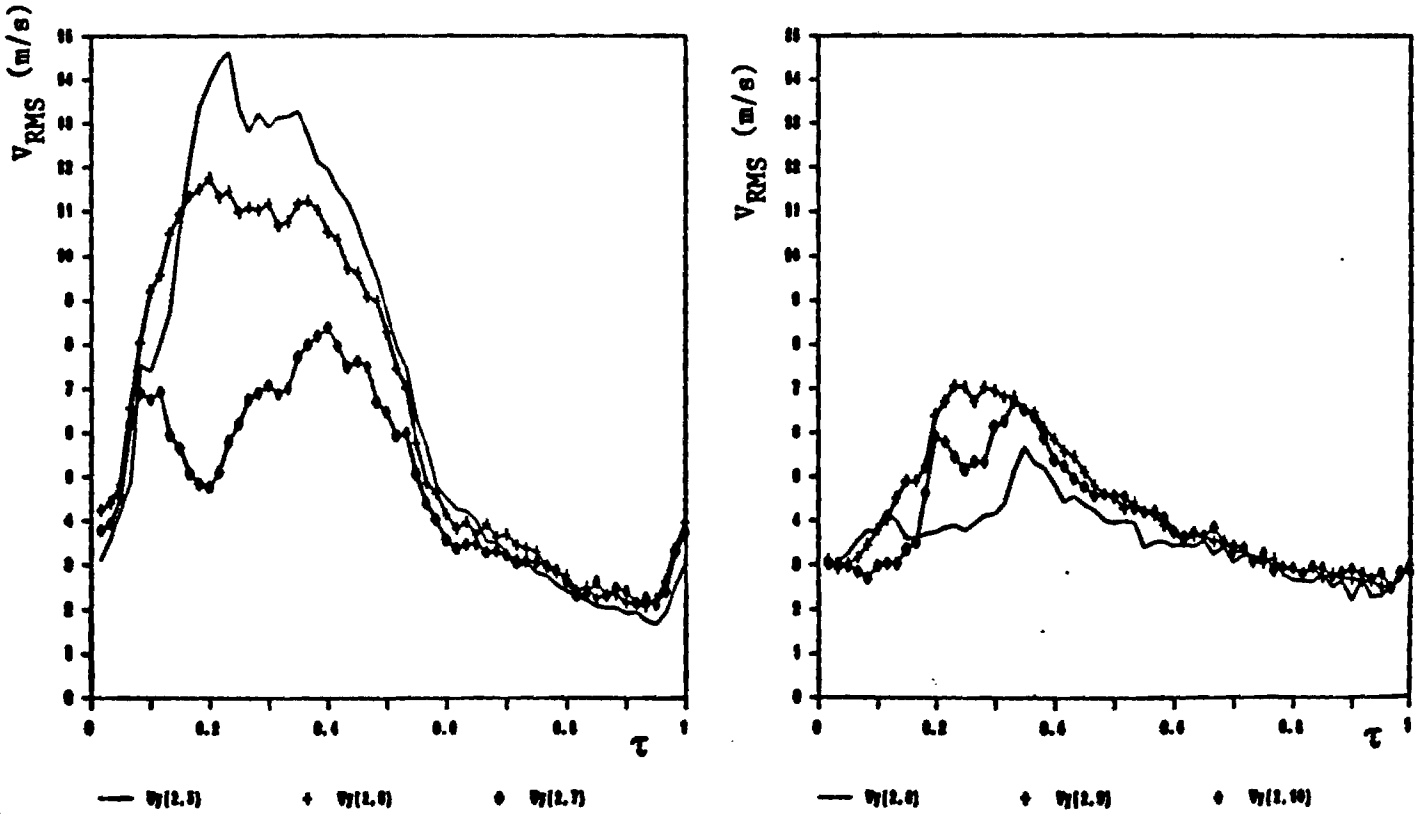

Fig. 19 Variation of the Vertical Turbulence Intensity During a Cycle for Locations along the Line m = 2.

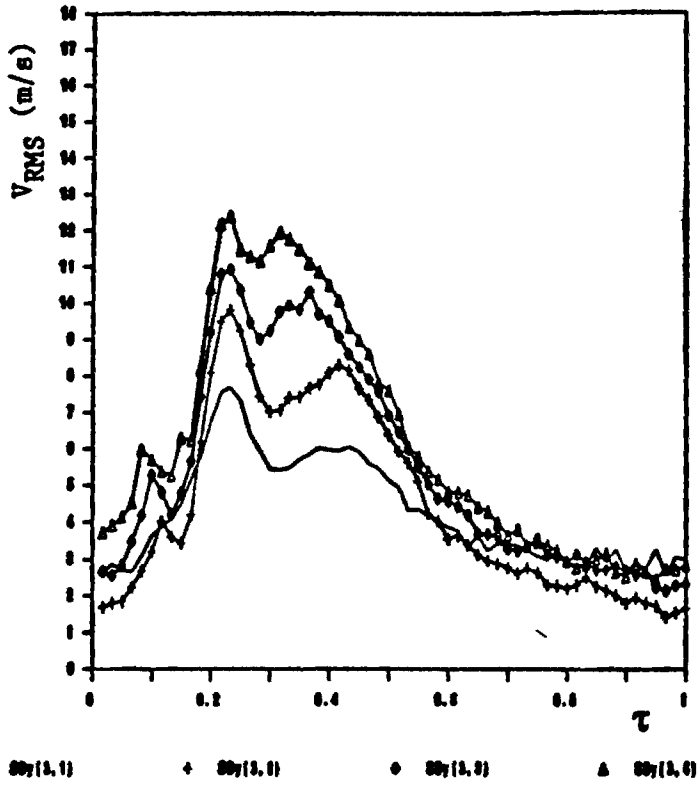

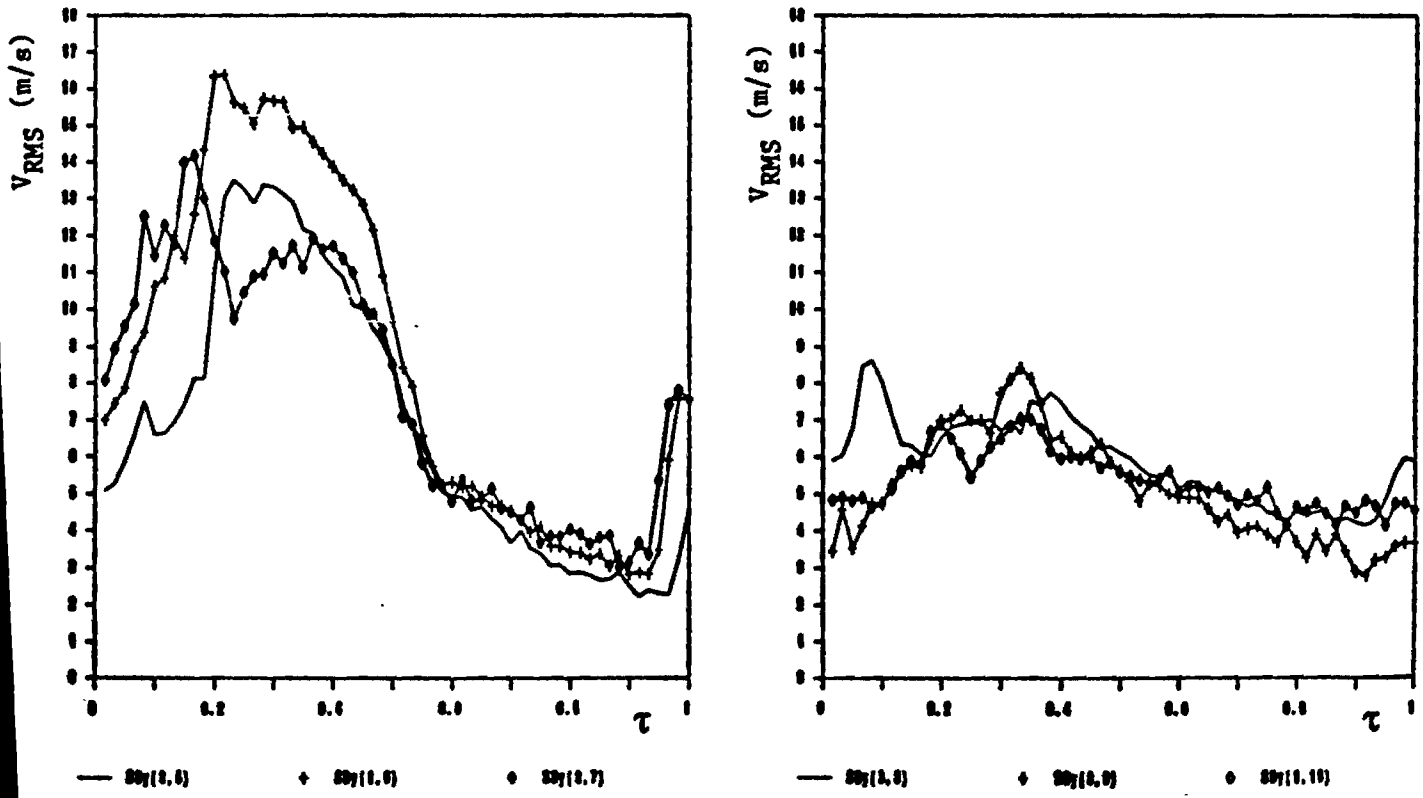

Fig. 20 Variation for the Vertical Turbulence Intensity During a Cycle for Locations along the Line m = 3.

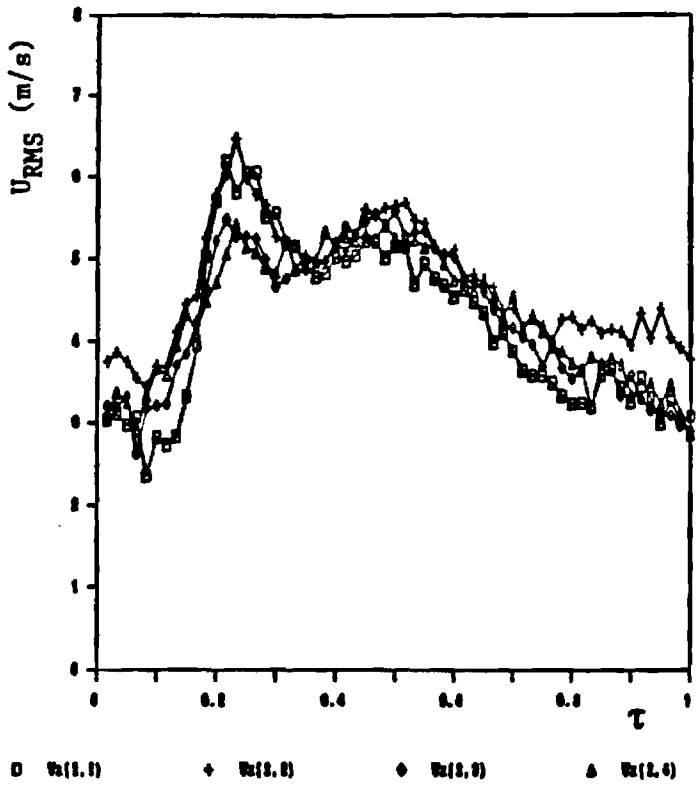

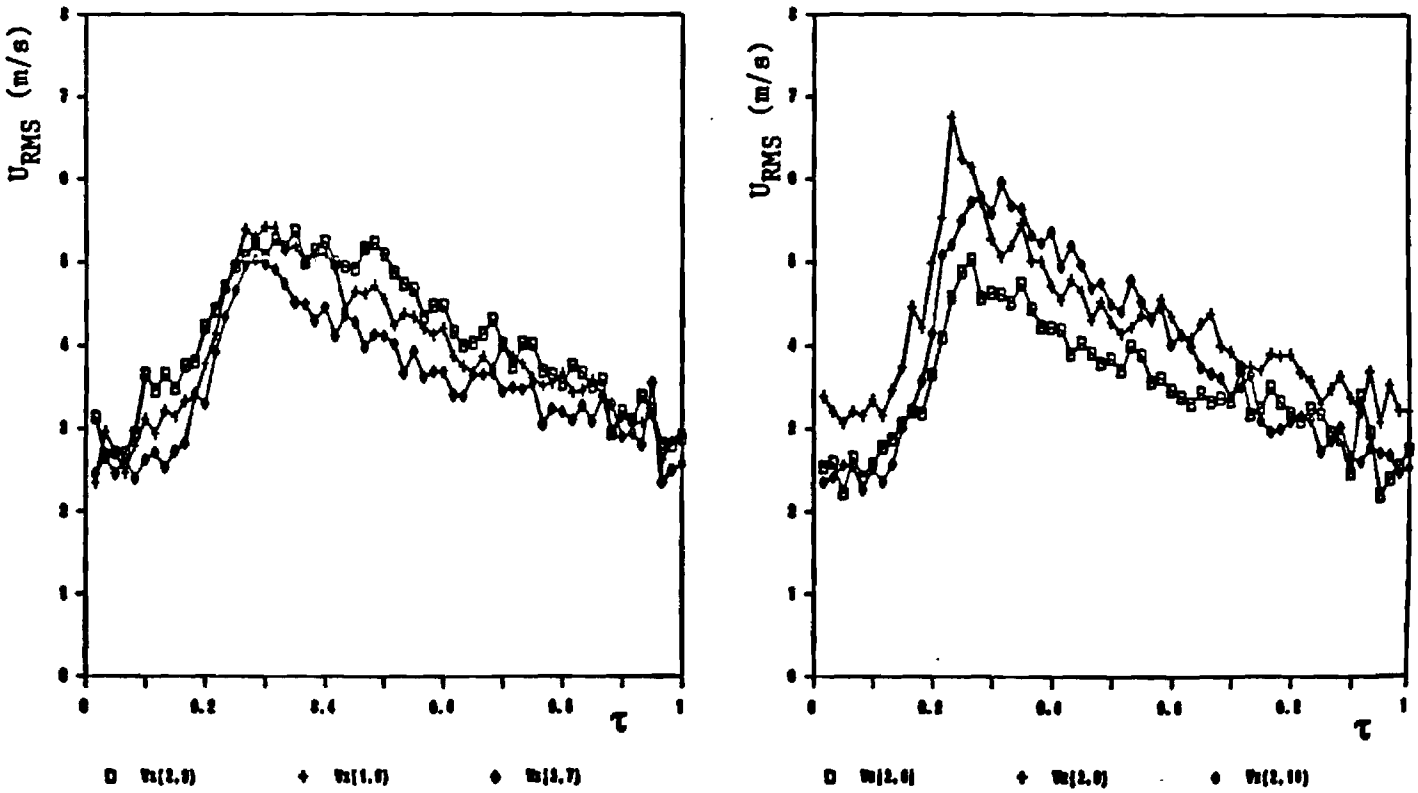

Fig. 21 Variation of the Axial Turbulence Intensity During a Cycle for Locations along the Line m = 1.

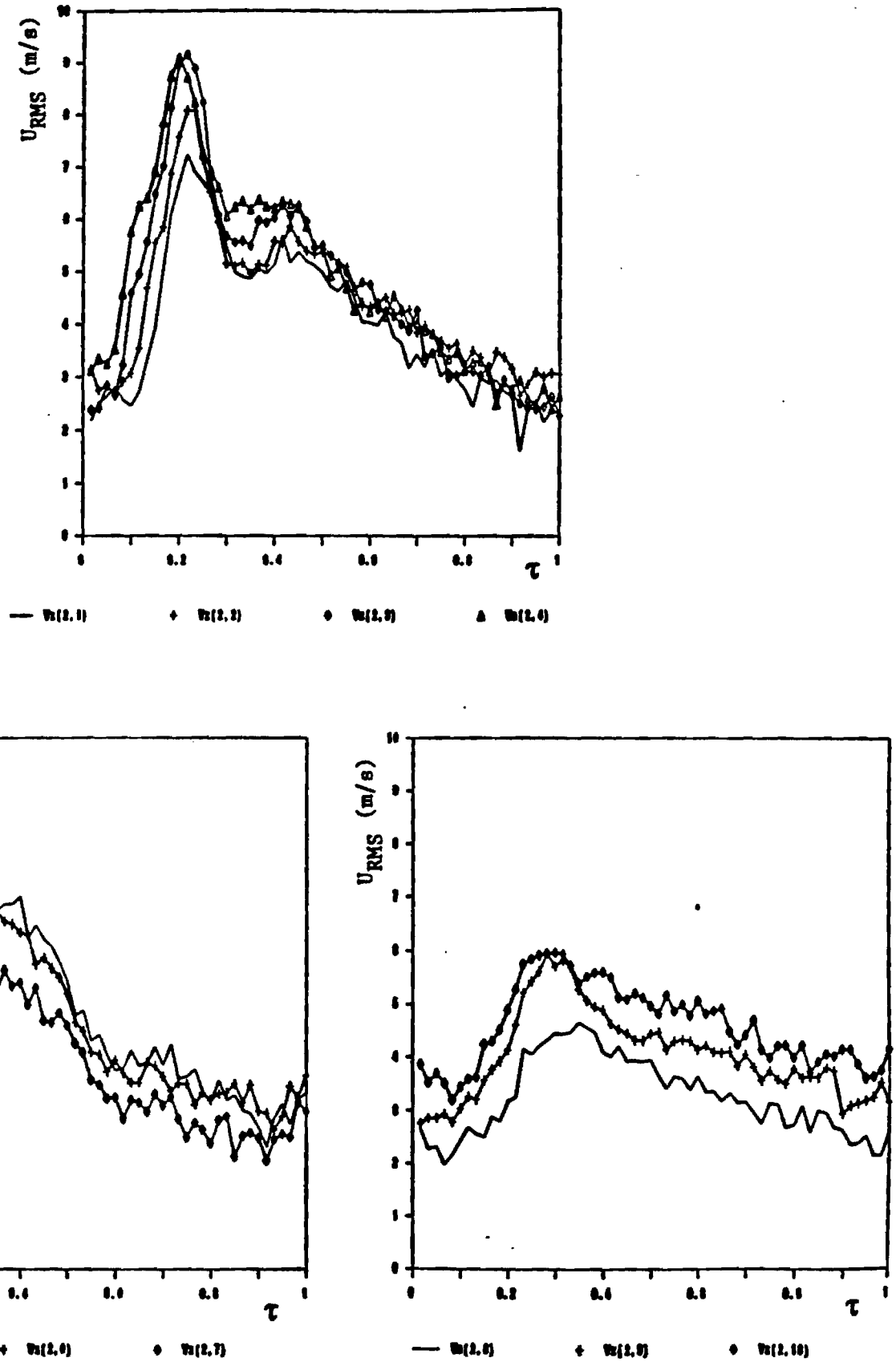

Fig. 22 Variation of the Axial Turbulence Intensity During a Cycle for Locations along the Line m = 2.

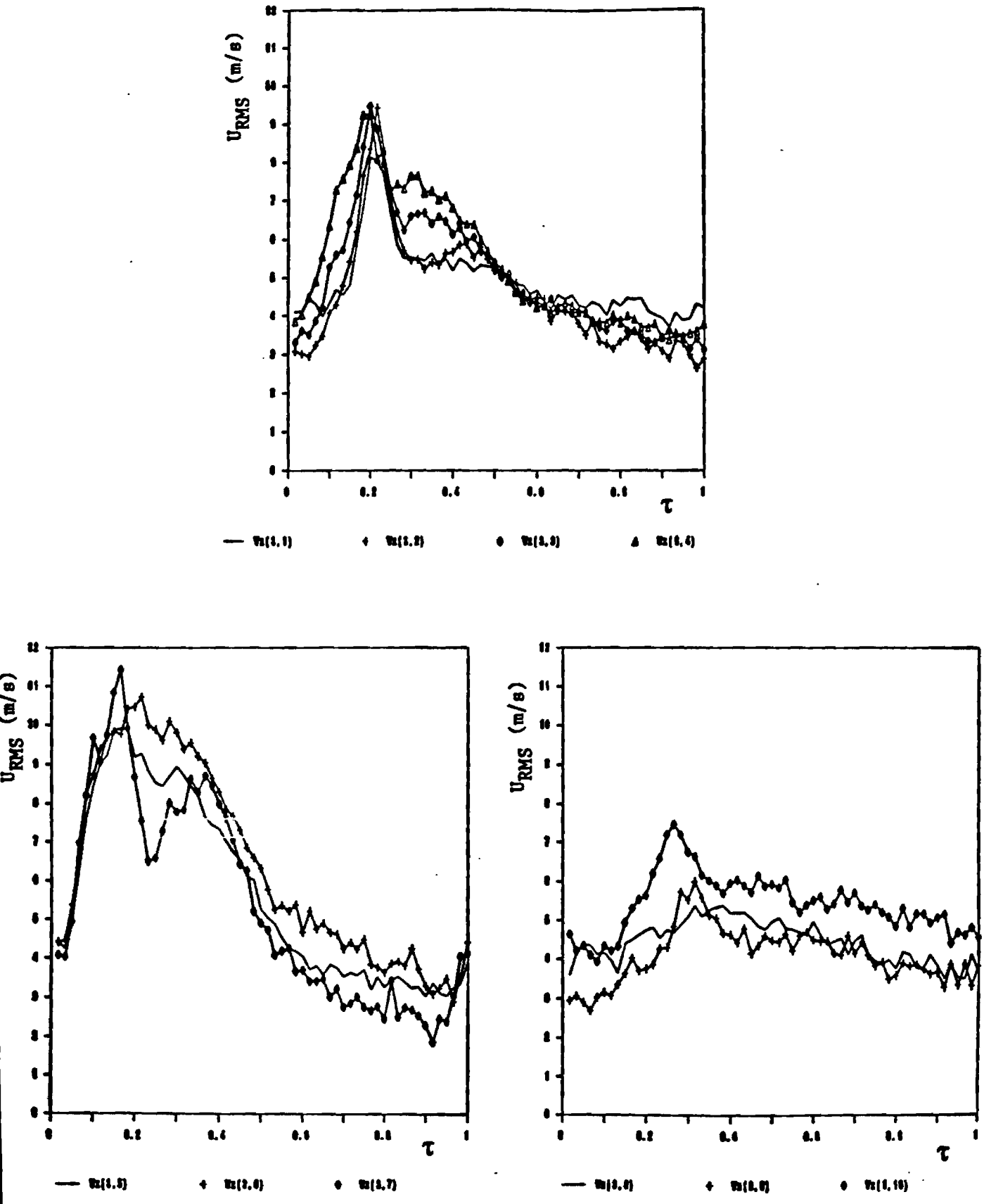

Fig. 23 Variation of the Vertical Turbulence Intensity During a Cycle for Locations along the Line m = 3.

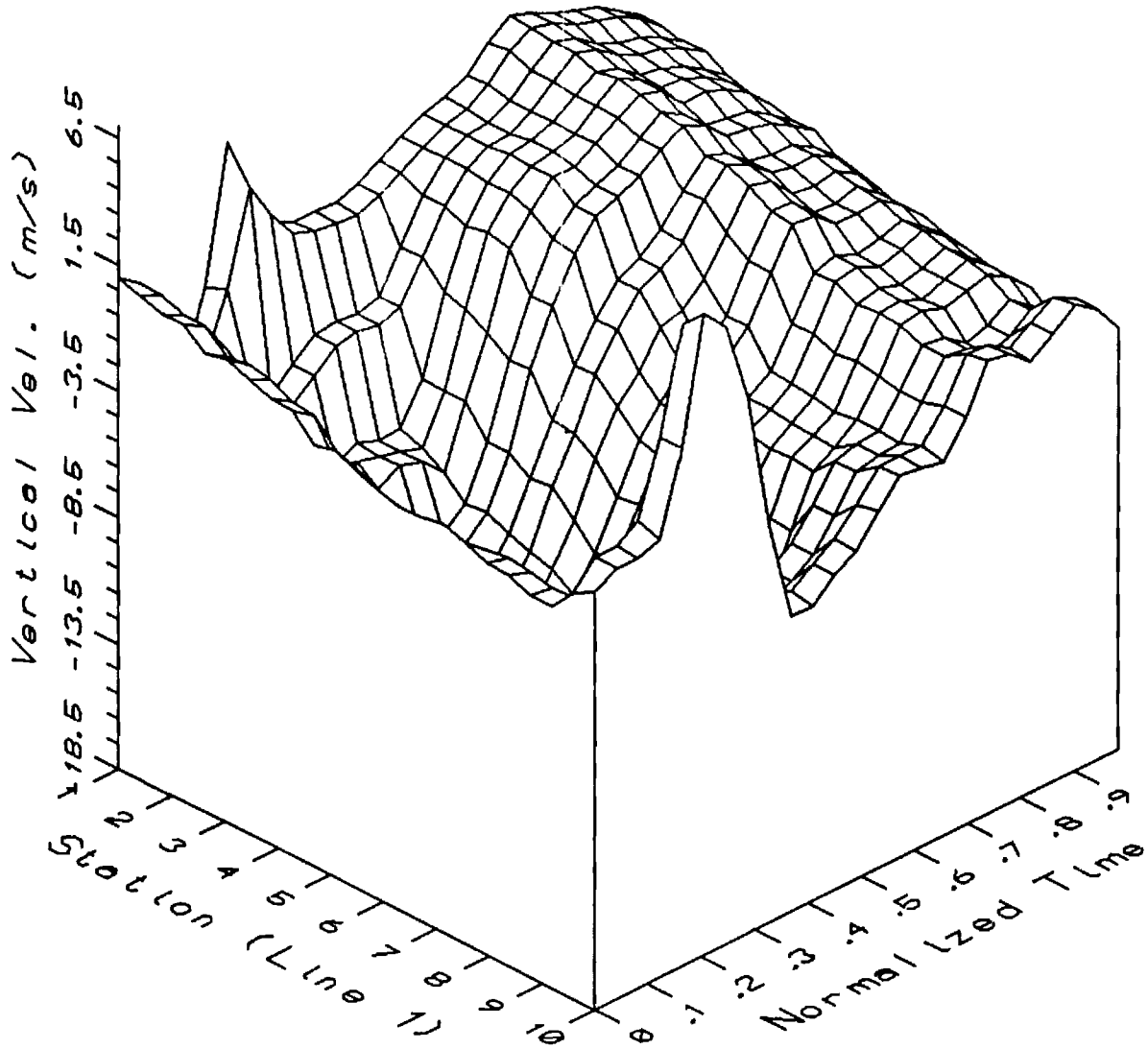

Fig. 24 Three Dimensional Plot of Vertical Mean Velocities during a Cycle for Locations along the Line m = 1.

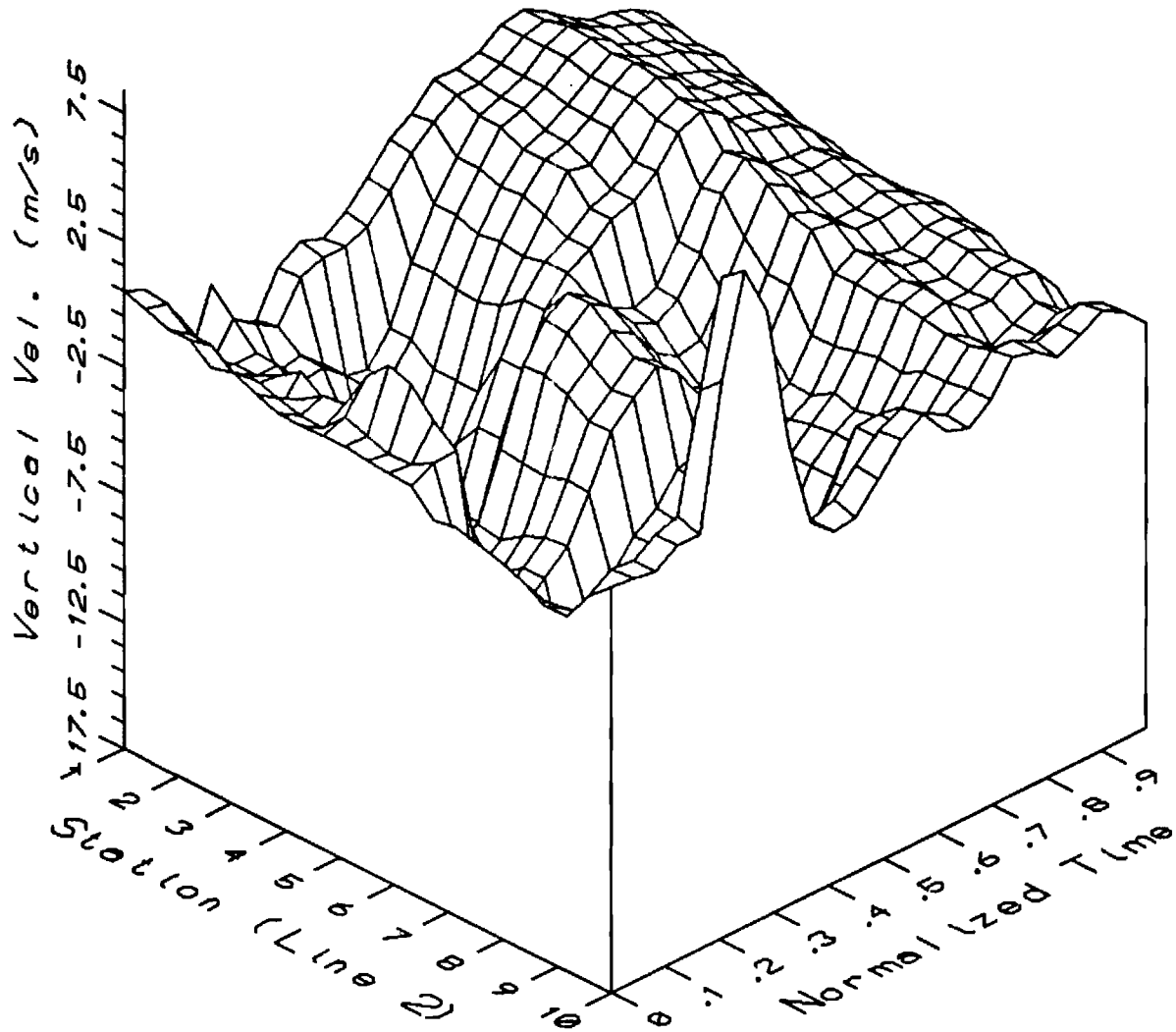

Fig. 25 Three Dimensional Plot of Vertical Mean Velocities during a Cycle for Locations along the Line m = 2.

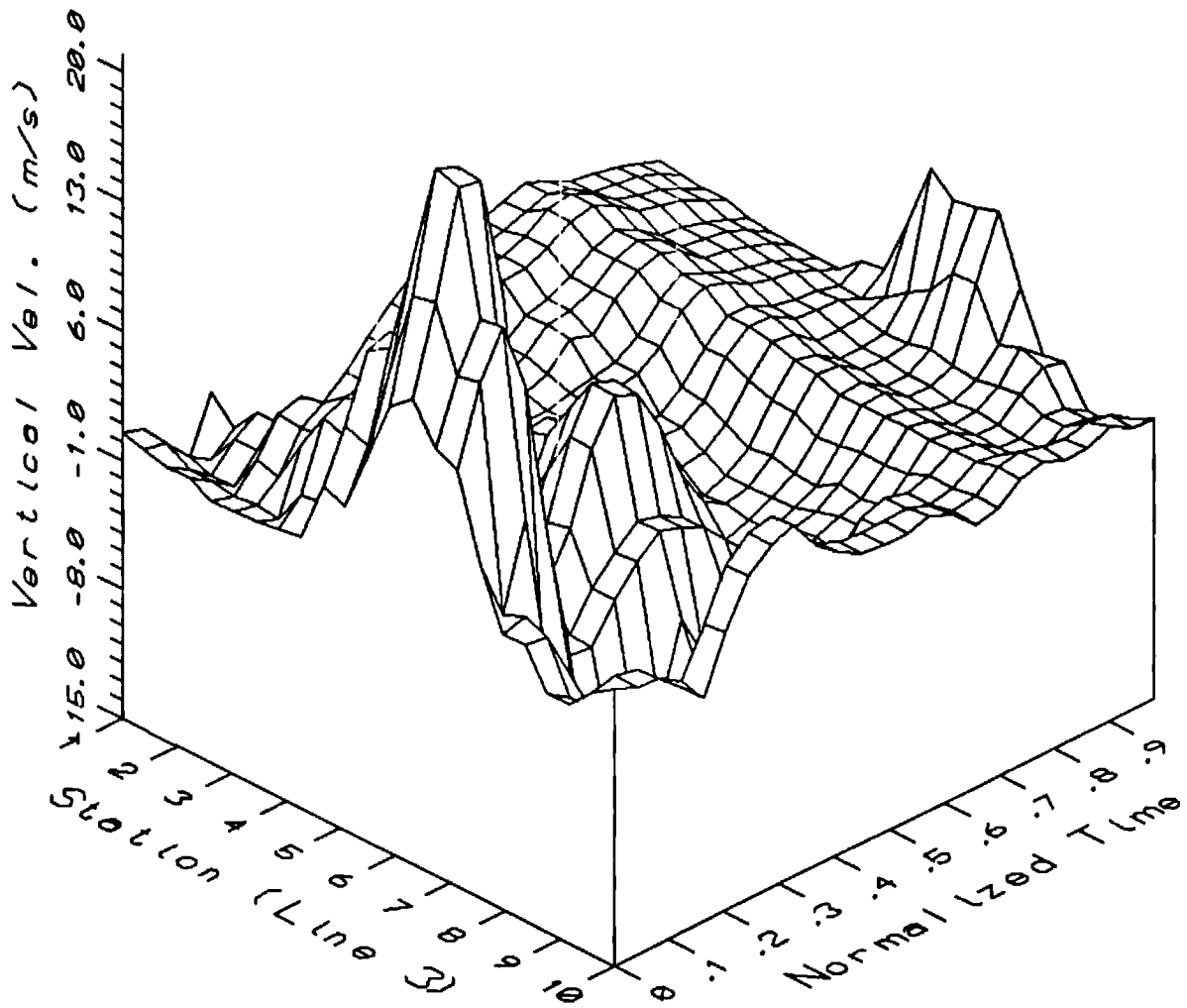

Fig. 26 Three Dimensional Plot of Vertical Mean Velocities during a Cycle for Locations along the Line m = 3.

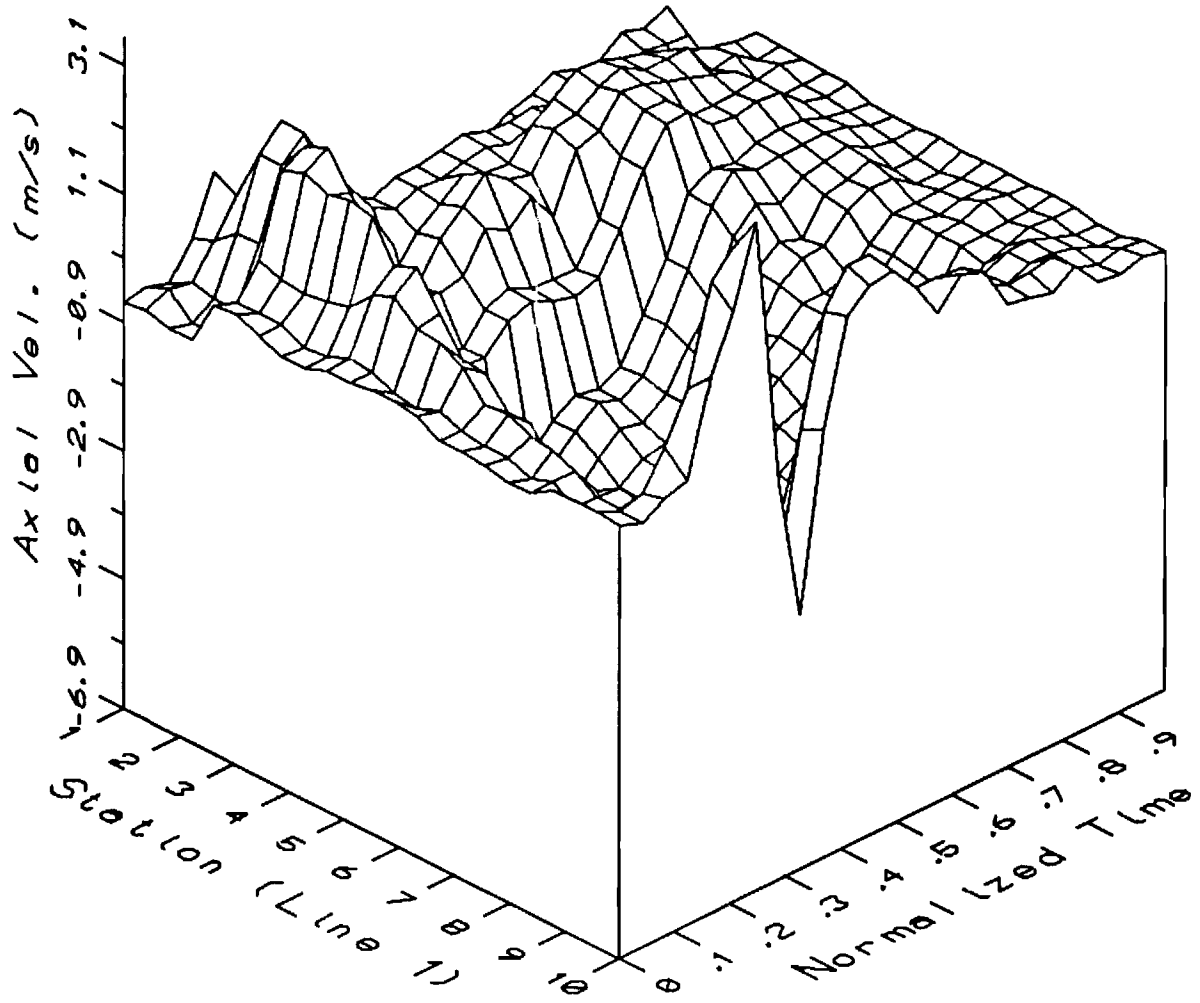

Fig. 27 Three Dimensional Plot of Axial Mean Velocities during a Cycle for Locations along the Line m = 1.

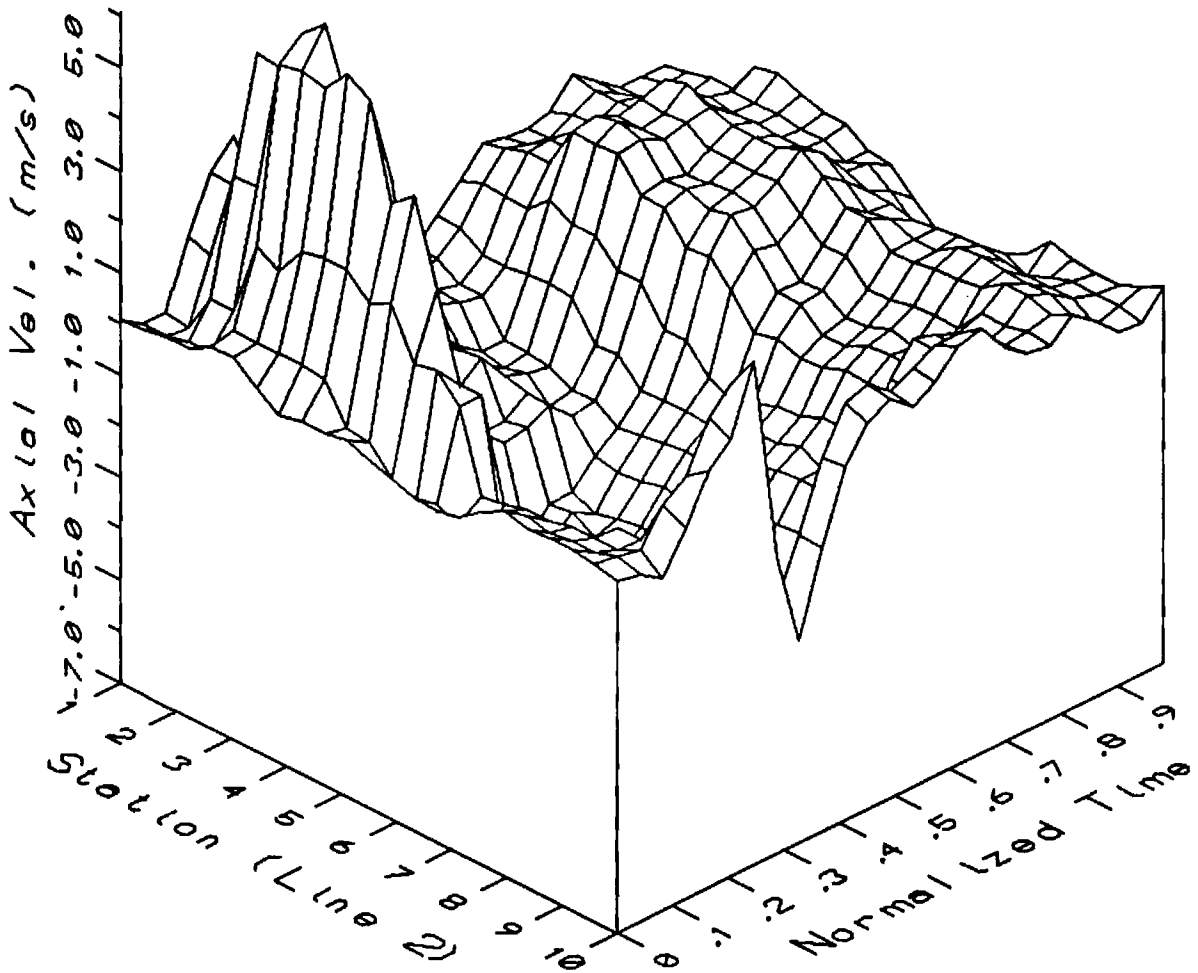

Fig. 28 Three Dimensional Plot of Axial Mean Velocities during a Cycle for Locations along the Line m = 2.

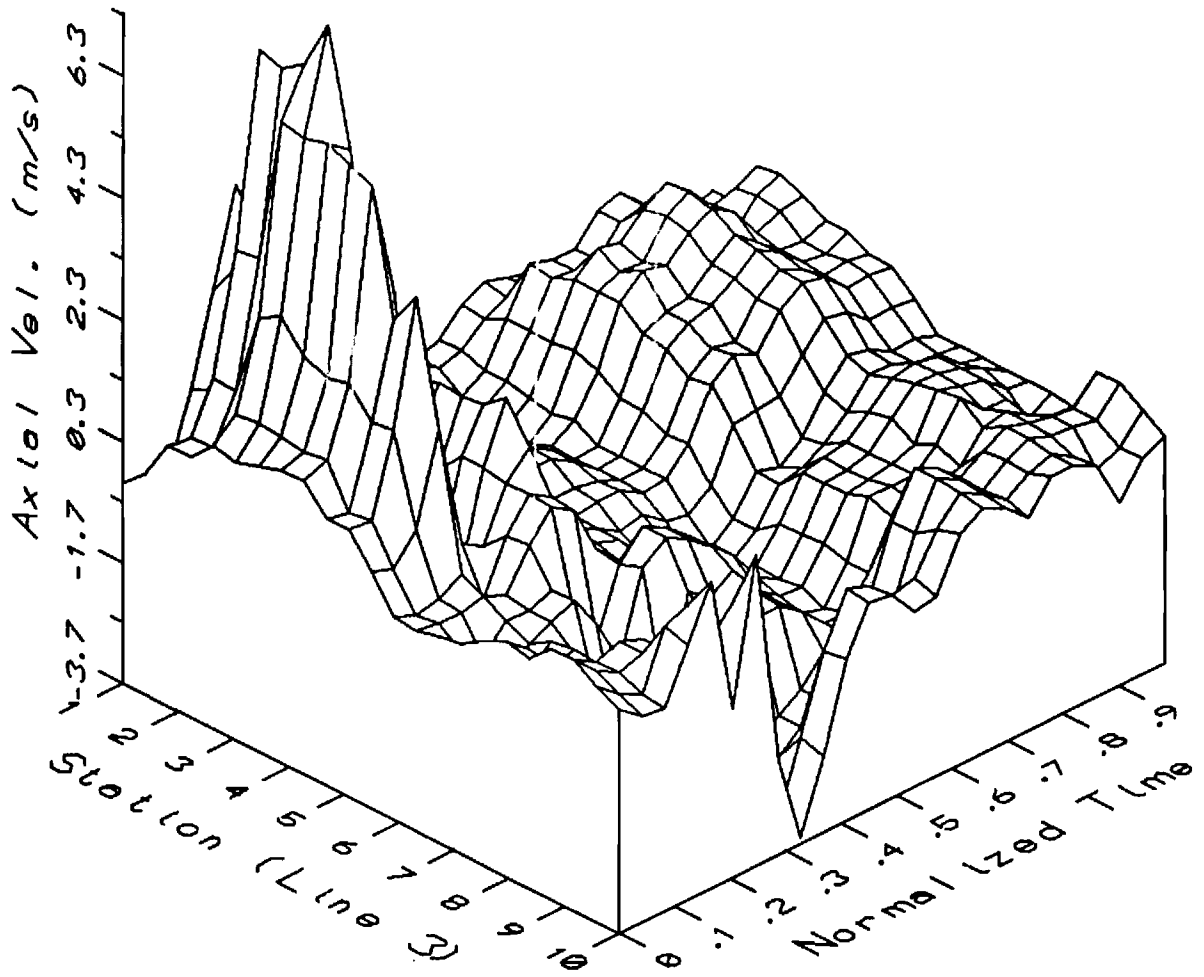

Fig. 29 Three Dimensional Plot of Axial Mean Velocities during a Cycle for Locations along the Line m = 3.

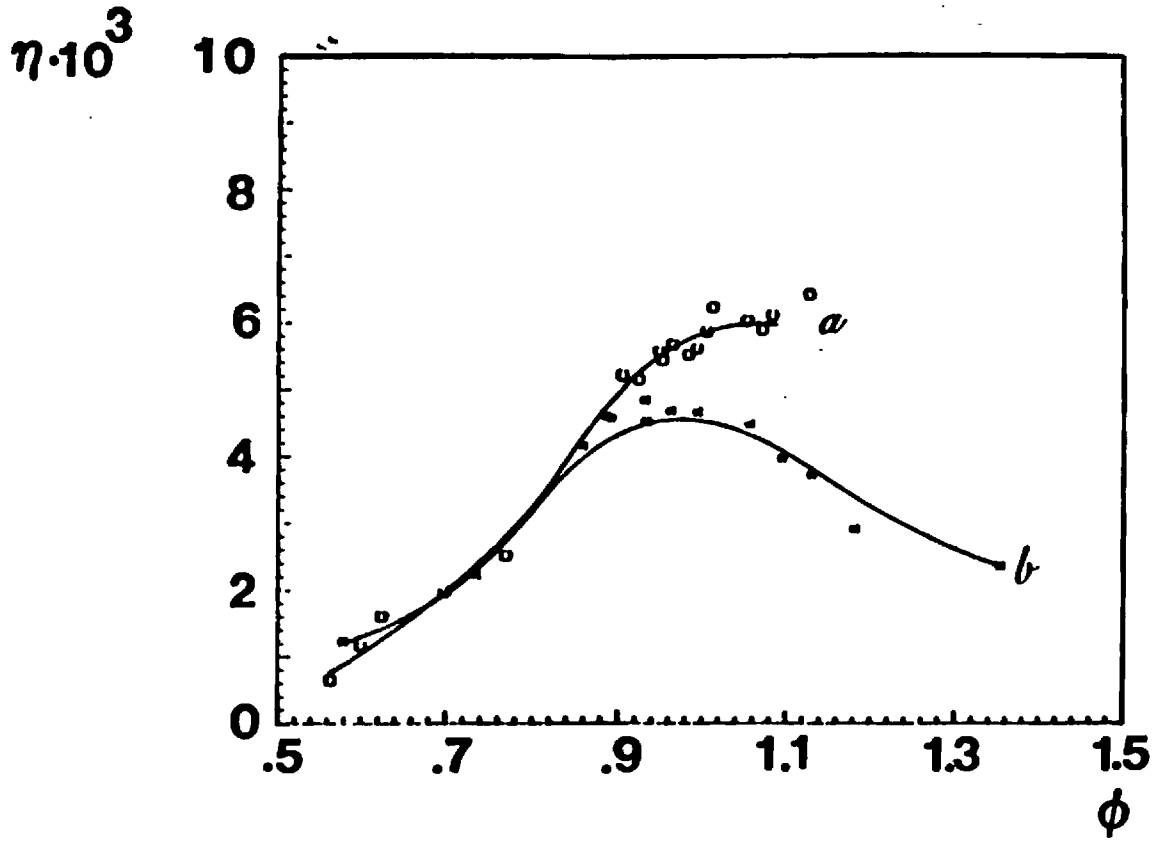

Fig. 30 Rayleigh Efficiency as a Function of Equivalence Ratio for The Combustor Fitted with the a) Standard and b) Long Tailpipes.

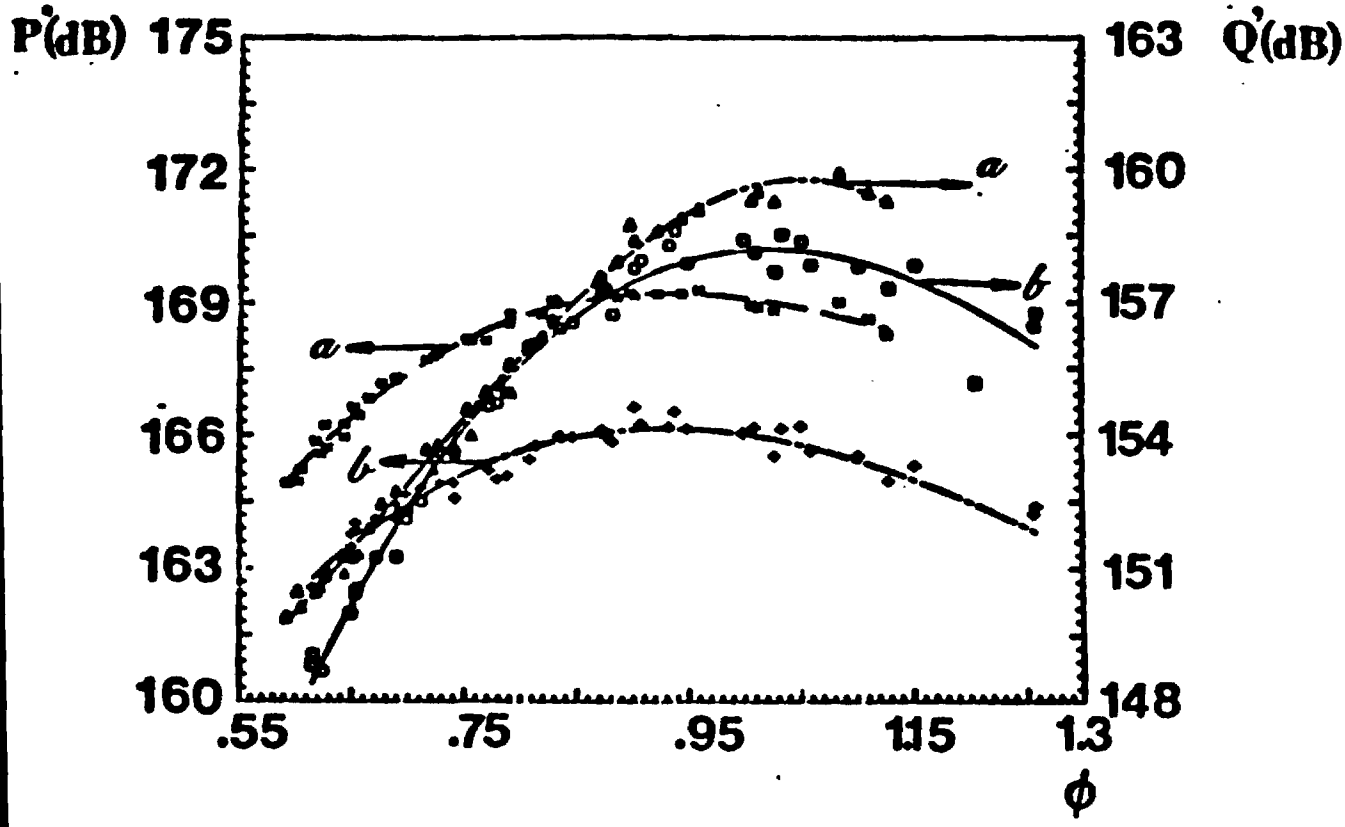

Fig. 31 Pressure and Heat Release Fluctuations as a Function of Equivalence Ratio for the Combustor Fitted with the Standard (a) and Long (b) Tailpipes.

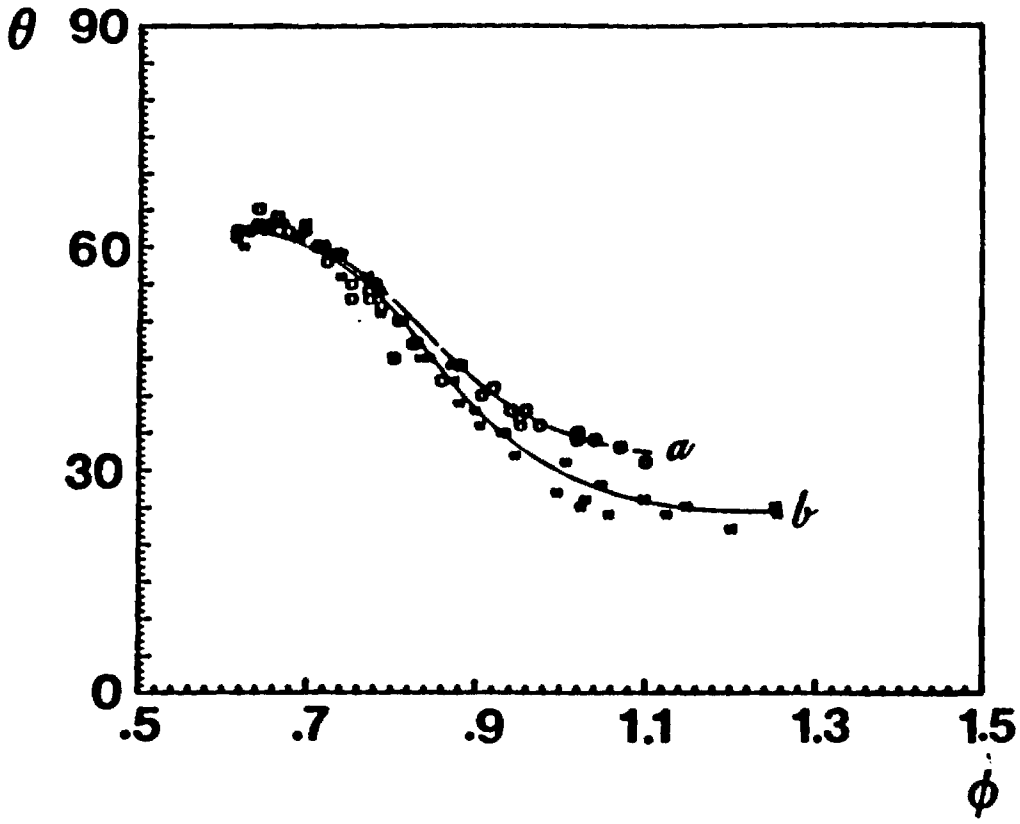

Fig. 32 Phase Angle by which the Heat Release Leads the Pressure as a Function of Equivalence Ratio for the Combustor Fitted with the a) Standard and b) Long Tailpipes.

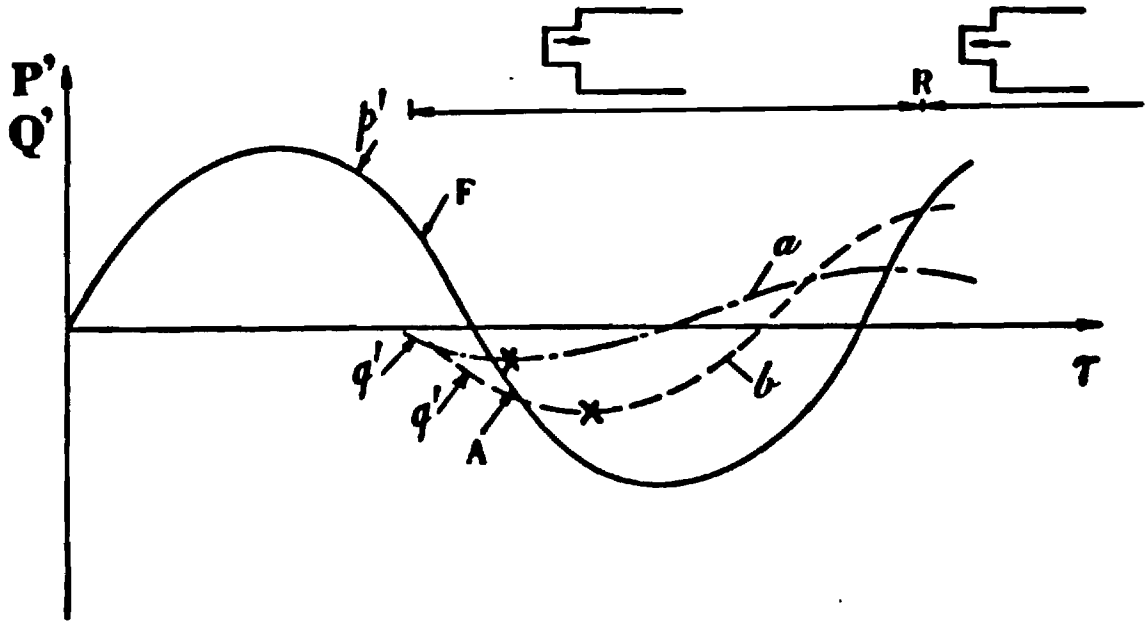

Fig. 33 Normalized Pressure (P') Cycle Showing the Timing of the Heat Release Oscillations (Q') for a) Lean and b) Rich Limits of Operation; Fuel Enters at "F", Air Enters at "A", Backflow into the Mixing Chamber Starts at "R"; the "X"s Denote the Instants of Reignition of the Fresh Fuel Charges.

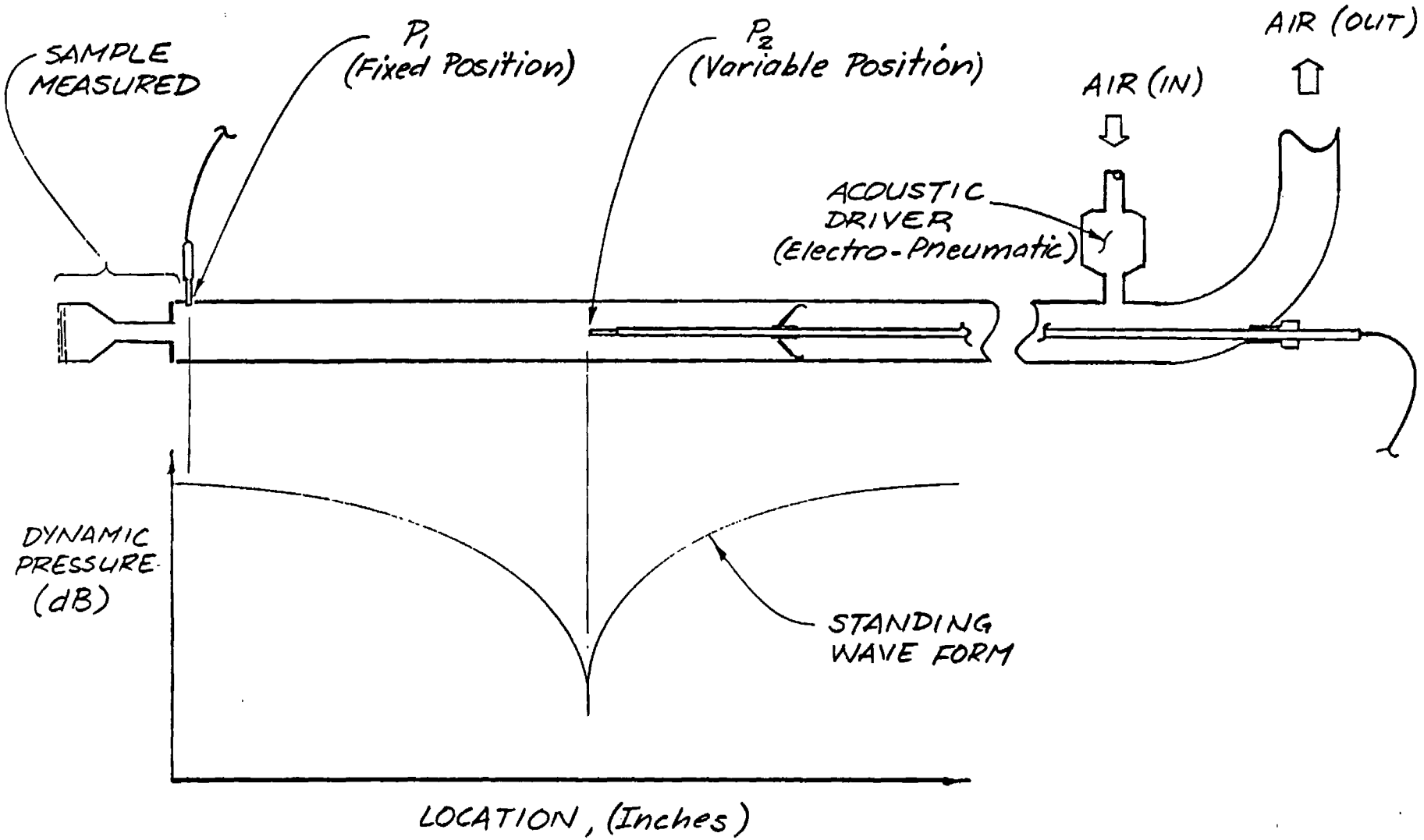

Fig. 34 Schematic of the Impedance Tube Experiment.

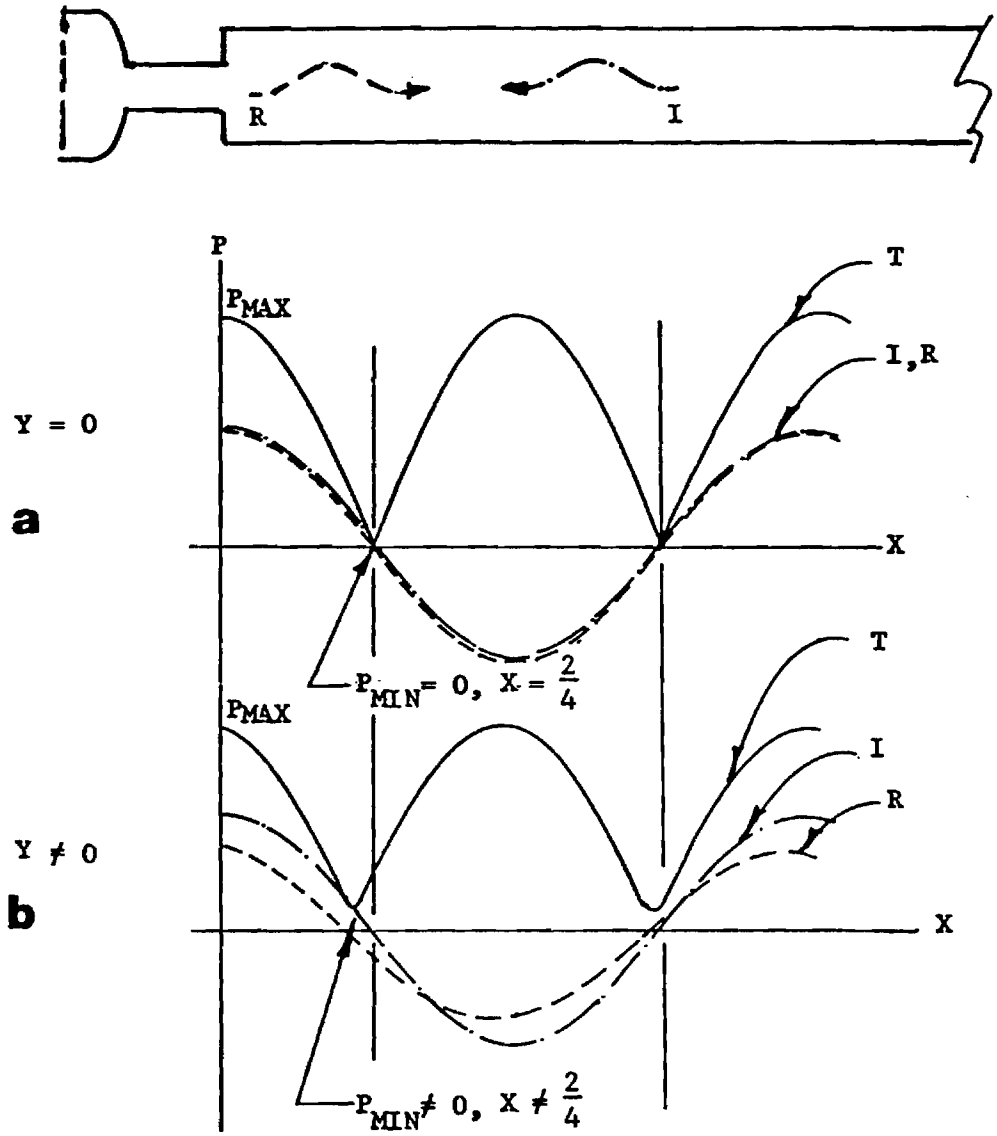

Fig. 35 Wave Form of the Incident (I), Reflected (R) and Total (T) Standing Wave for a) Hard Termination and b) Termination with Finite Admittance.

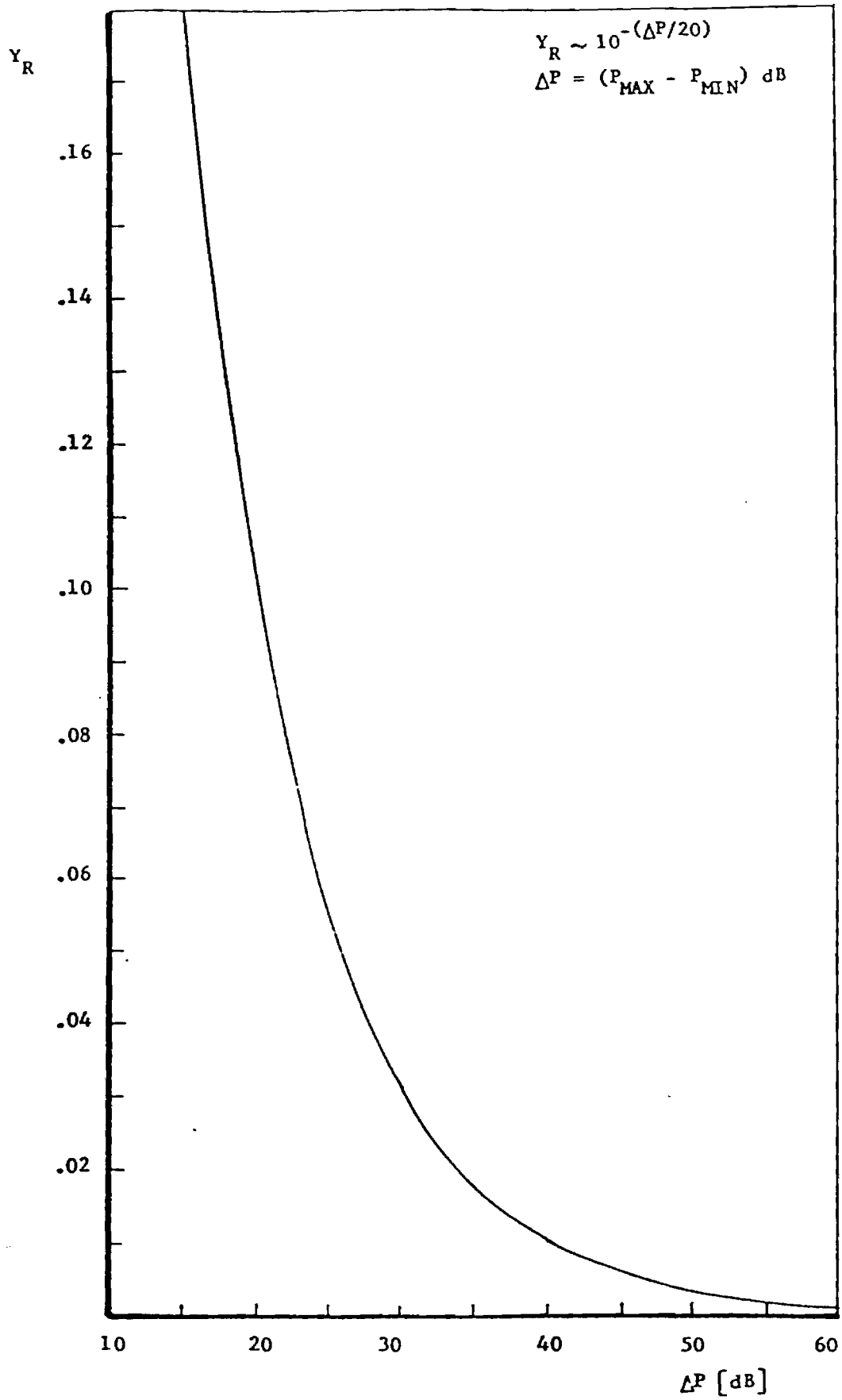

Fig. 36 Sensitivity of the Real Part of the Admittance to the Measured Pressure Difference between the Pressure Maximum and the Pressure Minimum.

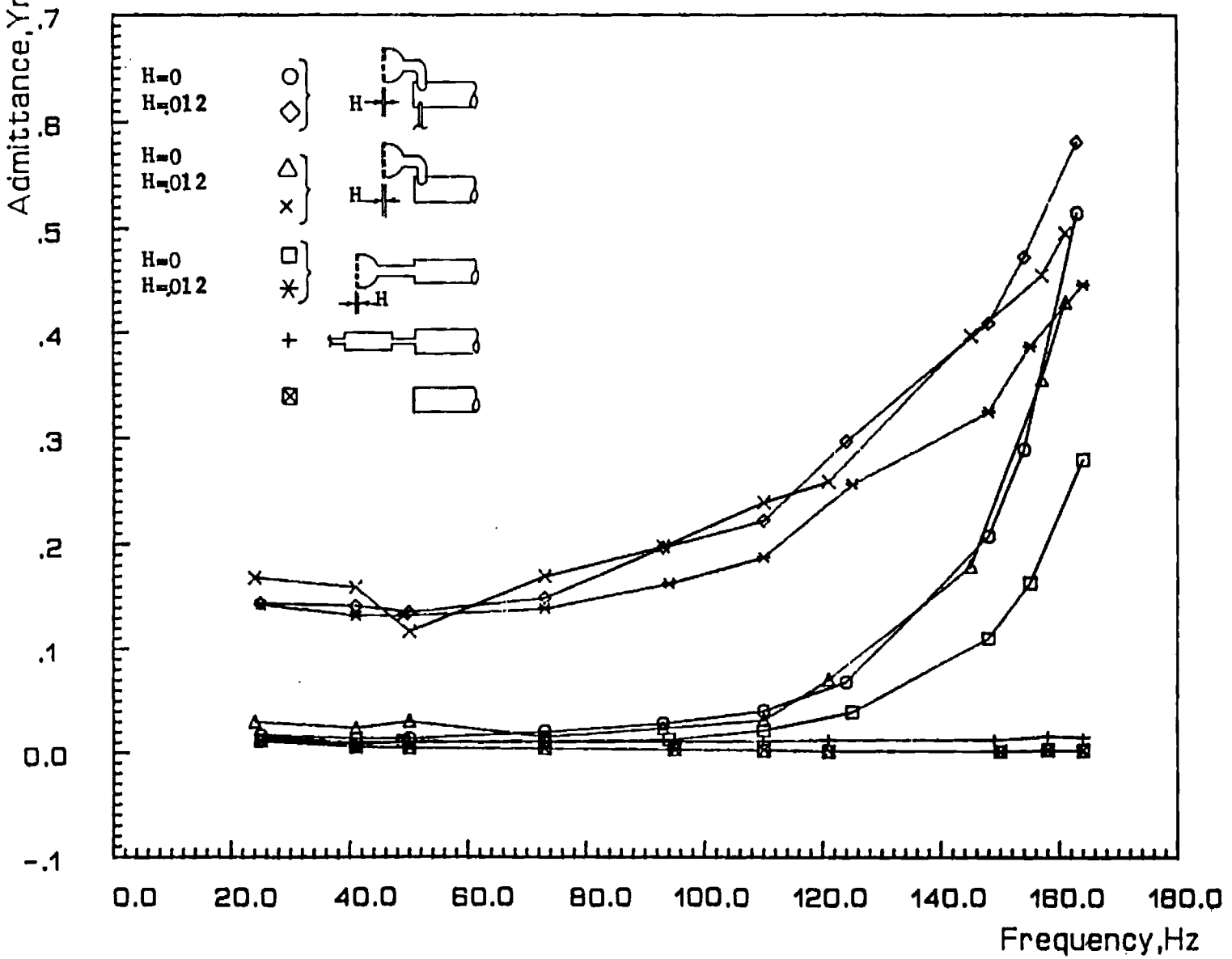

Fig. 37 Real Part of the Admittance as a Function of Frequency for Various Impedance Tube Terminations. H Denotes the Valve Gap Setting in Inches.

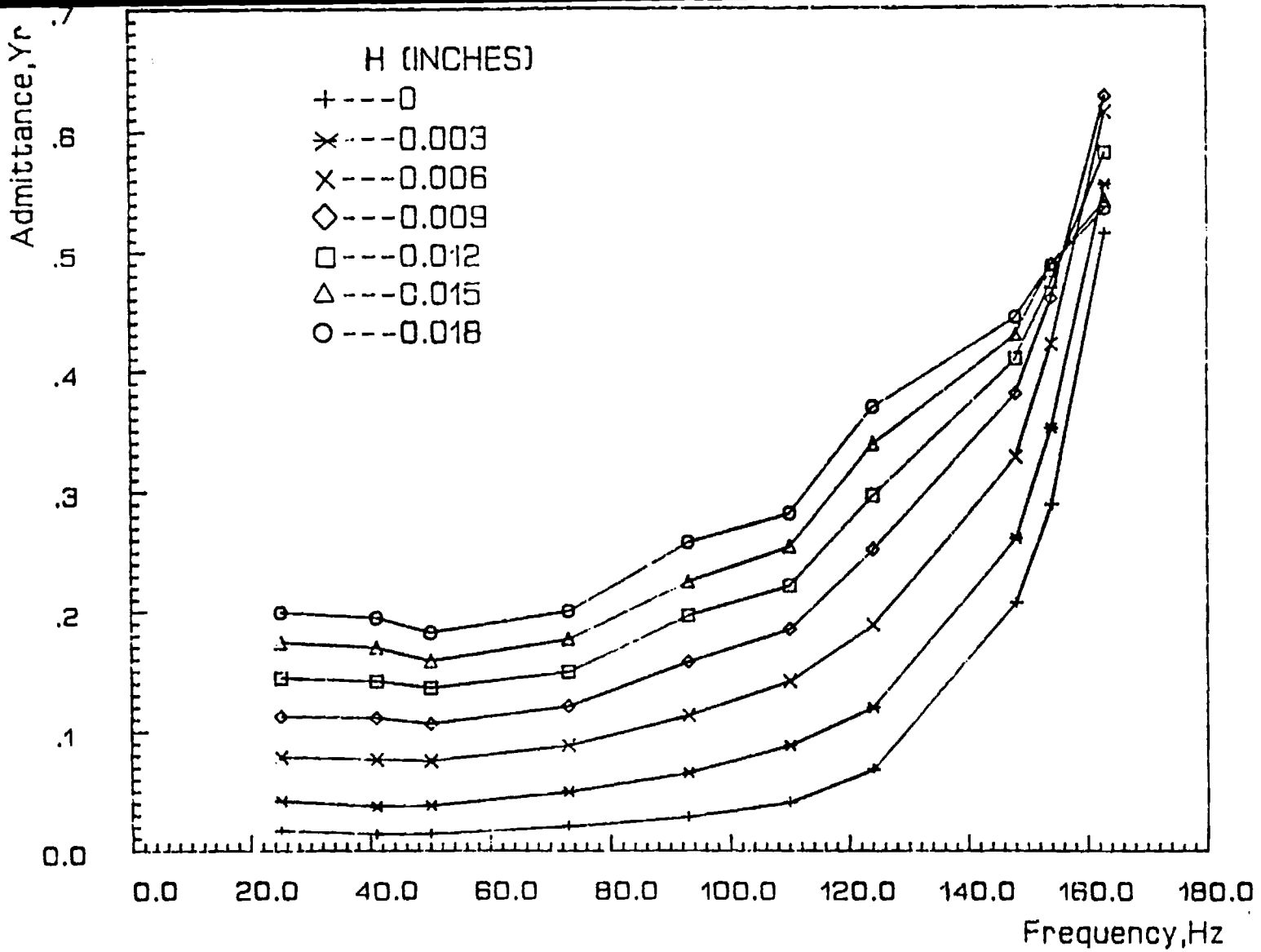

Fig. 38 Real Part of the Admittance of the Mixing Chamber Assembly as a Function of Frequency for Different Air Valve Gap Settings (H).

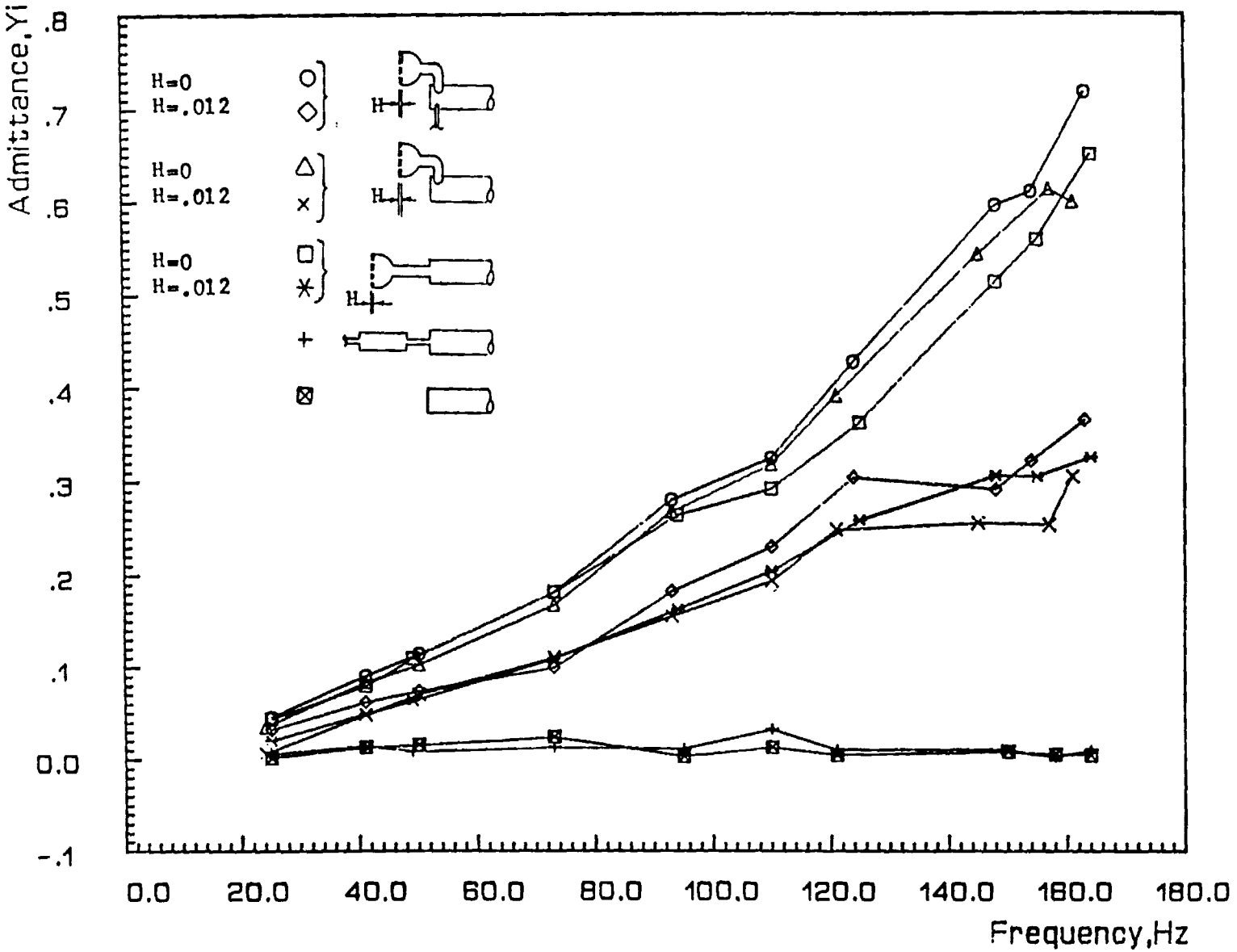

Fig. 39 Imaginary Part of the Admittance as a Function of Frequency for Various Impedance Tube Terminations. H Denotes the Valve Gap Setting in Inches.

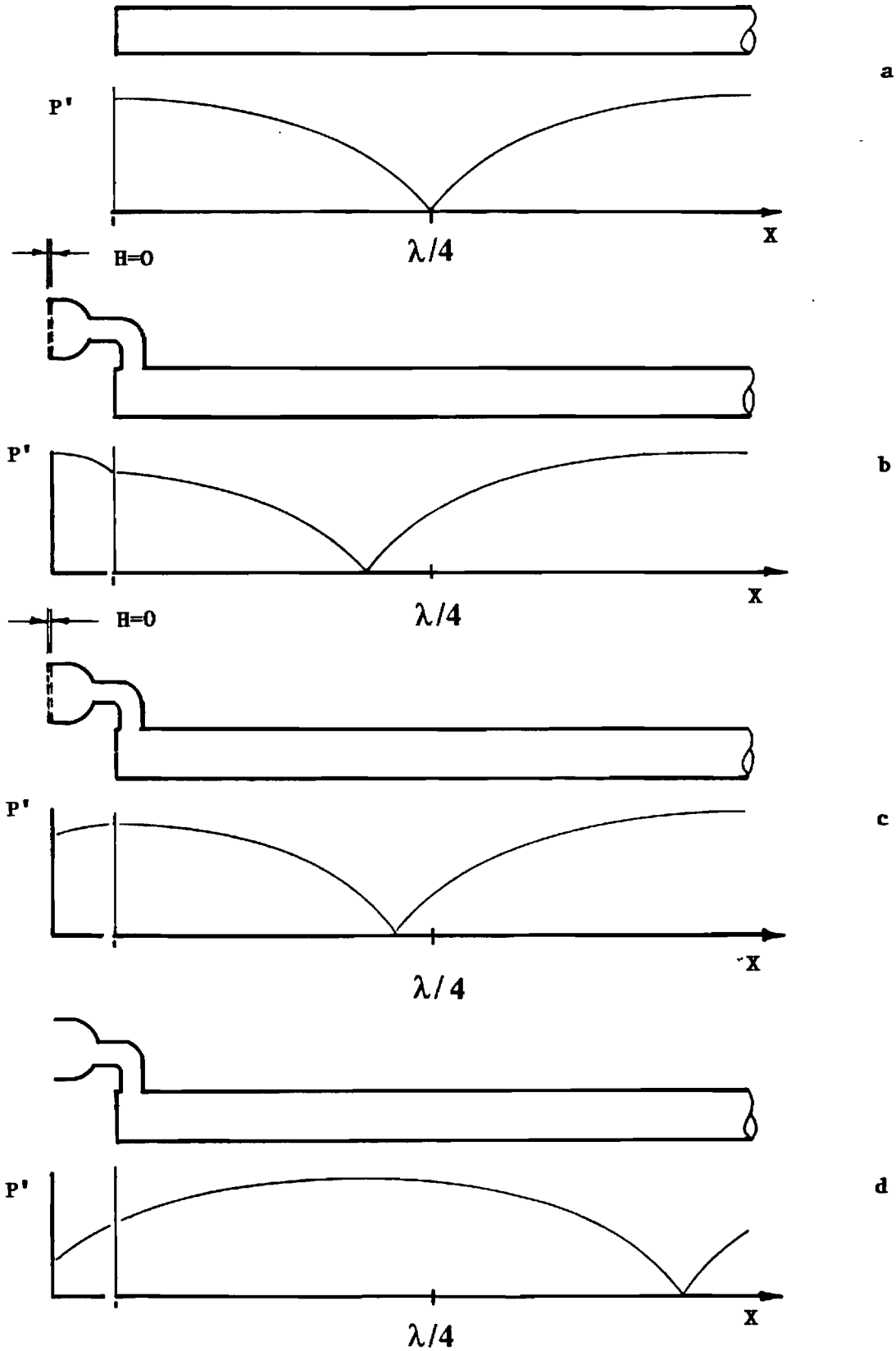

Fig. 40 Comparison of Standing Wave Pattern in the Impedance Tube Fitted with a) Hard Termination, b) Closed Air Valve, c) Open Valve and d) Valve Housing with Valve Plates Removed. The Actual Wave Pattern in the Valve Housing is More Complex Due to the Geometry of the Housing.

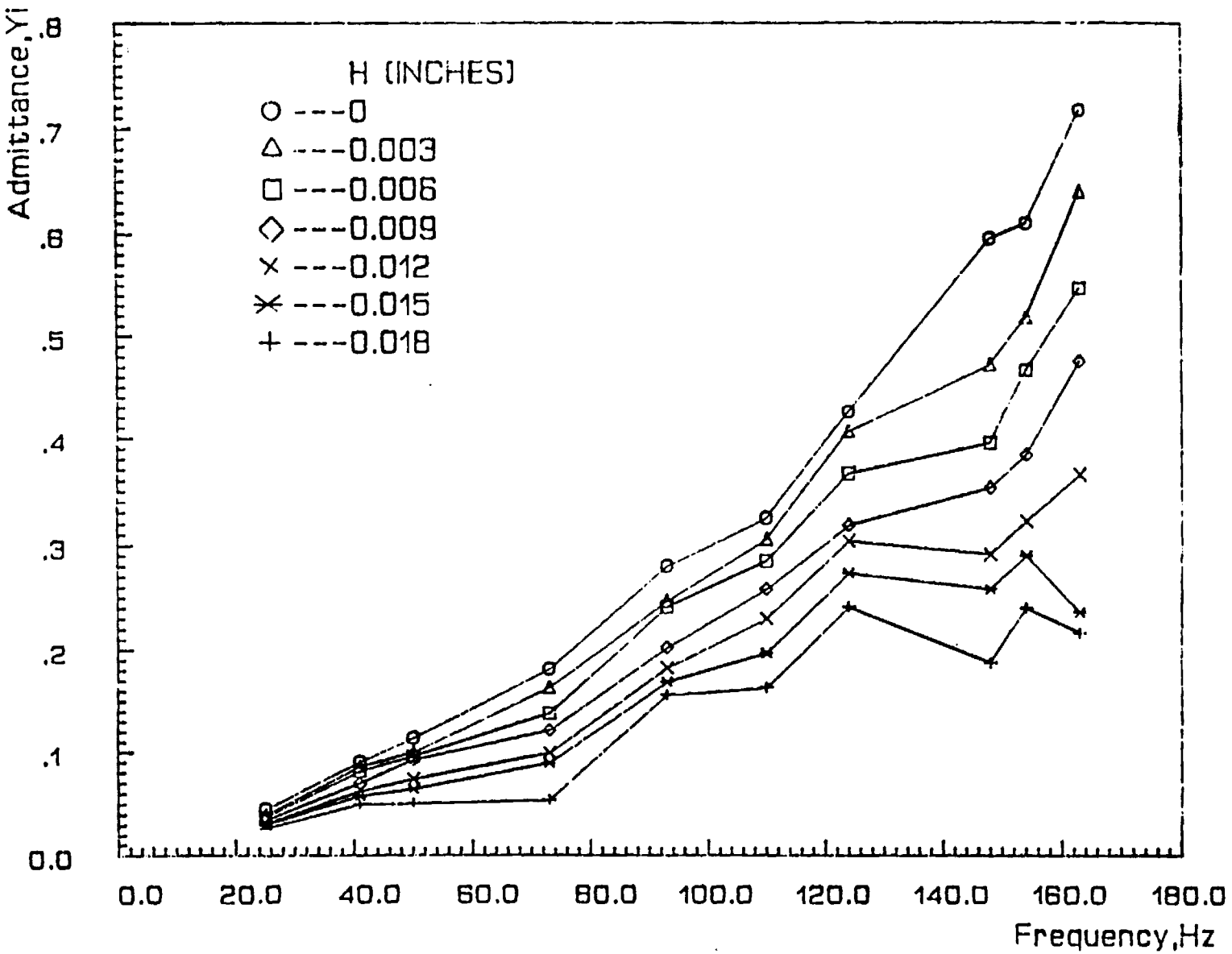

Fig. 41 Imaginary Part of the Admittance of the Mixing Chamber Assembly as a Function of Frequency for Different Air Valve Gap Settings (H).

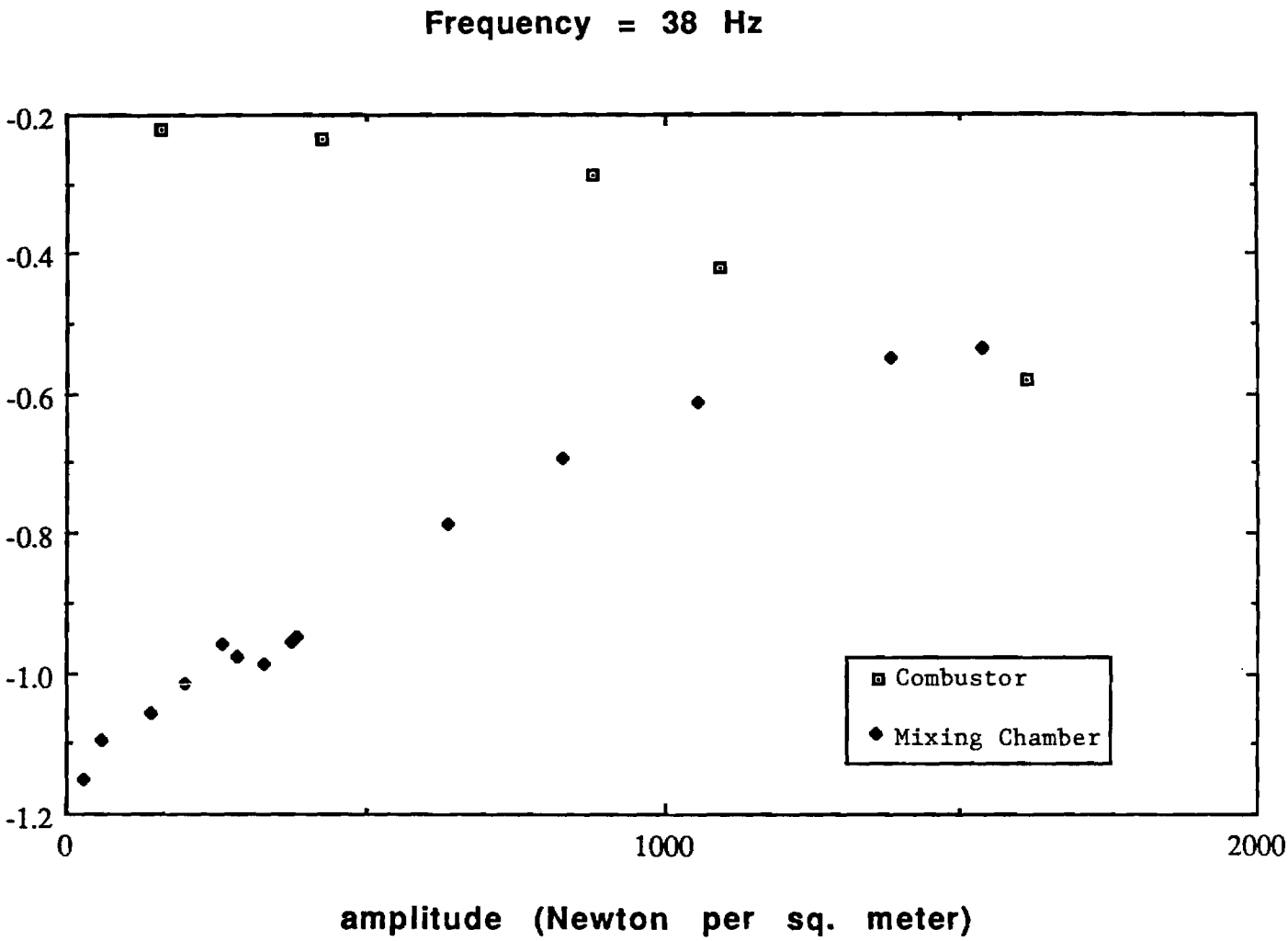

Fig. 42 Comparison of the Real Part of the Admittance as a Function of Pressure Amplitude for the Mixing Chamber Assembly only and for the Entire Helmholtz Combustor.

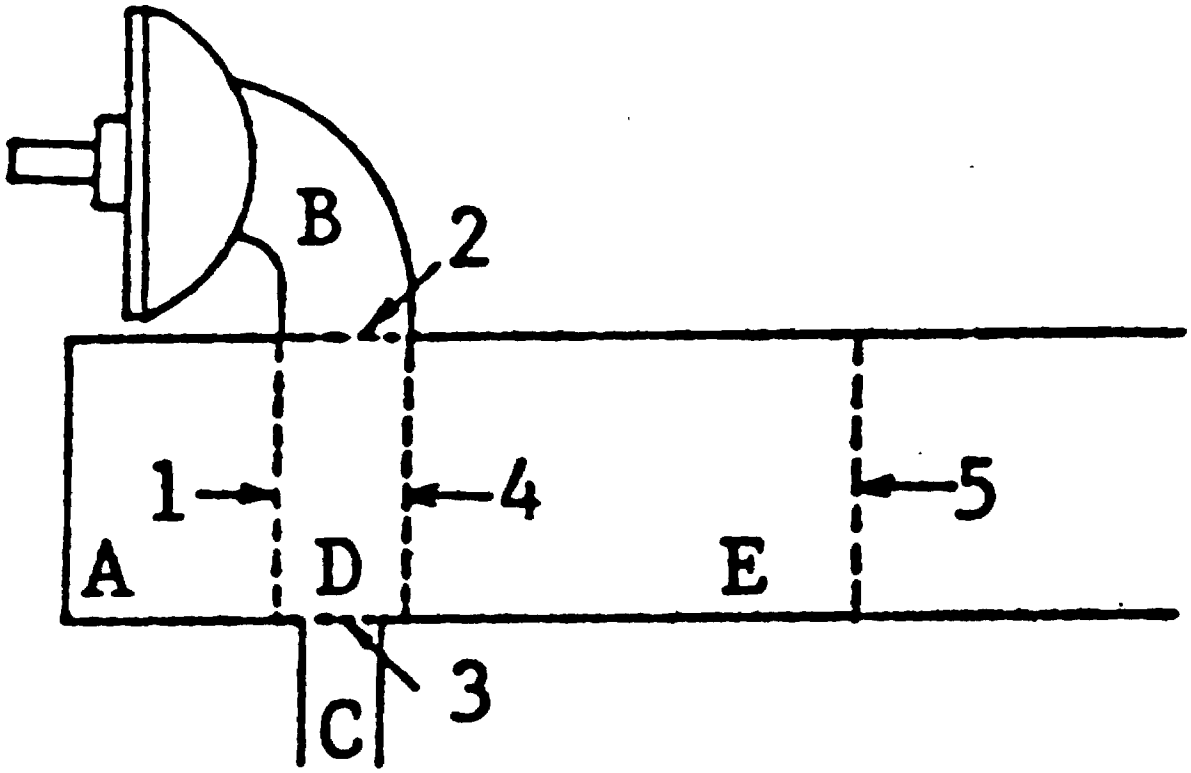

Fig. 43 Schematic Showing the Five Regions into which the Mixing Chamber Assembly has been Divided.

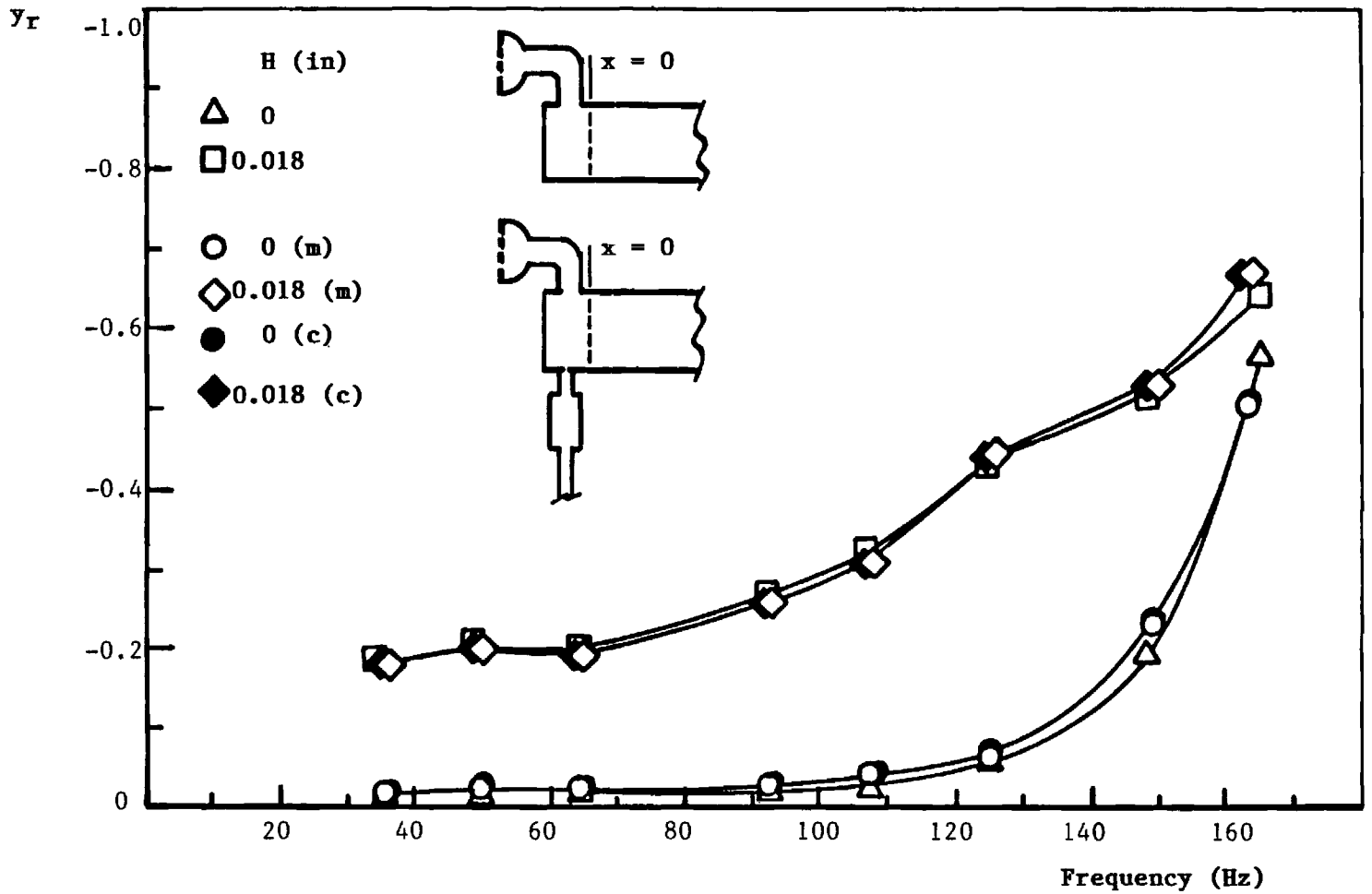

Fig. 44 Comparison between the Measured (m) and Calculated (c) Real Parts of the Admittance of the Mixing Chamber Assembly over a Range of Frequencies.

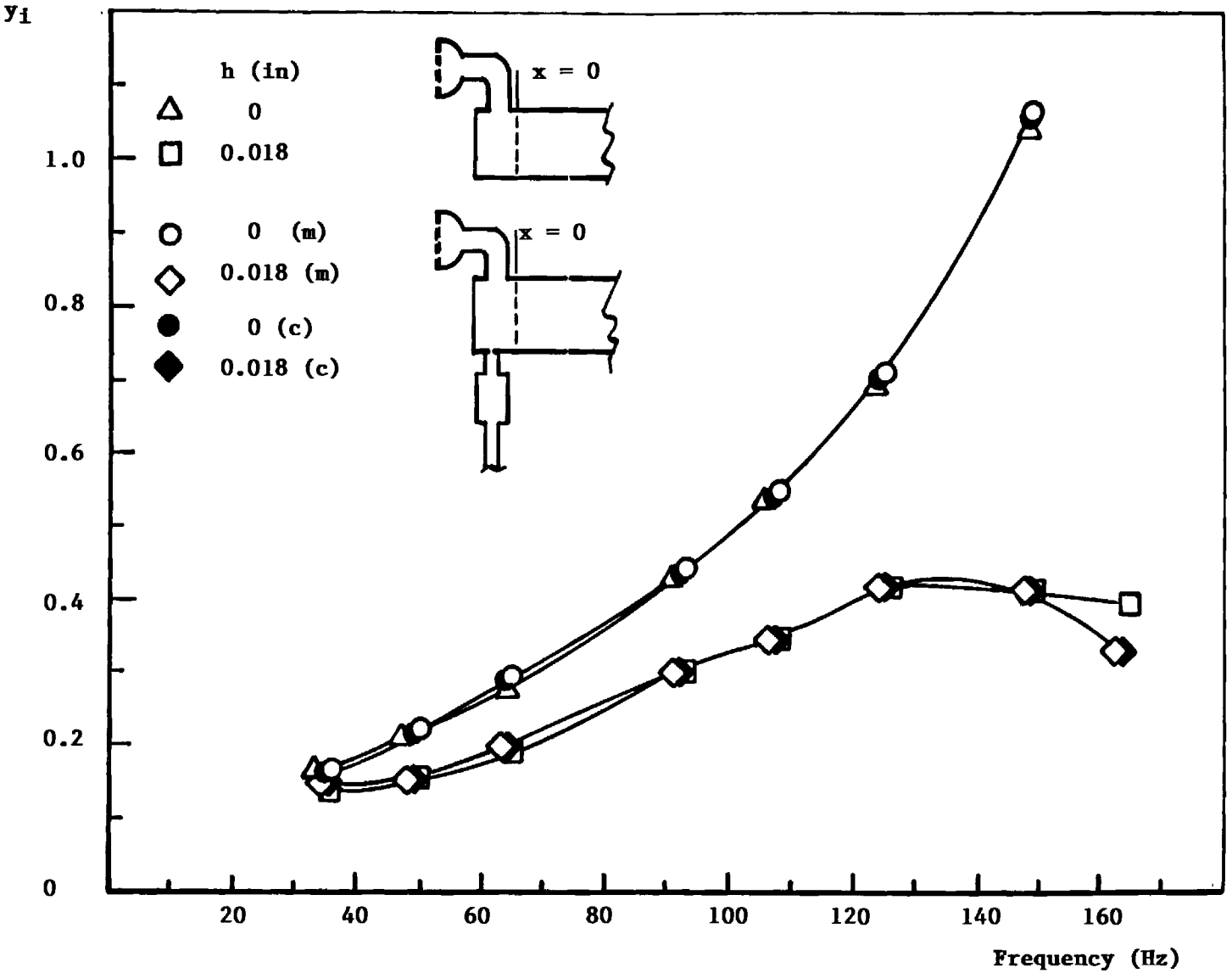

Fig. 45 Comparison between the Measured (m) and Calculated (c) Imaginary Parts of the Admittance of the Mixing Chamber Assembly over a Range of Frequencies.

GRI-91/0105

PULSATING BURNERS
CONTROLLING MECHANISMS AND PERFORMANCE

FINAL REPORT
(January 1, 1987 - June 30, 1991)

Gas Research Institute
8600 West Bryn Mawr Avenue
Chicago, Illinois 60631

Pulsating Burners - Controlling Mechanisms and Performance

Final Report

January 1, 1987 - June 30, 1991

Prepared by

J.I. Jagoda, B.R. Daniel and B.T. Zinn

School of Aerospace Engineering

Georgia Institute of Technology

For

Gas Research Institute

Grant No. 5087-260-1466

GRI Project Managers

James A. Kezerle and Thomas R. Roose

Combustion

June 1991

GRI DISCLAIMER

LEGAL NOTICE: This report was prepared by the Georgia Institute of Technology as an account of work sponsored by the Gas Research Institute (GRI). Neither GRI, members of GRI, nor any person acting on behalf of either:

a. Makes any warranty or representation, express or implied, with respect to the accuracy, completeness, or usefulness of the information contained in this report, or that the use of any apparatus, method, or process disclosed in this report may not infringe privately owned rights; or

b. Assume any liability with respect to the use of, or for damages resulting from the use of, any information, apparatus, method, or process disclosed in this report.

50272-101

REPORT DOCUMENTATION PAGE	1. REPORT NO. GRI-91/0105	2.	3. Recipient's Accession No.
4. Title and Subtitle "Pulsating Burners - Controlling Mechanism and Performance"			5. Report Date January 1991
			6.
7. Author(s) J.I.Jagoda, B.R.Daniel and B.T.Zinn			8. Performing Organization Rept. No. -
9. Performing Organization Name and Address School of Aerospace Engineering Georgia Institute of Technology Atlanta, Georgia 30332			10. Project/Task/Work Unit No. E-16-601
			11. Contract(C) or Grant(G) No. (C) 5087-260-1466 (G)
12. Sponsoring Organization Name and Address Gas Research Institute 8600 West Bryn Mawr Avenue Chicago, IL 60631			13. Type of Report & Period Covered Final Jan.'87-June '91
			14.

15. Supplementary Notes

16. Abstract (Limit: 200 words)

The objective of this study was to increase our understanding of the physical processes which control the mixing and heat release processes in valved, natural gas fired, pulse combustors. The effects of combustor geometry and heat transfer upon the performance of the pulse combustor were investigated. The flow and flame spread in the pulse combustor were visualized using high speed shadowgraphy and radical imaging, respectively. In addition, the flow field has been quantified using laser Doppler velocimetry. The resulting data were used to explain the dependence of the pulse combustor's performance upon the timing of the entry of the reactants and the complex interaction between the fuel and air jets. Furthermore, the reasons for the existence of lean and rich limits of operation were determined. Under a separate task, the acoustic characteristics of the various parts which make up a pulse combustor were determined using an impedance tube technique. Finally, an analytical scheme was developed which allows the calculation of the admittance of entire sections of the pulse combustor from measured admittances of its component parts.

17. Document Analysis a. Descriptors

Pulse Combustion

b. Identifiers/Open-Ended Terms

Performance, Flow Visualization, Reignition, Flame Spread, Limits of Operation, Admittance Measurements.

c. COSATI Field/Group Combustion

18. Availability Statement: Distribution Unlimited	19. Security Class (This Report) unclassified	21. No. of Pages
	20. Security Class (This Page) unclassified	22. Price

RESEARCH SUMMARY

Title: Pulsating Burners - Controlling Mechanisms and Performance

Contractor: Georgia Tech Research Corporation

Contract Number: 5087-260-1466

Reporting Period: January 1987- June 1990, Final Report

Principle Investigators: B. T. Zinn, B. R. Daniel and J. I. Jagoda

Objective: The objective of this study was to gain further insights into the detailed physical mechanisms which control the mixing and heat release processes in pulse combustors. In addition, the acoustic damping characteristics of various components and subsystems of the pulse combustor were to be determined over a range of operating conditions.

Technical Perspective: Natural gas fired pulse combustors have been on the market for a number of years. Nevertheless, their controlling mechanisms are still not sufficiently well understood to permit the design

of pulse combustors for different applications without resorting to costly trial and error development efforts. Proper operation of pulse combustors requires that the timing of the mixing, cycle to cycle reignition and flame spread processes produce oscillatory heat release in phase with the pressure oscillations. In addition, the thus generated driving must be sufficient to overcome the damping by the pulse combustor. To develop a rational design procedure for pulse combustors, it is necessary that the various processes responsible for energy addition to and removal from the pulsations be understood. Furthermore, data describing the acoustic properties of various pulse combustor components under different operating conditions are needed. Finally, the interaction between the acoustic characteristics of the various combustor components and the fundamental fluid mechanical, heat transfer and combustion processes must be understood.

Technical Approach: In order to elucidate the mechanisms which control the operation of a natural gas fired, Helmholtz type, pulse combustor and to determine the acoustic characteristics of different components and

subsystems which make up this pulse combustor, the following tasks were performed:

1) The flow field characteristics, mixing and heat release distributions in the pulse combustor were investigated using LDV, Schlieren, mixing visualization and radical radiation imaging.

2) The acoustic characteristics of various components and subsystems which make up the pulse combustor were measured using the impedance tube technique.

Results: A natural gas fired, valved, Helmholtz type, pulse combustor based upon an AGA design was studied. High speed shadowgraphy showed that the injection of the fuel jet leads the entry of the air jet by one quarter of a cycle. The latter creates large axial and transverse vortices in the mixing chamber. Comparison of the flow field with spatially and time resolved heat release measurements indicated that the order in which the reactants enter the combustor is critical to the spread of the combustion process through the mixing chamber. While the fuel jet begins to react with air left over from the previous cycle as soon as it enters the mixing chamber, the main ignition of the new fuel occurs near the combustor wall opposite of the fuel port. Combustion is then convected by the leading edge vortex of the air jet through the remainder of

the mixing chamber. It is this complex interaction between the fuel and air jets which stabilizes the combustion process in the mixing chamber. An increase in the combustor temperature by 30°K (54°F) was found to lower the lean limit of operation of the pulse combustor from a fuel air ratio (ϕ) of 0.64 to 0.55. However, the period of pulsations had to be extended or combustion air had to be supplied under pressure to extend its rich limit from ϕ = 1 to 1.3. This rich limit occurs near stoichometric conditions because no air is left over from the previous cycle. The combustion process is then confined to the time interval between the entry of the new air jet and the quenching of the reaction by the combustion products returning to the mixing chamber. For the standard AGA combustor this time is too short to permit sufficient heat release to drive the pressure oscillations. Further investigation of the importance of the timing between the heat release and the pressure oscillations revealed that at low operating frequencies (less than 25 Hz) the combustion process can excite higher pressure harmonics in the combustor unless the timing of the heat release is delayed. Furthermore, reduction of heat transfer to the combustor walls was found to significantly reduce the operating frequency of the device. The

results of ensemble averaged mean velocity and turbulence intensity measurements are used to qualitatively describe the complex, turbulent flow field in the mixing chamber at various instants during the cycle. These measurements are currently being completed by the graduate student as part of his Ph.D. thesis work. Under a separate task, an impedance tube technique was used to measure the acoustic characteristics (i.e., the admittance) of the fuel and air valves and of the mixing chamber fitted with both valves. These measurements indicated that, while the fuel valve behaves acoustically like a hard termination, the damping by the air valve increases with increasing frequency and valve opening and decreases with increasing pressure amplitude. Comparisons of the admittance measurements of the mixing chamber with those of the entire combustor showed that the damping by the Helmholtz volume formed by the combustion chamber overshadows the effect of the damping by the air flapper valve for the pulse combustor configuration under investigation. In addition to these measurements, an analytical scheme was developed which permits the determination of the admittance of the entire mixing chamber - valve assembly from the measured admittances of its component parts.

In summary:

- The detailed interactions between the flow field, the reignition and the flame spread during the cycle were determined
- The importance of the relative timing between the heat release and pressure fluctuations was investigated.
- The reasons for the existence of lean and rich operating limits for the Helmholtz type pulse combustor were established.
- The ensemble averaged velocity and turbulence intensity fields were quantified using laser Doppler velocimetry.
- The acoustic behavior of the pulse combustor and its component parts were determined.
- An analytic technique for predicting the acoustic damping by different combustor configurations from the acoustic characteristic of its component parts was developed.

Project Implications: This research has obtained important results and insights pertaining to pulse combustion. The knowledge gained in this contract is important to moving pulse combustion from an "art" to a science. The results explain the dependence of the pulse combustor's performance upon the timing of the reactant entry and the interaction among the fuel and air jets. Important fundamental data

characterizing the acoustics of pulse combustor components was obtained. These results will be used in models which are underway to describe pulse combustion. Additional pulse combustion research is being done at the Georgia Institute of Technology and at Forbes Energy Engineering, Inc. as part of the work scope for GRI's Pulse Combustion Engineering Research Laboratories. Pulse combustion continues to offer the potential for high efficiency with low NO_x emissions.

Thomas R. Roose
Principal Scientist, Engineering Sciences
Physical Sciences Department

TABLE OF CONTENTS

LIST OF FIGURES

INTRODUCTION

A recent increase in interest in pulse combustors has been driven by such advantages as high combustion and thermal efficiencies[1,2], excellent heat transfer characteristics[3,4] and low CO, NO_x[5] and soot emissions. Development of new pulse combustor applications has been hampered, however, by a lack of adequate understanding of the fundamental processes which control the operation of these devices. It was the purpose of this program to shed new light upon the mechanisms which control the operation of pulse combustors and to provide the designer with additional insight which would help him in the development of new and the scaling of existing pulse combustion devices.

The natural gas fired, valved, Helmholtz type, pulse combustor whose operating characteristics were investigated in this program is based upon an AGA design[6]. It is shown schematically in Fig. 1. The combustor consists of cylindrical mixing and combustion chambers, a tailpipe, a cylindrical decoupling chamber and a short vent pipe. Natural gas and air enter the combustor at right angle to each other through separate flapper valves attached to the curved side wall of the mixing chamber. During start up, the reactants are allowed to mix and are ignited using a spark plug. As the natural gas burns (a process which has previously been shown to take place primarily in the mixing chamber) the pressure in the combustor rises. This closes the flapper valves which prevents further reactants from entering the mixing chamber. This pressure rise also pushes the combustion products out through the tail pipe. The momentum

of the expelled exhaust gases causes the pressure in the mixing chamber to drop which reopens the flapper valves. New reactants now enter the combustor where they mix and are ignited by burning pockets of gas left over from the previous cycle. The cycle now repeats itself. Thus, pulse combustion operation can be maintained indefinitely without the use of the spark plug.

The gap in the fuel flapper valve is fixed while that in the air valve can be adjusted using a micrometer, see Fig. 2. The overall equivalence ratio in the pulse combustor is, therefore, varied by adjusting the air flapper valve setting which changes the air flow rate.

OBJECTIVES

It was the objective of this study to gain further insight into the fundamental processes responsible for the operation of pulse combustors in general and natural gas fired, valved, Helmholtz type, pulse combustors in particular. Emphasis was placed upon obtaining practical information which will permit designers to develop new and/or larger scale pulse combustors without resorting to costly trial and error based development efforts.

More specifically, the goal was to determine the effect of the combustor geometry and temperature upon its performance. In addition, the velocity, mixing and heat release distributions in the mixing and combustion chambers were measured both qualitatively and quantitatively and used to establish the nature of the interaction between

the combustion process and the acoustics of the combustor. This would lead to a physical explanation of the operating characteristics of the natural gas fired, valved, Helmholtz type, pulse combustor. In addition, the admittance of various components and subsystems which make up the pulse combustor were to be determined under a variety of operating conditions.

PROGRAM PLAN

The program is divided into two major tasks as outlined below:

Task I: Investigation of the Oscillatory Flow and Heat Release Fields and their Interaction in the Pulse Combustor

A. Performance Evaluation A limited number of measurements were carried out in modified, gas fired, valved, Helmholtz and Schmidt type pulse combustors in order to complement the performance studies carried out under a previous contract.

B. Shadow Visualization High speed shadowgraph cinematography was carried out parallel and normal to the axis of the combustor. These shadowgrams were then correlated in order to obtain a complete picture of the three-dimensional flow field in the pulse combustor.

C. Mixing Visualization An attempt was made to visualize mixing patterns photographically by heavily seeding one of the reactant flows and illuminating the combustor using an expanded laser sheet.

D. Spectroscopy Local and global heat release in the pulse combustor were determined by measuring the radical radiation emitted from the combustor. Instantaneous readings were ensemble averaged using the pressure signal as a clock. Planar spectroscopy using an intensified CCD camera resulted in local heat release measurements with excellent spatial and temporal resolution.

E. Laser Doppler Velocimetry Velocities were measured in the periodically varying, turbulent flow field at selected locations in the combustor. These velocities were then ensemble averaged which permitted the determination of mean velocities and turbulence intensities at various locations, at each instant during the cycle.

All Task I measurements were carried out in a pulse combustor whose mixing and combustion chambers were fitted with flat windows. The results from the different investigations outlined above were then correlated with each other and with the phase in the cycle at which they were obtained using the pressure oscillation as a clock. Such a coordination between the pressure, flow field and heat release measurements was

necessary to shed further light upon the fundamental processes which control the operation of the pulse combustor.

Task II: Admittance Measurements of Pulse Combustor Components

The acoustic admittances of various components and subsystems which make up a natural gas fired, valved, Helmholtz type, pulse combustor were measured using an impedance tube technique. These measurements yielded information on the frequency and amplitude dependances of the damping caused by the various pulse combustor subsystems. In addition, a methodology was developed which permits the designer to predict the damping in the pulse combustor from the acoustic properties of its component parts.

TECHNICAL PROGRESS AND RESULTS

Task I

Performance Evaluation:

This part of the study dealt with the investigation of the dependance of the performance of the pulse combustor upon the combustor geometry, the temperature in the combustion chamber and the relative duration and phase between the heat release and pressure oscillations.

Effect of the Combustor Geometry. The AGA based pulse combustor design[6] consists of a small diameter mixing chamber attached to a larger diameter combustion chamber, see Fig. 1 . This introduces a

step at the interface between the mixing and combustion chambers which has long been assumed to be critical for stabilizing the combustion process. This hypothesis was tested by constructing a pulse combustor with the same combustion chamber volume but without the step; i.e., a combustor whose mixing and combustion chamber diameters are equal. Tests revealed that the performance characteristics of the stepless pulse combustor are identical to those of the standard combustor. The combustion process in this type of pulse combustor is, therefore, not stabilized by the flow behind the backward facing step but by the complex interaction between the fuel and air jets in the mixing chamber.

Investigations under a previous contract[7] have shown that the Helmholtz type pulse combustor fitted with a standard tailpipe (i.e.,183 cm long) operates well for equivalence ratios between 0.61 and 1.03. When the tailpipe of the Helmholtz combustor was extended to 366 cm the rich limit of operation increased to an equivalence ratio 1.43. On the other hand, when the tailpipe was shortened to 69 cm the lean limit of operation was lowered to an equivalence ratio of 0.56. For tailpipes shorter than 69 cm the air supply had to be significantly pressurized in order to maintain the pulsation. If the pressurization was reduced the combustor switched from a pulsating to a non-pulsating mode of operation. The reasons for the existence of the limits of operation mentioned above will be addressed later.

Effect of Temperature upon Combustor Performance. The temperature in the pulse combustor was increased by insulating its

mixing and combustion chambers either externally or internally. When the combustor was externally insulated the temperature increased by approximately 30 °K (54 °F). Nevertheless, the kinetics of the combustion process were noticeably affected. For example, the CO level in the exhaust increased by 15%. However, the amplitude of the pressure pulsations remained unchanged. More importantly, the addition of thermal insulation lowered the lean limit of operation from an equivalence ratio of 0.64 to 0.55. The rich limit of operation was not affected by the increase in temperature. This suggests that the lean limit of operation of the pulse combustor is, at least in part, kinetically controlled. A more detailed explanation of the reason for the existence of the rich limit will be given later.

The temperature in the pulse combustor was increased by an additional 50 °K (90 °F) when the combustor was internally insulated using high temperature ceramic padding. However, the acoustic losses caused by this insulating material significantly decreased the amplitude of the pulsations. Since the mass flow rates of the reactants through the flapper valves depend upon the pressure amplitudes, the operating range of the pulse combustor was decreased. In some cases it was necessary to increase the gap in the air flapper valve and/or to pressurize the air supply to maintain the pulsations. In addition, it was noted that the internal insulation decreased the frequency of the pulsations. An analytical model currently being developed under a new program does, indeed, predict a dependence of the frequency of pulsation upon the rate of heat transfer to the walls of the combustor. More details of the effect of temperature upon the operating characteristics of the pulse combustor are given in Ref. 8.

Effect of Heat Release Duration and Timing. The effect of the relative timing between the heat release and pressure oscillations were investigated by varying the duration of the pressure cycle between 12 msec. and 67 msec. Both the Helmholtz and a Schmidt tube pulse combustors were used in this investigation. The Schmidt (or quarter wave) pulse combustor used the same fuel and air injection system as the Helmholtz pulse combustor. However, the mixing chamber, the combustion chamber and the tail pipe were replaced by a single, constant diameter pipe.

Tests showed that lengthening of the tailpipe of the Helmholtz combustor from 60 cm to 550 cm (24 in. to 217 in.) caused the pulsating frequency to decrease from 80 Hz to 24 Hz. At that point, the operating frequency of the combustor "jumped" to the tailpipe's first harmonic, i.e., 48 Hz, see Fig. 3a. If the tailpipe was further lengthened to 660 cm (260 in.), the frequency, once again, decreased from 48 Hz to 45 Hz. A similar trend was observed when the Schmidt pulse combustor was lengthened from 200 cm to 800 cm (79 in. to 315 in.) At 520 cm (205 in.) the frequency jumped from 20 Hz to 60 Hz, as shown in Fig. 3b. It should be noted that a "jump" to the higher harmonic of the Helmholtz combustor's tailpipe and of the Schmidt pulse combustor causes a doubling and tripling of the frequencies, respectively. However, if the mixing of the reactants and, therefore, the heat release process was delayed with respect to the pressure oscillations this frequency jump could be avoided. Such a delay could be introduced by moving the fuel injection port 7.5 cm (3 in.) downstream of its normal location.

The above phenomena is explained using Rayleigh's criterion which states that an oscillating heat release will drive pressure fluctuations if both are in phase. The timing and duration of the heat release due to the combustion process are determined by the injection of the reactants and their mixing. At relatively high frequencies, above 25 Hz, (i.e., short cycle durations) the heat release is primarily in phase with the fundamental mode of the combustor, as is shown schematically in Fig. 4a. If the frequency of pulsations is decreased below 20 Hz the cycle duration lengthens. The heat release is then confined to the early part of the fundamental pressure fluctuation (see Fig. 4b). However, the same figure also shows that the phase angle between the heat release and the first harmonic of the pressure oscillation is now closer to zero. Therefore, it is this harmonic that is excited. Finally, if the combustion process is delayed the phase angle between the heat release and the fundamental pressure oscillation is, once again, close to zero, see Fig. 4c. This causes the fundamental mode to be excited. This work is described in more detail in Refs. 8 and 9.

Finally, pressure amplitude measurements along the axis of the Schmidt pulse combustor indicated that as long as the air valve is in place this pulse combustor behaves like a true quarter wave tube even when the flapper valve gap is fully opened, see Fig. 5. However, once the air valve is completely removed the standing wave pattern is closer to that characteristic of a Rijke tube[10]. In that configuration the combustor is open at both ends, at the valve housing and at the downstream end, both of which are pressure nodes. Combustion takes place at approximately

one quarter of the combustor length from the air inlet. Since in the Rijke tube the length of the combustor represents one half of the acoustic wavelength, compared with one quarter of the wavelength in the Schmidt tube, the frequency of pulsations increases once the air valve is removed. This is discussed in more detail in Ref. 9.

Shadow Visualization

During a previous contract[7], the flow in the mixing chamber was visualized using high speed shadowgraphy through flat quartz walls at the end of the mixing chamber and the quartz transition between the combustion chamber and the tailpipe, see Fig 6. Briefly, a fast moving, highly turbulent fuel jet was seen to enter the mixing chamber followed by a wider, slower moving air jet, see Fig. 7. (Precise velocities will be discussed in the section on laser Doppler velocimetry.) The air jet impinges upon the fuel jet at approximately the same instant at which the latter reaches the mixing chamber wall opposite the fuel port. The leading edge vortex of the air jet then rapidly "scoops up" the fuel and sets up two, counter rotating vortices in the mixing chamber. Combustion occurs under conditions of intense, small scale turbulence and is nearly completed when the fuel for the next cycle enters the mixing chamber. Some of these shadow visualizations were repeated under different operating conditions during the present contract period. These tests indicated that the entry of the air jet is delayed as the fuel - air ratio in the combustor is increased.

In addition, the axial flow field in the pulse combustor was visualized using high speed shadow photography through the flat quartz windows in

the curved side walls of the mixing and combustion chambers, see Fig. 8. Particular attention was focused on the flow field in the mixing chamber and in the vicinity of the combustion chamber - tail pipe interface.

Since the air and fuel ports are located off axis, the flow field is not cylindrically symmetric. Once again, the high speed shadowgraphy showed that the fuel jet enters the mixing chamber shortly after the pressure there has passed through its maximum. Just before the pressure minimum is reached the air jet enters the mixing chamber. The addition of this air into the combustor increases the axial flow velocities further downstream in the mixing chamber. A little later, during the combustion phase of the cycle, a large, axial recirculation region forms in the mixing chamber. As the pressure maximum is reached the flow becomes axial again. Shortly thereafter, the new fuel jet enters and the cycle repeats itself.

High speed shadowgraphy was also carried out at the downstream end of the combustion chamber where the combustor connects with the tail pipe. As the pressure in the combustor decreases, combustion products from the tail pipe are seen to flow back into the combustion chamber. This backflow penetrates a distance of only two to three inches back into the combustor. As the acoustic pressure begins to rise again the flow reverses and reenters the tail pipe.

Mixing Visualization

Attempts were made to visualize the mixing process between the fuel and air as they enter the mixing chamber. For this purpose, the air jet

was heavily seeded with micron sized titanium dioxide particles while the fuel jet was left unseeded. As the reactants entered the mixing chamber, slices through this chamber were illuminated using vertical sheets of light produced by expanding the beam from a five watt argon ion laser using a cylindrical lens. The resulting light scattered by the particles in the flow was then recorded using a high speed camera capable of framing rates of up to 11,000 frames per second.

Unfortunately, the particle streak images obtained were not very clear. In spite of mirror generated, multiple traverses by the laser sheet through the mixing chamber not enough light was scattered by the particles to mark the film at framing rates above 2,500 frames per second. At these framing rates it was difficult to freeze the fast moving flow. In addition, seed particles remaining in the mixing chamber from previous cycles tended to obscure the details of the mixing flow field of the newly entering reactants. It was, therefore, decided to abandon this part of the investigation, at least until a more powerful pulsed laser, such as a copper vapor becomes available at this laboratory.

Spectroscopy

This investigation makes use of the fact that the intensity of spontaneously emitted CH, CC or OH radiation has been shown to be a measure of the local reaction rate[11]. Under a previous contract[7] the temporal oscillations of the overall reaction rate in the combustor were compared with those of the pressure. It was shown that the global radiation from the combustor fluctuates with the same frequency as the combustor pressure. The heat release fluctuations lead those of the

pressure by a phase angle which decreases as the equivalence ratio in the combustor is increased. As predicted by Rayleigh's criterion[12], this leads to an increase in sound pressure level in the combustor when the equivalence ratio is increased. At the same time it was shown that the combustion process never stops entirely during the cycle.

Under the present contract these experiments were extended to cover spatially as well as temporally resolved radiation measurements. A newly acquired intensified imaging system was used in these experiments. The radiation from the combustor is allowed to pass through a quartz window in the combustor wall before being focused through an interference filter onto an image intensifier. The intensifier is connected via an optical fiber bundle to the face plate of an 128 x 128 pixel CCD array. The array is read by an Omnicomp frame grabber and the data are transfered to the memory of a MicroVAX II workstation. The workstation is equipped with a 200 Mbite disk and a tape drive. The image intensifier can be gated which results in exposure times down to 50 nanoseconds, faster than necessary to freeze the fast, highly turbulent flow in the combustor. Images can be read and transfered at a rate of 200 frames per second from the array to the computer. In addition, up to four channels of scalars can be recorded simultaneously with the images. In these studies, the acoustic pressure signal was recorded and used to identify the instant during the cycle at which the image was obtained.

Once the images have been obtained they are manipulated using a wide range of software. Images are sorted, added, subtracted and averaged, contrasts are enhanced and contour maps are plotted using

false colors. Furthermore, the intensities recorded by selected, individual pixels during consecutive frames are plotted versus time. The frequency of any oscillations in these signals are determined by Fourier analysis and the phase angle between the fluctuations in the pixel intensities and the pressure signal are calculated. This allows the determination of the local driving of the pulsations by the combustion process using Rayleigh's criterion.

Local radical radiation and, therefore, heat release rates in the combustor were measured by imaging CC radiation through the flat quartz window at the upstream end of the mixing chamber. Images obtained at the same instants during consecutive cycles indicate that while the overall features of the flame shape are very similar at given instants during the cycle, the precise path over which the flame has spread varies somewhat from cycle to cycle. Figure 9 shows four frames which indicate the locations of the ignition and flame spread during one cycle in the pulse combustor. Each "frame" actually represents the average of 128 separate images obtained at the same phase during different cycles. The mechanism of flame spread is best illustrated by comparing the instantaneous flow fields and heat release distributions in Fig. 9. Early in the cycle (Fig. 9a), as the fuel jet enters the mixing chamber, it begins to react weakly with the air left over from the previous cycle. Main ignition of the new fuel occurs at the time and location where the fuel jet impinges upon the opposite wall, as shown in Fig. 9b. At that instant the new air jet has just reached the center of the mixing chamber. Shortly thereafter, the upper part of the leading mushroom vortex of the air jet entrains the reacting fuel which intensifies the combustion process and

spreads it throughout the upper part of the mixing chamber(Fig. 9c). Only after a pair of counter-rotating vortices have established themselves does the flame spread throughout the entire mixing chamber, as shown in Fig. 9d.

In order to quantify the flame spread in the mixing chamber, software was developed which permits the calculation of the phase angle between the maximum heat release rate at every location and the maximum pressure. The distribution of these phase angles then gives an indication of the instantaneous shape of the flame and of its spread through the combustor. Figure 10 shows a contour plot obtained using this technique. The numbers indicate the phase by which the local heat release leads the pressure. The flame, thus, spreads from the upper left hand side of the mixing chamber, opposite the fuel port, towards the lower left hand side and, finally, towards the right hand side of the mixing chamber into the region between the fuel and air ports.

These results indicate that, for the present valve configuration, it is essential that the fuel enter the mixing chamber prior to the air jet. Otherwise the momentum of the air jet would prevent the fuel jet from penetrating significantly into the mixing chamber. This would result in poor mixing of the fuel and air. At the same time, a different fuel and air port configuration or dual fuel inlets would, probably, result in a quicker, more uniform distribution of the combustion process in the mixing chamber. The results of these heat release measurements are discussed further in Refs. 13 and 14.

Laser Doppler Velocimetry

Velocity measurements in the mixing chamber were carried out using a two component LDV system based on a five watt argon ion laser. The results of the flow visualization experiments had indicated that reverse flow exists in the mixing chamber. Therefore, Bragg cells were incorporated into both components of the system. Because the flow in the combustor is periodic, mean flow velocities and turbulence intensities at different instances during the cycle had to be determined using conditional sampling. This was achieved by detecting the start of each cycle which was taken to be the positive zero crossing of the pressure signal. Each cycle was then divided into 60 equal time intervals based upon the previously obtained operational frequency of the combustor. Finally, the data were sorted into the relevant bins according to their time of arrival during the cycle. Ensemble averaged mean and RMS velocities were, thus, obtained at 60 equally spaced instances during the cycle.

Early tests of the performance of the LDV indicated that the system and its data reduction software produced reproducible mean velocities which were in good agreement with quantitative observations from the flow visualization[15]. However, the apparent level of turbulence, as measured by the RMS value of the conditionally sampled velocities, was considerably higher than that observed in other turbulent flows, (e.g. in the turbulent shear layer behind a backward facing step). It is important to realize that it is possible that only a part of this RMS may be due to true turbulence. Since the values of the velocity fluctuations were obtained by ensemble averaging, they may contain contributions due to 1) the finite width of the slots into which each cycle was divided; 2) the

slight variations in the flow field from cycle to cycle; and 3) slight variations in the combustor frequency during the experiment. In order to eliminate at least the effect of variations in the operating frequency of the combustor the data reduction software was modified. In the updated data reduction routine the pulse duration for each cycle was determined from the actual pressure oscillations measured during the experiment rather than from a previously determined mean frequency.

Typical spatially and temporally resolved mean velocity and turbulence intensity data in the axial (u) and vertical (v) directions are shown in Figs. 11 through 29. Figure 11 shows the locations at which these LDV data were obtained. All measurement points lie in a plane which bisects the right angle between the fuel and air injection ports, equi-spaced along lines which are normal to the axis of the combustor. Each measurement location is labeled (m,n) where m represents the number of the line counting from the flat end of the mixing chamber and n denotes the point number on this line counting from the curved wall of the chamber opposite to the fuel and air ports.

Each of the velocity and turbulence intensity figures represents one cycle starting at the negative zero crossing of the pressure signal; i.e., at an instant after the fuel has started to enter but before the air has entered the mixing chamber. Figures 12 through 23 represent velocity and turbulence intensity traces at each of the ten points along one measurement line; i.e., along a given value of m. For greater clarity, each of these figures consists of three plots one of which also shows the pressure signal for reference. Figures 24 through 29 show a different

representation of the same data which is more qualitative but conveys a better physical picture of the variation of the complex flow field in the mixing chamber during a cycle. These are three - dimensional "carpet plots" in which one axis represents the location of the measurement station along a given measurement line, the second axis represents the normalized time (i.e., 0 to 1 for one cycle) and the third axis shows either the u or v components of the velocity. This results in two carpet plots (one for u and one for v) for each value of m.

Figures 24, 25 and 26 show the carpet plots of the vertical velocities for the three measurement lines closest to the closed, upstream end of the mixing chamber. These are best analyzed in conjunction with the instantaneous velocity vs. time plots in Figs. 12, 13 and 14. Large positive (upward) velocity peaks are seen early in the cycle along all three lines. At m = 3, which lies in the paths of the fuel and air jets, (Fig. 26) the maximum velocity is 22 m/s (73 ft/s) which occurs very early in the cycle, near the center of the mixing chamber (n = 4 to 7). Further upstream, at m = 1 and 2 (Figs 24 and 25), the velocities peak at 8 m/s (26 ft/s). These maxima occur later, and are confined to locations n = 9 and 10, which lie within 12 mm (0.5 in.) of the curved mixing chamber wall between the fuel and air ports. Immediately following the peak at m = 3 and coincident with the peaks at m = 1 and 2, deep, wide and wide valleys (downward velocities) are seen near the center of all three measurement lines. The early peak at m = 3 is caused by the entry of the fuel jet which results in an upward component of velocity, close to 22 m/s (73 ft/s). The valley observed later in the cycle is due to the downward component of velocity of 18 m/s (59 ft/s) caused by the entering air jet.

Since the positive peaks along m = 1 and 2 occur at the same instant in the cycle as the valley they must be due to the leading edge vortex of the air jet observed in the flow visualization. Later in the cycle the flow near the wall opposite to the inlet ports is generally upward while that near the ports is directed downward. This suggests the existence of a large vortex in the plane normal to the axis of the combustor.

The time dependence of the instantaneous axial velocities and their carpet plots at the same locations are shown in Figs. 15 through 17 and 27 through 29, respectively. Early in the cycle, when the fuel jet enters the mixing chamber, a significant downstream velocity directed towards the combustion chamber is observed. These positive velocity peaks are particularly large, up to 8 m/s (26 ft/s), along lines m = 2 and 3 (Figs. 16 and 17), where the effect of the fuel jet is felt most strongly. It is also confined to an area within 20 mm (.8 in.) of the curved mixing chamber wall opposite the injection ports. This wall deflects the incoming jet. In addition, the initial combustion process and the associated expansion of the combustion products are concentrated in this area. Shortly thereafter, the air jet enters the mixing chamber. It has very little effect upon the axial velocities along the line m = 3 which coincides with the centerline of the jet. However, at locations m = 1 and 2 large valleys representing upstream velocities of up to 7 m/s (23 ft/s) can be seen. These are formed by the leading edge vortex of the incoming air jet which has an upstream component of velocity. After this vortex has passed, a small upstream velocity, of the order of 2 m/s (7 ft/s), continues to be observed. This flow causes the acoustic pressure in the mixing chamber to increase. As the acoustic pressure approaches its maximum the flow

reverses direction and the combustion products exhaust towards the combustion chamber for the remainder of the cycle.

The instantaneous turbulence intensities for all measurement lines are plotted versus phase in the cycle in Figs. 18 through 23. Early in the cycle the turbulence levels at all locations are relatively low (u_{RMS} = 3 m/s, 10 ft/s). At the central locations (n = 3,4,5 and 6) along the lines m = 2 and 3, which lie directly in the path of the fuel jet, the turbulence intensity increases as soon as this jet enters the mixing chamber to a value of u_{RMS} close to 8 m/s (26 ft/s). At all other locations the turbulence intensity does not significantly increase until the entry of the air jet is detected in the mean velocities. The turbulence levels then remain close to u_{RMS} = 6 m/s (20 ft/s) for part of the cycle and then slowly drop to their initial values.

These LDV measurements are presently continuing as part of the Ph.D. thesis work of the graduate student responsible for this work. Velocity measurements in the mixing chamber will be completed and velocity measurements at the combustion chamber - tailpipe interface will be added. The complete set of velocity results will then be submitted for publication to a suitable journal and as a "Topical Report" to GRI.

Rich Limit of Pulse Combustor Operation

As mentioned in the section dealing with performance measurements, the Helmholtz type pulse combustor fitted with the standard, 163 cm (64.2 in.) long tail pipe has a rich limit of operation at an equivalence ratio of 1.03. This limit exists even though the pulse combustor appears to be operating near its optimal condition immediately before this limit is reached. This operational limit can, however, be

extended if the tail pipe is lengthened; i.e., the period of the pulsations is prolonged, or if the combustion air is supplied under pressure[13]. Based upon the results of the measurements discussed above, the following mechanism appears to control this rich limit.

In order to attain pulse combustion, the driving of the pulsations by the combustion process must overcome the acoustic damping due to, for example, viscous dissipation and acoustic radiation from the combustor. A limit of operation of the pulse combustor occurs if this balance between the driving and damping processes fails to materialize. According to Rayleigh's criterion, the driving by the combustion process can be quantified by the Rayleigh efficiency[16] η which is defined by

$$\eta = \frac{R}{C_P \bar{P}\bar{Q}} \int_0^1 P' Q' \, d\tau \approx \frac{|P||Q|\cos\theta}{C_P \bar{P}\bar{Q}}$$

where P and Q are the total pressure and combustion heat release rate, θ is the phase angle between the pressure and the heat release rate oscillations, R and C_p are the ideal gas constant and the specific heat at constant pressure, respectively, and τ is the time normalized by the duration of one cycle. Bars, primes and brackets represent the steady state, oscillating components and amplitudes of the indicated quantities, respectively.

Figure 30 shows the variation of the Rayleigh efficiency of the combustor fitted with a standard tailpipe and an extended tailpipe as a function of equivalence ratio, ϕ. The maximum ϕ at which each curve stops

represent the rich limit of operation for each configuration. Clearly, near the lean limit, at ϕ = 0.55, the driving is small, just enough to overcome the damping in the system. In contrast, near the rich limit for the combustor fitted with a standard tailpipe, at ϕ = 1.03, the driving is close to its maximum. Thus, the mechanism which controls this rich limit appears fundamentally different from that which is responsible for the lean limit.

The Rayleigh efficiencies presented in Fig. 30 were calculated from the measured fluctuations of pressure and heat release and the phase angle between them. The dependences of these three variables upon the equivalence ratio in the combustor are shown in Figs. 31 and 32. The amplitudes of both, the pressure and heat release fluctuations reach their maxima near stoichometric conditions, at ϕ = 0.98. The phase angle by which the heat release leads the pressure, on the other hand, decreases with increasing equivalence ratio until it asymptotically reaches a constant value which depends upon the length of the tailpipe.

In order to understand the combustor behavior described above, it is helpful to consider the relative phases of the pressure and radiation oscillations and the instants of fuel and air injection. Figure 33 shows one normalized period of oscillation for both rich and lean operating conditions. The arrows indicate the instants at which fuel and air jets enter the mixing chamber. Horizontal lines at the top of the figure indicate those parts of the cycle when the combustion products move away from or towards the mixing chamber where most of the combustion process occurs. Finally, the points marked "X" indicate the instants at which the new fuel charges reignite, as indicated by the increase in the radiation

signal. All this information is based upon the high speed shadowgrams, pressure and CC radiation measurements described above.

Figure 33 indicates that for lean operation the new fuel ignites before the new air enters the mixing chamber. This is possible since there is air left over from the previous cycle. As the equivalence ratio is increased, less air is available from the previous cycle and ignition is delayed until, under stoichometric conditions, ignition of the fuel jet must await the entry of the air jet. Since the oscillations of heat release always lead those of pressure, the phase angle between the two decreases from 60° to 30° as the equivalence ratio is decreased, see Fig. 32. Since with decreasing phase angle the pressure and heat release fluctuations are more in phase, the Rayleigh criterion causes the pressure amplitudes in the combustor increase from 165 dB to 169 dB when the equivalence ratio is increased from 0.55 to 0.98, as observed in Fig. 31.

The rich limit of operation can now be explained with the aid of Fig. 33. The time available for the reactants to mix and burn is limited to the time interval between the instants when the new fuel charge ignites and when the reaction is quenched by the combustion products returning from the combustion chamber to the mixing chamber. If ignition is sufficiently delayed this time interval is too short and not enough heat is released to drive the pulsations. This occurs at the rich limit.

When the duration of the cycle is prolonged by extending the tailpipe the time available for combustion is increased and the rich limit is extended beyond $\phi = 1.3$. A similar result is obtained if ignition of the new

fuel is advanced by forcing the air to enter earlier or if mixing is improved by injecting the air jet under pressure. Conversely, delaying the entry of the air jet by, for example, extending the pipe which connects the air valve to the mixing chamber reduced the rich limit to an equivalence ratio of less than one. A more detailed description of this part of the work is given in Refs. 6 and 7.

Task II

In this task, the impedance tube technique[19] was used to measure the admittances (i.e., the complex ratio between the acoustic velocity and pressure) of different pulse combustor components. The admittance is a complex quantity which describes the acoustic behavior of the system. As discussed later, if the real part of the admittance is positive the system drives the acoustic pressure oscillations, if it is negative the system damps. All components which make up the pulse combustor damp the pressure oscillations in the absence of combustion. Therefore, the measured, real part of the admittance of the cold combustor provides an indication of how much driving the combustion process will have to provide to assure pulse operation.

In the impedance tube set-up, the investigated component is attached to one end of a long tube, see Fig. 34. An electro-pneumatic, acoustic driver is attached to the wall just upstream of the opposite, open end of the tube. The acoustic driver is used to excite an incident acoustic wave which moves towards the tested component. The interaction of this wave with the investigated sample produces a reflected wave with

modified amplitude and phase. The incident and reflected waves combine to establish a standing wave in the impedance tube. A piezo-electric pressure transducer mounted near the tested sample measures the acoustic pressure amplitude at the upstream end of the tube. A second pressure transducer, mounted at the end of a long rod, is translated inside the tube to measure the axial variation of the standing wave pressure amplitude along the impedance tube.

When measuring the admittance of a hard termination (i.e., zero admittance), the incident wave is reflected without a change in amplitude or a shift in phase. In this case, the combination of incident and reflected waves produces a standing wave with a zero-amplitude pressure minimum located one quarter of the wavelength ($\lambda/4$) from the hard termination, see Fig. 35a. On the other hand, if the complex admittance of the termination is non-zero, see Fig. 35b, the minimum pressure amplitude is non-zero and it occurs at a location other than $\lambda/4$ from the tested sample. Physically, the termination changes the pressure amplitude of the reflected wave and introduces an apparent change in the length of the pipe by introducing a phase shift in the reflection process. The measured values of P_{max}, P_{min} and the distance of P_{min} from the tested sample can be used to determine the real and imaginary parts of the admittance of the termination and, thus, of the component under investigation. A more detailed analysis shows that the real part of the admittance, which is calculated from the difference between the maximum and minimum pressure amplitudes (i.e., $P_{max} - P_{min}$) determines the damping (or driving) provided by the component under investigation. On the other hand, the imaginary part of the admittance

provides information which affects the frequency of the system which utilizes the tested component.

The above described technique was used to measure the real and imaginary parts of the admittances of different pulse combustor components under cold and "hot" operating conditions. Admittance measurements under cold conditions were completed as part of this project. The system was also prepared for measurements with combustion under the present program but most actual measurements were carried out under a new contract.

The admittances were measured under cold flow conditions for the following configurations: (1) a hard termination at the end of the impedance tube; (2) the gas valve and its decoupler at the end of the tube; (3) the air valve at the end of the tube; (4) the mixing chamber fitted with the air valve only; and (5) the mixing chamber fitted with both the fuel and the air valves. The air valve opening was varied between 0 and .018 inches for configurations 3, 4 and 5. In these tests the acoustic driver was set to generate sound pressure levels of approximately 160 dB near the tested component. This corresponds to typical dB levels in pulse combustors. Furthermore, the driving frequencies were varied between 20 and 170 Hz. In addition, the admittance of the air flapper valve and of the entire pulse combustor including valves, mixing and combustion cambers were measured as a function of amplitude. All tests were carried out at mean pressures in the impedance tube equal to the previously determined boost pressure in the pulse combustor.

Before presenting the obtained results, it would be helpful to consider Fig. 36. It shows the dependence of the real part of the admittance upon ΔP (i.e., $P_{max} - P_{min}$). Clearly, when the magnitude of the real part of the admittance (i.e., Y_r) is small, the value of Y_r is relatively insensitive to the accuracy of the measurement of ΔP. However, as the magnitude of Y_r increases, the sensitivity of the Y_r to the measured ΔP increases rapidly. Thus, the error in the determined Y_r increases with increasing value Y_r. In addition, while the real part of the admittance depends largely upon the value of ΔP, the value of the imaginary part of the admittance is primarily determined by the location of P_{min}. Since the standing pressure wave has a relatively flat minimum at 40 Hz, which is the operational frequency for the pulse combustor under investigation, it was easier to determine the value of the minimum than its location. The real parts of the admittances were, therefore, measured with better accuracy than their imaginary parts.

The real parts of the admittances for the above configurations with the air valve (when included) closed and open (to .012 inches) measured over a 20 to 170 Hz frequency range are shown in Fig. 37. An air valve opening of .012 inches was selected since it corresponds to a typical setting for the pulse combustor under normal operating conditions. Both, the hard termination and the fuel flapper valve with its decoupling chamber showed no damping over the entire range of investigated frequencies (i.e., $Y_r = 0$). This indicates that the fuel valve orifice behaves, essentially, like a solid surface.

For all of the tested configurations which contain an air flapper valve Y_r is essentially zero at low frequencies as long as the air valve is closed. As the frequency is increased, Y_r and, thus, the damping by the air valve and its housing increases until it becomes quite significant at high frequencies. The real part of the admittance is increased even further if the closed air valve is attached via an elbow to the mixing chamber. On the other hand, adding the fuel valve to the mixing chamber - air valve assembly has no significant effect upon the admittance at any investigated frequency. This provides further indication that the fuel valve behaves like a solid surface.

Figure 37 also shows that opening the air valve substantially increases the real part of the admittance over the entire range of investigated frequencies. Once again, the effect of attaching the air valve housing to the side of the mixing chamber is significantly greater than adding the fuel valve to the mixing chamber - air valve assembly. The increase in the real part of the admittance with increasing air valve opening is illustrated in more detail in Fig. 38 for a range of valve openings and driving frequencies for the mixing chamber fitted with both valves.

The variation of the measured imaginary part of the admittance (i.e., Y_i) for these configurations over the 20 to 170 Hz frequency range are shown in Fig. 39. Once again, Y_i is zero for the hard termination as well as for the fuel valve only. However, once the closed air valve was added to any of the three investigated configurations the imaginary part of the admittance increased substantially. The latter effect increased with

increasing frequency. This occurred because adding the valve assembly moves the termination, in the form of the valve plates, further away from the end of the impedance tube, see Fig. 40. The minimum of the standing pressure wave in the impedance tube was, therefore, moved upstream resulting in an increase in Y_i. Because of the size of the mixing chamber and the elbow that connects the air valve to it, this effect is more pronounced for the valve - mixing chamber assembly than for the air valve alone.

Once the air valve is opened the pressure anti-node moves away from the valve plates towards the driver end of the impedance tube, see Fig. 40. (If the valve plates are completely removed the resulting open end corresponds to a pressure node). This causes the decrease in the magnitude of Y_i observed in Fig. 39. Because of the above discussed difficulty in determining the precise location of the minimum of the standing pressure wave, no clear difference between the imaginary part of the impedance of the air valve only and that of the valve - mixing chamber assembly could be established. However, Fig. 41 clearly shows that the magnitude of Y_i decreases as the opening of the air valve increases. This effect is particularly pronounced at higher frequencies. The lack of smoothness of the curves is, once again, due to the difficulty in determining the precise location of the flat minimum of the standing wave. More details of these results are given in Ref. 20.

Additional admittance measurements were carried out in which either the mixing chamber with its valves or the entire combustor consisting of mixing and combustion chambers and the flapper valves

were attached to the impedance tube. In these tests, the admittances were measured as a function of applied sound pressure level for a given air valve opening. Figure 42 shows that for the mixing chamber assembly only the damping decreases with increasing sound pressure level. Since it has been shown that the only significant acoustic losses in the mixing chamber assembly occur in the air flapper valve it can be concluded that it is the damping in the air valve that decreases with increasing acoustic excitation. However, the damping of the entire combustor (including the combustion chamber) increases with increased applied sound pressure level, as shown in Fig. 42. This suggests that the damping in the Helmholtz volume formed by the combustion chamber overshadows the effect of the damping in the air flapper valve for this pulse combustor configuration.

In addition to the above detailed measurements an analytical scheme was developed which permits the determination of the admittance of the entire mixing chamber - valve assembly from the measured admittances of its component parts. As shown in Fig. 43, the assembly was divided into five sections. The admittance at location "1" was calculated from that of the solid wall (Y = 0) which closes the upstream end of the mixing chamber using a transfer function. The admittance at "2" was determined from the measured admittance values of the valve. The admittance at "3" was taken to be zero since the fuel valve had been shown to behave like a solid surface. The acoustic mass conservation equation was then applied to the control volume bounded by interfaces 1,2,3 and 4 to calculate the admittance at "4" from the admittances at the other interfaces. Finally, the admittance at "5" was calculated from that at "4" using a transfer function. Details of these calculations are given in Ref. 20. The results of these

calculations for different valve openings and over a range of frequencies are compared with the experimentally measured values of the real and imaginary parts of the admittance of the mixing chamber - valve assembly in Figs. 44 and 45. Clearly, the agreement is excellent.

At the end of this contract the impedance tube set up was modified to accommodate tests with combustion. Because of heat transfer to the impedance tube wall a temperature gradient existed along the axis of the impedance tube. A measurement technique was developed to determine the temperature gradient using thermocouples and the classical impedance tube theory was modified to account for it. The actual measurement of the driving by the unsteady combustion process was initiated and completed under a new contract.

Publications

Apart from the semiannual and annual reports specified in the contract, the following papers were presented and published during the contract period:

"Dependence of Pulse Combustion Performance upon Interior Temperature, Acoustic Losses and Combustion Time", X.C. Cheng, B.R. Daniel, J.I. Jagoda and B.T. Zinn, International Gas Research Conference, Tokyo, Japan, November, 1989.

"Dependence of Pulse Combustor Frequency upon Combustion Process Timing", X.C. Cheng, B.R. Daniel, J.I. Jagoda and B.T. Zinn, Twelfth Annual Energy Sources Technology Conference and Exhibition, Fossil Fuels Combustion Symposium, PD-Vol. 25, pp 39-42, Houston, TX, January, 1989.

"Radiation Measurements in a Gas Fired Pulse Combustor", S.H. Ku, X.C. Cheng, B.R, Daniel, J.I. Jagoda and B.T. Zinn, Proceedings of the Spring Technical Meeting, Central States Section of The Combustion Institute, Chicago, IL, May, 1987.

"The Interaction between Fluid Mechanics and Combustion in a Helmholtz Type Pulse Combustor", J.M. Tang, B.R. Daniel, J.I. Jagoda and B.T. Zinn, Fall Technical Meeting, Eastern Section of The Combustion Institute, Orlando, FL, December, 1990.

"Frequency Modeling and Velocity Measurements in Gas Fired, Valved Pulse Combustors", S.H. Ku, B.R. Daniel, J.I. Jagoda and B.T. Zinn, Fall Technical Meeting, Eastern Section of The Combustion Institute, Clearwater Beach, FL, December, 1988.

"Flame Spread and Limits of Operation of Gas Fired, Mechanically Valved Pulse Combustor", S.H. Ku, B.R. Daniel, J.I. Jagoda and B.T. Zinn, Poster at the Twenty-Second Symposium (International) on Combustion, Seattle, WA, August, 1988.

"Controlling the Rich Limit of Operation of Pulse Combustors", J.M. Tang, S.H. Ku, B.R. Daniel, J.I. Jagoda and B.T. Zinn, Twenty-Third Symposium (International) on Combustion, Orleans, France, August 1990, (in print).

"The Acoustic Characteristics of Pulse Combustor Flapper Valves and Mixing Chambers", D. Xu, B.R. Daniel, J.I. Jagoda and B.T. Zinn, Thirteenth Annual Energy Sources Technology Conference and Exhibition, Fossil Fuel Combustion Symposium, PD-Vol. 30, pp 21-28, New Orleans, LA, January, 1990.

CONCLUSIONS

The physical mechanisms which control the performance of a natural gas fired, valved Helmholtz type pulse combustor were investigated. Comparison of flow and flame spread visualization indicated that the fuel jet enters the mixing chamber ahead of the air jet. Under lean operating conditions the fuel begins to react as soon as it enters the combustor. Main ignition occurs once the fuel is scooped up by the leading edge vortex of the air jet. Combustion then spreads by the convection of this vortex throughout the mixing chamber. It is this complex interaction between the fuel and air jets entering the mixing chamber which stabilizes the combustion process. The lean limit of operation of the pulse combustor could be extended by reducing the heat losses to the combustor walls while its rich limit was increased by reducing the pulsation frequency or supplying the combustion air under pressure. The rich limit of operation near stoichometric conditions exists because of the limited time available for combustion during the cycle if no air from the previous cycle is available for early ignition. In addition to the visualization experiments the flow field is currently being quantified by laser Doppler velocimetry.

Under a separate task the acoustic characteristics of the air flapper valve were determined by an impedance tube technique. In addition, an analytical scheme was developed which allows the determination of the admittance of entire sections of a pulse combustor from the measured admittances of its component parts.

In summary:

- The detailed interactions between the flow field, the reignition and the flame spread during the cycle were determined
- The importance of the relative timing between the heat release and pressure fluctuations was investigated.
- The reasons for the existence of lean and rich operating limits for the Helmholtz type pulse combustor were established.
- The ensemble averaged velocity and turbulence intensity fields were quantified using laser Doppler velocimetry.
- The acoustic behavior of the pulse combustor and its component parts were determined.
- An analytic technique for predicting the acoustic damping by different combustor configurations from the acoustic characteristic of its component parts was developed.

REFERENCES

1. "Lennox-Pulse-G14 Series Up-Flo Gas Furnaces," Engineering Data, Heating Units, Gas, pp. 21-24, published by Lennox Industries, Inc.

2. Hydropulse by Hydrotherm," information about pulsed combustion water hearing published by Hydrotherm, Rolfland Ave., Northvale, NJ 07647

3. Hanby, V. I.: "Convective Heat Transfer in a Gas-Fired Pulsating Combustor," Paper No. 68-WA/FU-1, 1968.

4. Fedorov, B. N.: "Experimental Study of the Effect of Acoustic Oscillations on Heat Transfer in a Gas Flow", Juzherno-Fisicherkii Zhurnal, 32, No. 1, pp. 167-180, 1977.

5. Belles, F. E.: "R & D and Other Needs for Exploitation of Pulse-Combustion in Space-Heating Applications," Proceedings of the Symposium on Pulse Combustion Technology for Heating Applications, Argonne National Laboratory, pp. 167-180, 1979.

6. Corliss, J. M, Battelle Columbus Laboratories : Annual Report, Gas Research Institute Report GRI 85/0029, April, 1985.

7. Reuter, D., Daniel, B. R., Jagoda, J. I. and Zinn, B. T.: Combustion and Flame, 65, pp. 281-290, 1986.

8. Cheng, X.C., Daniel, B.R., Jagoda, J.I. and B.T. Zinn, B.T.: "Dependence of Pulse Combustion Performance upon Interior Temperature, Acoustic Losses and Combustion Time", presented at the International Gas Research Conference, Tokyo, Japan, November, 1989.

9. Cheng, X.C., Daniel, B.R., Jagoda, J.I. and B.T. Zinn, B.T.: "Dependence of Pulse Combustor Frequency upon Combustion Process Timing", presented at the Twelfth Annual Energy Sources Technology Conference and Exhibition, Fossil Fuels Combustion Symposium, PD-Vol. 25, pp 39-42, Houston, TX, January, 1989.

10. Miller, N., Carvalho, J.A., Daniel, B.R. and Zinn, B.T.: Proceedings of the Nineteenth Symposium (International) on Combustion, pp. 1197-1203, 1982.

11. Gaydon, A. G. and Wolfhard, H. T.: "Flames," Chapman, R. and Hall Ltd, 1970.

12. Lord Rayleigh: "The Theory of Sound," Vol. II, pp. 224-235, Dover, 1945.

13. Ku, S.H., Cheng, X.C., Jagoda, J.I., Daniel B.R. and Zinn B.T.: "Radiation Measurements in a Gas Fired Pulse Combustor", Proceedings of the Spring Technical Meeting, Central States Section of The Combustion Institute, Chicago, IL, May, 1987.

14. Tang, J.M., Daniel, B.R., Jagoda, J.I., and Zinn B.T.:" The Interaction between Fluid Mechanics and Combustion in a Helmholtz Type Pulse Combustor", presented at the Fall Technical Meeting, Eastern Section of The Combustion Institute, Orlando, FL, December, 1990.

15. Ku, S.H., Daniel, B.R., Jagoda, J.I., and Zinn B.T.: "Frequency Modeling and Velocity Measurements in Gas Fired, Valved Pulse Combustors", presented at the Fall Technical Meeting, Eastern Section of The Combustion Institute, Clearwater Beach, FL, December, 1988.

16. Keller, J. O., Dec, J. E., Westbrook, C. K. and Bramlette, T. T.: Combustion and Flame, 75, pp. 33-44, 1989.

17. Ku, S.H., Daniel, B.R., Jagoda, J.I., and Zinn B.T.: "Flame Spread and Limits of Operation of Gas Fired, Mechanically Valved Pulse Combustor", Poster at the Twenty-Second Symposium (International) on Combustion, Seattle, WA, August, 1988.

18. Tang, J.M. Ku, S.H., Daniel, B.R., Jagoda, J.I., and Zinn B.T., "Controlling the Rich Limit of Operation of Pulse Combustors", Twenty-Third Symposium (International) on Combustion, Orleans, France, August 1990, (in print).

19. Scott, R.A.: Proceedings of the Physical Society, 58, pp. 253-264, 1946.

20. Xu, D., Daniel, B.R., Jagoda, J.I. and Zinn, B.T.: "The Acoustic Characteristics of Pulse Combustor Flapper Valves and Mixing Chambers", presented at the Thirteenth Annual Energy Sources Technology Conference and Exhibition, Fossil Fuel Combustion Symposium, PD-Vol. 30, pp 21-28, New Orleans, LA, January, 1990.

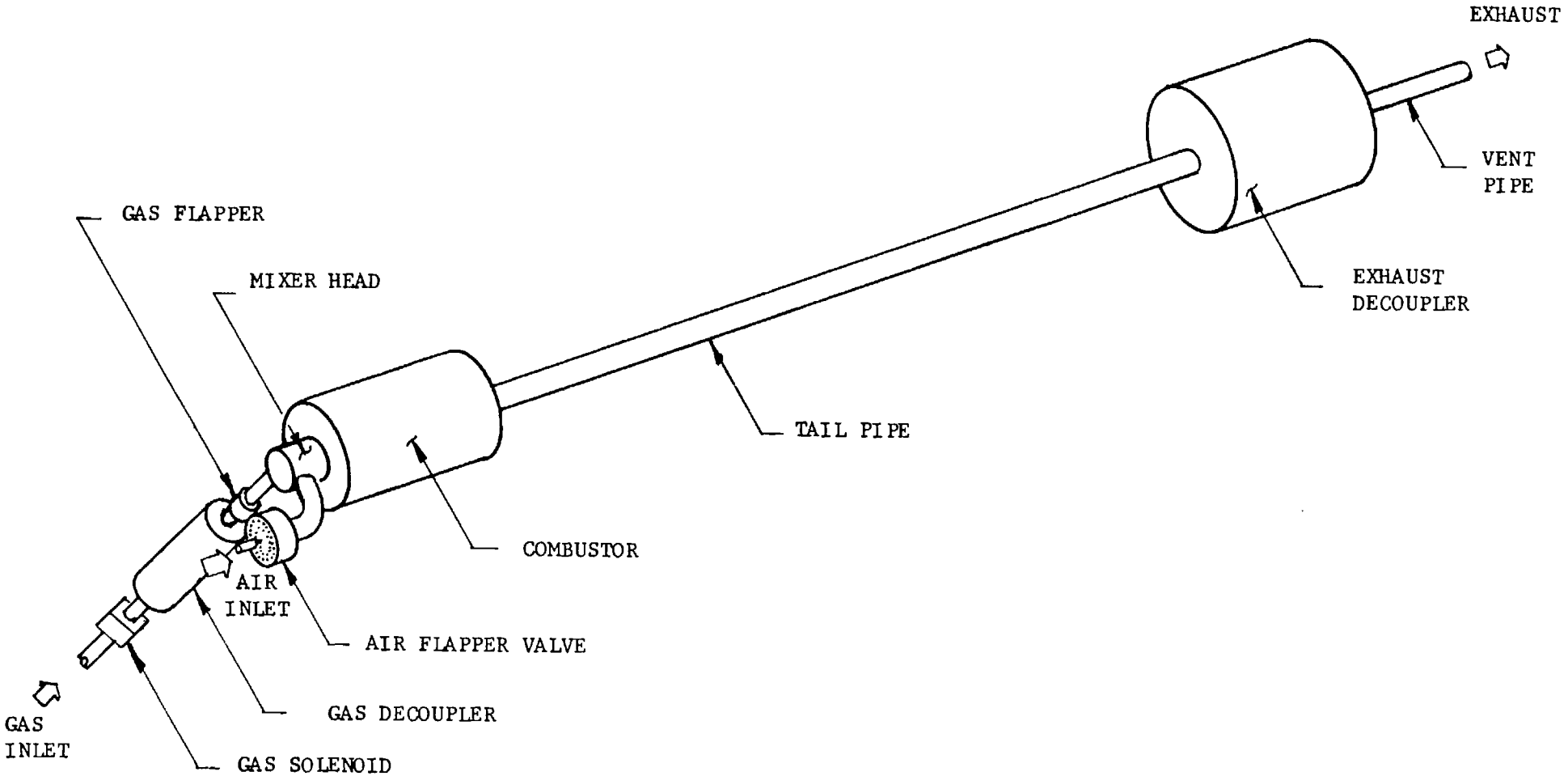

Fig. 1 Schematic of the Helmholtz Type Pulse Combustor

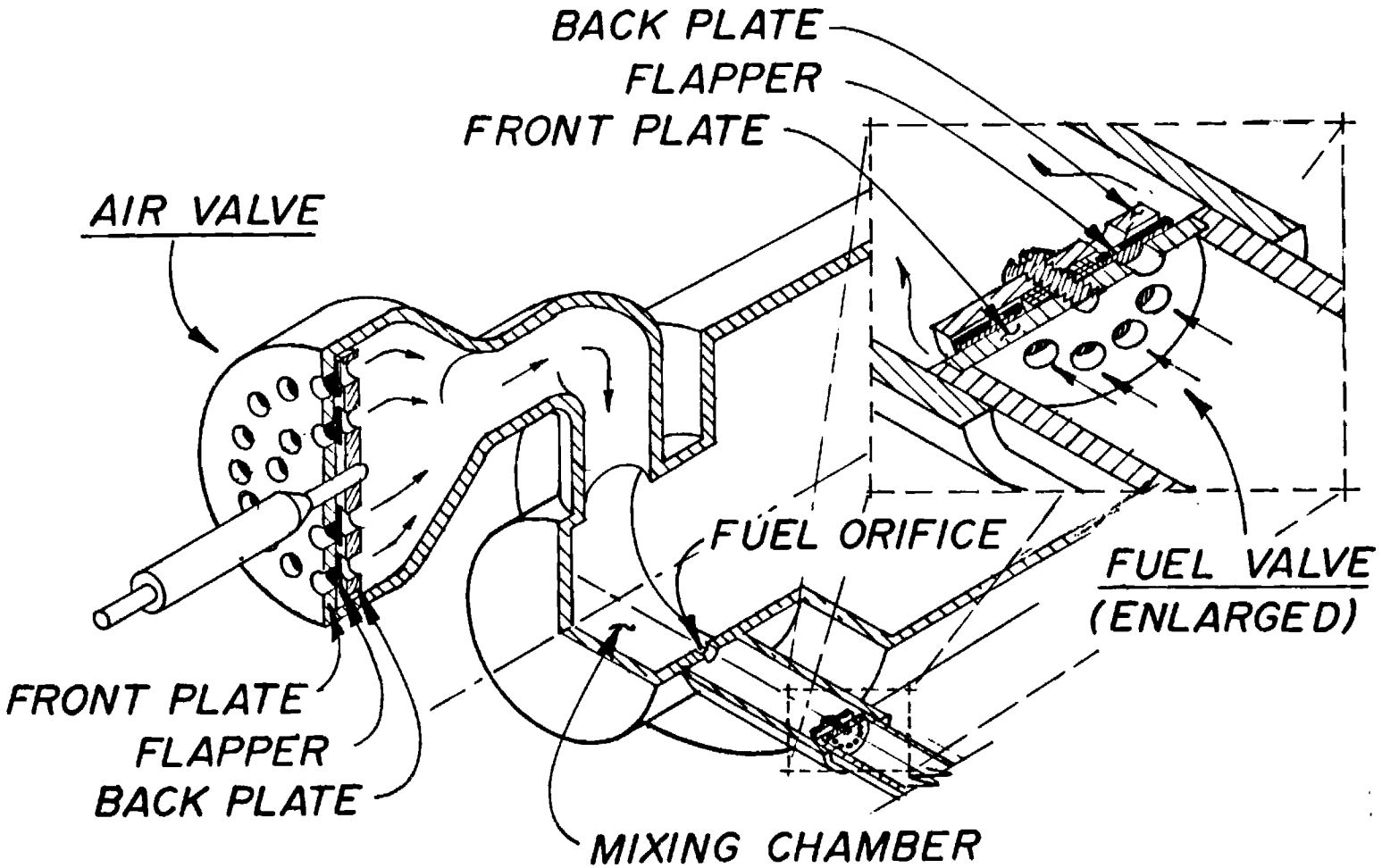

Fig. 2 Schematic of the Mixing Chamber Showing the Fuel and Air Flapper Valves

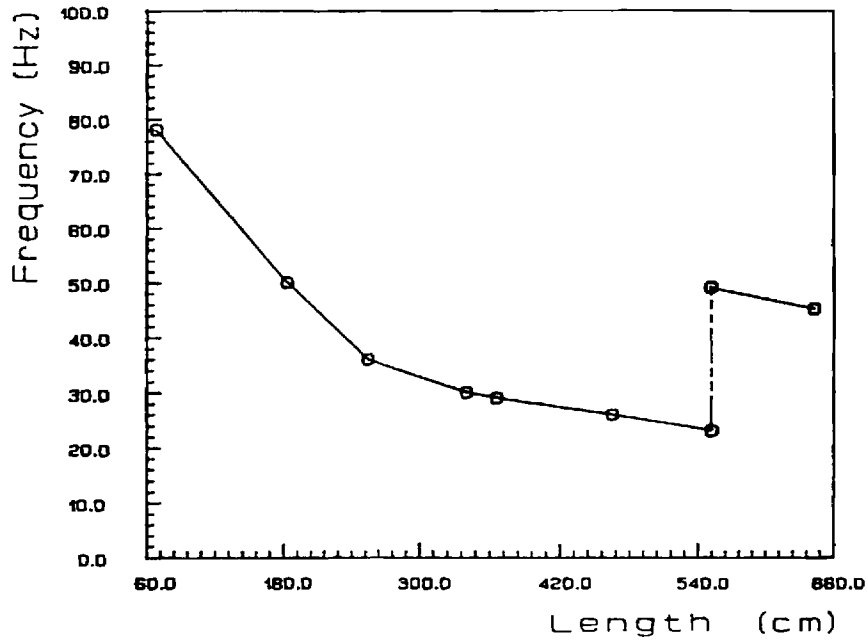

a

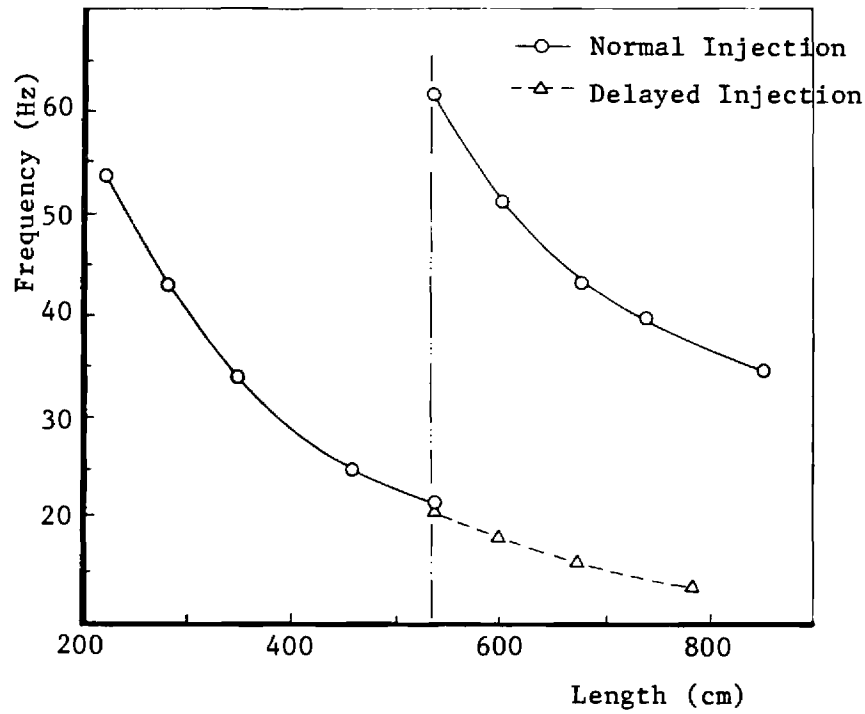

b

Fig. 3 Operational Frequency of the a) Helmhotz and b) Schmidt Combustors as a Function of Tailpipe or Combustor Length Respectively.

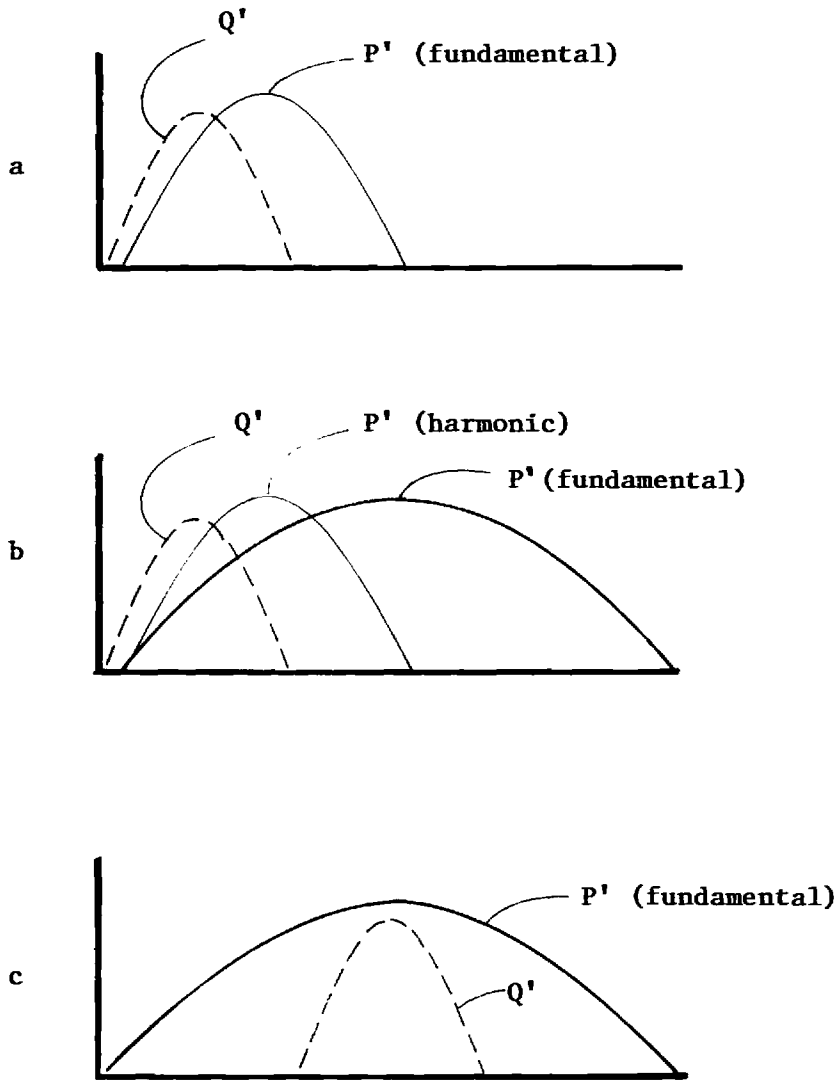

Fig. 4 Schematic of Relative Timing of Heat Release (Q') and Pressure (P') Oscillations for a) High Frequencies, b) Low Frequencies with Standard Fuel Injection and c) Low Frequencies with Displaced Fuel Injection Leading to Delayed Heat Release.

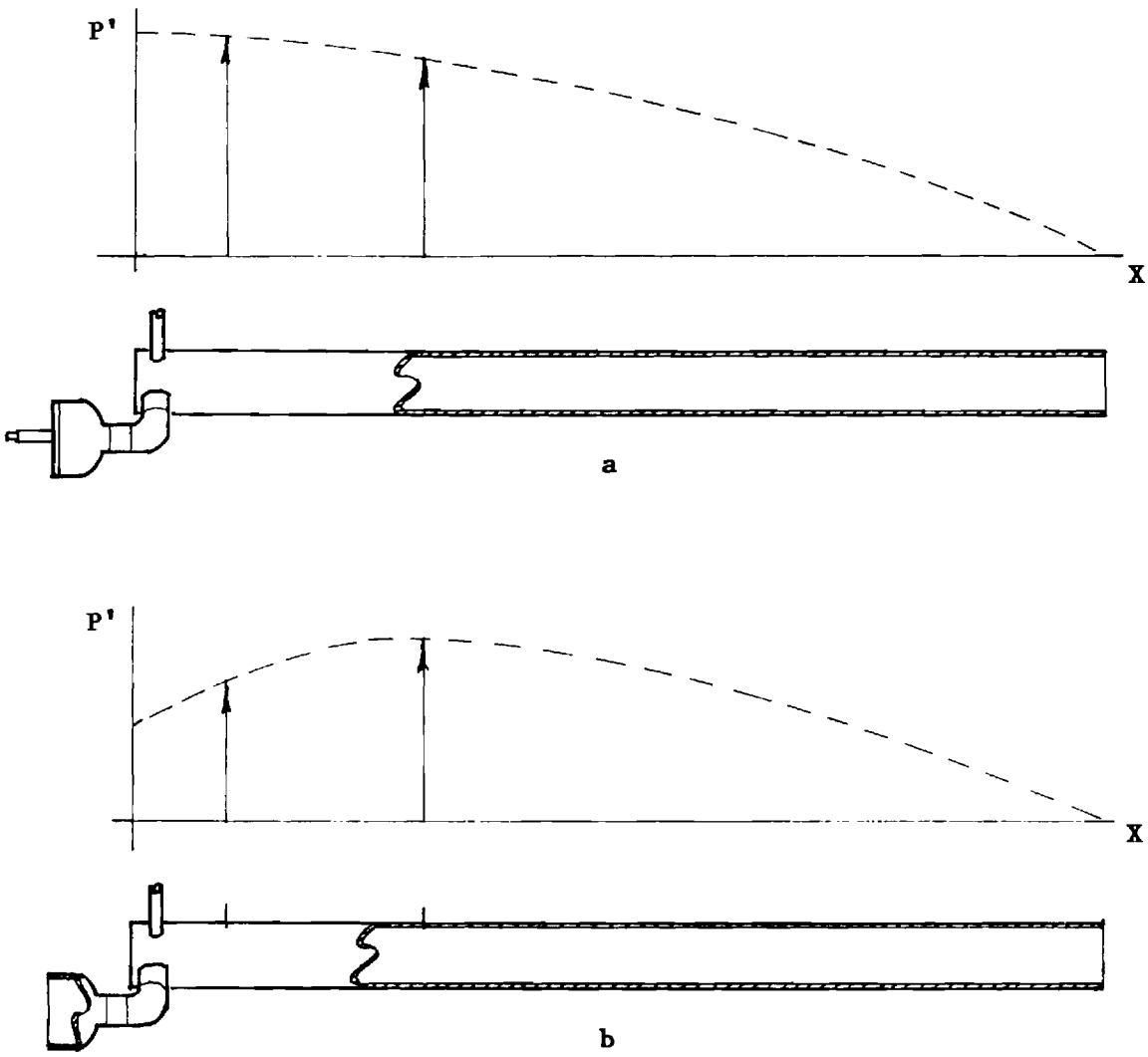

Fig. 5 Plot of Pressure Amplitude (P') vs. Axial Distance along the Combustor (X) Showing Standing Wave Pattern along Schmidt Combustor a) with Air Valve and b) without Air Valve.

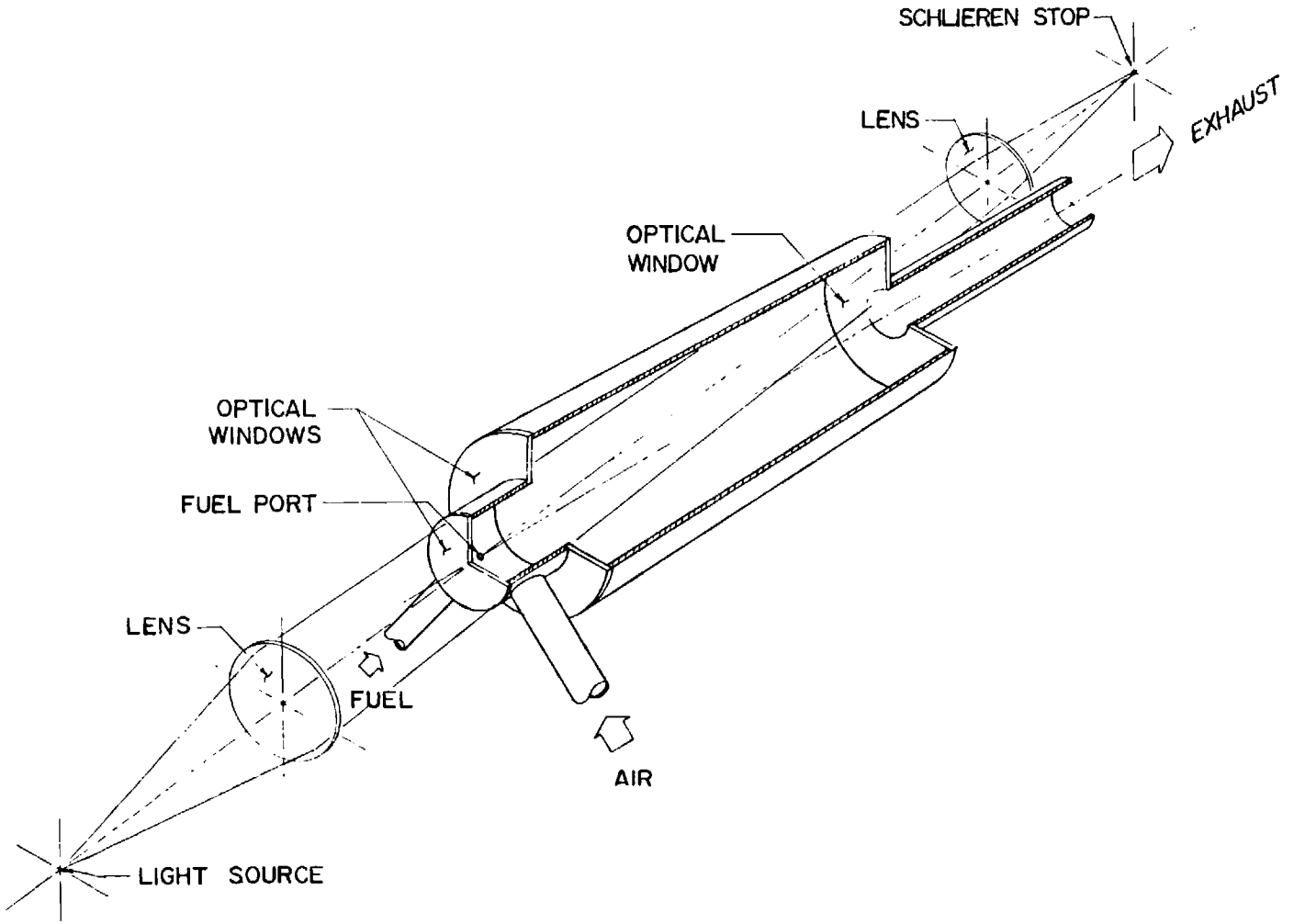

Fig. 6 Schematic of the Schlieren Set-up along the Combustor Axis

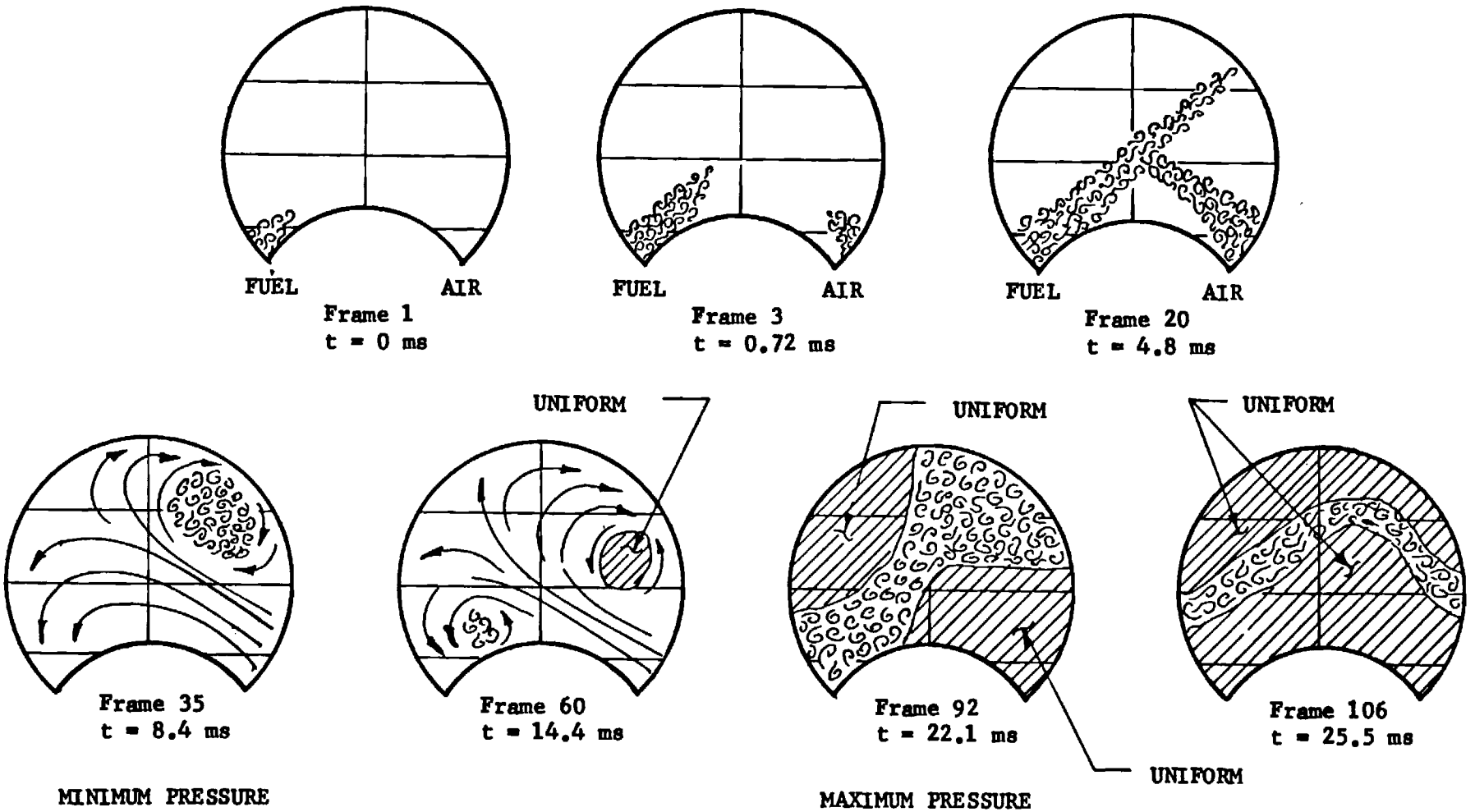

Fig. 7 Schematic of Selected Frames from the High Speed Shadow Movie Showing the Flow Field at Different Instances during the Cycle as Seen along the Combustor Axis

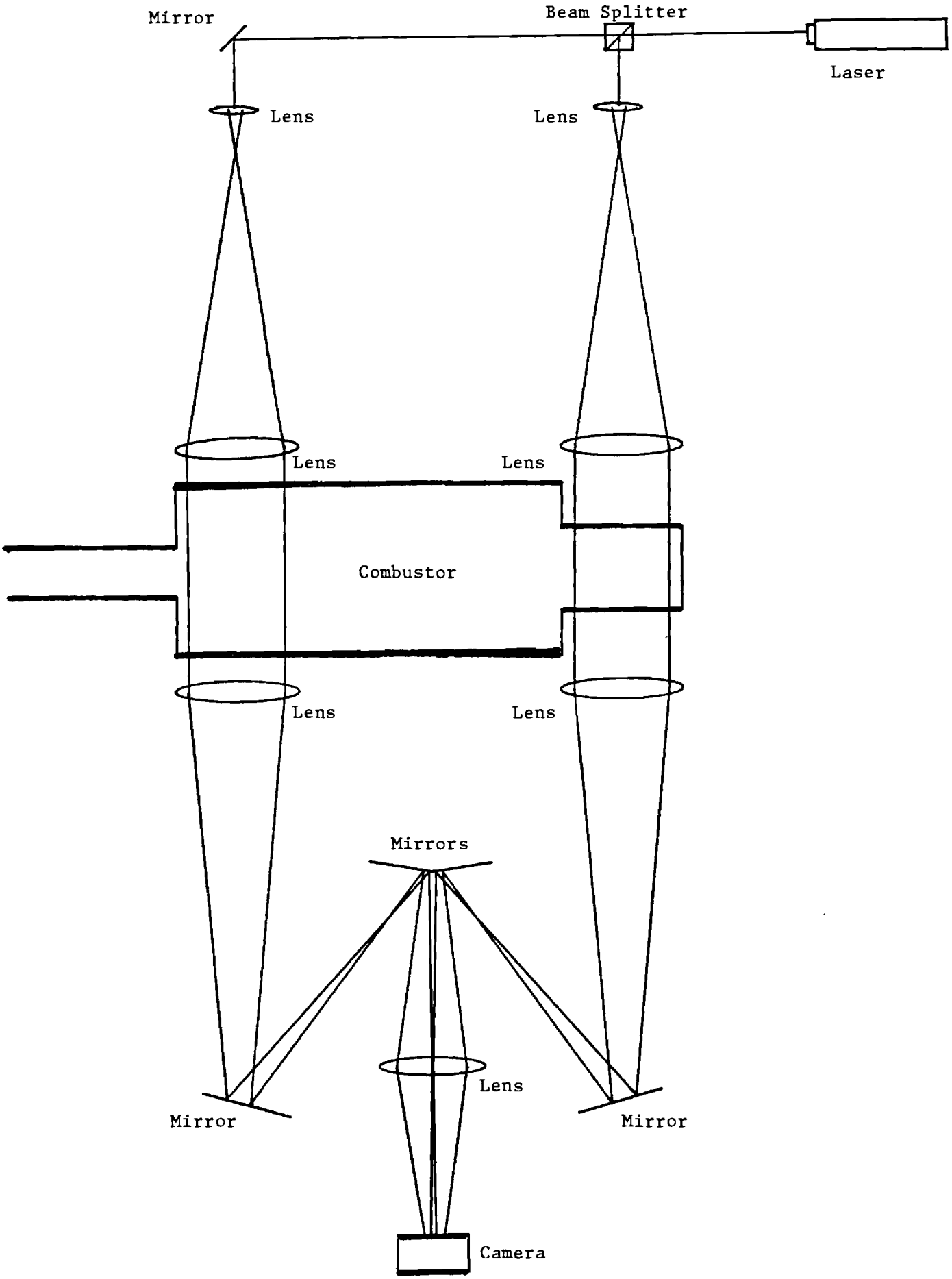

Fig. 8 Schematic of the Schlieren Set-up normal to the Combustor Axis

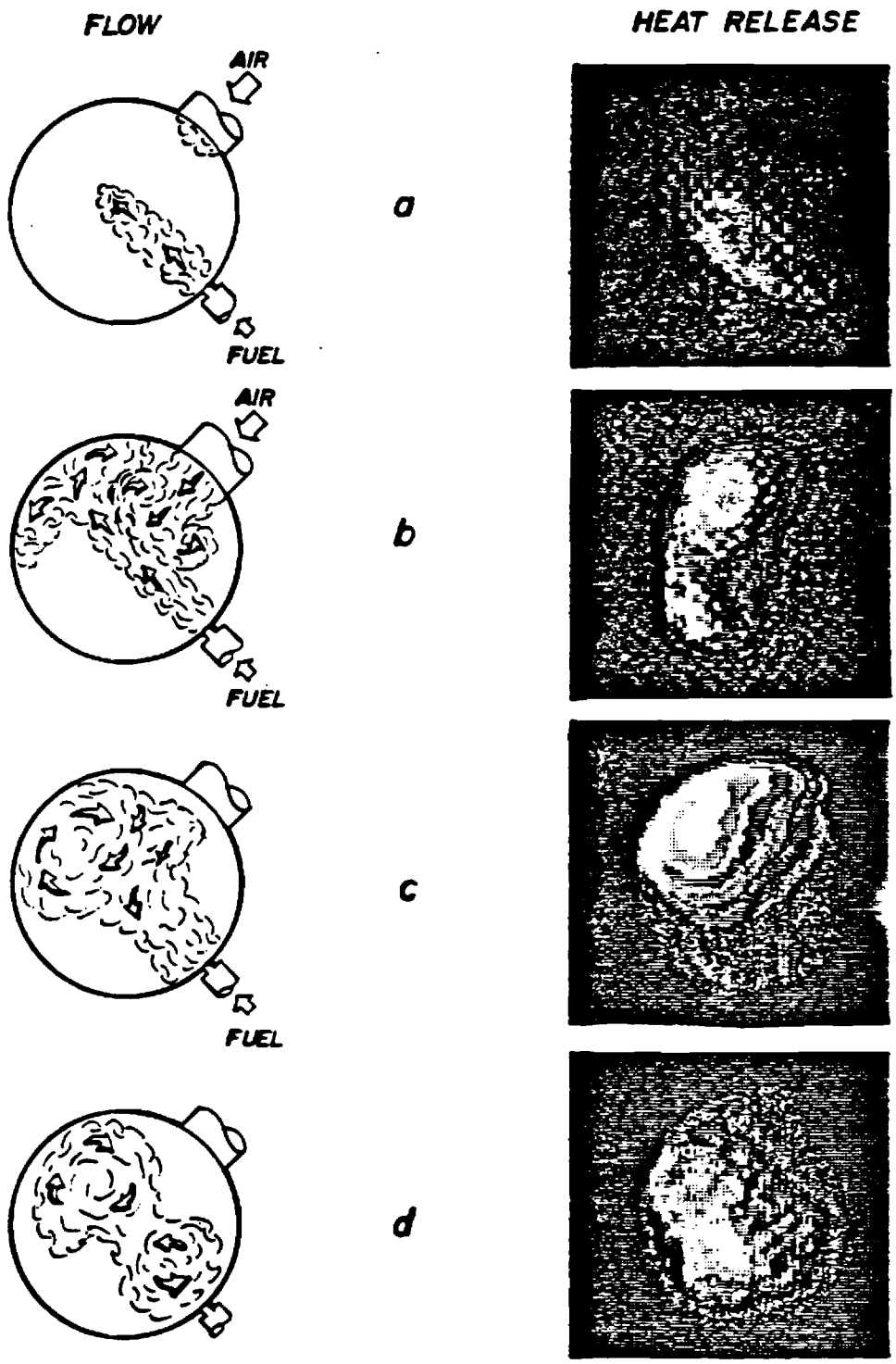

Fig. 9 Comparison of the Flow Field and the Heat Release Distribution as Seen along the Combustor Axis at Four Instants during the Cycle.

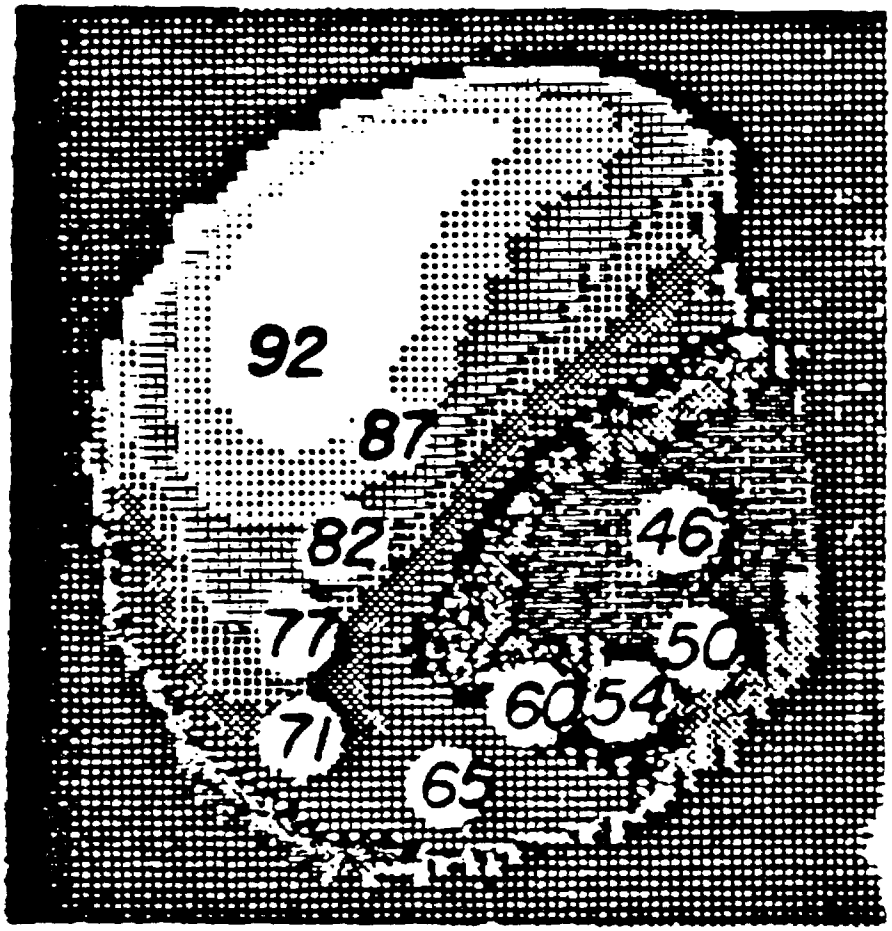

Fig. 10 Contour Plot of Phase Angle by which the Heat Release Oscillations Lead the Pressure Oscillations.

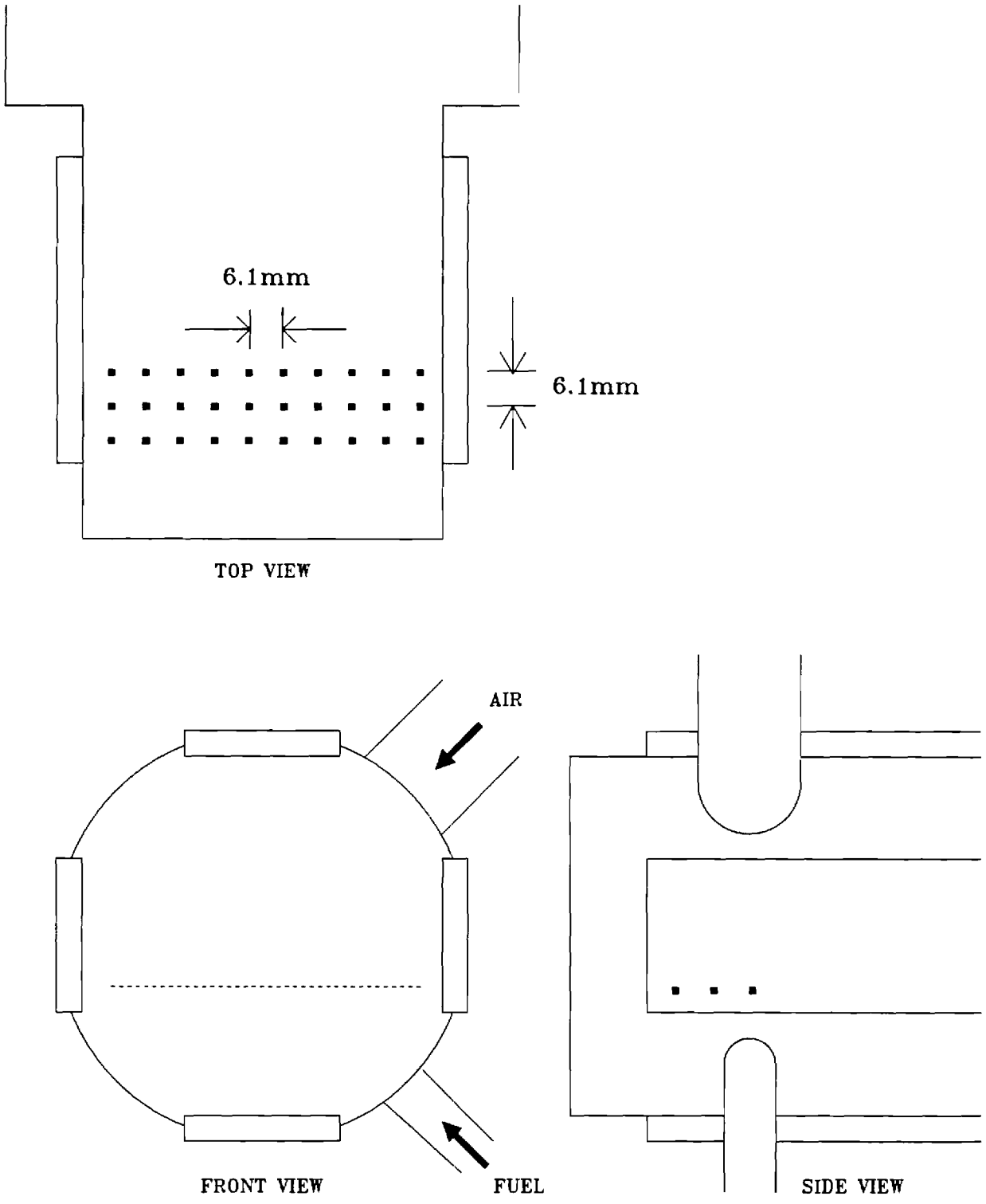

Fig. 11 Locations at which the Laser Doppler Velocimeter Results Shown in Figures 12 through 29 were Obtained. Each Location is Labeled (m,n).

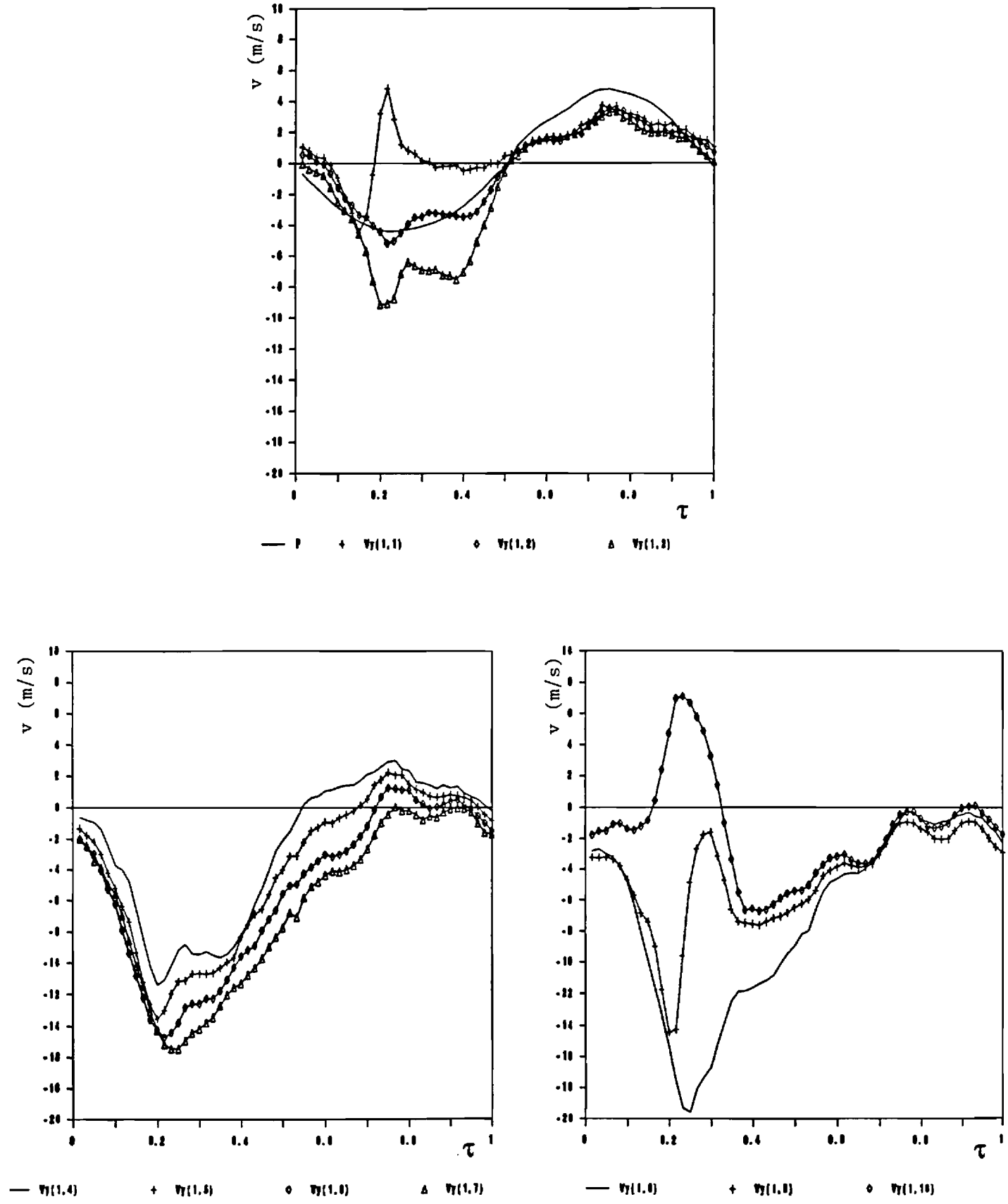

Fig. 12 Variation of the Vertical Mean Velocity (v) with Instant During a Cycle (τ) for Locations along the Line m = 1. The Top Plot includes the Pressure Trace for Reference.

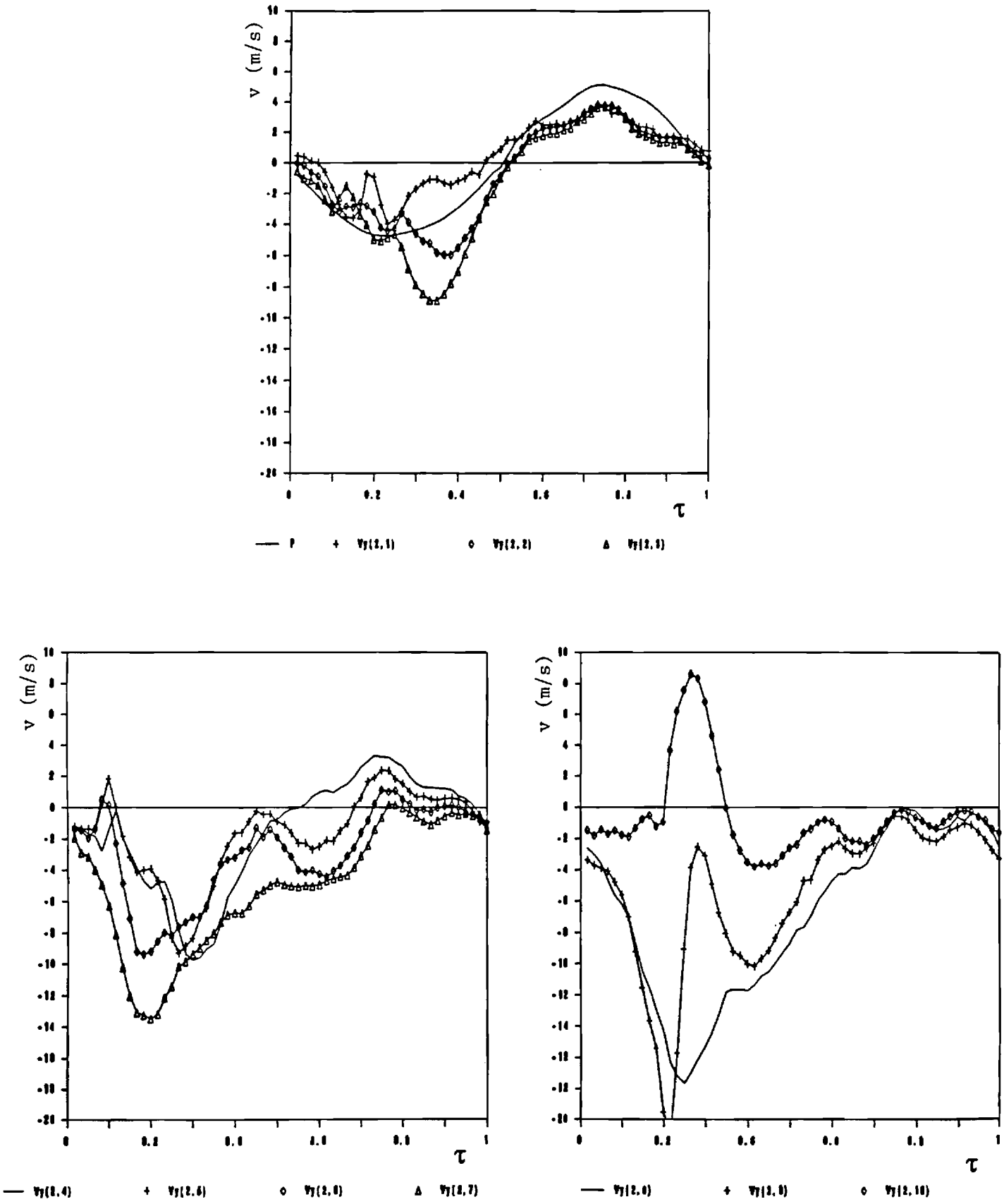

Fig. 13 Variation of the Vertical Mean Velocity (v) with Instant During a Cycle (τ) for Locations along the Line m = 2. The Top Plot includes the Pressure Trace for Reference.

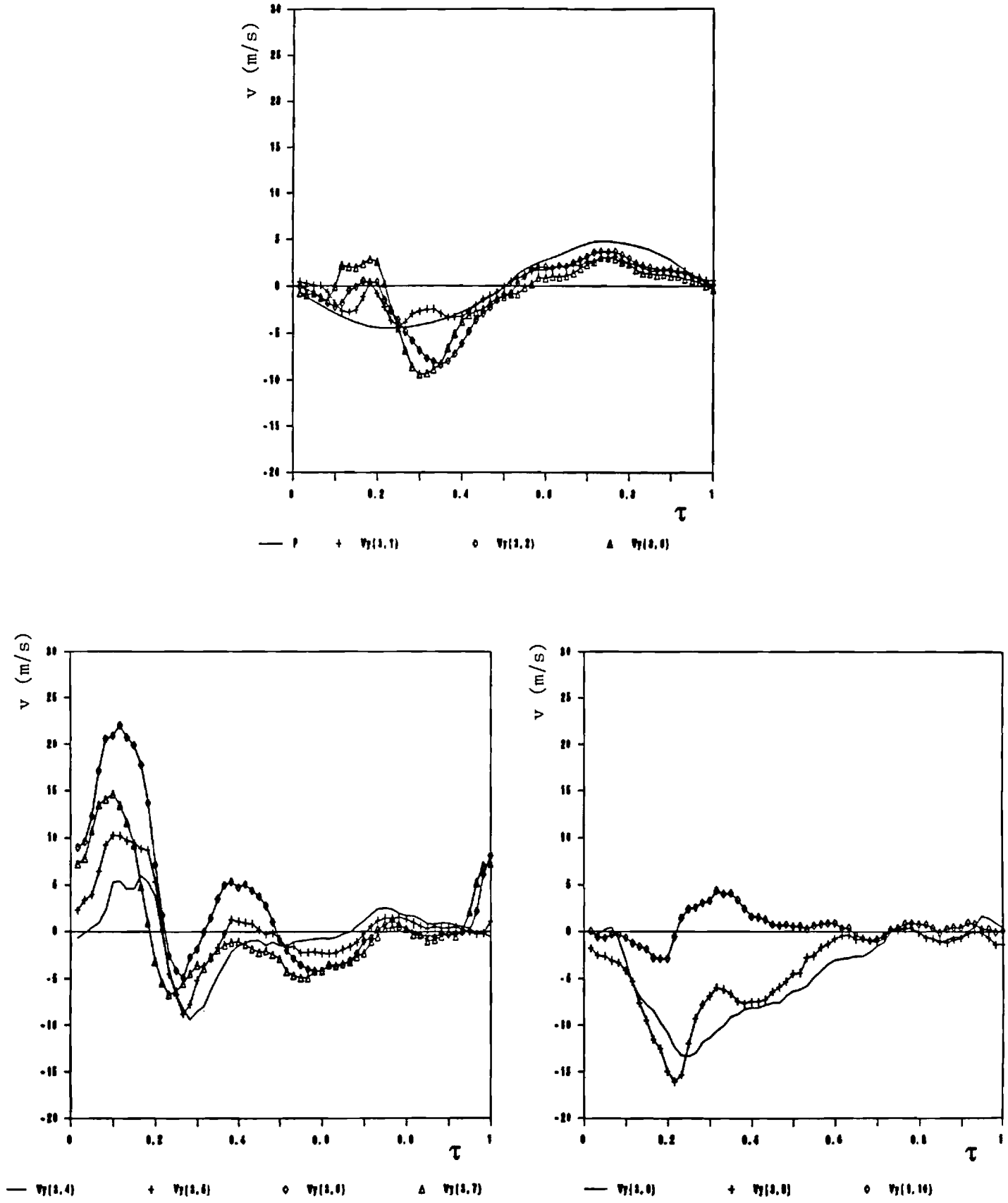

Fig. 14 Variation of the Vertical Mean Velocity (v) with Instant During a Cycle (τ) for Locations along the Line m = 3. The Top Plot includes the Pressure Trace for Reference.

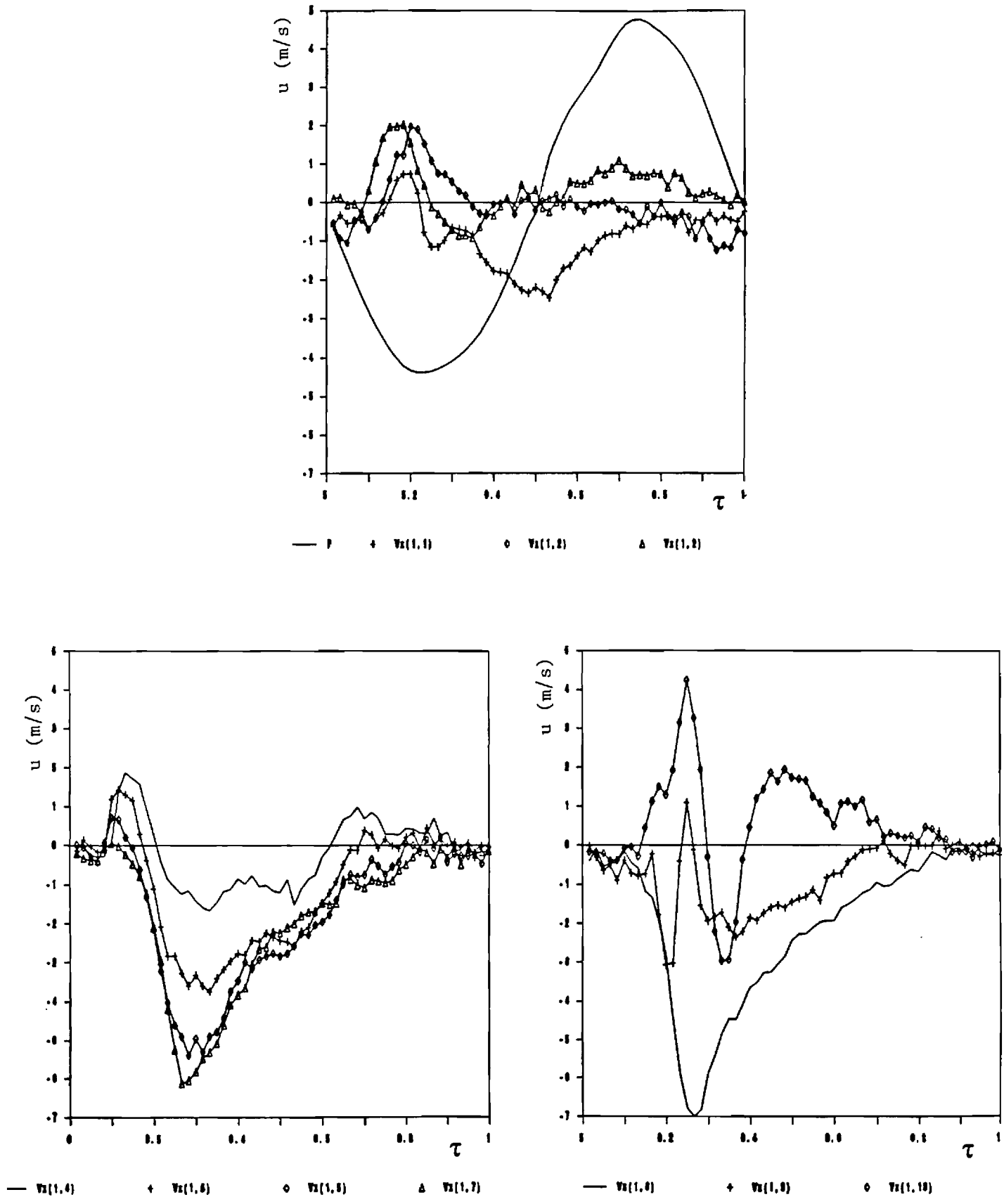

Fig. 15 Variation of the Axial Mean Velocity (u) with Instant During a Cycle (τ) for Locations along the Line m = 1. The Top Plot includes the Pressure Trace for Reference.

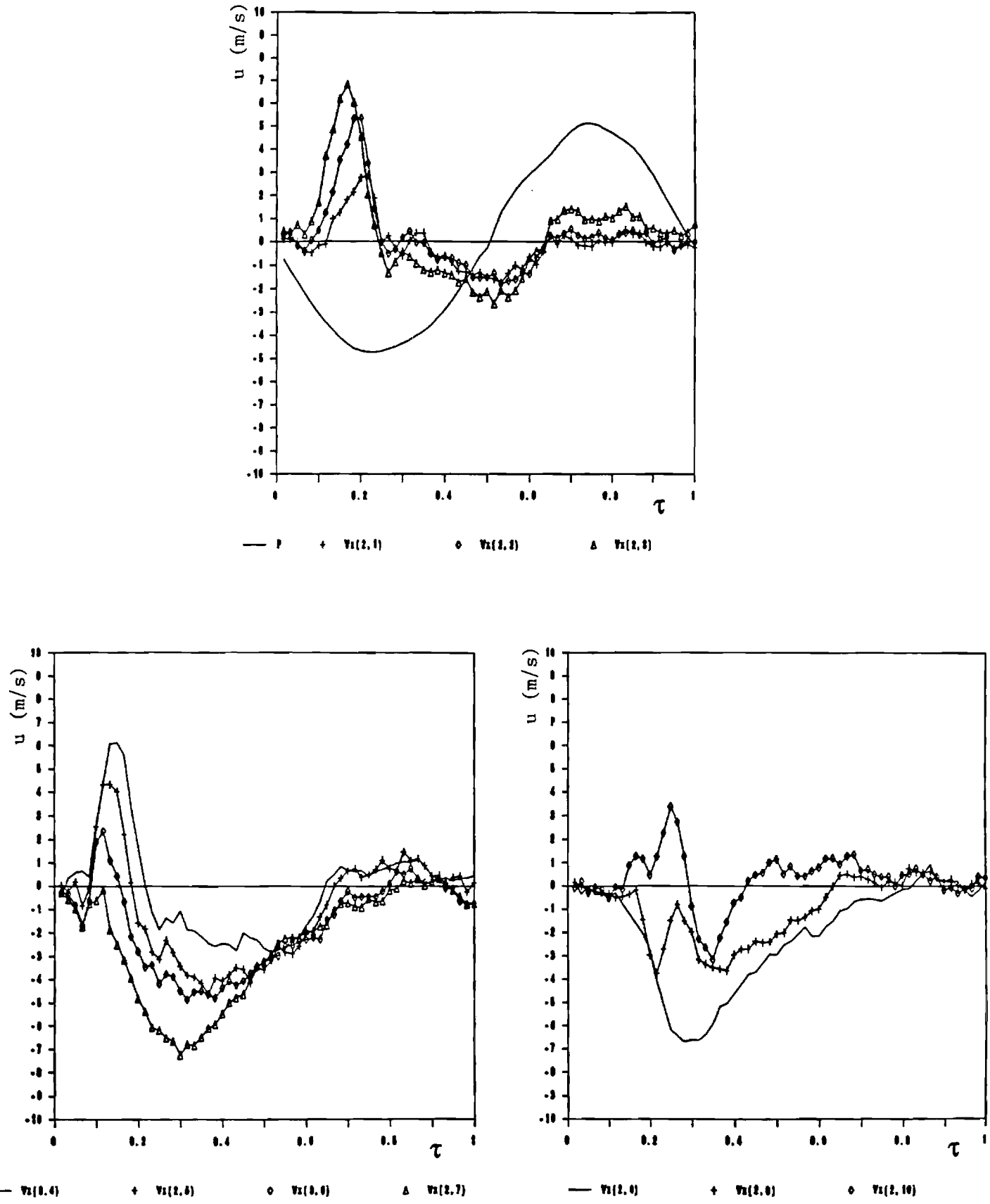

Fig. 16 Variation of the Axial Mean Velocity (u) with Instant During a Cycle (τ) for Locations along the Line m = 2. The Top Plot includes the Pressure Trace for Reference.

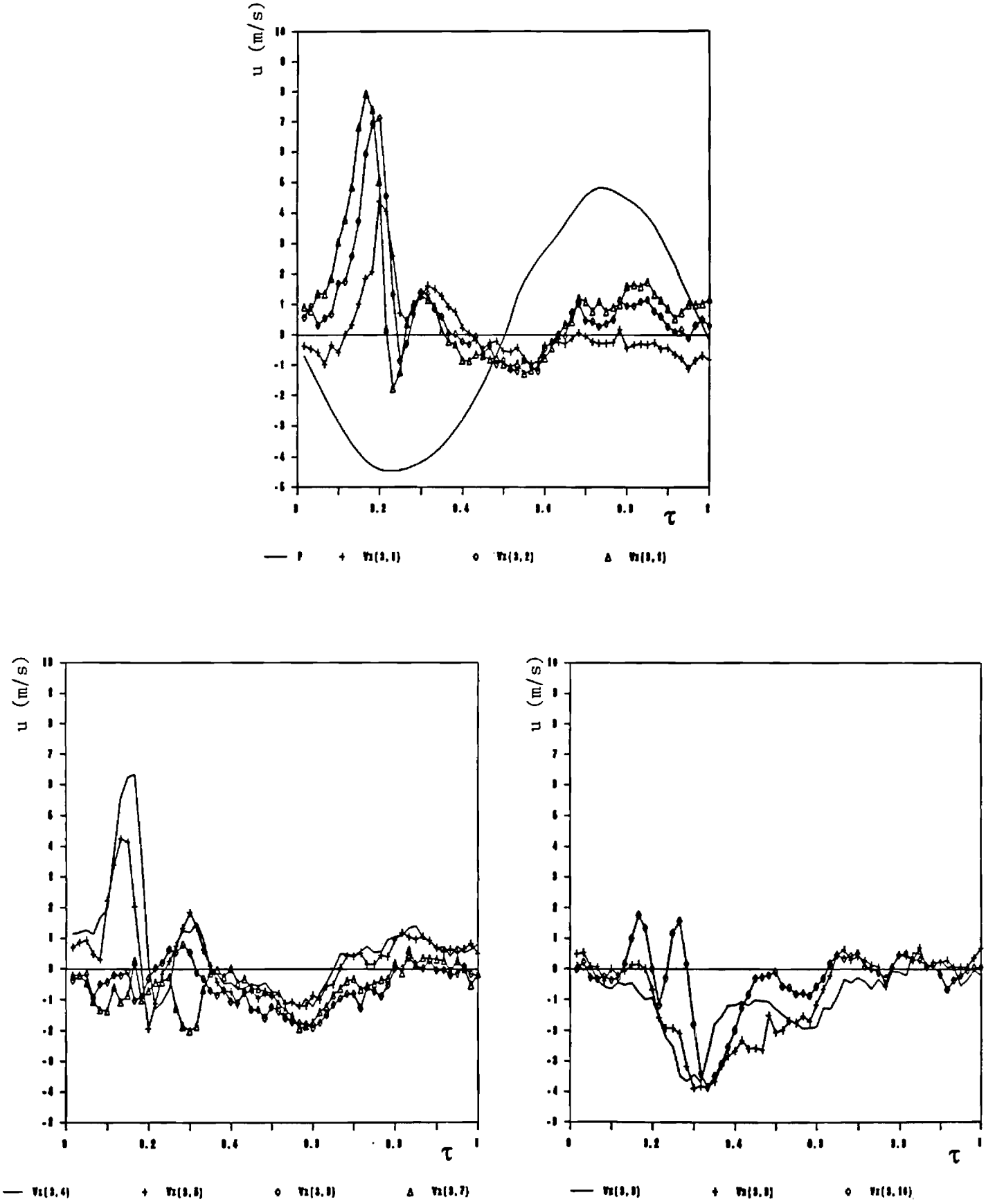

Fig. 17 Variation of the Axial Mean Velocity (u) with Instant During a Cycle (τ) for Locations along the Line m = 3. The Top Plot includes the Pressure Trace for Reference.

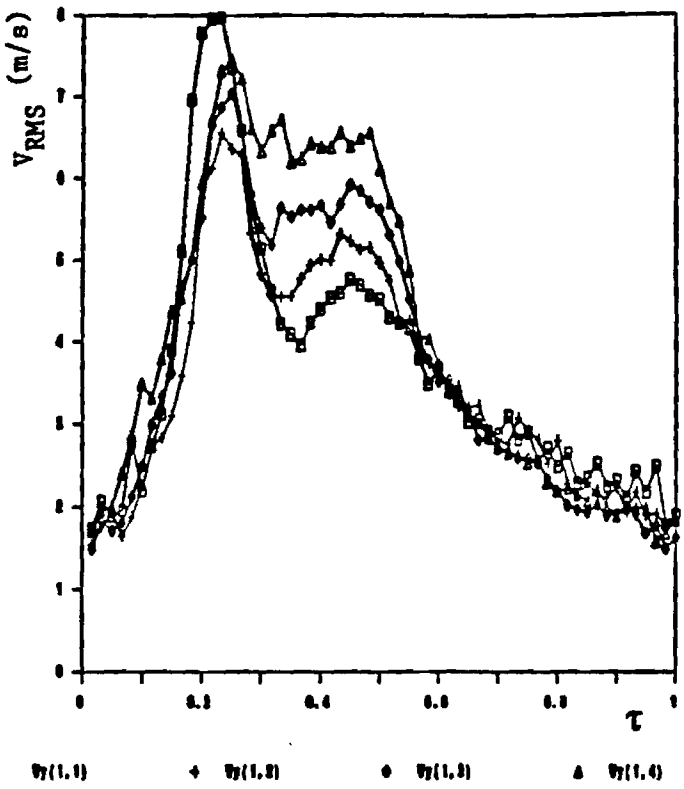

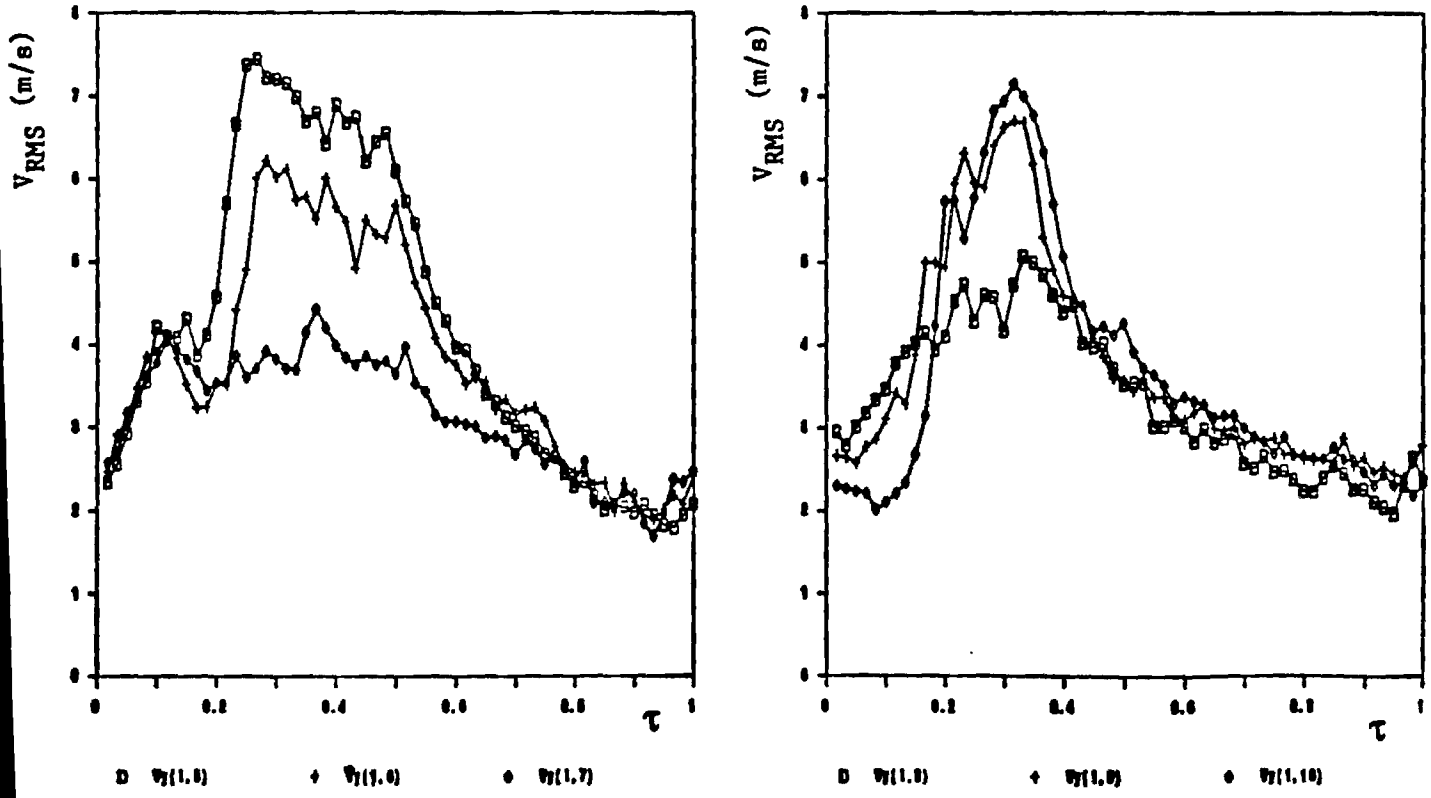

Fig. 18 Variation of the Vertical Turbulence Intensity (v_{RMS}) with Instant During a Cycle (τ) for Locations along the Line m =1.

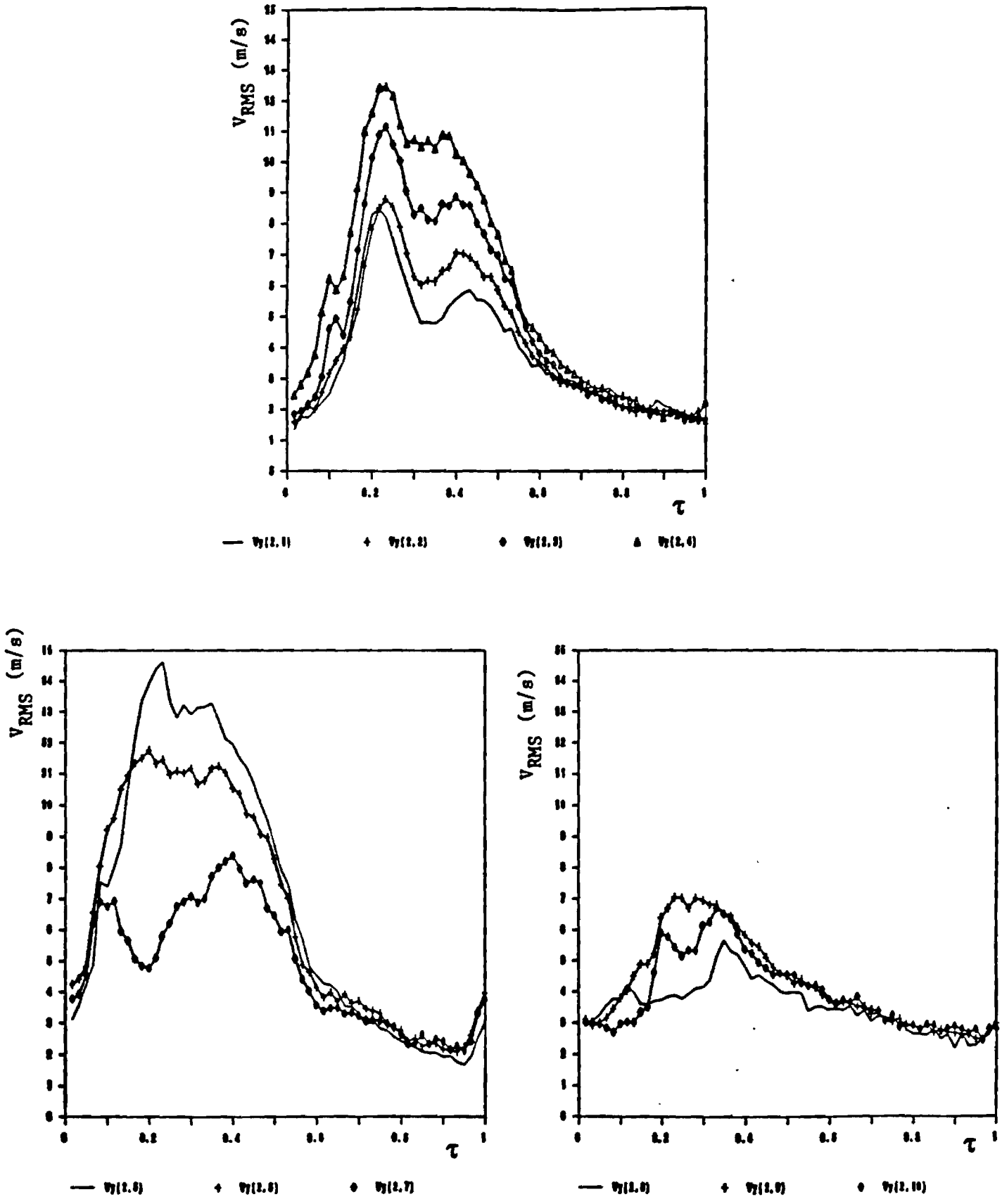

Fig. 19 Variation of the Vertical Turbulence Intensity (v_{RMS}) with Instant During a Cycle (τ) for Locations along the Line m = 2.

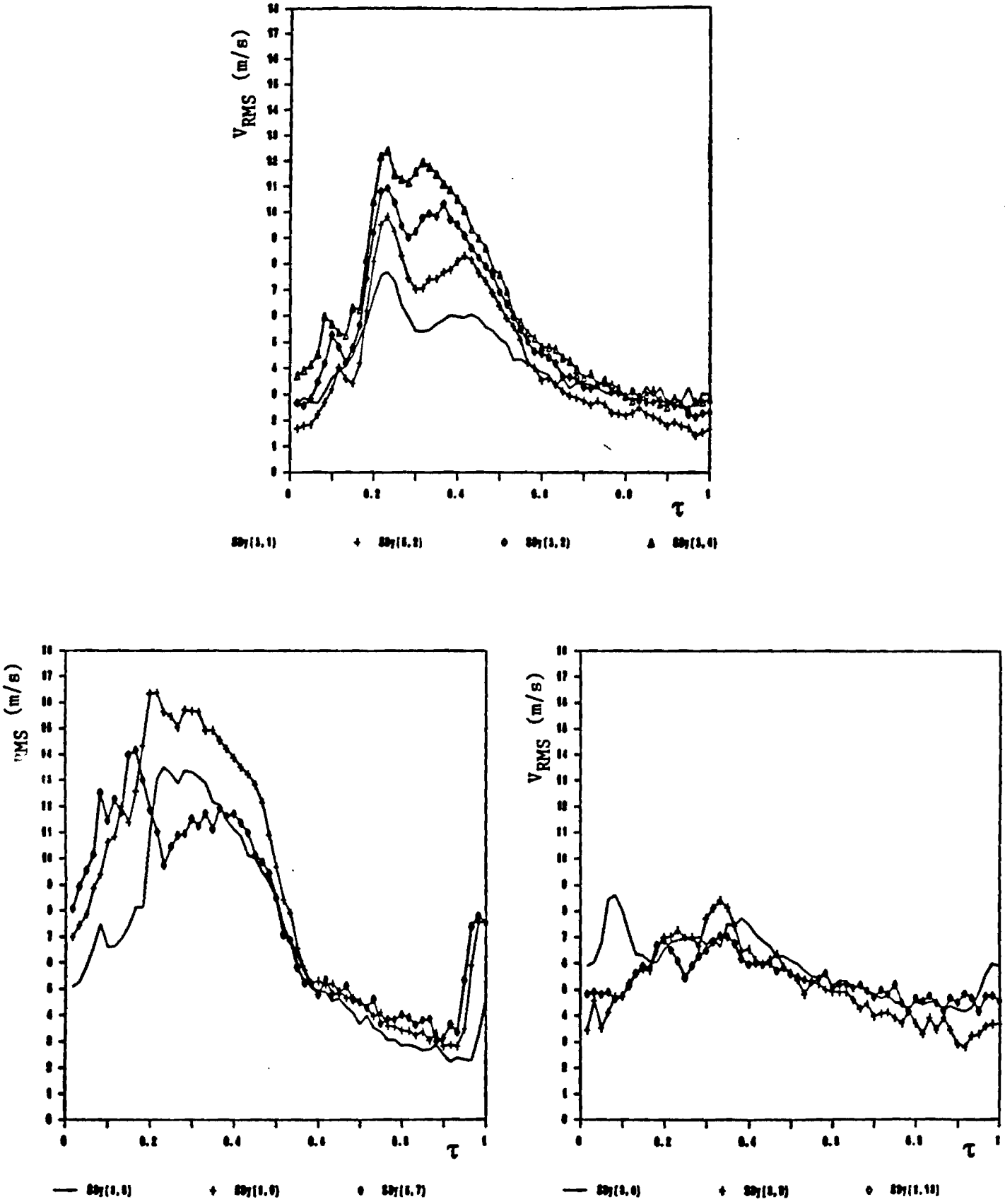

Fig. 20 Variation of the Vertical Turbulence Intensity (v_{RMS}) with Instant During a Cycle (τ) or Locations along the Line m = 3.

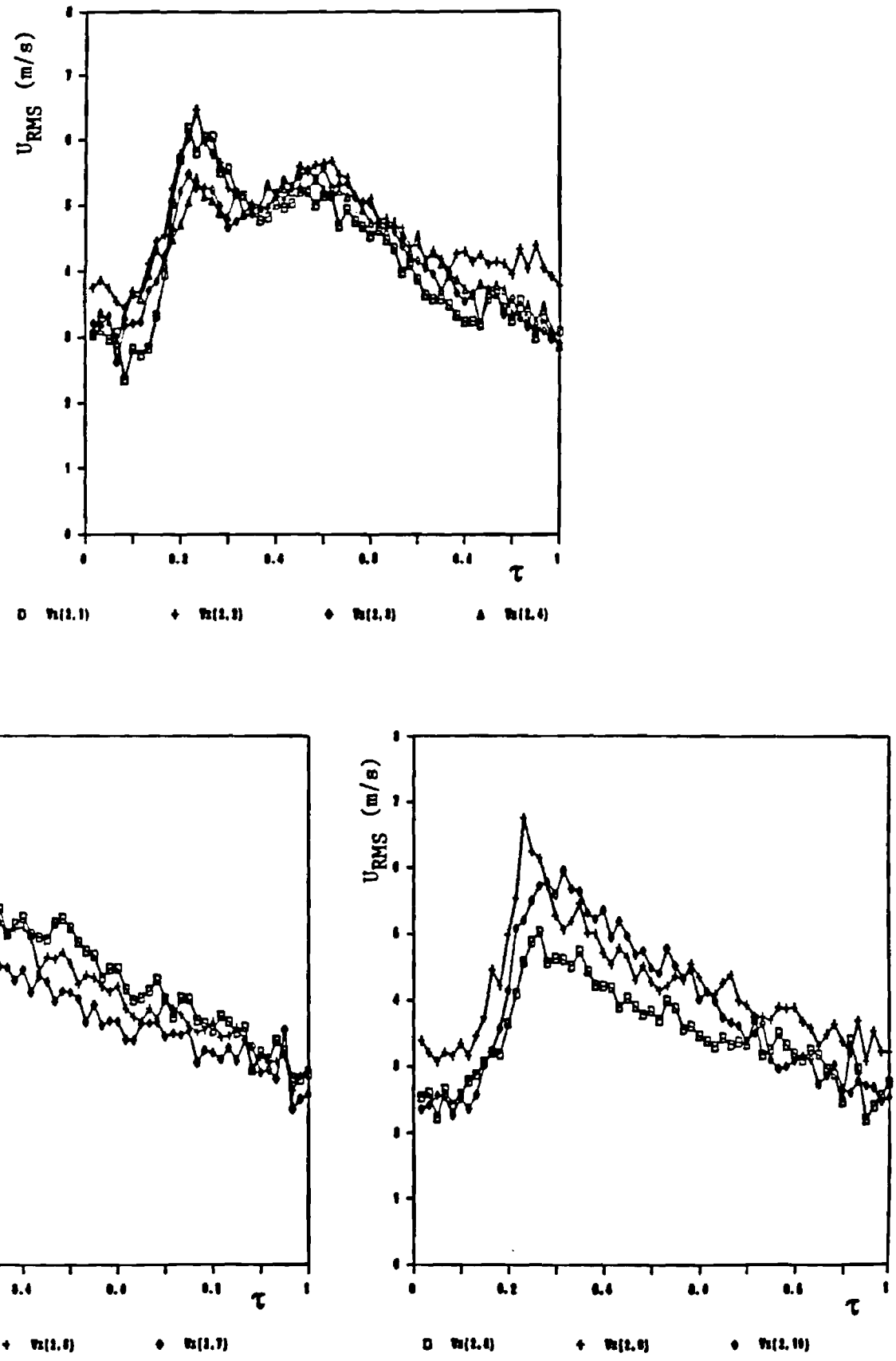

Fig. 21 Variation of the Axial Turbulence Intensity (u_{RMS}) with Instant During a Cycle (τ) for Locations along the Line m = 1.

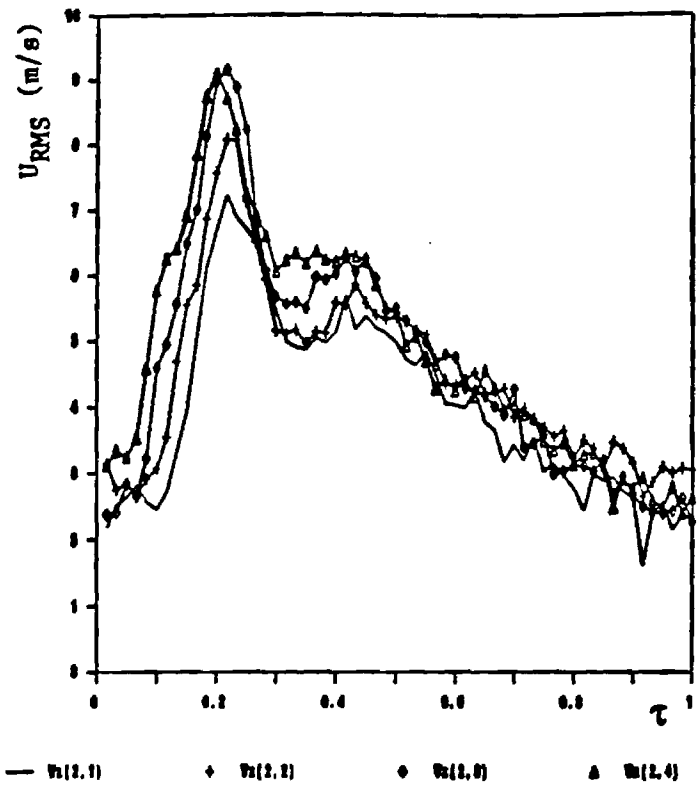

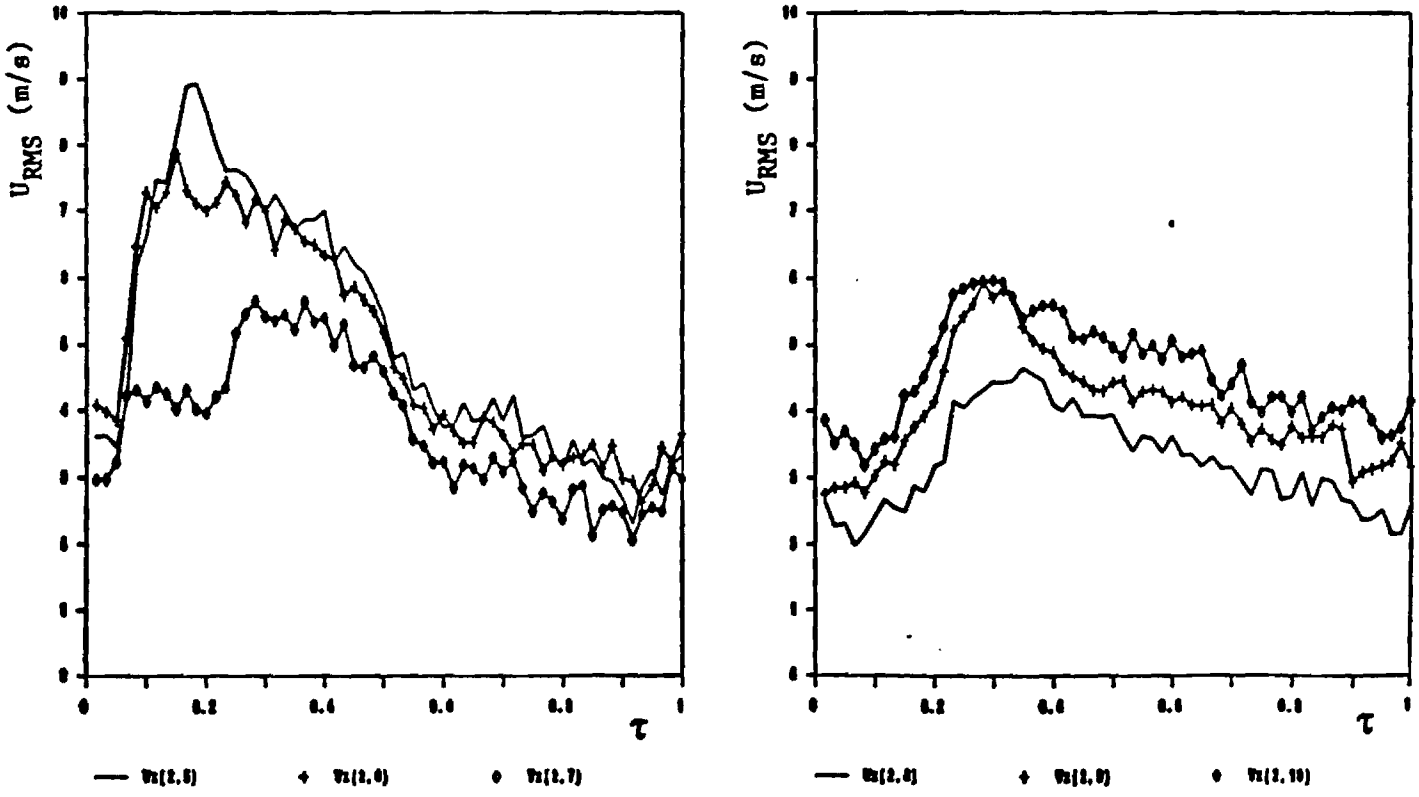

Fig. 22 Variation of the Axial Turbulence Intensity (u_{RMS}) with Instant During a Cycle (τ) for Locations along the Line m = 2.

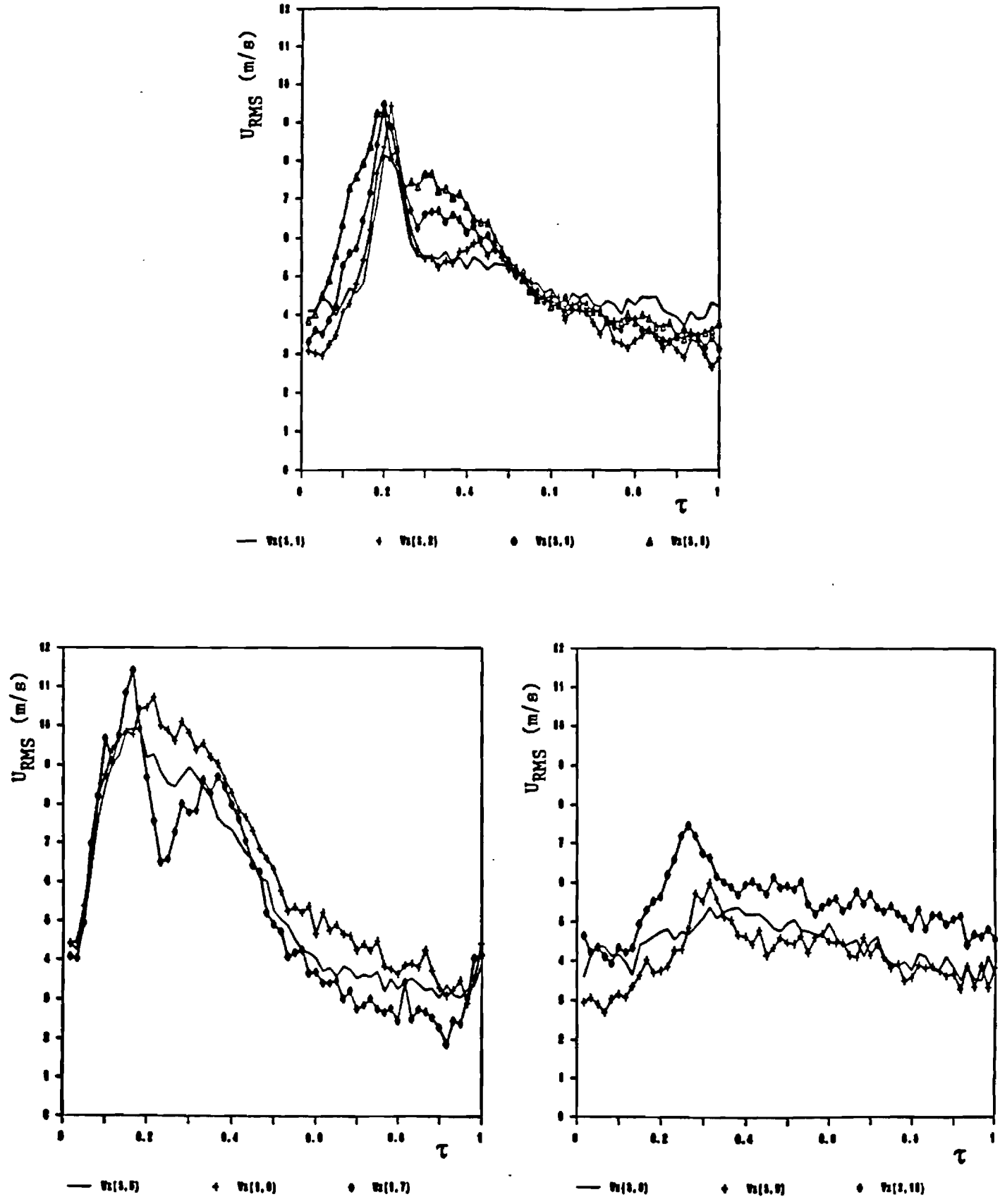

Fig. 23 Variation of the Axial Turbulence Intensity (u_{RMS}) with Instant During a Cycle (τ) for Locations along the Line m = 3.

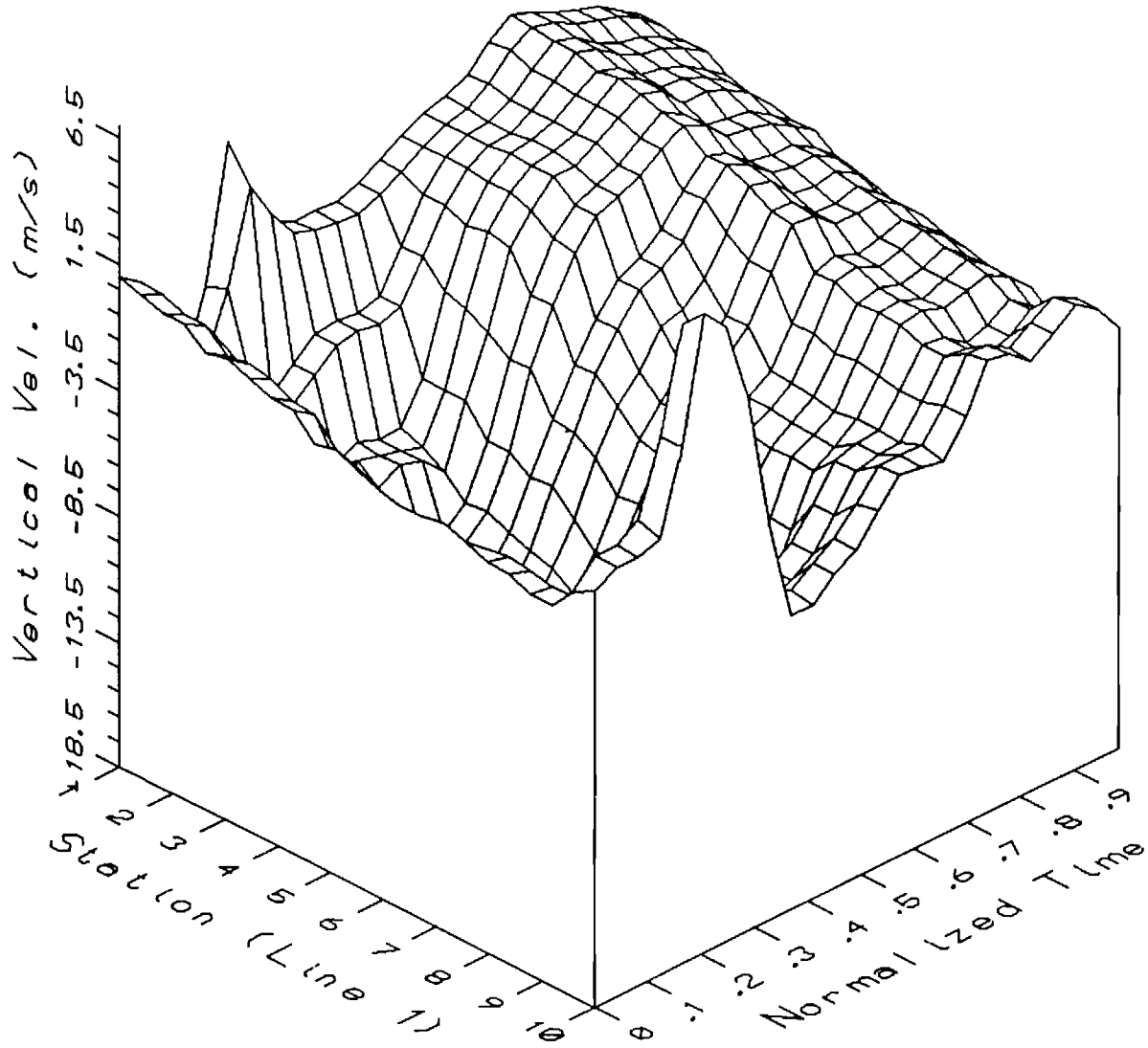

Fig. 24 Three Dimensional Plot of Vertical Mean Velocities during a Cycle for Locations along the Line m = 1.

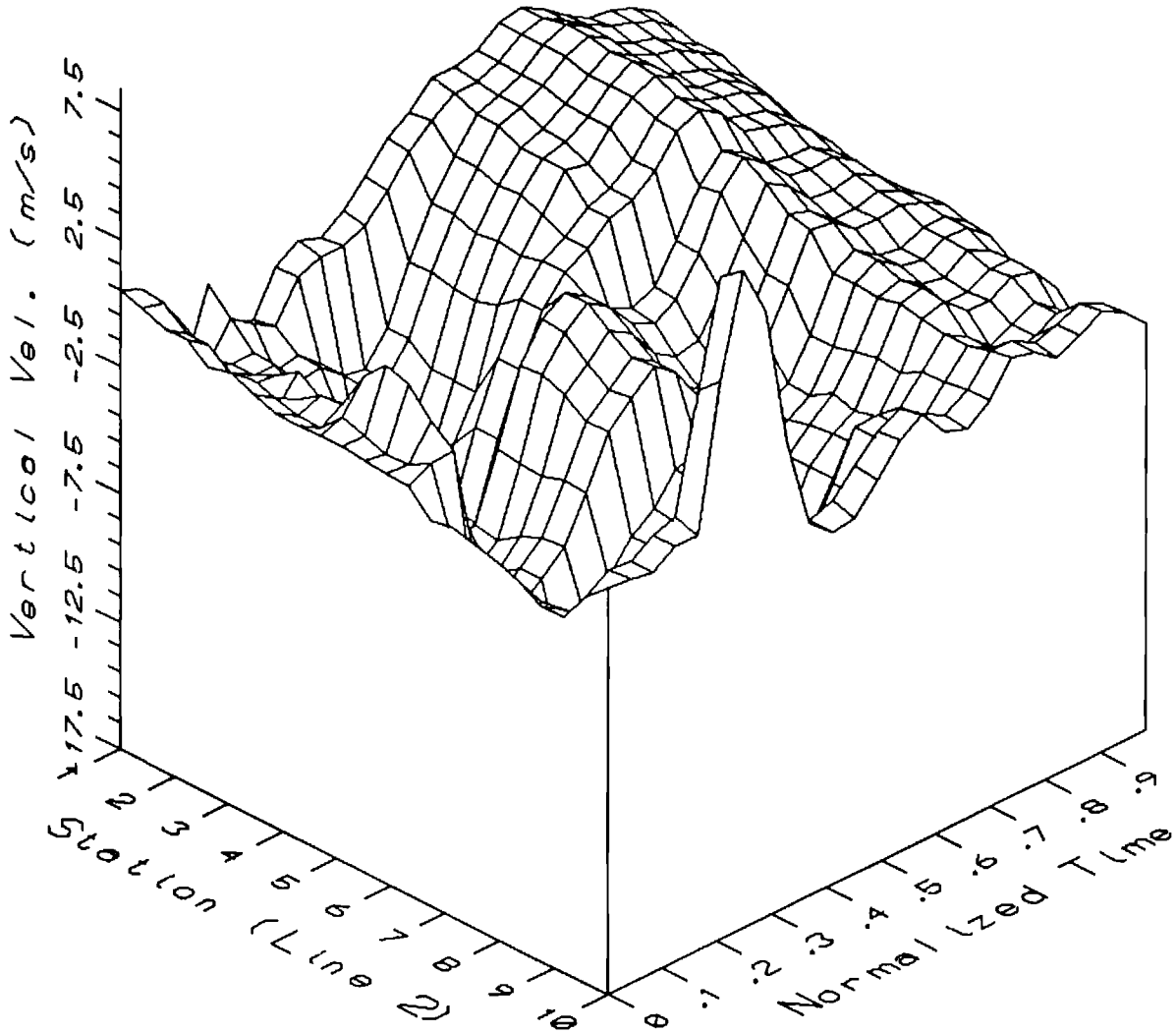

Fig. 25 Three Dimensional Plot of Vertical Mean Velocities during a Cycle for Locations along the Line m = 2.

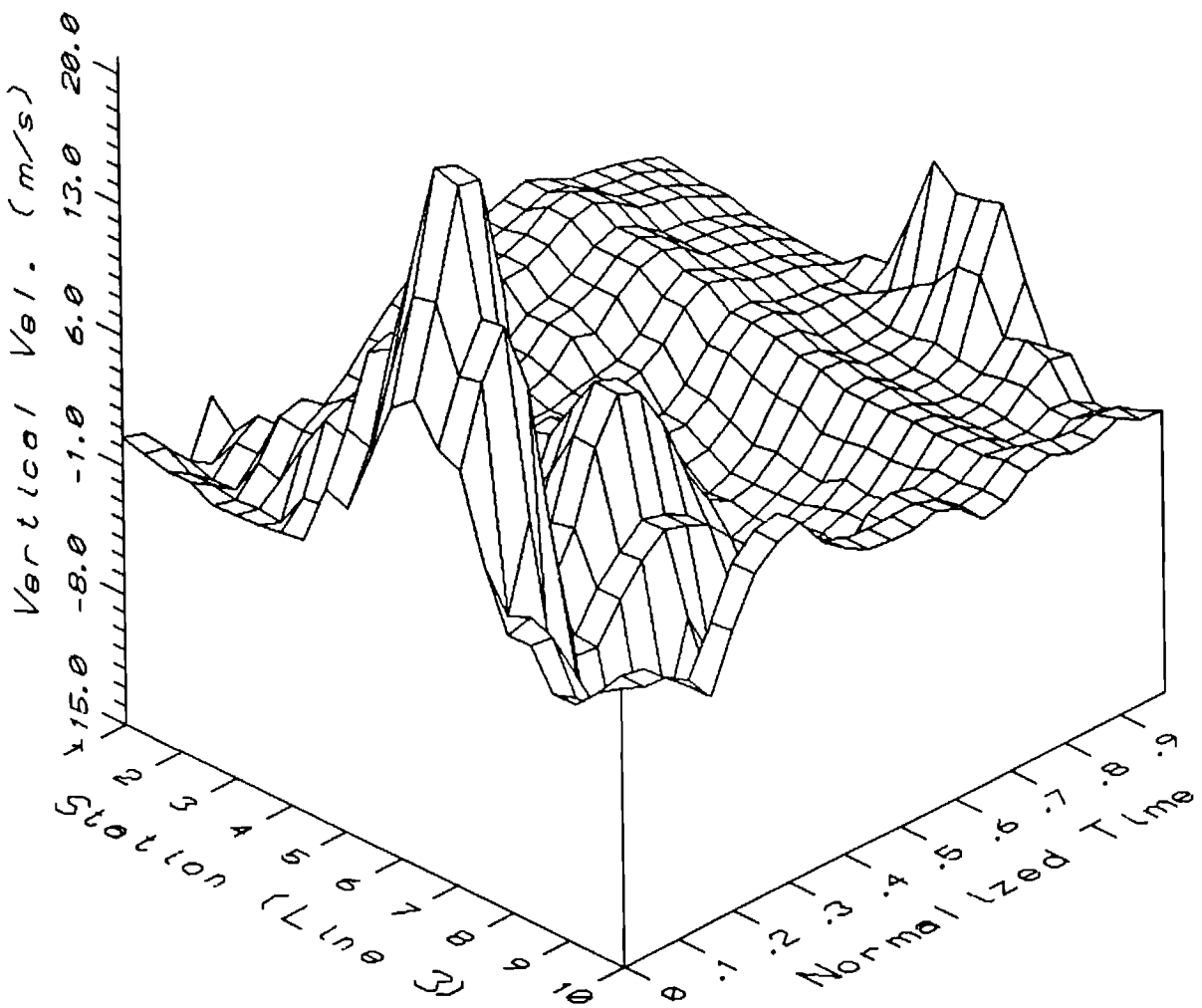

Fig. 26 Three Dimensional Plot of Vertical Mean Velocities during a Cycle for Locations along the Line m = 3.

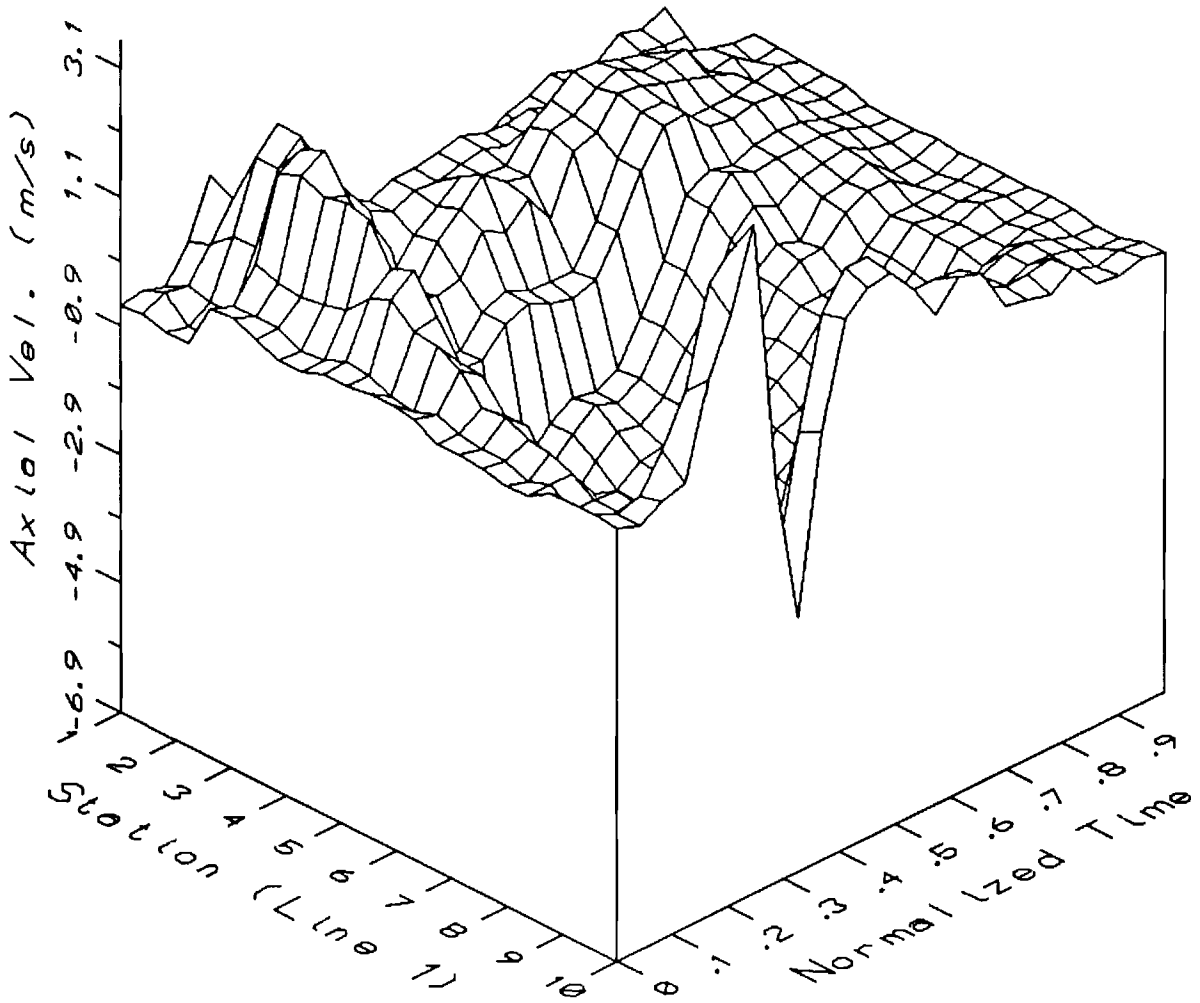

Fig. 27 Three Dimensional Plot of Axial Mean Velocities during a Cycle for Locations along the Line m = 1.

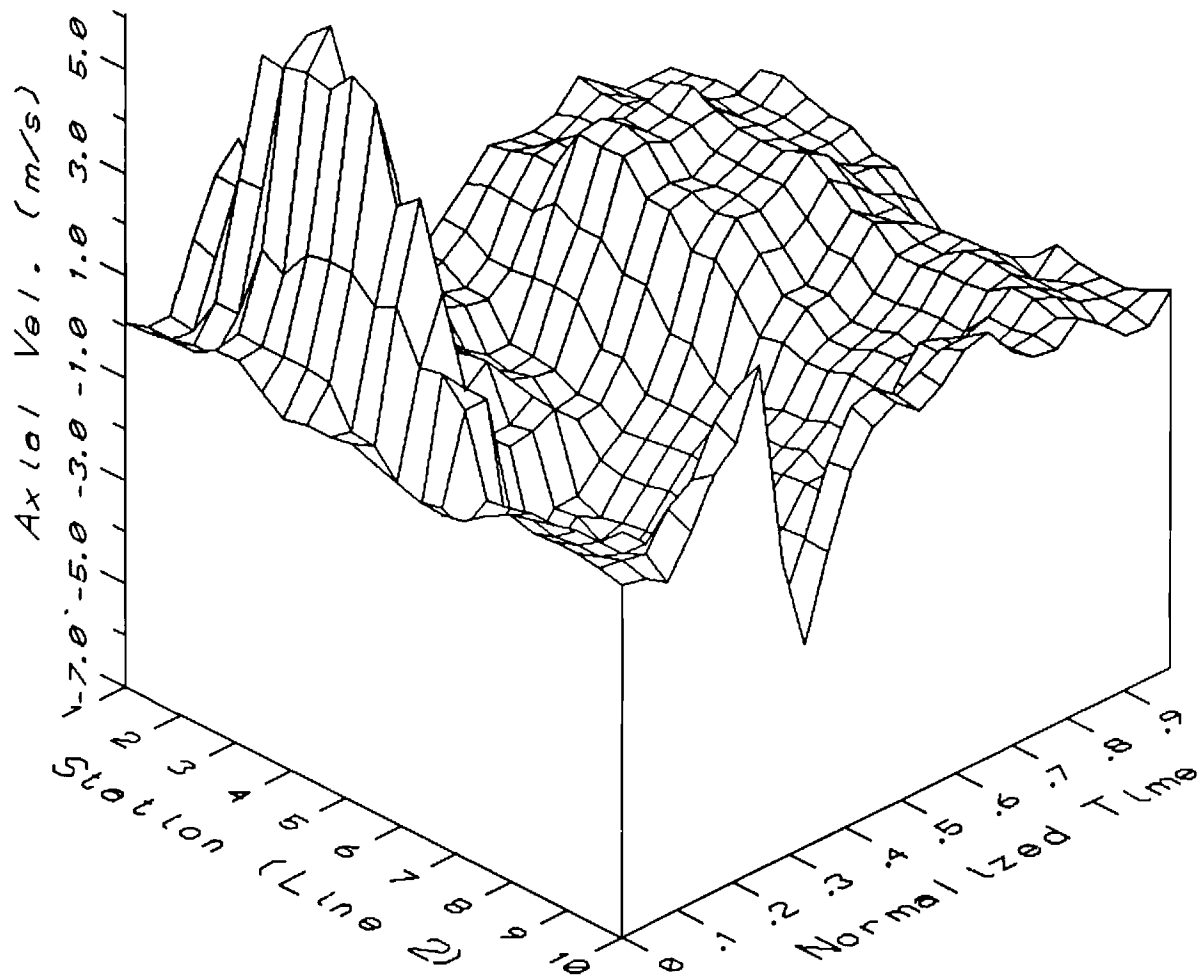

Fig. 28 Three Dimensional Plot of Axial Mean Velocities during a Cycle for Locations along the Line m = 2.

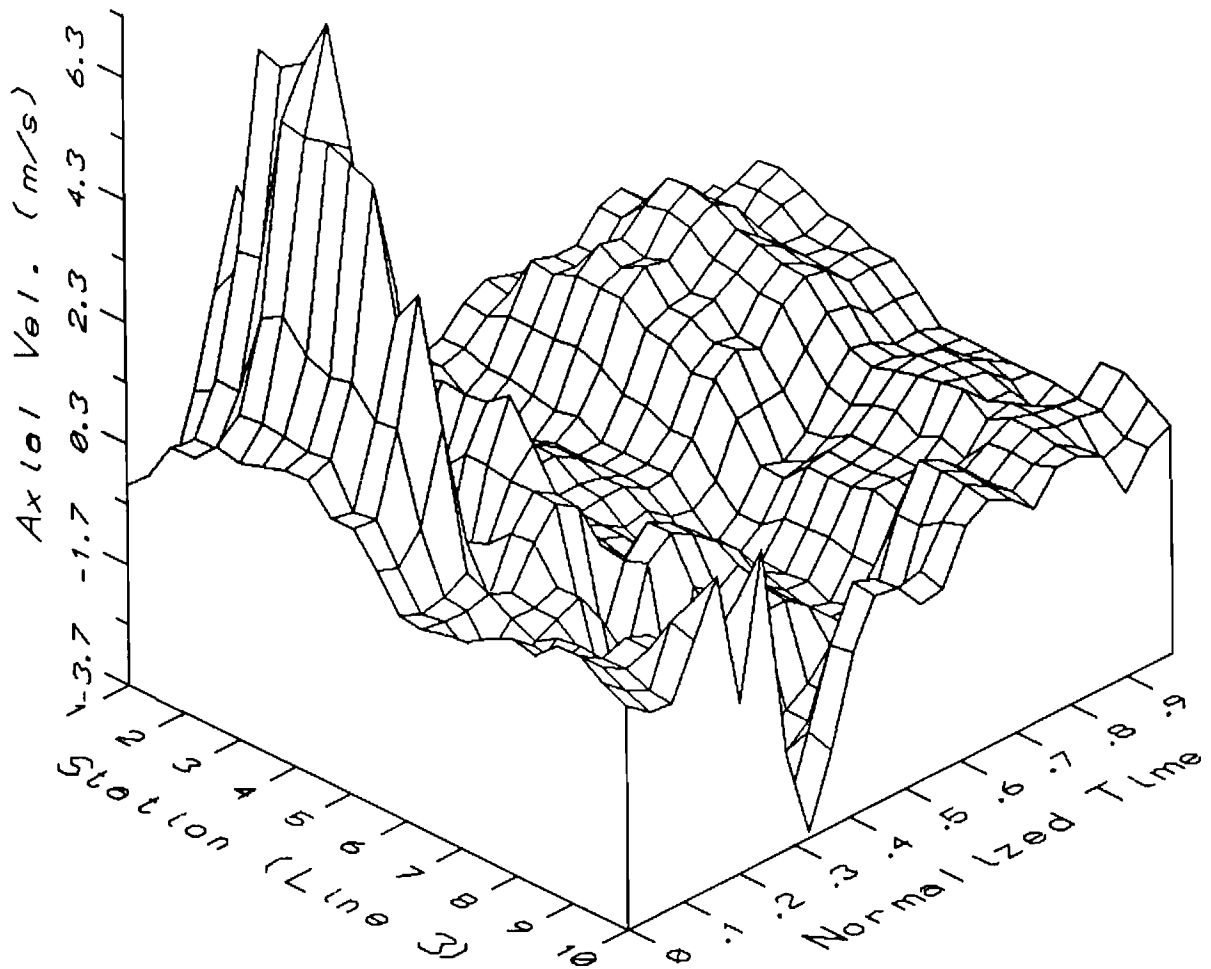

Fig. 29 Three Dimensional Plot of Axial Mean Velocities during a Cycle for Locations along the Line m = 3.

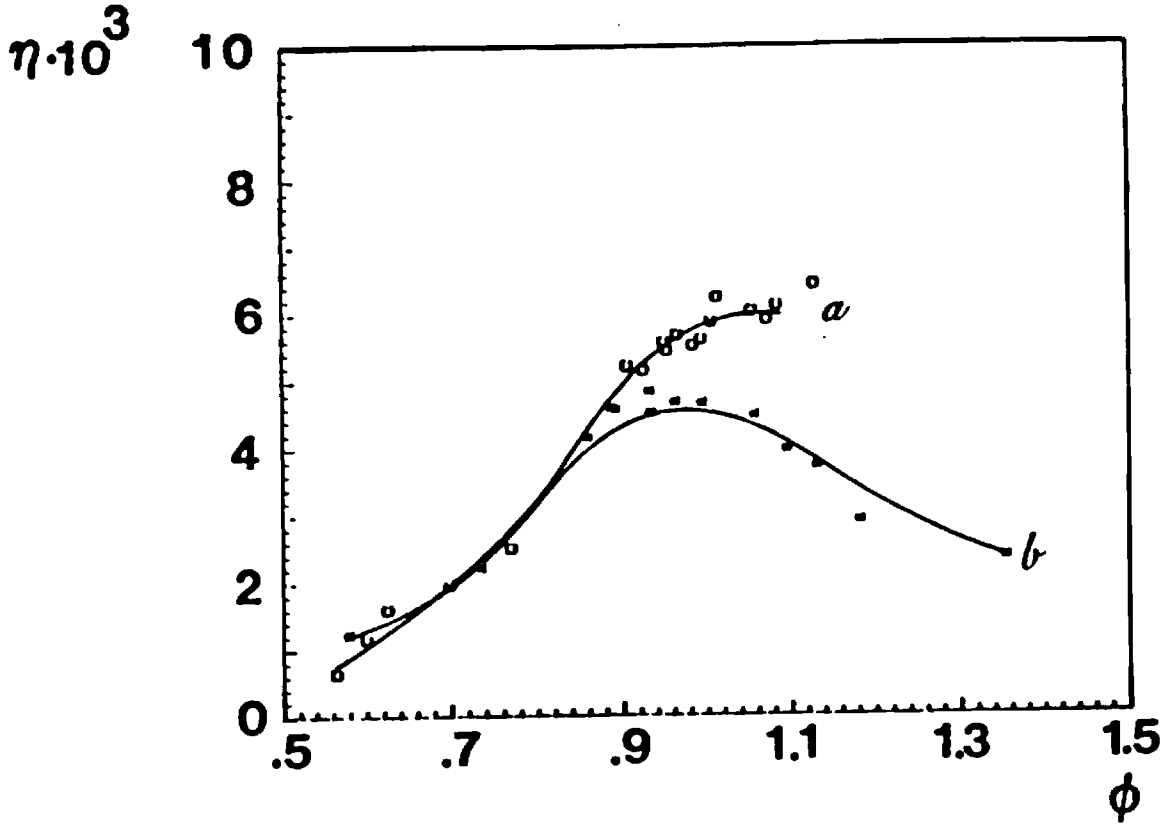

Fig. 30 Rayleigh Efficiency (η) as a Function of Equivalence Ratio (ϕ) for the Combustor Fitted with the a) Standard and b) Long Tailpipes.

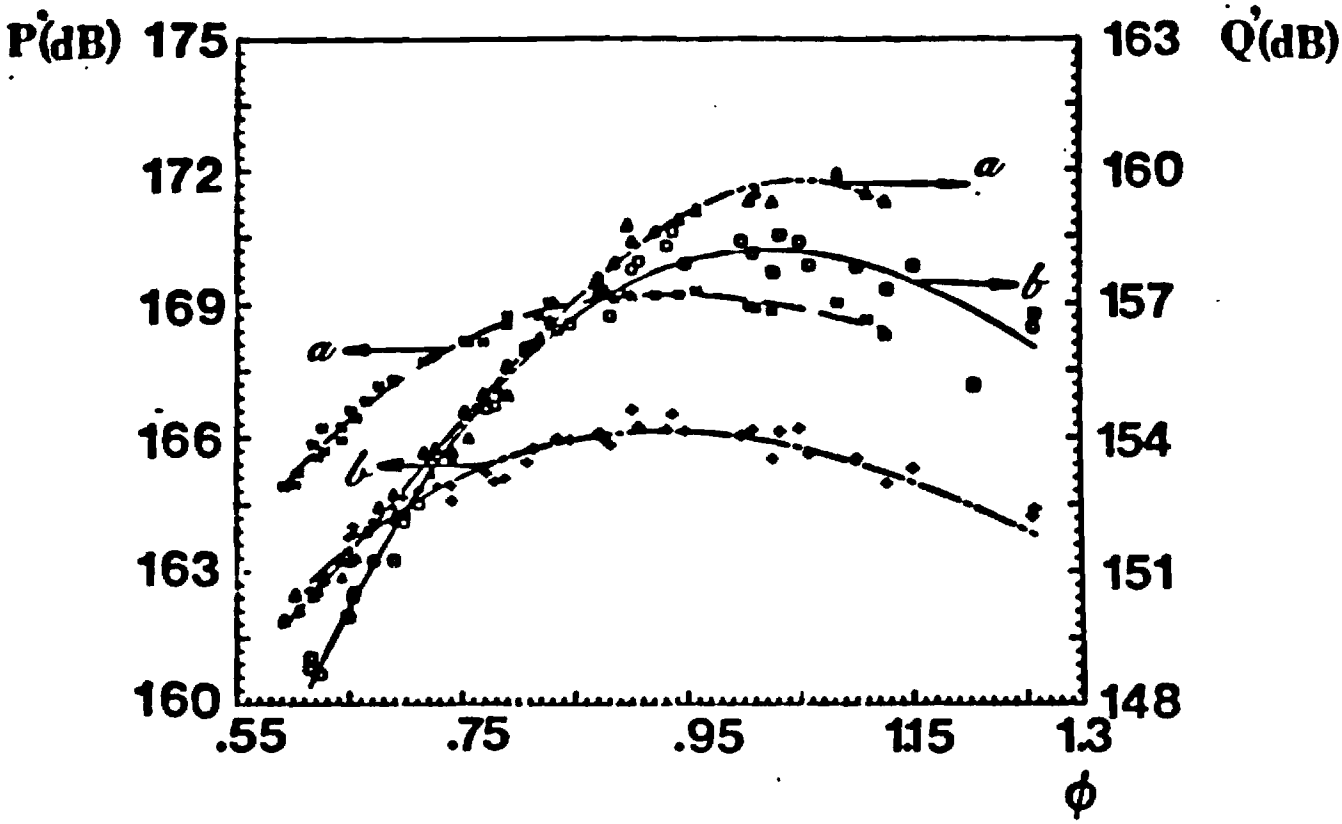

Fig. 31 Pressure (P') and Heat Release Fluctuations (Q') as a Function of Equivalence Ratio (ϕ) for the Combustor Fitted with the a) Standard and b) Long Tailpipes.

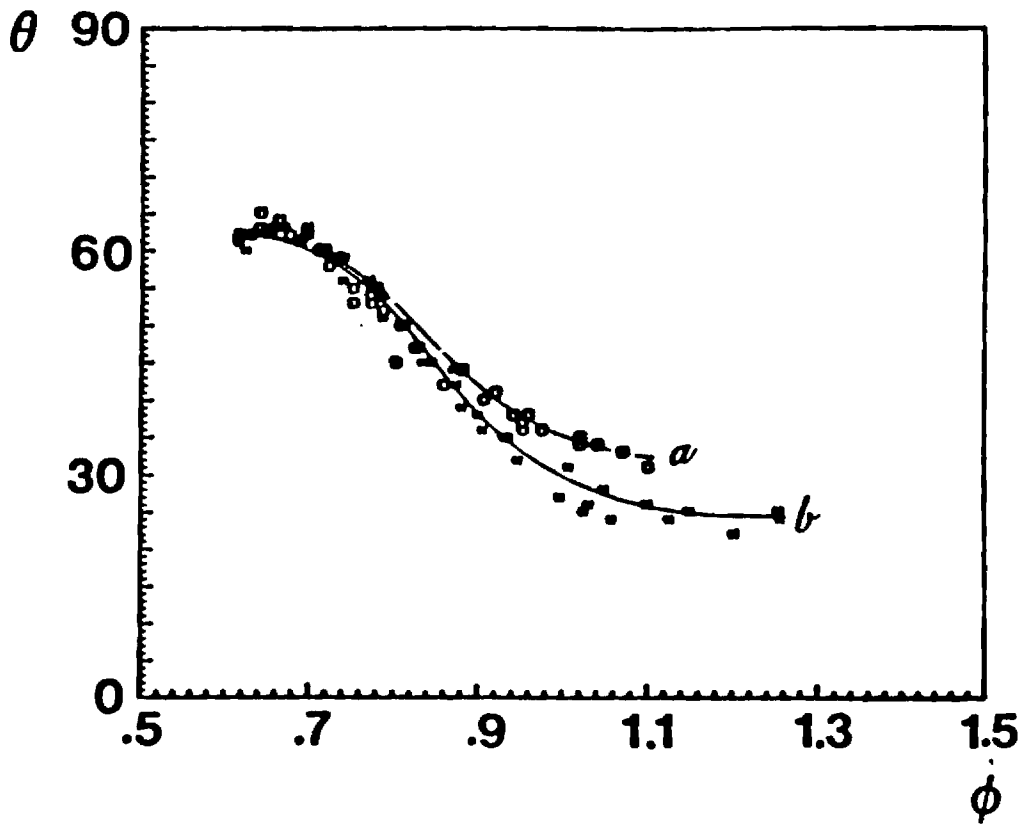

Fig. 32 Phase Angle (θ) by which the Heat Release Leads the Pressure as a Function of Equivalence Ratio (ϕ) for the Combustor Fitted with the a) Standard and b) Long Tailpipes.

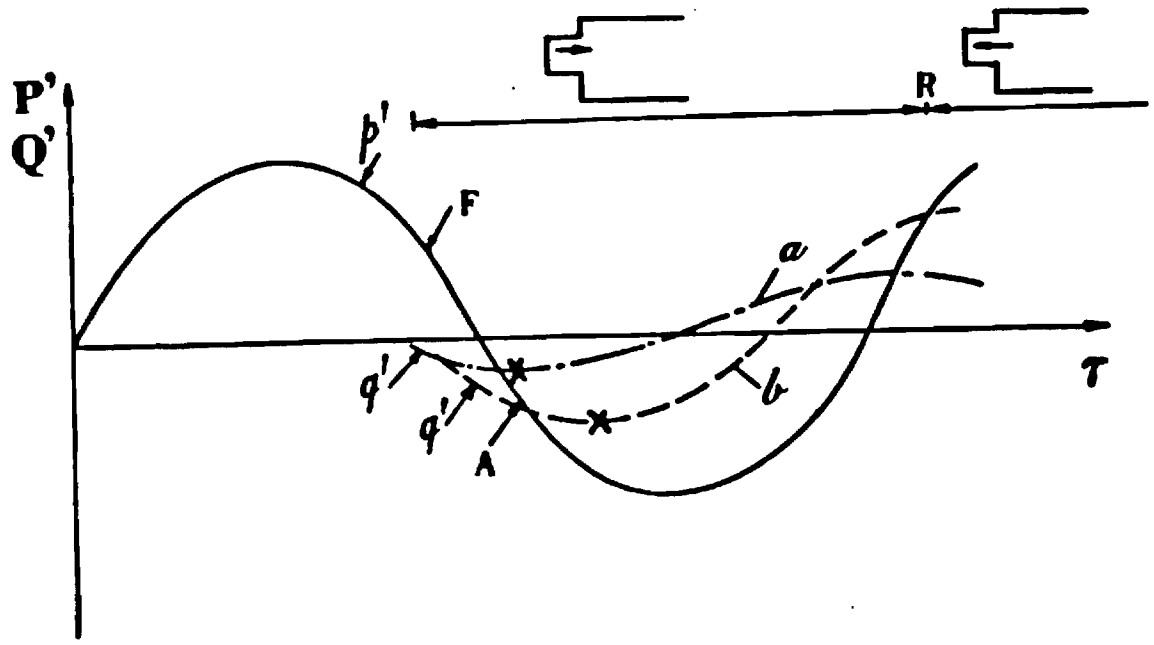

Fig. 33 Normalized Pressure (P') Cycle Showing the Timing of the Heat Release Oscillations (Q') for a) Lean and b) Rich Limits of Operation; Fuel Enters at "F", Air Enters at "A", Backflow into the Mixing Chamber Starts at "R"; the "X's" Denote the Instants of Reignition of the Fresh Fuel Charges.

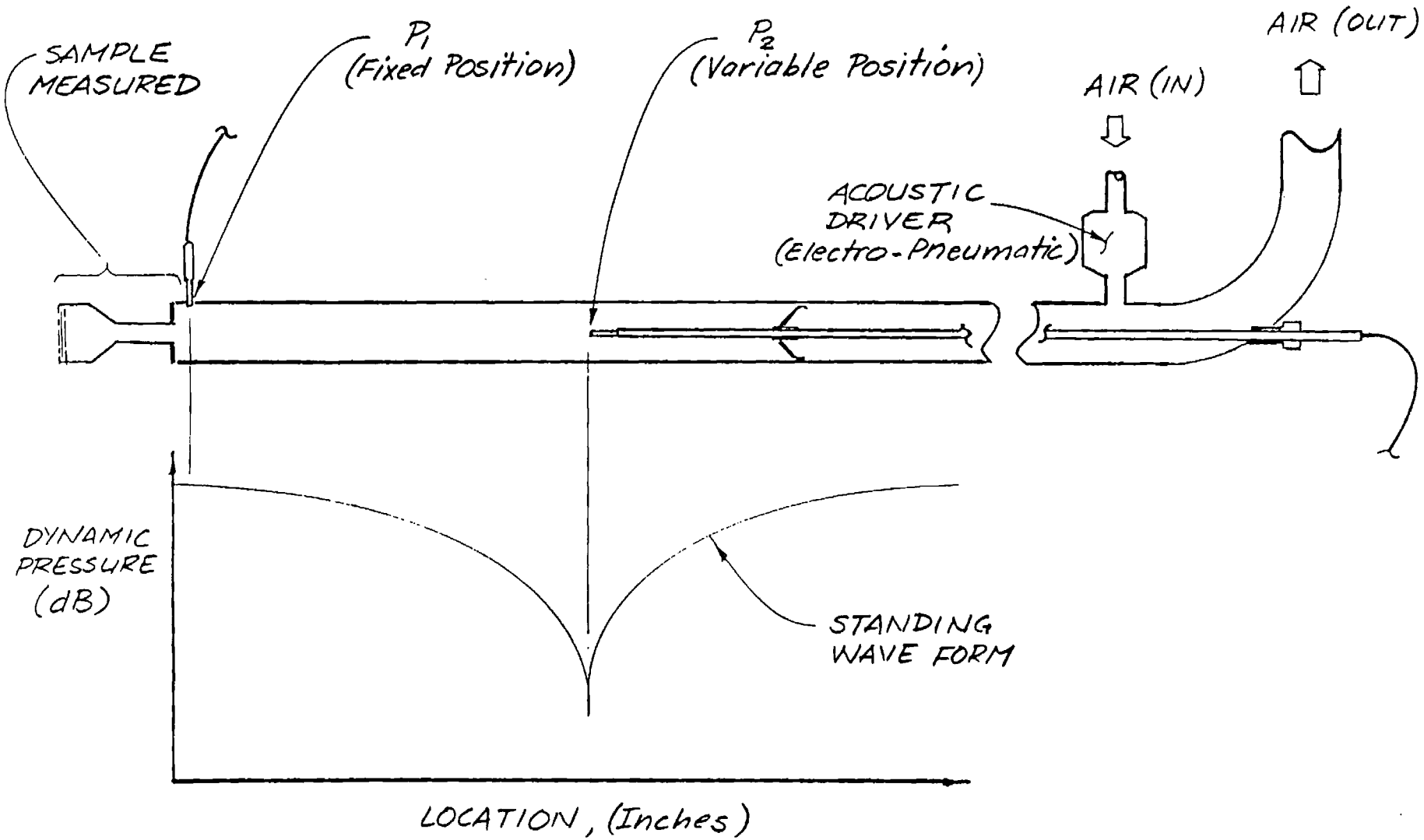

Fig. 34 Schematic of the Impedance Tube Experiment.

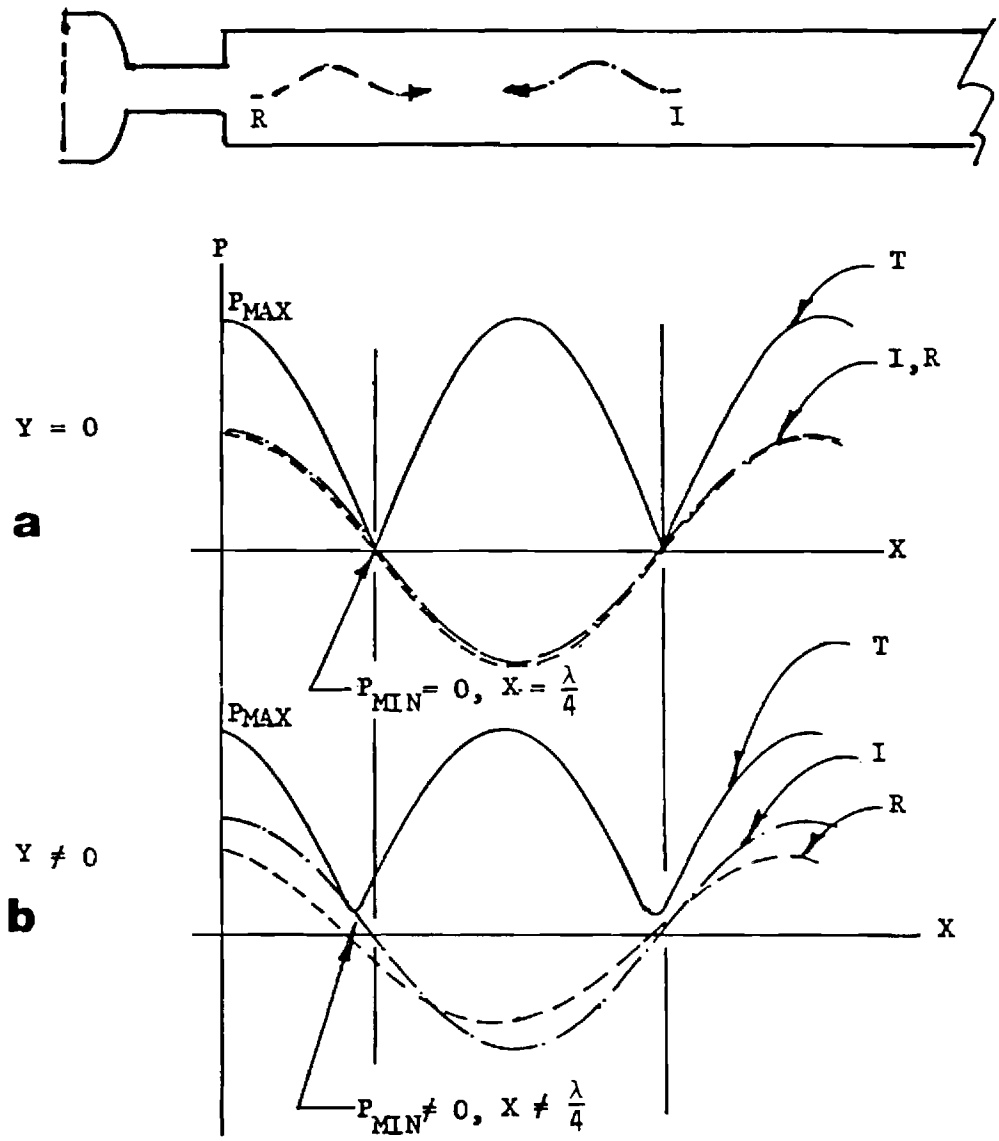

Fig. 35 Wave Form of the Incident (I), Reflected (R) and Total (T) Standing Wave for a) Hard Termination and b) Termination with Finite Admittance, as Shown by Plots of Pressure Amplitudes (P) versus Axial Distance along the Impedance Tube (X).

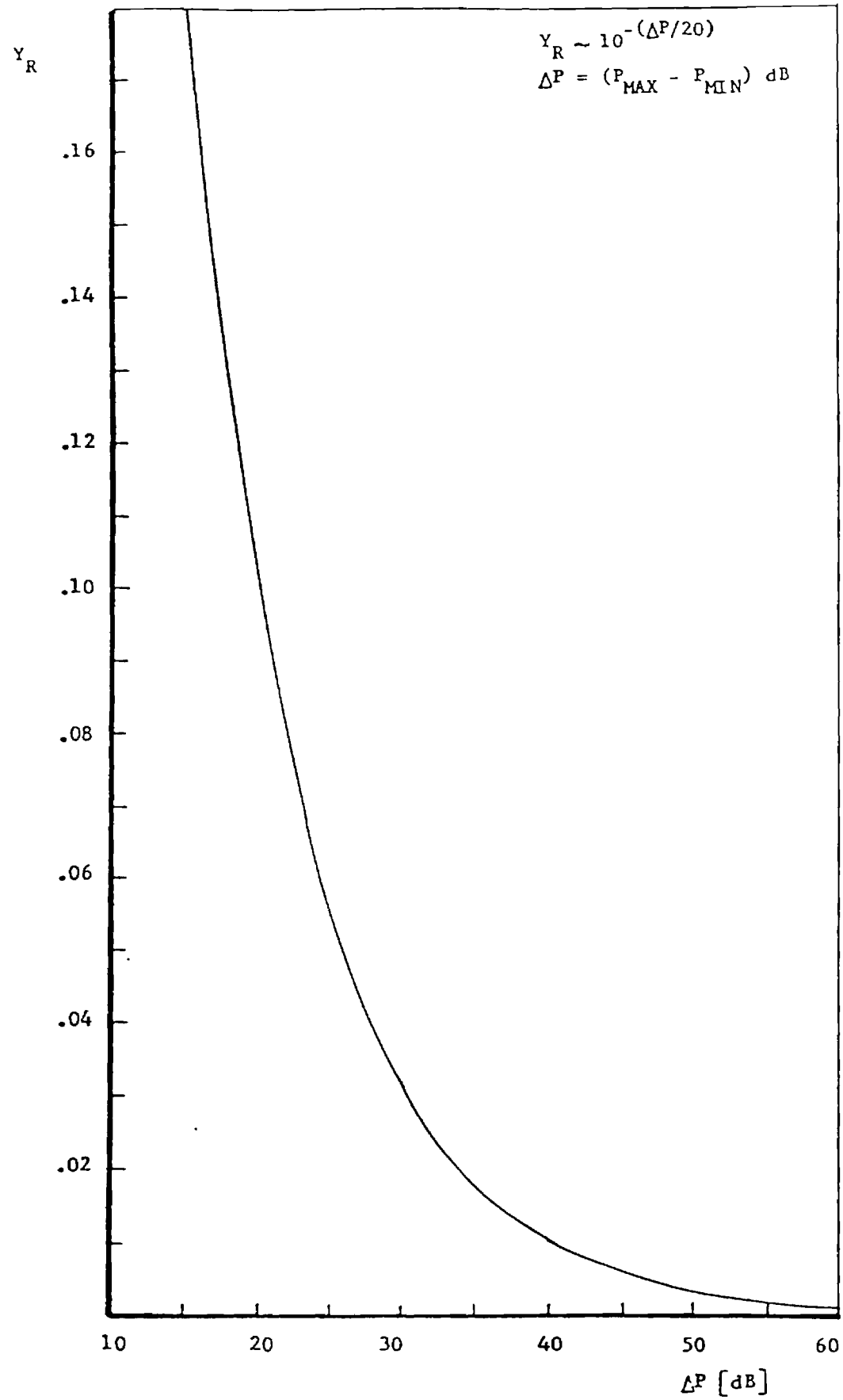

Fig. 36 Sensitivity of the Real Part of the Admittance (Y_R) to the Measured Pressure Difference between the Pressure Maximum and the Pressure Minimum (Δp).

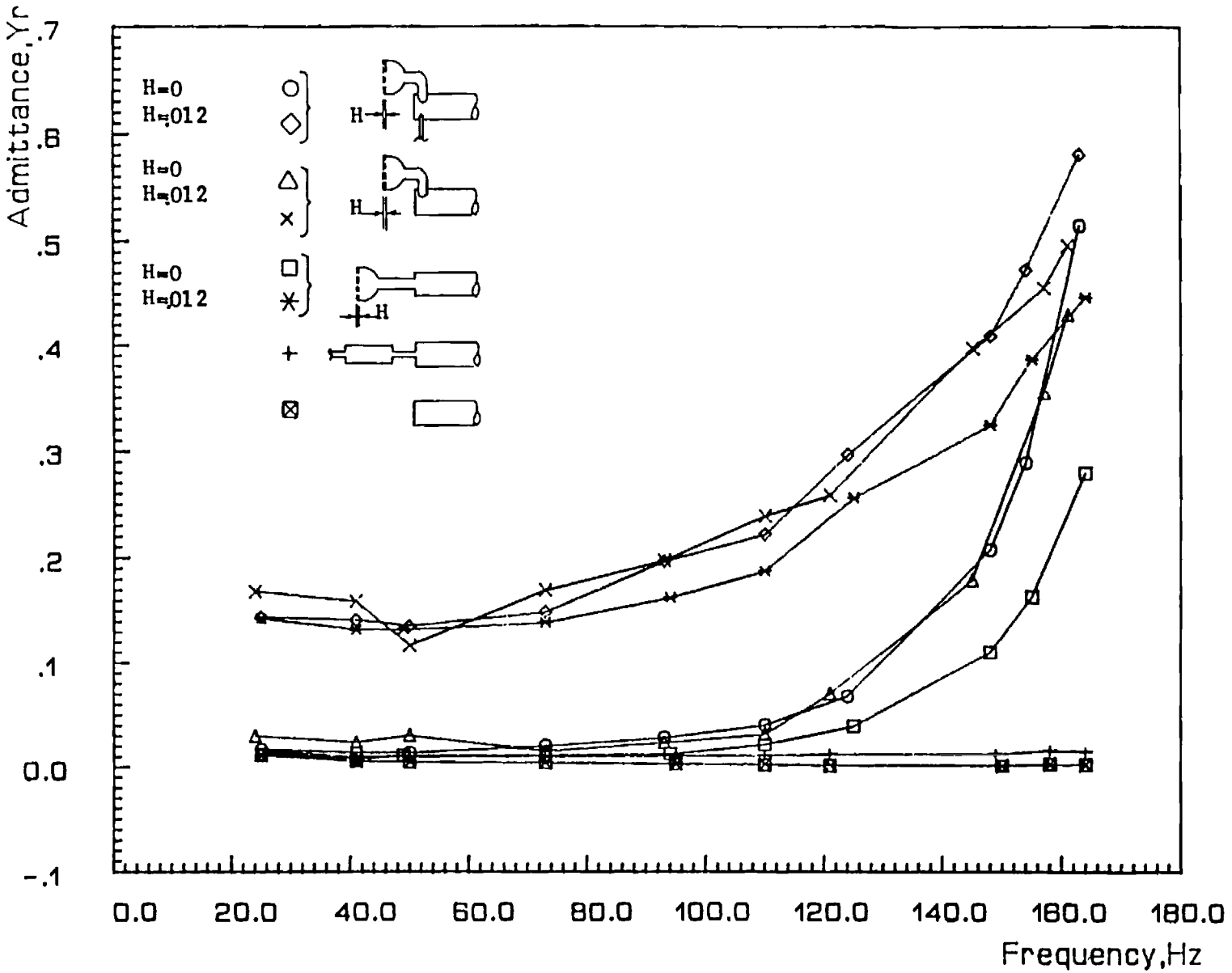

Fig. 37 Real Part of the Admittance (Y_r) as a Function of Frequency for Various Impedance Tube Terminations. H Denotes the Valve Gap Setting in Inches.

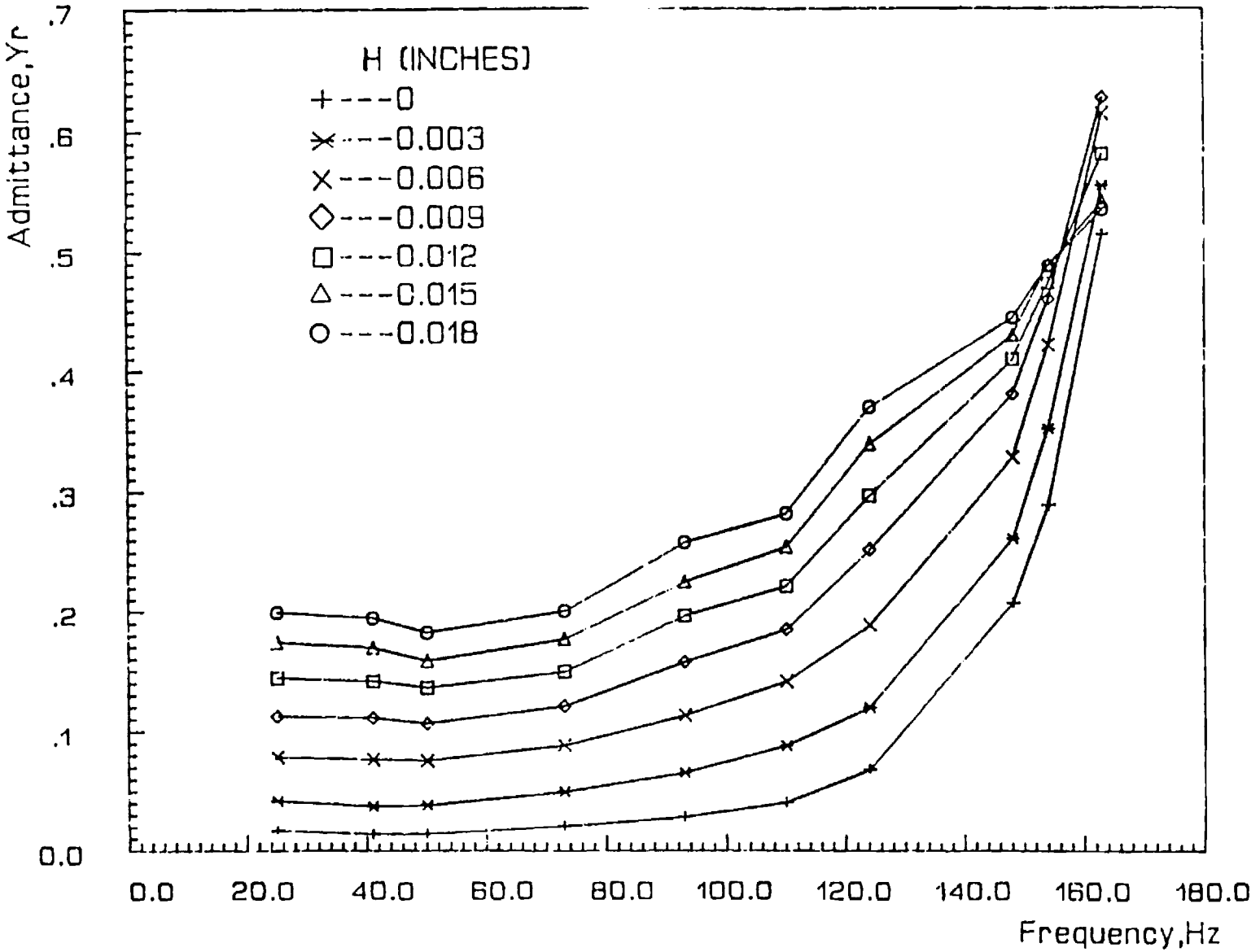

Fig. 38 Real Part of the Admittance (Y_r) of the Mixing Chamber as a Function of Frequency for Different Valve Gap Settings (H).

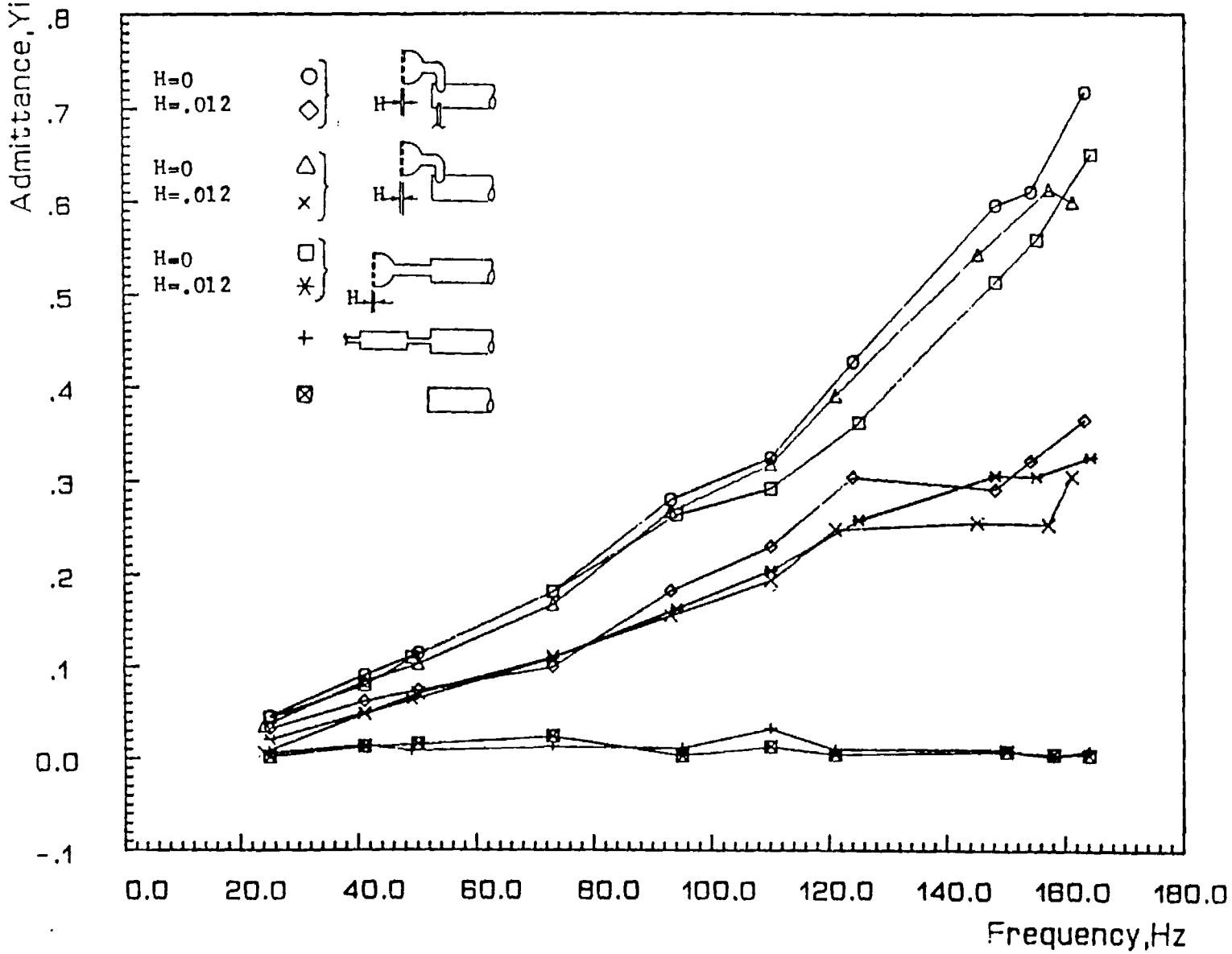

Fig. 39 Imaginary Part of the Admittance (Y_i) as a Function of Frequency for Various Impedance Tube Terminations. H Denotes the Valve Gap Setting in Inches.

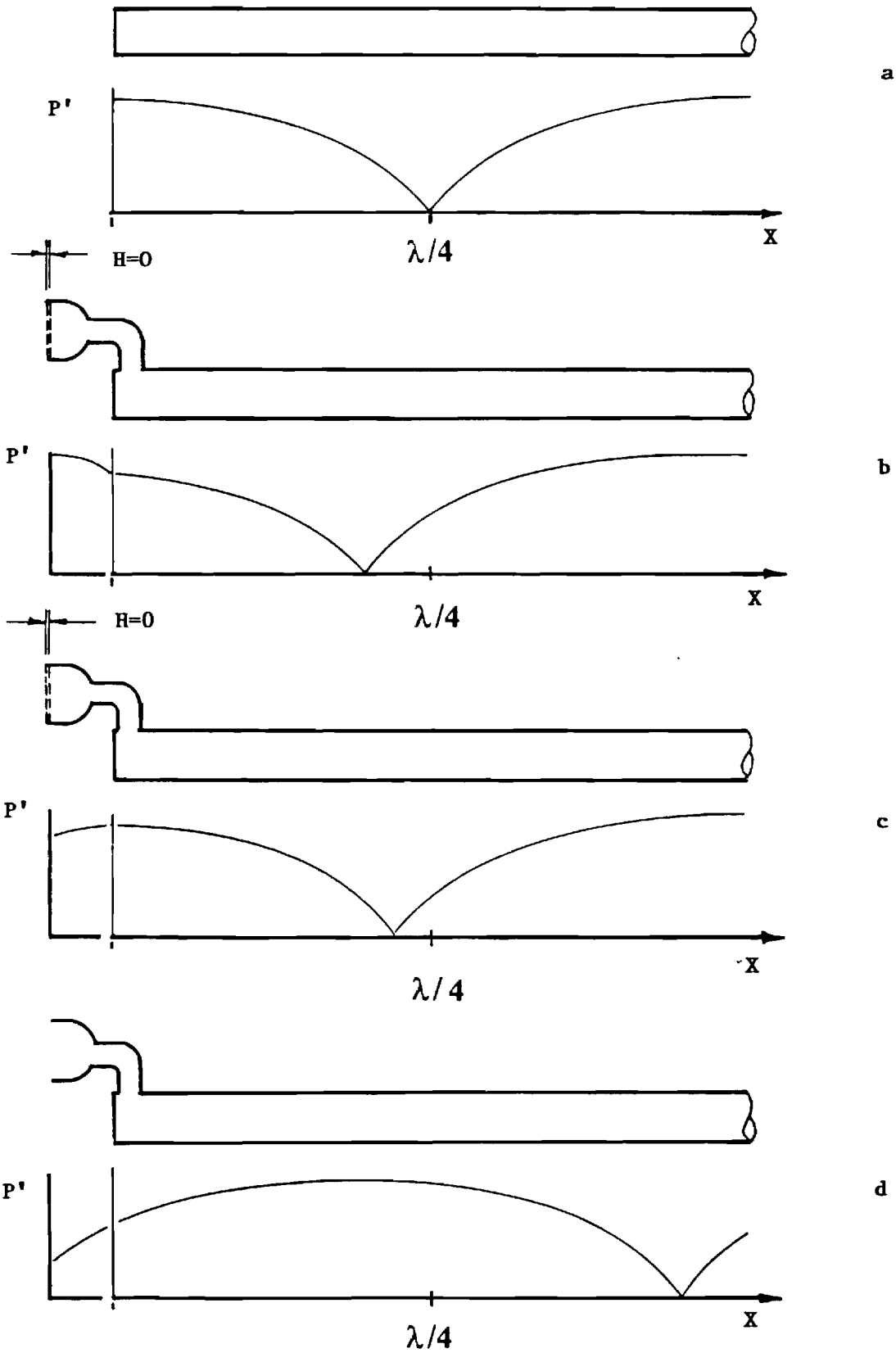

Fig. 40 Comparison of Pressure Amplitudes (P') along the Impedance Tube (X) Fitted with a) Hard Termination, b) Closed Air Valve, c) Open Valve and d) Valve Housing with Valve Plates Removed. The Actual Wave Pattern in the Valve Housing is More Complex Due to the Geometry of the Housing. H Denotes the Valve Gap Setting.

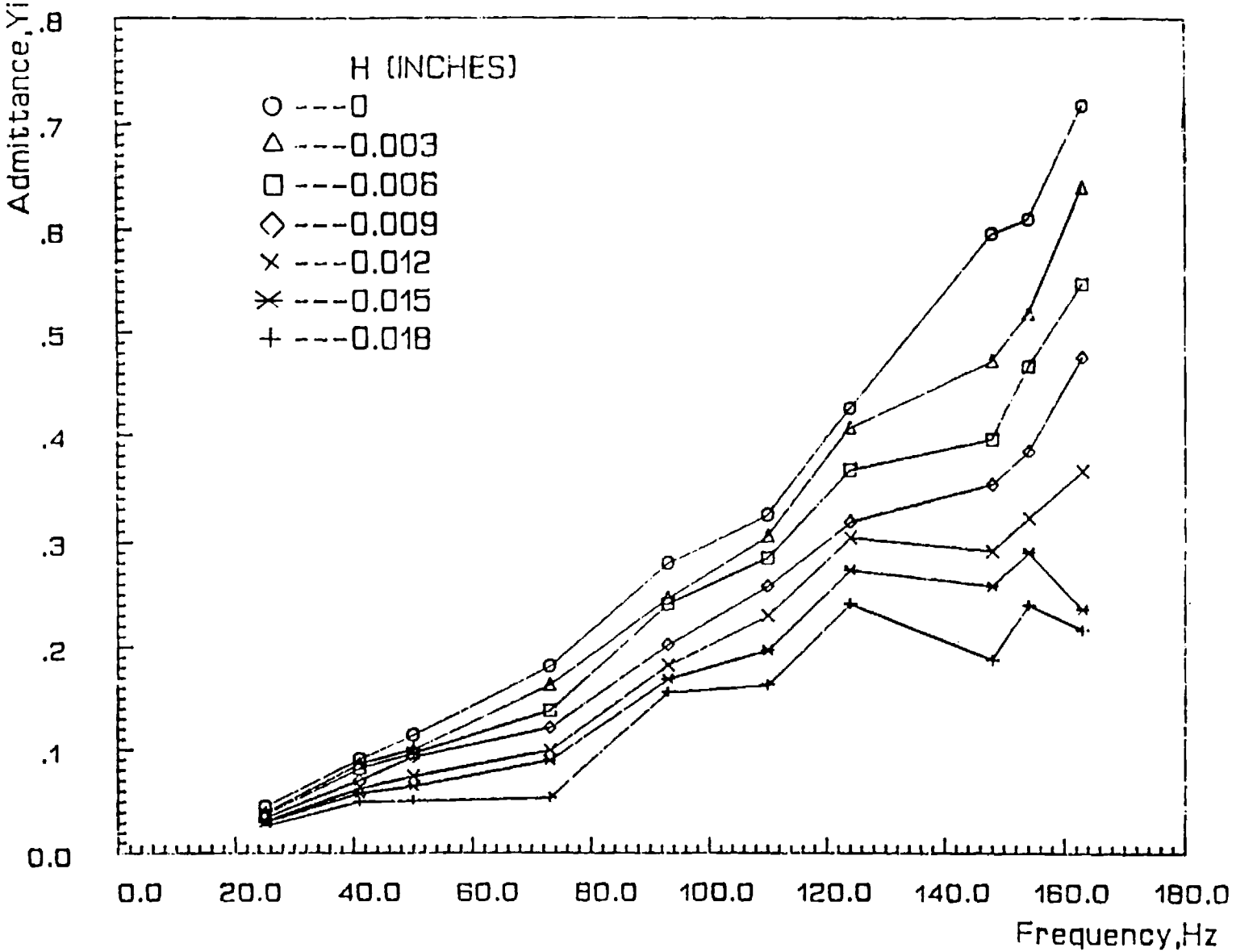

Fig. 41 Imaginary Part of the Admittance (Y_i) of the Mixing Chamber Assembly as a Function of Frequency for Different Air Valve Gap Settings (H).

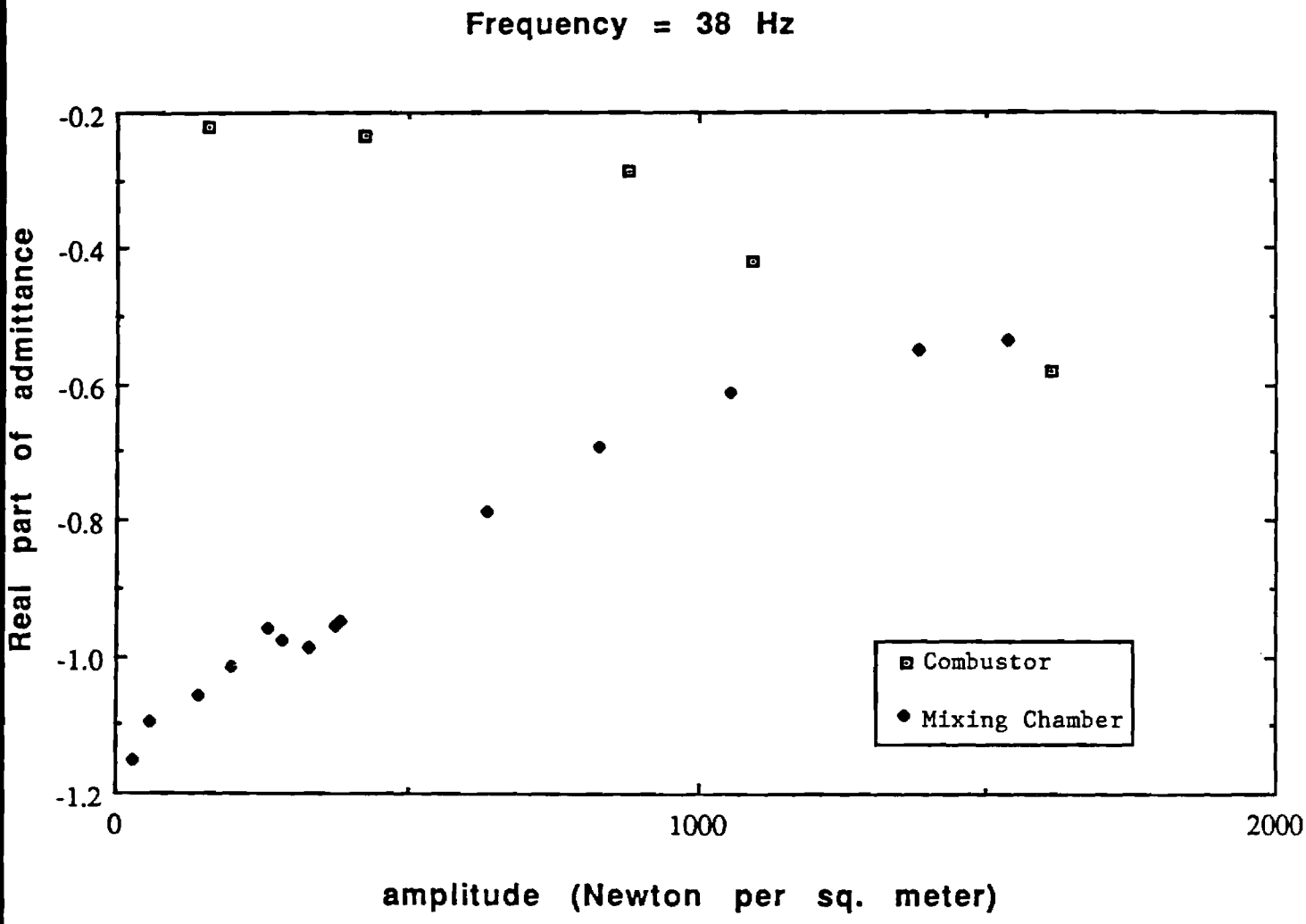

Fig. 42 Comparison of the Real Part of the Admittance as a Function of Pressure Amplitude for the Mixing Chamber Assembly only and for the Entire Helmholtz Combustor. ($1N/m^2 = 1.45 \times 10^{-4}$ psi)

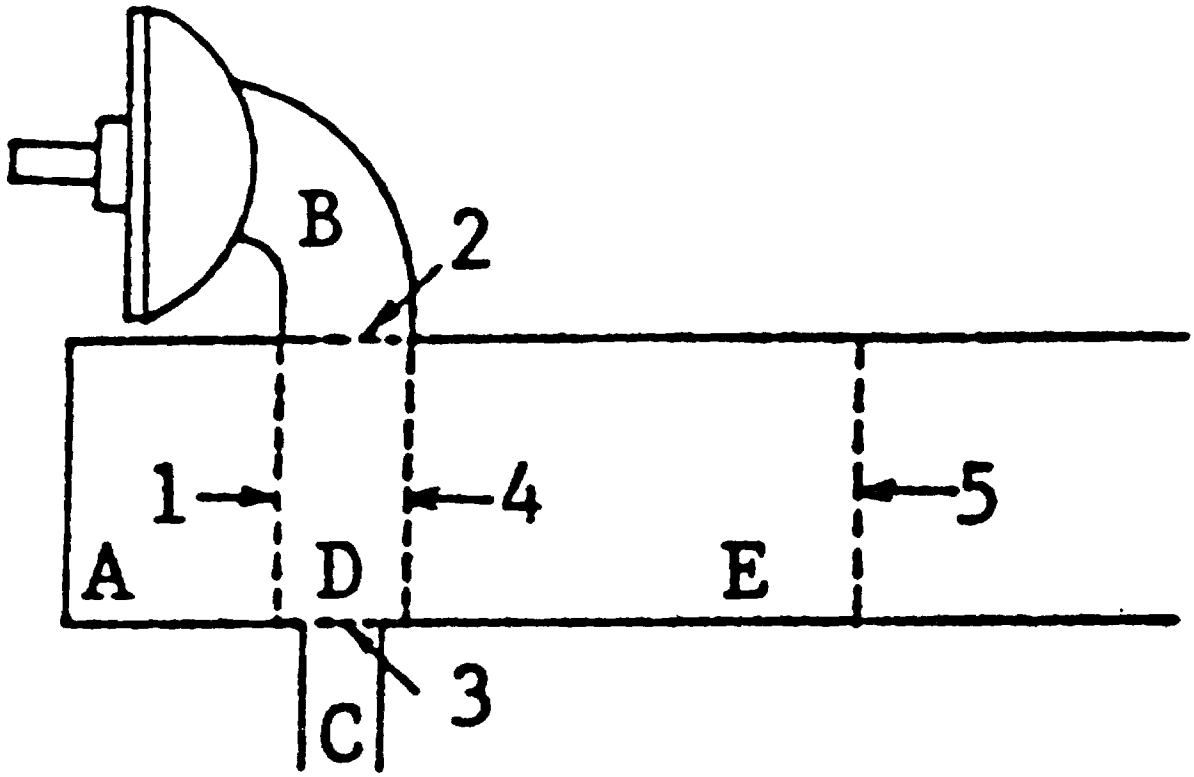

Fig. 43 Schematic Showing the Five Regions into which the Mixing Chamber Assembly has been Divided.

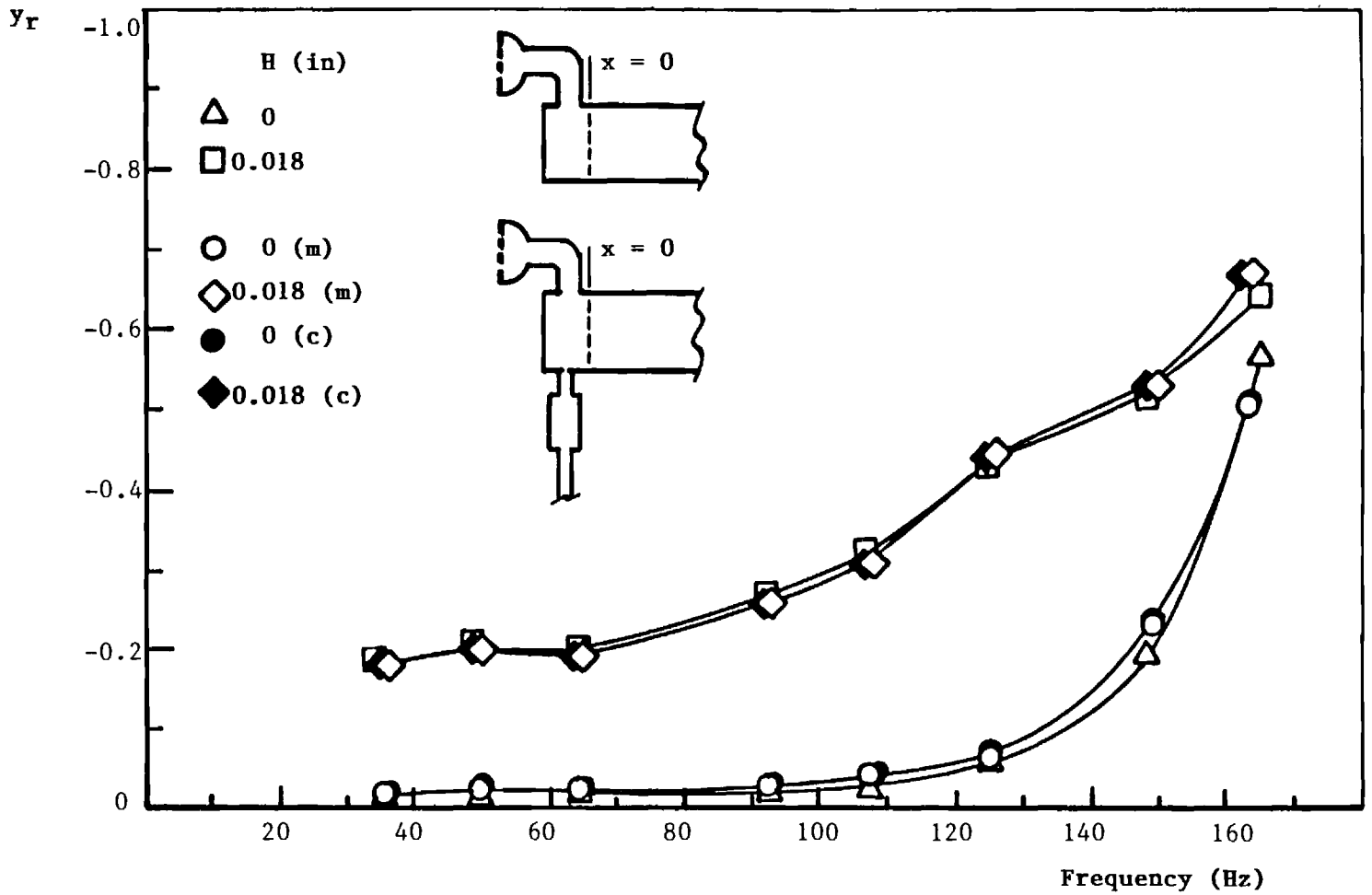

Fig. 44 Comparison between the Measured (m) and Calculated (c) Real Parts of the Admittance of the Mixing Chamber Assembly over a Range of Frequencies. H Denotes the Air Valve Gap Setting in Inches.

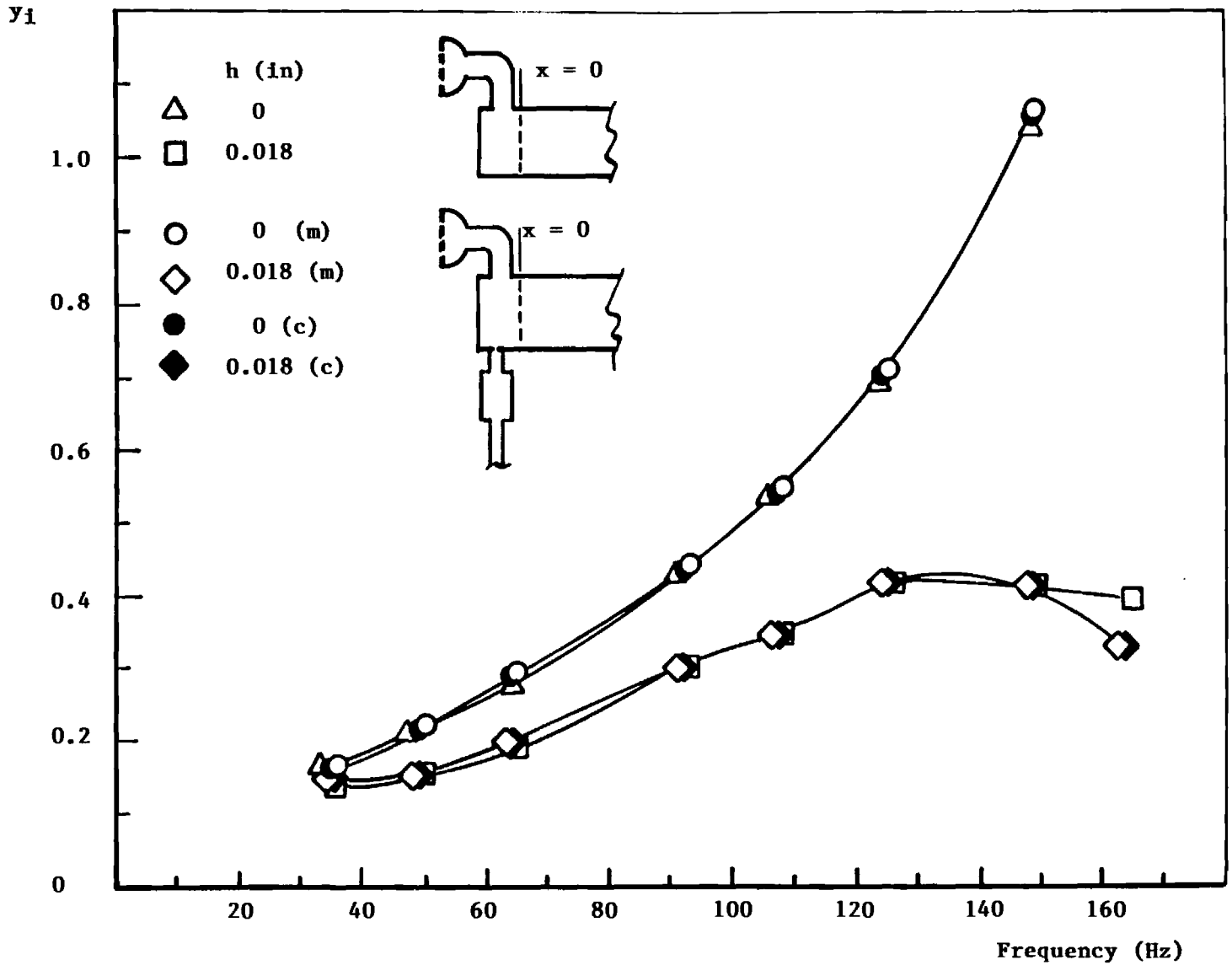

Fig. 45 Comparison between the Measured (m) and Calculated (c) Imaginary Parts of the Admittance of the Mixing Chamber Assembly over a Range of Frequencies. H Denotes the Air Valve Gap Setting in Inches.